

ELECTRON SPIN RESONANCE STUDIES ON  
IRRADIATED INORGANIC SOLIDS

by

M.B.D. Bloom

A thesis submitted for the degree of  
Doctor of Philosophy in the Faculty  
of Science of the University of  
Leicester.

February 1971

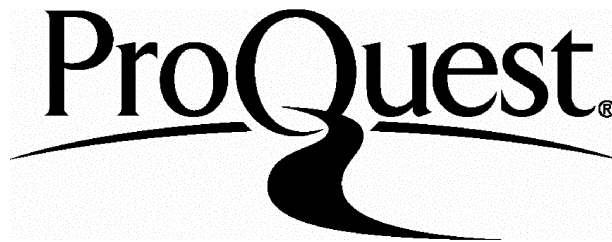
ProQuest Number: U377632

All rights reserved

INFORMATION TO ALL USERS

The quality of this reproduction is dependent upon the quality of the copy submitted.

In the unlikely event that the author did not send a complete manuscript and there are missing pages, these will be noted. Also, if material had to be removed, a note will indicate the deletion.



ProQuest U377632

Published by ProQuest LLC(2015). Copyright of the Dissertation is held by the Author.

All rights reserved.

This work is protected against unauthorized copying under Title 17, United States Code.  
Microform Edition © ProQuest LLC.

ProQuest LLC  
789 East Eisenhower Parkway  
P.O. Box 1346  
Ann Arbor, MI 48106-1346

X75305350X

*Theris*

*395906*

*13-9-1971*

*X The author*

STATEMENT

The work described in this thesis was carried out by the author in the Department of Chemistry of the University of Leicester during the period October 1966 to November 1969. The work has not been presented and is not being concurrently presented for any other degree. In the case of cojoint work a substantial part was the original work of the author.

Signed:

*M.B.D. Bloom*

M.B.D. Bloom.

TO MY PARENTS

### ACKNOWLEDGEMENTS

The author wishes to thank the following:

Professor M.C.R. Symons for his constant encouragement and invaluable guidance during the course of this work.

Dr. J.B. Raynor for his helpful advice on matters concerning Part I of this thesis.

Dr. R.S. Eachus with whom the work outlined in Part II of this thesis was jointly carried out.

Members of the Chemistry Department, too numerous to mention by name, for their freely given advice and friendship, who helped make my stay in Leicester an enjoyable one.

Mrs. P. Spicer for helping me with the diagrams for this thesis.

My Father for his encouragement and for typing most of this thesis.

The Science Research Council for a maintenance grant.

## CONTENTS

### CHAPTER 1

#### General Introduction

I.	Some Aspects of Electron Spin Resonance Spectroscopy	1
II.	Experimental Methods	7
III.	Instrumentation	8
	References	11

### PART I      SPECTROSCOPIC STUDIES UPON SOME TRANSITION

#### METAL NITROSYL COMPLEXES.

	<u>Introduction to Part I</u>	14
	References	18

### CHAPTER 2

#### Paramagnetic Species Obtained from Anhydrous Nitroprusside

	Introduction	19
	Experimental	19
	Results	21
	Discussion	22
	References	36

### CHAPTER 3

#### Paramagnetic Species Obtained from Hydrated Nitroprusside

	Introduction	37
	Experimental	37
	Results	40
	Discussion	48
	References	70

## CHAPTER 4

### Spectroscopic Studies on Chromium and Manganese

#### Pentacyanonitrosyls in Alkali Halide Lattices

Introduction	72
Experimental	73
Results	76
Discussion	86
References	106

## PART II STABILISED RADICALS IN PRECIPITATED POWDERS

<u>Introduction to Part II</u>	108
--------------------------------	-----

## CHAPTER 5

### Interaction of Trapped Hydrogen Atoms with

#### Alkali Metal Ions in Barium Sulphate.

Introduction	112
Experimental	112
Results	113
Discussion	115
Related Systems	120
Other Systems: The $H_2^-$ and $H_2^+$ Ions	122
References	128

## CHAPTER 6

### The 33 Valence-electron $ClO_4^{2-}$ Anion and Related Species

Introduction	130
Experimental	131
Discussion	132
References	143

APPENDIX I

Calculation of Principal g- and A- Values from  
Single Crystal Data.

145

APPENDIX II

Calculation of the Dipolar Interaction between an  
Electron Confined to a Hydrogen 1s-orbital and an  
Adjacent Sodium Nucleus.

153

CHAPTER 1.

GENERAL INTRODUCTION.

## I. Some Aspects of Electron Spin Resonance Spectroscopy.

For a detailed exposition of fundamental e.s.r. theory, the reader is referred to several excellent comprehensive reviews recently published.<sup>1-11</sup> In this introductory section we shall briefly cover the methods involved in the extraction of structural information from the spin-resonance parameters of transition metal complexes and simple inorganic radicals.

### a) g-Values.

The application of a magnetic field to the energy levels of the free atom, formed by the successive operations of the electronic repulsion and spin-orbit Hamiltonians as perturbations on the Schrodinger equation, results in a splitting into  $2J + 1$  sublevels. For Russell-Saunders coupling  $\vec{J} = \vec{L} + \vec{S}$ , where  $L$  and  $S$  are the orbital and angular momentum quantum numbers. Now, in the free atom all directions are equivalent, and by operating on the wavefunction  $\{L, S, J, M_J\}$  with the Zeeman operator  $\beta \underline{H}(\underline{L} + 2\underline{S})$ , where  $\beta$  is the Bohr magneton and  $\underline{H}$  the magnetic field operator, we obtain for the z-axis as field direction:

$$E = g \beta H_z M_J,$$

$$\text{where } g = 1 + \frac{J(J+1) - L(L+1) + S(S+1)}{2J(J+1)}.$$

The term  $g$  is commonly known as the Lande  $g$ -factor, and for the case where the orbital angular momentum is completely quenched (i.e.  $L = 0$ ) we obtain the free spin value of  $g = 2$ , (actually 2.0023).

In an electron spin resonance experiment, the degeneracy of the ground state is removed by the application of a magnetic field; the

energy separation being  $\Delta E = g \beta H$ . Transitions between these levels are now induced by interaction with electromagnetic radiation of frequency  $\nu$ , such that  $\Delta E = h\nu$ , where  $h$  is Planck's constant. We can thus describe the electron spin resonance condition as  $h\nu = g \beta H$  (Figure 1.1).

In transition metal compounds, the values of the  $g$ -factors often differ widely from those predicted for the free atom or the free spin value. For first row transition metals, however,  $g$ -values close to free spin are often obtained; deviations being due to spin-orbit coupling. In general, there are competing excited states that can combine with the ground state of the molecule. If there is mixing with an empty orbital, the orbital motion of the electron will be such that the induced magnetic field will tend to oppose the applied field, resulting in a negative  $g$ -shift. If there is mixing with a filled orbital the resulting  $g$ -shift will be positive. Thus the  $g$ -values give valuable information about the proximity of magnetically coupled excited states.

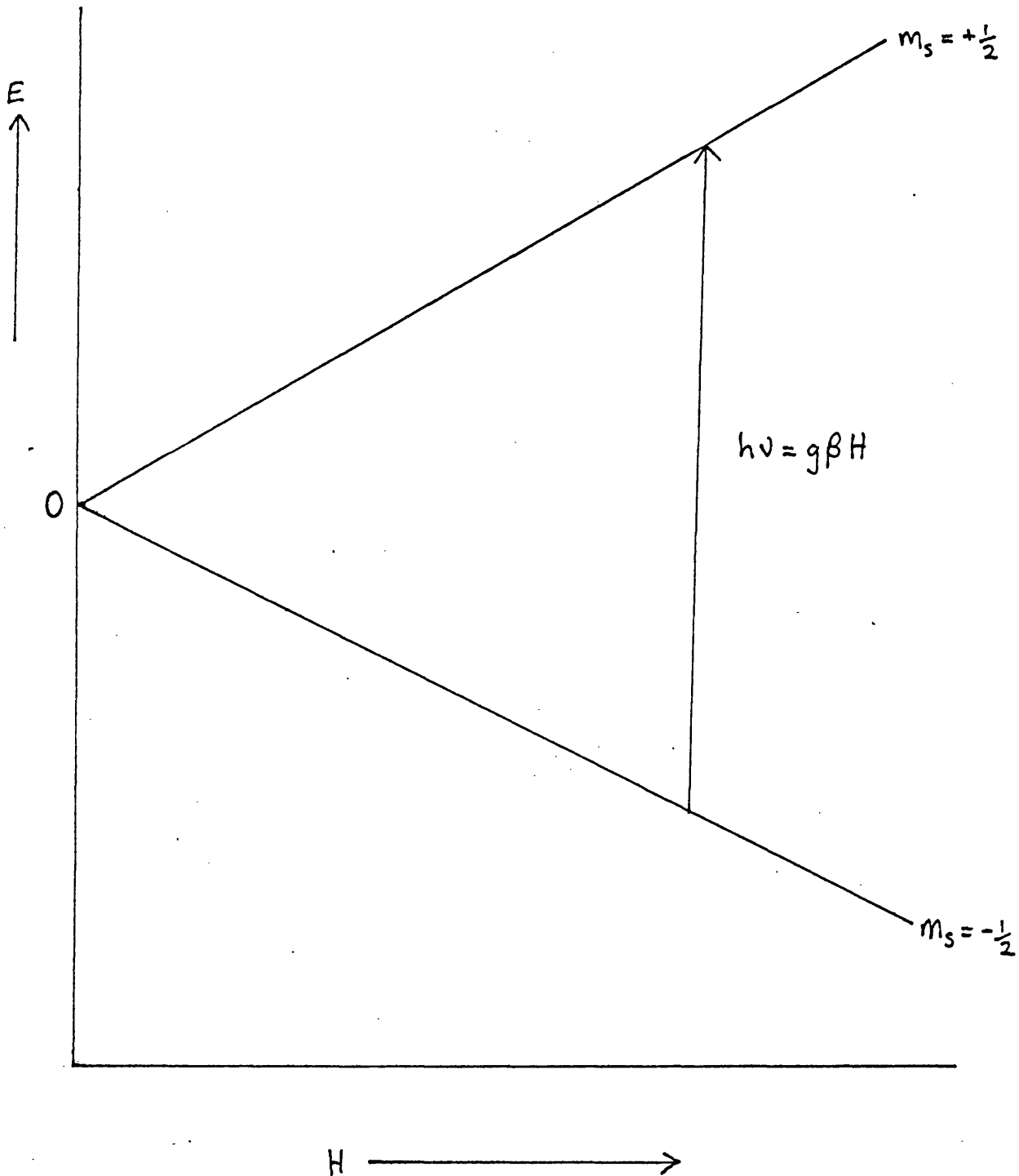
In the presence of a ligand field, the  $g$ -values are found to be dependant upon the symmetry of the field. The resonance condition now becomes  $h\nu = g_k \beta H_k$ , where  $k$  represents an arbitrary axis. For an octahedral complex  $g_x = g_y = g_z$ , and the  $g$ -value is said to be isotropic. In fields with non-cubic symmetry, however, anisotropy of the  $g$ -factor is observed, e.g. for molecules with axial symmetry two  $g$ -values,  $g_{\parallel}$  and  $g_{\perp}$  are observed, whereas in fields of lower symmetry three distinct  $g$ -values are obtained. The general Hamiltonian for the Zeeman interaction when the magnetic field,  $H$ , is applied in an arbitrary direction (whose direction cosines are  $l, m, n$ ) is:

$$\mathcal{H} = H(lg_x S_x + mg_y S_y + ng_z S_z),$$

where for convenience the  $x, y, z$  axes are chosen to be the principal axes of the  $g$ -tensor.

Figure 1.1

Zeeman Energy Levels for a Single Unpaired Electron  
as a Function of Magnetic Field.



When the e.s.r. experiment is performed using a single crystal, it is usual to rotate the crystal in turn about three mutually perpendicular axes. The principal values of both the  $g$ - and  $A$ -tensors and their direction cosines relative to the crystal axes can then be deduced from the observed angular variations of the  $g$ - and  $A$ - factors. Detailed descriptions of the techniques involved, and convenient methods of processing the experimental information are given by Geusic and Brown,<sup>12</sup> Pryce,<sup>13</sup> Weil and Anderson,<sup>14</sup> and Schonland.<sup>15</sup> The method used to evaluate the spin-resonance data for an irradiated single crystal of sodium nitroprusside, included in Chapter 3, follows closely that of Schonland and is fully described in Appendix I.

In fluid solution, where rotation of the paramagnetic compound is rapid compared to the time required for resonance, all anisotropic effects will be averaged out and an isotropic spectrum will be observed. The  $g$ -value will simply take the average of the single crystal values:

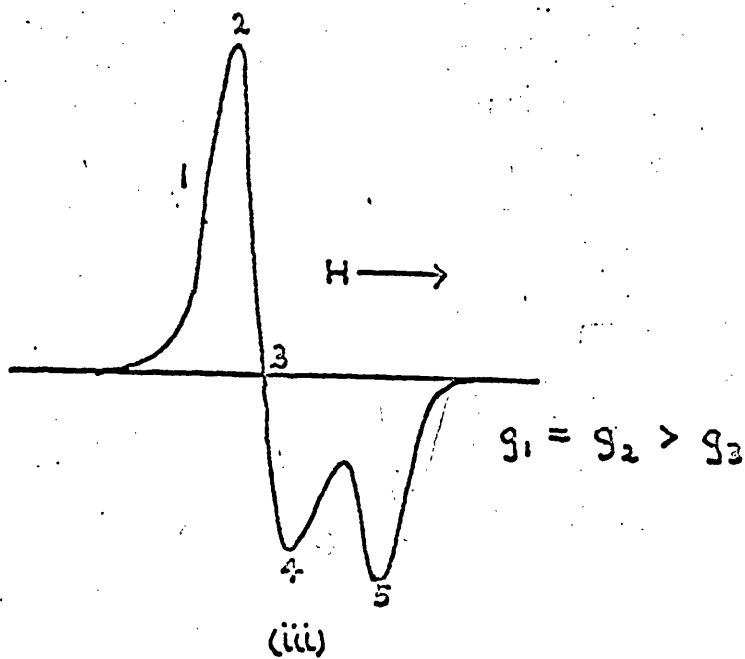
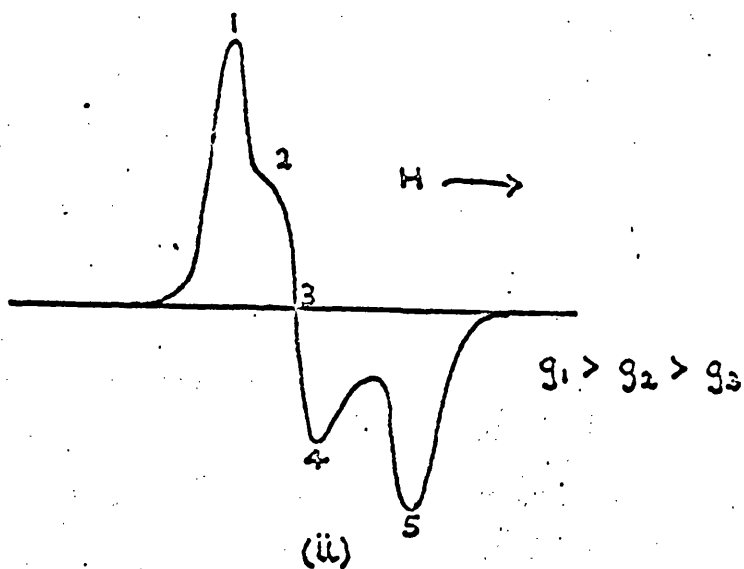
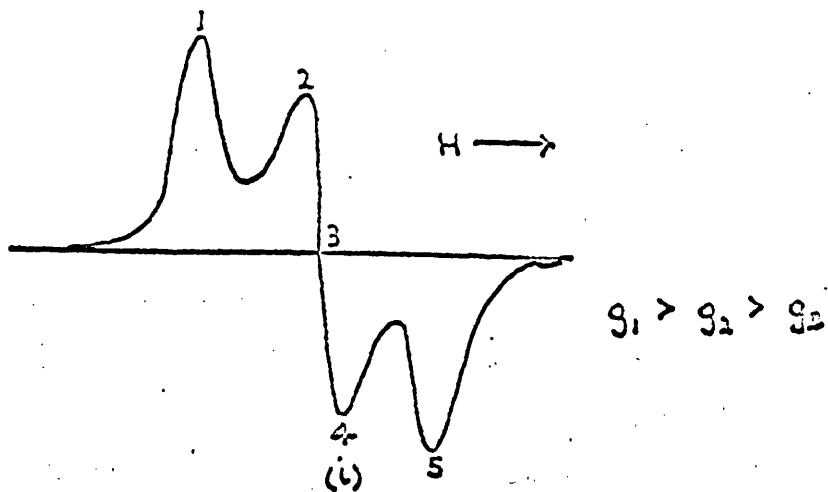
$$\text{i.e. } g_{\text{iso}} = 1/3(g_x + g_y + g_z).$$

In a frozen solution or polycrystalline sample an average spectrum is again observed, but this time it consists of a superimposition of all the lines of the single crystal spectra. Powder spectra provide a useful check on the diagonalisation results from single crystal studies, and should always be obtained and compared with the single crystal spectra.

Several authors<sup>16-26</sup> have performed calculations on the line shapes of polycrystalline spectra with different amounts of asymmetry. Figure 1.2 illustrates the changes observed with varying degrees of asymmetry of the  $g$ -tensor. Figure 1.2(i) gives an example of the spectrum obtained when there is a marked triaxial anisotropy. The three

Figure 1.2

ESR Lineshapes for Species Exhibiting Varying Degrees of Assymetry.



principal  $g$ -values are given by points 1,3 and 5. Figure 1.2(ii) illustrates a similar spectrum, but with values of  $g_1$  and  $g_2$  much closer together. In Figure 1.2(iii) the case for axial symmetry is illustrated, and, in this case according to Korolkov and Potapovich,<sup>26</sup> the field corresponding to  $g_{\perp}$ , i.e.  $H_{\perp}$ , occurs 2/5 of the way between points 2 and 3. Small deviations from axial symmetry may be detected by a lengthening of the distance 2 - 3 compared with the distance 1 - 2.

#### b) Nuclear Hyperfine Coupling.

The experimental tensor  $\underline{\underline{A}}$ , ( $A_{xx}$ ,  $A_{yy}$ ,  $A_{zz}$ ), representing the total hyperfine interaction between the unpaired electron and a given nucleus may be resolved into isotropic and anisotropic components as follows:

$$\underline{\underline{A}} = A_{\text{iso}} \cdot \underline{\underline{E}} + \underline{\underline{B}},$$

where  $\underline{\underline{E}}$  is the unit matrix, and  $\underline{\underline{B}}$  ( $B_{xx}$ ,  $B_{yy}$ ,  $B_{zz}$ ) the anisotropic component arises from a coupling between the electron and <sup>nuclear</sup> magnetic dipoles.

The isotropic part of the hyperfine tensor stems solely from the presence of unpaired electron spin-density at the nucleus. This can arise in one of three ways:

- (i) from spin-density directly in an ns-orbital,
  - (ii) from a configurational interaction which admixes excited states with appreciable s-character into a ground-state which has no s-orbital contribution,
- or (iii) from polarisation of inner s-electrons by unpaired electron density in outer s-, p-, d- or f-orbitals.

The hyperfine coupling between an electron in an ns-orbital and the nucleus at the centre of that orbital is given by:

$$A_{\text{iso}} = a_{\text{ns}}^2 \left(\frac{8\pi}{3}\right) g_n \beta_n \left|\psi_{\text{ns}}(0)\right|^2 \text{ gauss,}$$

where  $a_{\text{ns}}^2$  is the spin-population of the ns-orbital and  $\psi_{\text{ns}}(0)$  is the value of the ns-wavefunction at the nucleus. Thus, we can estimate the orbital population of the ns-orbital ( $a_{\text{ns}}^2$ ) quite simply from a comparison of the experimental ( $A_{\text{iso}}$ ) value with the theoretical value ( $A_{\text{iso}}^0$ ) calculated from an atomic wavefunction for an electron occupying the ns-orbital.

In transition metal compounds there is usually no population of s-levels by unpaired electrons so the mechanism of "core polarisation" mentioned in (iii) above, is an important factor in placing unpaired electron density in s-orbitals. An unpaired electron is able to polarise electrons in closed shells so that the electrons with  $\alpha$ -spin have slightly different radial distributions from electrons with  $\beta$ -spin. This core polarisation is most noticeable with 's-electrons', since only a small degree of imbalance is required to produce quite large contributions to the hyperfine structure. The spin-polarised Hartree-Fock wave functions of Watson and Freeman<sup>27</sup> for free atoms have shown that, for the first row transition elements, the contributions to the hyperfine field are negative for 1s and 2s electrons and positive for 3s and 4s electrons. These calculations also show that the 2s contribution is dominant, and thus the sign of the isotropic hyperfine coupling constant is negative.

When a ligand has a magnetic nucleus, superhyperfine structure is often observed. The two major effects which contribute to this are:

- (i) dipolar interaction between the unpaired electron in a metal orbital and the ligand nucleus,
- (ii) real spin-density on the ligands arising from the formation of molecular orbitals between ligand orbitals and the metal

(ii)(continued)

orbital containing the unpaired electron.

Mechanism (i) produces a purely anisotropic interaction, whereas mechanism (ii) often produces both isotropic and anisotropic components of the total superhyperfine coupling constant.

In the case of simple inorganic radicals, if d-orbitals are assumed not to contribute appreciably to the molecular orbital containing the unpaired electron, then the anisotropic component of the hyperfine tensor may lead directly to the np-orbital population.

The contribution of unpaired spin in a p-orbital to the anisotropic hyperfine tensor when the external field is applied along the symmetry axis is given by the expression:

$$2B = a_{np}^2 \left(\frac{4}{5}\right) g_N \beta_N \langle r^{-3} \rangle_{np} \text{ gauss,}$$

where  $\langle r^{-3} \rangle_{np}$  is the average value of  $r^{-3}$ ,  $r$  being the distance of the nucleus from the electron in the np-orbital, and  $a_{np}^2$  is the electronic population of the orbital. We can estimate  $a_{np}^2$  from a comparison of the experimental  $2B$  value with the theoretical value ( $2B^0$ ) calculated from the free-atom value of  $\langle r^{-3} \rangle$  and taking  $a_{np}^2$  as unity.

Anisotropic couplings of an order of magnitude smaller than those stemming directly from np-density can arise from the dipolar coupling of a magnetic nucleus and an unpaired electron in an orbital on a neighbouring atom. When the distance between the unpaired electron and the interacting nucleus is greater than 1.5 Å these indirect couplings can be satisfactorily estimated, to first-order, by a simple point-dipole approximation. However, when this separation approaches 1.5 Å it is necessary to use the more sophisticated approach of McConnell and Strathdee.<sup>28</sup>

Thus, the isotropic and anisotropic components of the hyperfine tensor, representing the interaction of the unpaired electron with a single magnetic nucleus, can yield estimates of both the s- and p-characters of the molecular orbital of the electron at that nucleus (provided that d-orbital contributions to this molecular orbital are neglected). It is now possible to deduce the hybridisation ratio  $\lambda$  (where  $\lambda^2 = a_p^2/a_s^2$ ) which is related to the bond angles in certain radicals by Coulson's orthogonality relationships.<sup>29</sup> Values of bond angles calculated from spin-resonance data generally agree well with those obtained by more conventional techniques, which is indeed remarkable in view of the drastic assumptions involved in the method of population analysis we have outlined.

## II. Experimental Methods.

### a) Crystal Growing.

Crystals of alkali halides doped with complex ions were grown by slow evaporation of aqueous solutions containing 1 - 0.001% of the complex. This solution method has the advantage of being relatively simple, but it is difficult to grow large crystals, and to control the amount of impurity incorporated. In some cases the impurities are incorporated more easily than the required ion. Infra-red spectra showed that all crystals grown by this method contained an appreciable amount of water incorporated into the lattice.

### b) Coprecipitation.

Barium sulphate powders doped with required impurity ions were prepared by precipitation at 370 K from near saturated aqueous solutions of barium chloride containing approximately 10% of the microcomponent

salt using pure sulphate salts and sometimes pure sulphuric acid. The resulting suspension, resembling a gel, was allowed to digest at 353 K overnight. In some cases the powders were annealed at high temperatures (ca. 900 K) in a furnace in order to diffuse the impurity ions throughout the lattice and thus render the solid phase homogeneous.

c) Pressed Discs.

Samples suitable for i.r. were conveniently prepared by compressing the finely powdered doped alkali halides in a steel die at about 20 tons per square inch and about 2 mm of Hg pressure.<sup>30</sup> The preparation of potassium chloride and bromide discs was straightforward, but sodium salts, because of their higher melting point, did not form good discs. In this case a disc was formed by adding potassium chloride to the sample, followed by careful mixing in an agate ball mill. The main advantage of these pressed discs is that they can be irradiated easily and a series of spectra can be run of the same sample after different irradiation times.

III. Instrumentation.

i) Electron Spin Resonance Spectrometers.

Five e.s.r. spectrometers were used in this study, three at X-band, one at Q-band and one at S-band frequencies. Measurements at 9.3 GHz on polycrystalline samples were obtained using either a commercial X-band Varian V4502-03 or Varian E3 high resolution spectrometer with 100 kHz field modulation. The method employed for the calibration of the magnetic field has been described in detail elsewhere,<sup>31</sup> and the estimated accuracy of the  $g$ -values and hyperfine coupling constants measured in this way are  $\pm 0.0004$  (in 2.0000) and  $\pm 0.03$  gauss respectively. Measurements

at 77 K were made with the paramagnetic samples immersed in liquid nitrogen in a quartz Dewar which could be inserted directly into the spectrometer cavity. Measurements at temperatures between 77 and 295 K were made using a variable-temperature accessory designed and constructed in these laboratories;<sup>32</sup> the absolute temperature of the sample could be controlled within  $\pm 0.5$  K. Spectra at 4.2 K were obtained employing a Varian V4545B liquid helium accessory and superheterodyne detection. Spectra at 19 K were obtained by passing boiling helium rapidly through the variable-temperature accessory referred to above.<sup>32</sup>

Powder spectra were occasionally measured at 34.0 GHz on a Q-band spectrometer which employed superheterodyne detection,<sup>33</sup> whilst spectra were measured at 3.1 GHz using an S-band spectrometer incorporating a 64 channel averaging computer.<sup>32,34</sup> Single-crystal spectra at 77 and 295 K were obtained using an X-band spectrometer on which the magnetic field was calibrated against a proton n.m.r. magnetometer.<sup>31</sup> In this machine the sample cavity is mounted in an insulating bath so that, using liquid nitrogen as coolant, the sample could be kept at a constant temperature of 77 K. This instrument was ideal for single crystal spectra, and runs as long as 15 hours at 77 K have been performed, the microwave frequency and the temperature remaining stable. The Q-band cavity could be cooled by placing a copper extension of the cavity in a bath of coolant, and temperatures down to about 100 K could be reached. All of these spectrometers, except the first two, were designed and constructed by Mr. J.A. Brivati, and have been fully described elsewhere.<sup>31-34</sup>

#### ii) Infra-red Spectrometer.

All the i.r. spectra were recorded on a Perkin Elmer 225 double beam instrument. A low temperature attachment of the cold finger type<sup>30</sup> was used to record spectra of pressed discs down to about 100 K. On slow

and expanded scans the spectra were reproducible to  $1 \text{ cm}^{-1}$ .

iii) Radiation Sources.

Irradiations with  $^{60}\text{Co}$   $\gamma$ -rays were carried out in a 'Gammacell-200' supplied by Atomic Energy of Canada Ltd., which produced an effective dose rate of approximately 0.15 Mrads per hour. Irradiations at 77 K were accomplished with the samples immersed in liquid nitrogen in a Pyrex Dewar which was designed to fit close to the radiation source. When samples were irradiated in sealed quartz tubes, to eliminate radicals produced in the quartz, one end of the tube was annealed to red heat using a blow-torch, keeping the other end immersed in liquid nitrogen where necessary. If this were not done, radicals produced in the radiation-damaged quartz would interfere with the desired sample spectrum.

Photolyses with  $3650 \text{ \AA}$  radiation were carried out with a high-pressure mercury arc lamp, and photolysis at 77 K was accomplished by placing the sample in a quartz tail-piece of a Dewar filled with liquid nitrogen.

References for Chapter 1.

1. P.B. Ayscough, "Electron Spin Resonance in Chemistry", Methuen, London, (1967).
2. A. Carrington and A.D. McLachlan, "Introduction to Magnetic Resonance," Harper & Row, New York, (1967).
3. M. Bersohn and J.C. Baird, "An Introduction to Electron Paramagnetic Resonance," Benjamin, New York, (1966).
4. C.P. Poole, "Experimental Techniques in Electron Spin Resonance," Wiley, New York, (1966).
5. H.G. Hecht, "Magnetic Resonance Spectroscopy," Wiley, New York, (1967).
6. M.T. Jones and W.D. Phillips, Ann. Rev. Phys. Chem., 17, 323, (1966).
7. A. Carrington and D.H. Levy, J. Phys. Chem., 71, 2, (1967).
8. E. Mueller, K. Rieker, K. Schleffer and A. Moosmayer, Angew. Chem. Intern. Ed. Engl., 5, 6, (1966).
9. N.M. Atherton, A.J. Parker and H. Steiner, Ann. Rept., 63, 62, (1966).
10. A. Horsfield, Ann. Rept., 64, 257, (1966).
11. P.W. Atkins and M.C.R. Symons, "The Structure of Inorganic Radicals," Elsevier, Amsterdam, (1967).
12. J. Geusic and L.C. Brown, Phys. Rev., 112, 64, (1958).
13. M.H.L. Pryce, Proc. Phys. Soc., A63, 25, (1950).

14. J.A. Weil and J.H. Anderson, J. Chem. Phys., 28, 864, (1958).
15. D.S. Schonland, Proc. Phys. Soc., 73, 788, (1959).
16. R.H. Sands, Phys. Rev., 99, 1222, (1955).
17. F.K. Kneubuhl, J. Chem. Phys., 33, 1074, (1960).
18. S.M. Blinder, J. Chem. Phys., 33, 748, (1960).
19. H. Sternlicht, J. Chem. Phys., 33, 1128, (1960).
20. R. Neiman and D. Kivelson, J. Chem. Phys., 35, 156, (1961).
21. H.R. Gersmann and J.D. Swalen, J. Chem. Phys., 36, 3221, (1962).
22. J.W. Sear, R.C. Smith and S.J. Wyard, Proc. Phys. Soc., A74, 491, (1959).
23. J.A. Ibers and J.D. Swalen, Phys. Rev., 127, 1914, (1962).
24. F.K. Kneubuhl and B. Natterer, Helv. Phys. Acta, 34, 710, (1961).
25. B. Eleaney, Proc. Phys. Soc., 75, 621, (1960).
26. V.S. Korolkov and A.K. Potapovich, Opt i Spek., 16, 461, (1963).  
(Eng. transl. 16, 251, (1964)).
27. A.J. Freeman and R.E. Watson, in "Magnetism Vol. IIA," ed. Rado and Suhl, Academic Press, 167, (1965).
28. H.M. McConnell and J. Strathdee, Mol. Phys., 2, 129, (1959).
29. C.A. Coulson, Volume Commemoratif Victor Henri, Contributions à l'Etude de la Structure Moleculaire, 15, (1948).

30. R.G.J. Miller (Ed), "Laboratory Methods in I.R. Spectra," Heydon and Son Ltd., London, (1965).
31. J.A. Brivati, N. Keen and M.C.R. Symons, J. Chem. Soc., 237, (1962).
32. J.A. Brivati, unpublished work.
33. J.A. Brivati, J.M. Gross, M.C.R. Symons and D.J.A. Tinling, J. Chem. Soc., 6504, (1965).
34. R.S. Eachus, Ph.D. Thesis, Leicester, (1969).

PART I

SPECTROSCOPIC STUDIES UPON SOME TRANSITION METAL

NITROSYL COMPLEXES.

INTRODUCTION TO PART I.

In part I of this thesis we report some interesting transition metal nitrosyl complexes in unusual valency states. E.s.r. and i.r. spectroscopic studies were used not only as an aid to their identification but as a probe of their molecular structure and geometry as well as their electronic configuration.

Several reviews have been published on nitrosyl compounds<sup>1-5</sup> and using the classification of reference 1, nitrosyl compounds may be divided into six categories:

- (i) simple nitrosyl compounds of the type  $M_x(NO)_y$ .
- (ii) nitrosyl carbonyls; several of these complexes have been reported, but to date all have been found to be diamagnetic.
- (iii) nitrosyl halide complexes.
- (iv) complexes involving sulphur ligands.
- (v) organometallic nitrosyl complexes.
- (vi) nitrosyl cyanide complexes.

We have exclusively studied  $d^5$  and  $d^7$  pentacyanonitrosyls in the present work. These complexes are particularly amenable to e.s.r. study since, being low-spin complexes, they have only one unpaired electron and any delocalisation of the unpaired electron onto the nitrogen of the nitrosyl group is readily observed as superhyperfine splitting ( $^{14}\text{N}$ ;  $I = 1$ , 99.6% isotopic abundance). Furthermore, delocalisation onto the cyanide ligands can also be observed ( $^{13}\text{C}$ ;  $I = \frac{1}{2}$ , 1.1% isotopic abundance) at high gain, or

more readily if the complex is synthesised using  $\text{Na}^{13}\text{CN}$ .

At this point it is instructive to give a general introduction to the bonding that can occur in nitrosyl complexes. On the basis of a wide range of infra-red measurements,<sup>6,7</sup> complexes with N-O stretching frequencies in the range  $1940\text{--}1575\text{ cm}^{-1}$  were assumed to have  $\text{NO}^+$  co-ordination, whereas those in the range  $1200\text{--}1040\text{ cm}^{-1}$  were assigned to  $\text{NO}^-$ . This latter group has since been assigned to compounds having a hyponitrite structure.<sup>8,9</sup> The former group then comprises all true nitrosyl complexes with the charge on the ligand varying from  $\text{NO}^+$  to  $\text{NO}^-$ .

Using Valence Bond theory we can consider the nitric oxide bonding to a metal in the following ways:

- (a) Transfer of the unpaired electron from NO to the metal followed by lone pair donation from  $\text{NO}^+$ .
- (b) Transfer of an electron from the metal to NO forming  $\text{NO}^-$ .
- (c) Donation of the lone pair on the nitrogen to the metal, with the unpaired electron being retained by the nitrosyl group.
- (d) Donation of the unpaired electron from the NO to the metal, followed by back donation from the metal to the ligand antibonding orbitals.
- (e) Transfer of three electrons to the nitrosyl group to form  $\text{NO}^{3-}$ , followed by strong electron donation from the nitrosyl group to the metal.
- (f) It is possible that the NO group could bond in a bridging position analogous to the carbonyl group in some polynuclear metal carbonyls.

Schemes (a) and (d) both involve the initial formation of the

nitrosonium ion ( $\text{NO}^+$ ) which is not energetically difficult, since the ionisation potential for nitric oxide is only 9.5 eV ( $74,000 \text{ cm}^{-1}$ ).<sup>10</sup> This would result in a considerable increase in the strength of the N-O bond since we are removing an antibonding electron, which is reflected by the infra-red stretching frequencies of nitric oxide gas ( $1880 \text{ cm}^{-1}$ )<sup>1,11</sup> and nitrosonium salts ( $2200-2300 \text{ cm}^{-1}$ ).<sup>1,12</sup> However, since the nitrosyl group is now positively charged, it is very improbable that further electron donation (i.e. the lone pair) can occur without some additional mechanism tending to neutralise the charge on the nitrosyl group. Thus a combination of schemes a) and d) could give a bonding scheme compatible with Pauling's charge neutrality rule,<sup>13</sup> which, although empirical, seems to have been justified by charge density calculations.<sup>14</sup>

Mechanism (b) might be expected to operate if the metal has a high formal oxidation state, although a simple donation will result in the presence of two unpaired electrons on the nitrosyl ligand (vide infra). However, the presence of additional electron density on the nitrosyl group would cause considerable weakening of the N-O bond with respect to nitric oxide gas. This is reflected in the i.r. stretching frequencies of a large number of nitrosyl complexes.<sup>1</sup> Bonding scheme (e) also results in an increase in the electron density on the nitrosyl group, and on the basis of i.r. data, it is difficult to distinguish between these two cases.

A much more satisfactory description of the bonding in nitrosyl complexes may be obtained by using M.O. theory. The unfilled orbitals of  $\text{NO}^+$  with lowest energy are the doubly degenerate  $\pi^*$ -orbitals, which can mix with the metal  $d_{xy}$  and  $d_{yz}$  orbitals. For a nitrosyl group on the z-axis, the back donation from the metal in scheme (d) will come from these orbitals. In fact, if the  $d_{xy}$  and  $d_{yz}$  orbitals

are filled, we can form molecular orbitals in which the electron density will be shared between the metal and the nitrosyl ligand; the electron density on the latter depending upon the initial energy difference between the  $d_{xz,yz}$  orbitals and the  $\pi^*(NO)$  orbitals.

On the basis of the above arguments we can draw up a molecular orbital scheme (Figure I.1) in which only the metal d-orbitals have been considered and any bonding between the metal and the other ligands (L) is assumed to be completely ionic.<sup>14</sup>

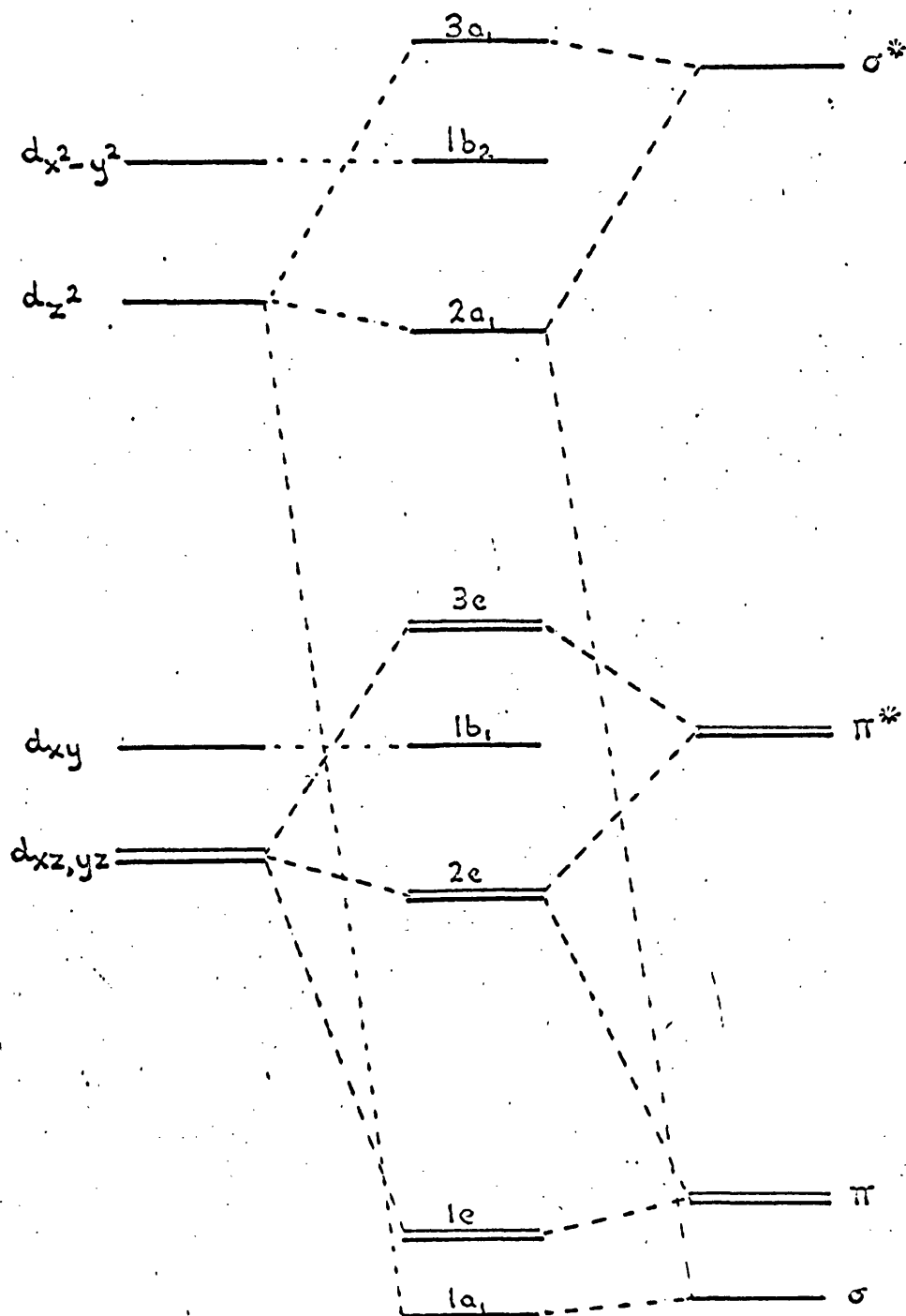
The molecular orbitals involved in scheme (e) are identical to those described above except that the  $\pi^*(NO)$  level is formally of lower energy than the  $d_{xz,yz}$  level.

Bonding scheme (b) involves the donation of an electron from the metal to the  $\pi^*(NO)$  level. This will now contain two unpaired electrons (isoelectronic with  $O_2$ ), which will remain unpaired unless there is a distortion in the molecule sufficient to separate the two  $\pi^*(NO)$  orbitals by an amount greater than the pairing energy of the electrons.

Scheme (c) is best interpreted in the molecular orbital picture as the case where there is just one electron in the  $3e$  level.

To summarise then: we can see that the six pictures of the bonding using the valence bond approach can be accommodated in the molecular orbital scheme shown in Figure I.1 with the appropriate number of electrons.

Simplified Molecular Orbitals for  $M(NO)L_5$ .



Metal orbitals    Molecular orbitals    NO orbitals

Figure I.1.

References for Introduction to Part I.

1. B.F.G. Johnson and J.A. McCleverty, *Prog. Inorg. Chem.*, 7, 277, (1966).
2. C.C. Addison and J. Lewis, *Q. Rev.*, 9, 115, (1955).
3. J. Lewis, *Sci. Prog.*, 47, 506, (1959)
4. W.P. Griffith, *Q. Rev.*, 16, 188, (1962).
5. P.T. Manoharan and H.B. Gray, *Inorg. Chem.*, 5, 823, (1966).
6. J. Lewis, R.J. Irving and G. Wilkinson, *J. Inorg. Nucl. Chem.*, 7, 32, (1958).
7. W.P. Griffith, J. Lewis and G. Wilkinson, *J. Inorg. Nucl. Chem.*, 7, 38, (1958).
8. J.B. Raynor, *J. Chem. Soc.(A)*, 997, (1966).
9. E.E. Mercer, W.A. McAllister and J.R. Durig, *Inorg. Chem.*, 6, 1816, (1967).
10. K. Watanabe, *J. Chem. Phys.*, 22, 1564, (1965).
11. E.L. Saier and A. Pozefsky, *Anal. Chem.*, 26, 1079, (1954).
12. D.J. Millen and D. Watson, *J. Chem. Soc.*, 1369, (1957).
13. L. Pauling, *The Nature of the Chemical Bond*, Cornell University Press, Ithaca, New York, (1940).
14. B.A. Goodman, Ph.D. Thesis, Leicester, (1968).

CHAPTER 2.

PARAMAGNETIC SPECIES OBTAINED FROM

ANHYDROUS SODIUM NITROPRUSSIDE.

### Introduction.

Prior to the commencement of this work Goodman et. al.<sup>1</sup>  $\gamma$ -irradiated anhydrous sodium nitroprusside, prepared by heating the dihydrate in vacuo, at 77 K and at room temperature and obtained a paramagnetic species with e.s.r. parameters similar to those of the  $\gamma$ -irradiated dihydrate.<sup>1</sup> The only point of difference between the two was that the former had axially symmetric g- and A- tensors whereas the latter did not.

One of the difficulties in low temperature work is the transfer of the sample at 77 K to the e.s.r. cavity without raising its temperature. If this happens, and it was suspected that this did occur in the above work, then any unstable radicals formed at 77 K would decay on warming and would therefore not be observed. It was decided to test this theory by repeating the experiment with two modifications. A more efficient and reliable method of dehydrating the sodium nitroprusside was used, together with a rapid transfer technique which minimised any chance of losing short lived radicals by thermal decay.

The present work was also undertaken in order to elucidate indirectly the part played by water molecules in the  $\gamma$ -ray damage mechanism. In particular to obtain new paramagnetic species and hence prove that a different mechanism of radiation damage was employed in the anhydrous material from that employed in the hydrated compound.

### Experimental.

Sodium nitroprusside was dehydrated by the following method. Reagent grade sodium nitroprusside was powdered and dissolved in

pure, dry dimethylformamide (D.M.F.). The anhydrous form was then precipitated out of solution using sodium-dried ether. After rapid filtration and washing with dry ether, the extremely hygroscopic material was stored over  $P_2O_5$  in vacuo. A portion of the powder was transferred in a dry box to a quartz tube which was then sealed and  $\gamma$ -irradiated at 77 K for approximately 12 hours. After annealing one end, the tube was then rapidly transferred to a Dewar containing liquid nitrogen, designed to fit into the cavity of an X-band e.s.r. spectrometer. A spectrum was first obtained at 77 K having ensured that the sample did not warm up to any extent during the transfer procedure. The microwave power was varied in order to obtain the highest signal to noise ratio and also as an aid to interpretation by determining which sets of lines had the same intensity versus power characteristics. The sample was then removed from the cavity, allowed to warm up for approximately five seconds, and then returned to the cavity and a new spectrum obtained. Since the spectrum of the annealed sample indicated that one of the radicals was decaying, the above procedure of warming and recooling the sample was repeated until the spectrum showed no further change. To monitor the decay of longer lived radicals, spectra were also obtained at 77 K after the sample had been at room temperature for 1 hour, 8 hours, 24 hours and one week.

Spectra of warmed samples were obtained at room temperature (298 K) as were samples  $\gamma$ -irradiated at room temperature. All spectra were calibrated using a proton resonance probe and the microwave frequency was checked using charred dextrose as a standard whose g-value is known accurately. To confirm the

interpretation of the X-band spectra, a spectrum of the  $\gamma$ -irradiated powder was obtained at S-band frequency at 77 K.

### Results.

At 77 K the original X-band spectrum (Figure 2.1) showed the presence of two predominant species, A and B, with some underlying weaker lines of a third species, C, in considerably lower yield. The spectrum of species A had axial symmetry, with  $g_{\perp} > g_{\parallel} > 2$  and no observable hyperfine structure on either the perpendicular feature or on the very sharp parallel line. The spectrum of the other main paramagnetic centre (species B) was interpreted in terms of a radical with three  $g$ -values and hyperfine coupling characteristic of interaction of the unpaired electron with a nucleus of spin  $I=1$ . The feature having the lowest  $g$ -value consisted of a rather broad line which could only just be resolved into three lines under optimum conditions. The highest  $g$ -value feature consisted of a single line whose hyperfine coupling constant was estimated from the line-width. The remaining  $g$ -feature was a clearly defined triplet.

On warming the sample for five seconds and recooling to 77 K there was a marked change in the spectrum. (Figure 2.2) The features assigned to species A disappeared completely, whereas species B remained with approximately a twenty five per cent loss in intensity, measured from signal height. The weak lines of species C also remained and their intensity was estimated to have increased concomitantly by approximately twenty five per cent. The spectrum of the sample after five minutes at room temperature followed by recooling to 77K showed a further decrease in

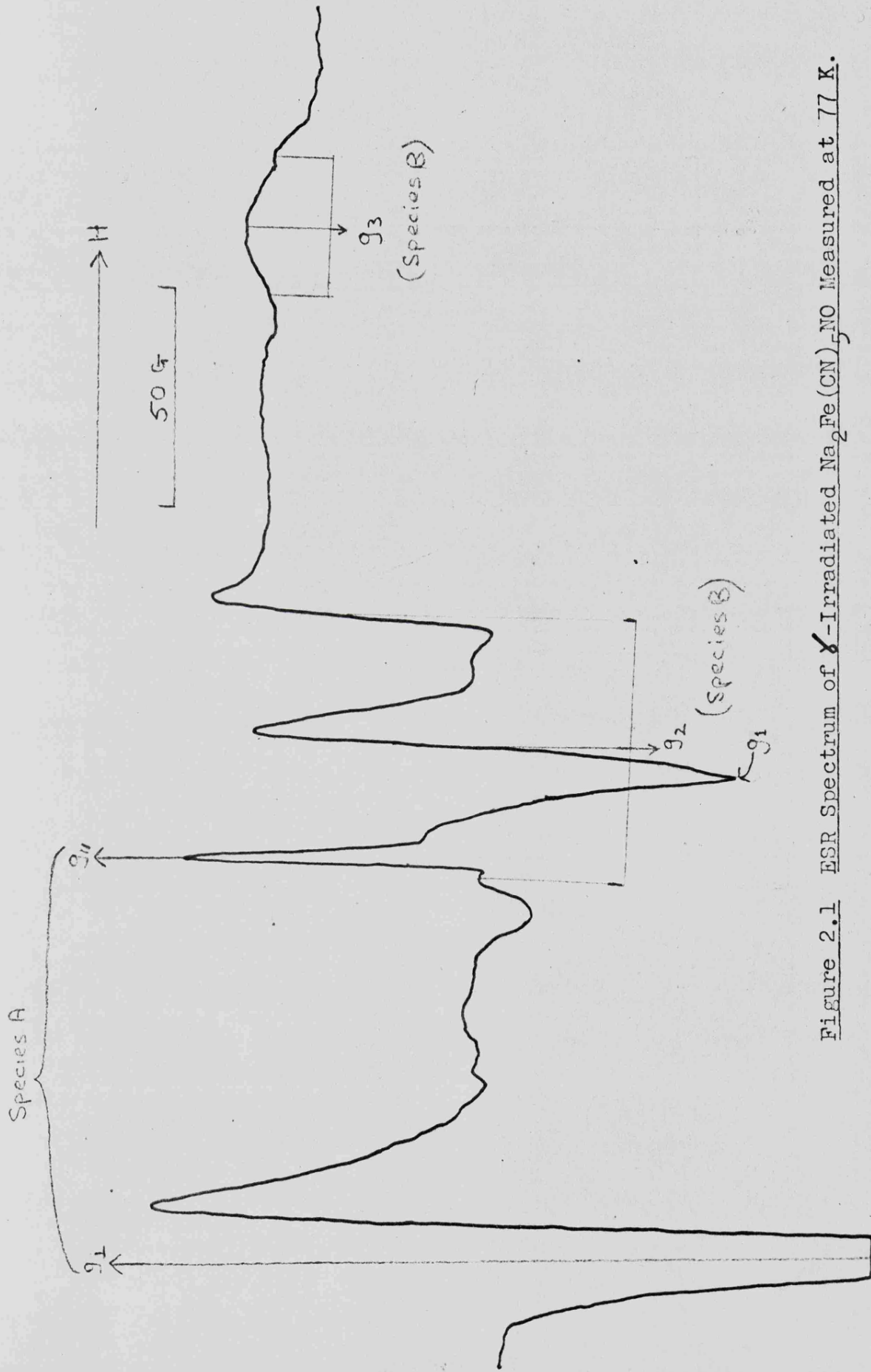


Figure 2.1 ESR Spectrum of  $\gamma$ -Irradiated  $\text{Na}_2\text{Fe}(\text{CN})_5\text{NO}$  Measured at 77 K.

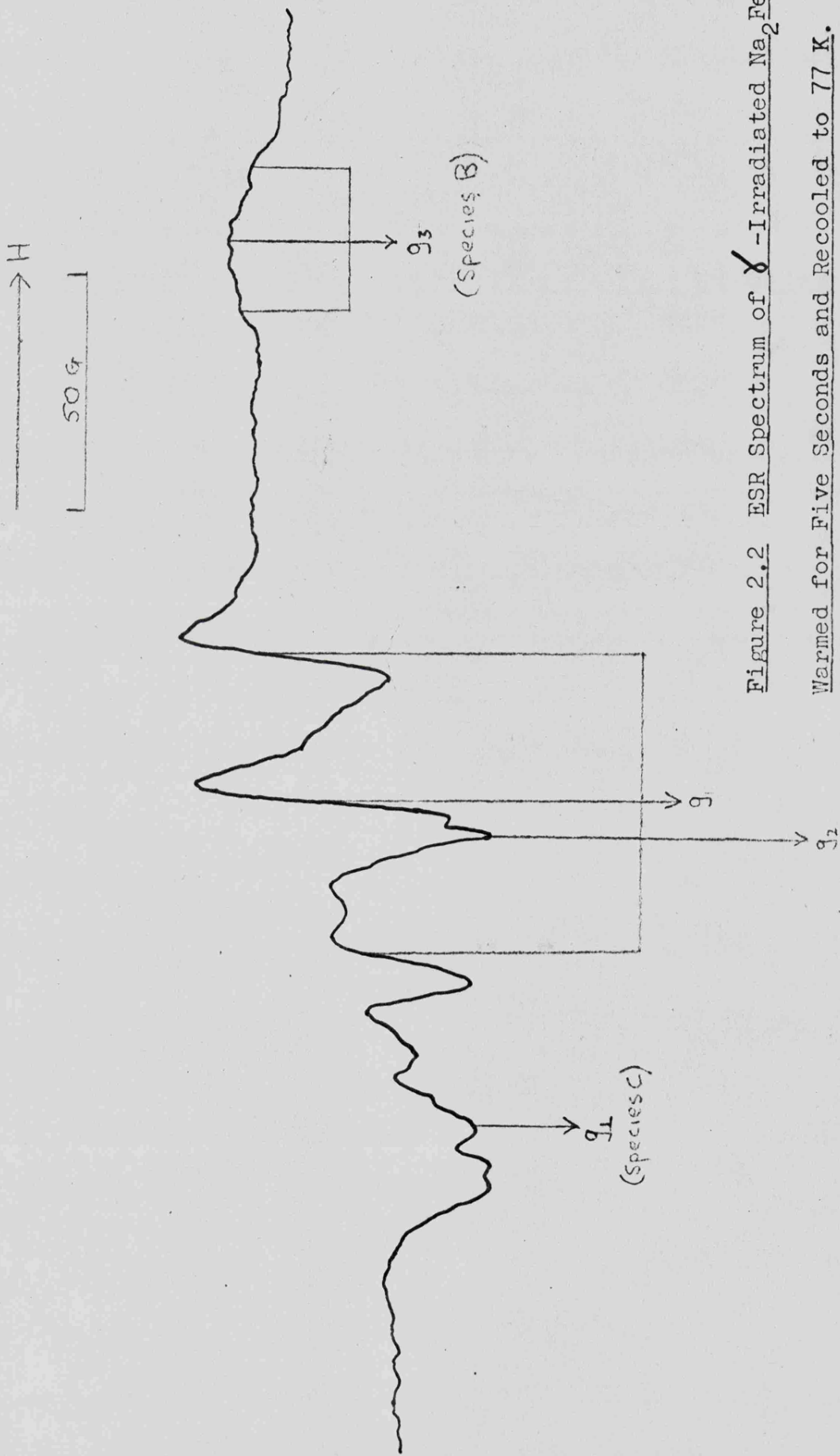


Figure 2.2 ESR Spectrum of  $\gamma$ -Irradiated  $Na_2Fe(CN)_5NO$

Warmed for Five Seconds and Recooled to 77 K.

intensity of species B with a concomitant increase in intensity of species C. A similar result was obtained after eight hours and twenty four hours at room temperature. After several days at room temperature, the spectrum of the sample run at 77K showed the presence of species  $C$  only. Spectra of samples run at room temperature showed only the presence of species C in all the above cases.

No new information was obtained from the S-band spectrum run at 77K (Figure 2.3) but it served to confirm the interpretation of the X-band spectrum.

### Discussion.

#### Identification of Species A.

Although in the absence of  $^{57}\text{Fe}$  data this cannot be positively identified as an iron centre it is considered that the species is most probably the pentacyanonitrosyl ferrate(III) anion for the following reasons.

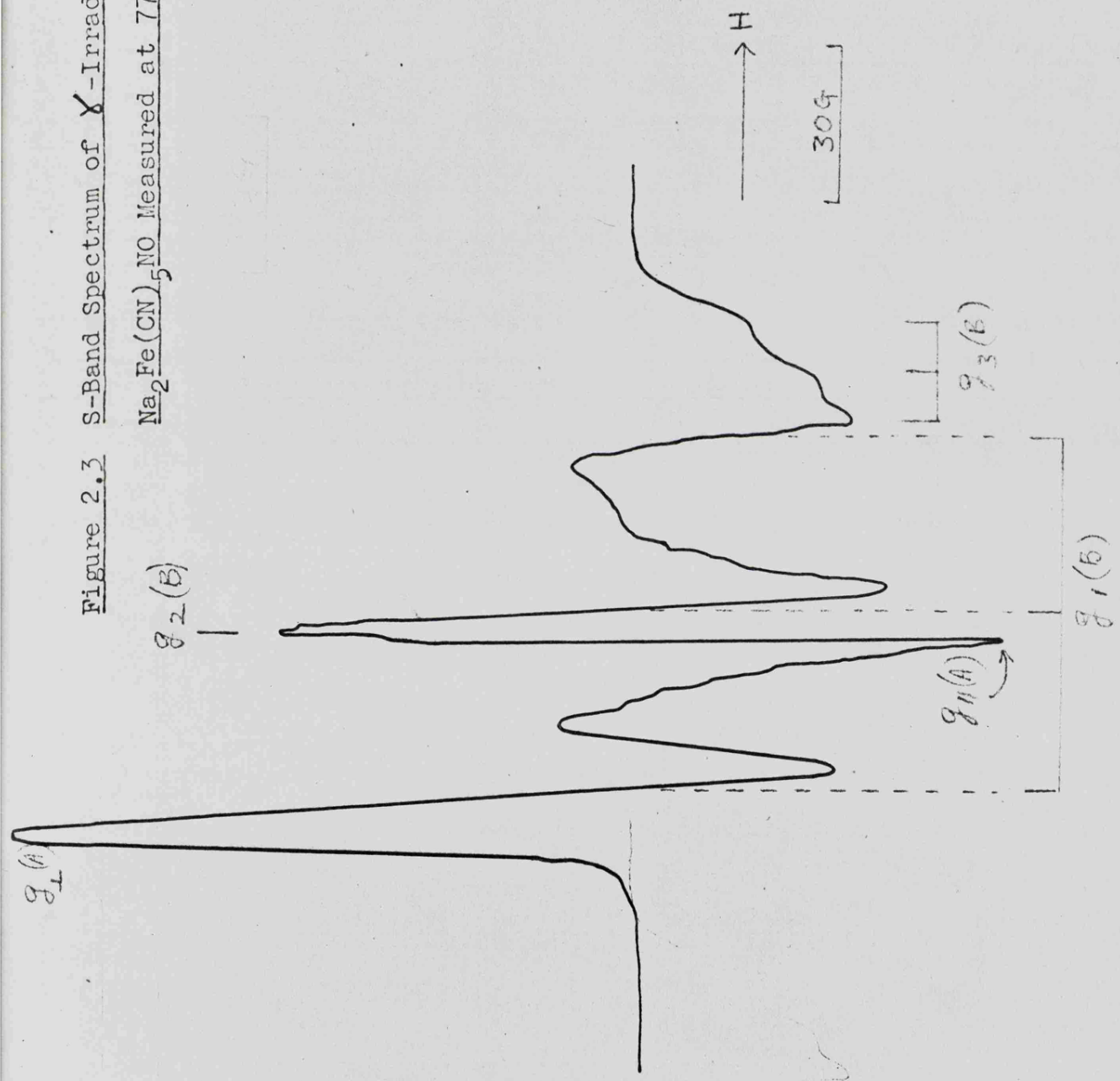
The absence of significant nitrogen hyperfine coupling precludes any form of iron (I) pentacyanonitrosyl since an electron in an iron  $d_{z^2}$  orbital or in an orbital mainly  $\sigma$  on nitrogen would give a very significant hyperfine coupling to nitrogen.

Similar arguments would also eliminate other nitrogen containing radicals such as NO or CN which could be derived from radiation damage of the sodium nitroprusside.

A choice remains then between the following paramagnetic iron species:  $\text{Fe}^{\text{I}}(\text{CN})_5$ , a  $d^7$  iron complex having completely lost the nitrosyl group; or  $\text{Fe}^{\text{III}}(\text{CN})_5\text{NO}$ , a  $d^5$  iron pentacyanonitrosyl complex either intact or having lost a cyanide or

Figure 2.3 S-Band Spectrum of  $\gamma$ -Irradiated

$\text{Na}_2\text{Fe}(\text{CN})_5\text{NO}$  Measured at 77 K.



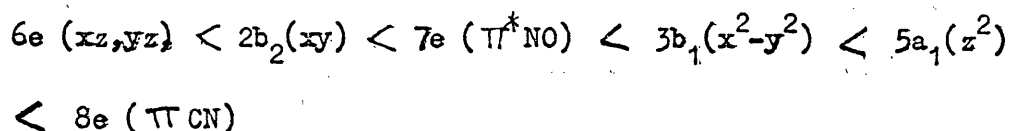
nitrosyl ligand.

The formation of an iron(I) species following the loss of a nitrosyl group is very unlikely indeed on mechanistic grounds. An argument based on a consideration of mechanism would similarly rule out the formation of an iron(III) species following the loss of a nitrosyl or cyanide group. This will be discussed in more detail in a later section. Furthermore it will be shown later that species B is an electron-excess centre, from which it can be inferred that species A is an electron deficient centre. We will now examine the g- and A- tensors of species A and by comparison with the corresponding spin-resonance parameters of the well characterised  $d^5$  ions  $\text{Cr}^{\text{I}}(\text{CN})_5\text{NO}^{3-}$  <sup>3-6</sup> and  $\text{Mn}^{\text{II}}(\text{CN})_5\text{NO}^{2-}$  <sup>2,7,8</sup>, we will show that it is most probably the isoelectronic  $\text{Fe}^{\text{III}}(\text{CN})_5\text{NO}^-$  ion.

#### The g- tensor.

Table 2.1 lists the g- factors for the three pentacyano-nitrosyls in question. We can explain the variation from the free-spin value of these g-factors in terms of a mixing of the ground and excited states via spin-orbit coupling.

Figure 2.4 shows the relevant molecular orbitals in a typical metal pentacyanonitrosyl<sup>8</sup> ( $\text{Mn}(\text{CN})_5\text{NO}^{2-}$ ) where the ordering of the electronic levels is:



The ground state in these  $d^5$  complexes is designated  ${}^2B_2$ . With the field along the z-axis (the M-N-O direction) the  $2b_2$

Table 2.1

Electron Spin Resonance Parameters for some Metal Pentacyanonitrosyl  
d<sup>5</sup> Complexes.

Complex	g-tensor			<sup>14</sup> N Hyperfine tensor (gauss)			Ref.
	g <sub>  </sub>	g <sub>⊥</sub>	g <sub>av</sub>	A <sub>  </sub>	A <sub>⊥</sub>	A <sub>av</sub>	
Cr(CN) <sub>5</sub> NO <sup>3-</sup>	1.9722	2.0045	1.9937	2.89	7.10	5.70	4
Cr(CN) <sub>5</sub> NO <sup>3-</sup>	1.9745	2.0052	1.9950	2.00	6.90	5.30	5
Cr(CN) <sub>5</sub> NO <sup>3-</sup>	1.9745	2.0051	1.9949	2.00	7.00	5.30	3
Mn(CN) <sub>5</sub> NO <sup>2-</sup>	1.9922	2.0311	2.0181	1.91	4.75	3.80	7,8
Species A	2.0142	2.0716	2.0535	≤ 1 <sup>b</sup>	≤ 3 <sup>b</sup>	≤ 2 <sup>b</sup>	a

a = This work.

b = Estimated from the line-width.

Manoharan and Gray's M.O. Diagram for  $[\text{Mn}(\text{CN})_5\text{NO}]^{2-}$

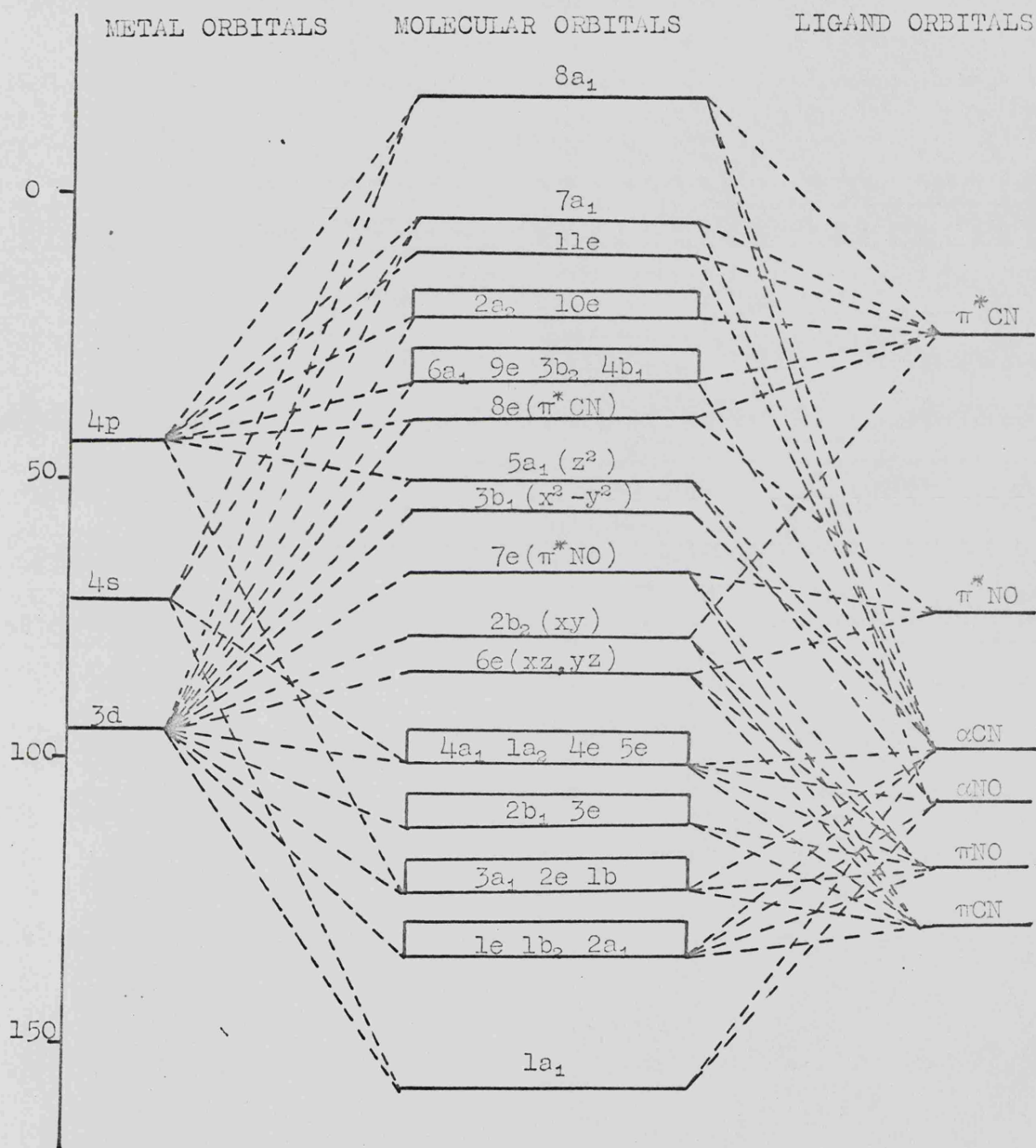


Figure 2.4

( $d_{xy}$ ) orbital is able to couple with the empty  $3b_1(d_{x^2-y^2})$  orbital and with the filled  $1b_1$  orbital. With the field perpendicular to the z-axis the  $d_{xy}$  orbital can couple with the filled degenerate  $6e(d_{xz,yz})$  pair and with the empty  $7e(\pi^*NO)$  orbitals.

Now in an isoelectronic series such as this, the effect of increasing the positive charge on the metal is to stabilise the metal orbitals with respect to the ligand orbitals. The most pronounced effect will be on the mainly non-bonding metal  $d_{xy}$  orbital in question; the orbital containing the unpaired electron. Thus on going from  $Cr^I$  to  $Mn^{II}$  to  $Fe^{III}$  the  $2b_2(d_{xy})$  orbital will be lowered in energy thereby moving closer to the  $1b_1$  and  $6e$  filled orbitals. (Figure 2.5) The effect of this is to make spin-orbit coupling with these filled levels increasingly more pronounced and so we would expect both the  $g_{||}$ - and  $g_{\perp}$ - factors to shift to more positive values, which is in fact the case. The rather large positive perpendicular g-shift for  $Fe^{III}$  may be explained by the additional effect brought about by coupling of the  $2b_2$  level with the filled  $5e$  level which is now close enough to make an important contribution to the overall g-value. That species A is an iron(III) complex would seem to be likely in view of this experimental trend in g-values.

#### The A-tensor. ( $^{14}N$ )

As seen in Table 2.1 the observed values for  $A_{(av)}^N$  decrease in the order  $Cr^I > Mn^{II} > Fe^{III}$ . Again there appears to be a consistent numerical trend in a spin-resonance parameter on increasing the charge on the metal.

Effect of Increasing Positive Charge on the Metal on the M.O.'s of some  $d^5$  Pentacyanonitrosyl Complexes.

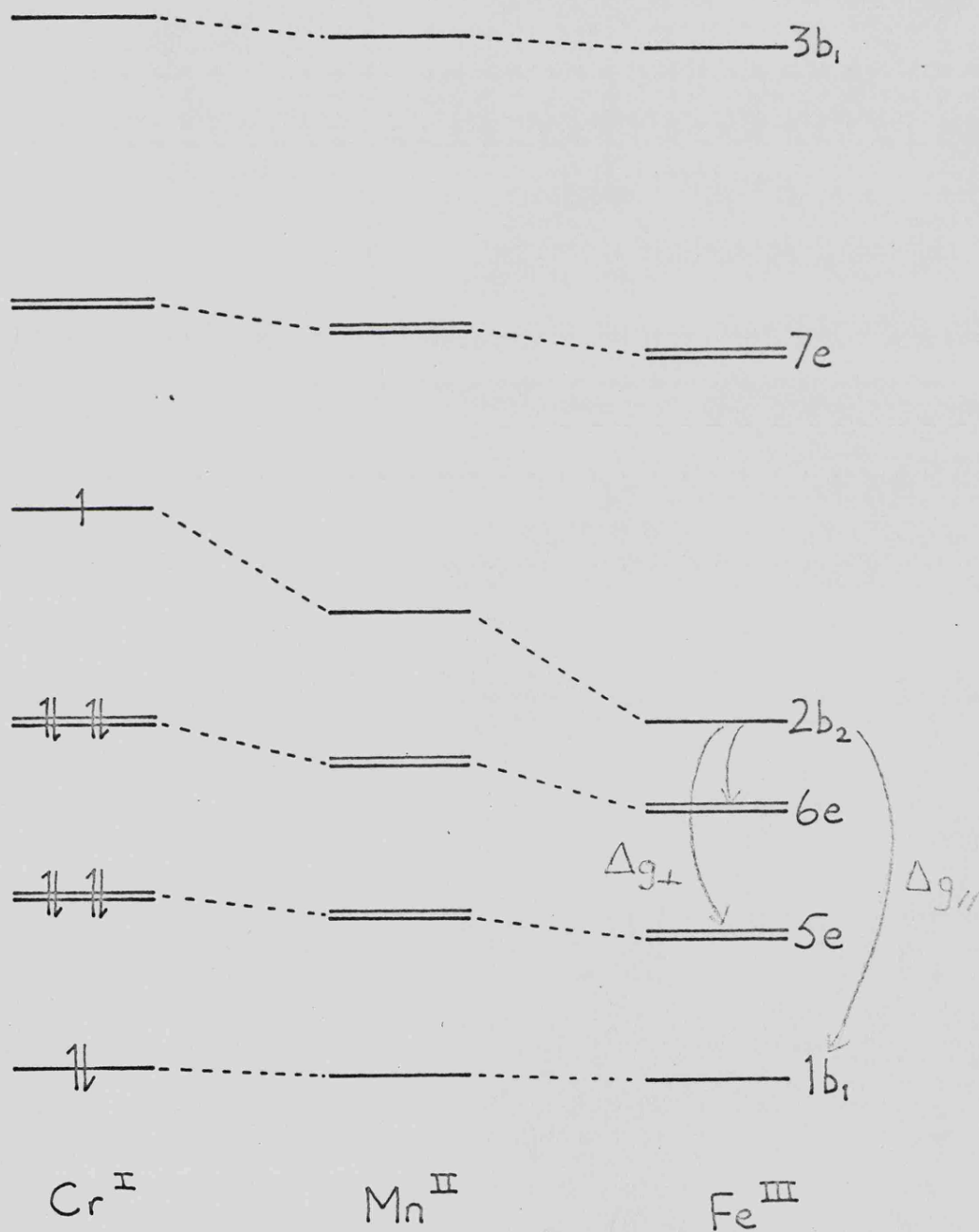


Figure 2.5

The mechanism for placing spin-density on the nitrosyl group is not known for certain. However some mechanisms can be discounted. For instance, direct overlap of the  $d_{xy}$  orbital with any NO orbital is clearly impossible unless there was some considerable bending of the NO group. There is no evidence for more than very slight bending in the case of the chromium<sup>3</sup> and manganese<sup>8</sup> complexes, and so, if iron follows this trend we can eliminate this particular mechanism.

Calculations for the chromium complex<sup>9</sup> have shown that remote dipolar interaction makes only a very small contribution to the overall coupling, so this can probably be discounted as a major contribution to the measured  $A^N$  for the manganese and iron complexes also. The mechanism of spin-orbit coupling, however, is able to account for the experimental trend. The  $6e$  ( $d_{xz,yz}$ ) level contains contributions from  $\pi^*(NO)$ <sup>8</sup> and calculations have shown that the contribution decreases in the order  $Cr^I > Mn^{II} > Fe^{III}$ .<sup>8</sup> Thus, spin-orbit coupling involving the  $6e$  orbital would place spin-density on NO and account for the decrease in hyperfine coupling constants in the observed order.

A possible alternative mechanism is spin polarisation. For example, mixing configurations  ${}^2B_2(6e^4 2b_2^1)$  and  ${}^2B_2(6e^3 2b_2^1 7e^1)$  would also place unpaired spin-density on the nitrogen of the nitrosyl group. For this particular case M.O. calculations of Manoharan and Gray<sup>8</sup> lend support to this mechanism by theoretically predicting the observed decrease in  $A^N$  on going from the chromium(I) to the manganese(II) complex. This result, which is attributed to the increased charge on the metal, may then be extrapolated to include the iron(III) complex.

**Table 2.2** E.S.R. Parameters for Nitric Oxide in Various Matrices.

Matrix	g-tensor			<sup>14</sup> N Hyperfine tensor (gauss)				Ref.
	g <sub>11</sub>	g <sub>22</sub>	g <sub>33</sub>	A <sub>11</sub>	A <sub>22</sub>	A <sub>33</sub>	A <sub>iso</sub>	
NH <sub>3</sub> OH.Cl <sup>a</sup>	1.998	1.999	1.886	36.4	5.4	11.5	6.4	10
MgO <sup>b</sup>	1.996	1.996	1.89	33	-	<10	~7	11
MgO <sup>c</sup>	1.995	1.995	1.91	32	-	<10	~7	11
ZnS	1.997	1.997	1.91	31	-	<10	~7	12
ZnO	1.999	1.999	1.94	30	-	<10	~7	12
species B	1.998	1.999	1.925	31	≤ 3	≤ 10	~6	This work
Be-Y zeolite	1.996	2.003	1.86	34	-	<10	~8	14
gas phase <sup>d</sup>	-	-	-	36	6	6	8	15

a)  $\gamma$ -irradiated hydroxylamine hydrochloride.

b) MgO degassed at 800°C.

c) MgO degassed at 300°C.

d) calculated from data in Ref. 15 by Dr.D.J.A. Tinling.

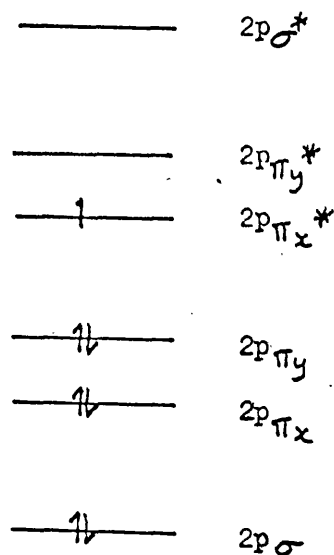
So although we have not proved conclusively that species A is  $\text{Fe}(\text{CN})_5\text{NO}^-$ , the  $g$ - and  $A$ - values are very much consistent with this assignment and it seems more than likely that it is the third member of an isoelectronic series of  $d^5$  pentacyanonitrosyls.

#### Identification of Species B.

Table 2.2 lists the  $g$ - and  $A$ - tensors for nitric oxide trapped in a variety of matrices <sup>10-14</sup> together with those of species B. The spin resonance parameters of the latter are so strikingly similar to those of trapped nitric oxide that we are led to the conclusion that it too is nitric oxide trapped in the host lattice, especially since there <sup>are</sup> no other known nitrogen-containing radicals with similar e.s.r. parameters.

Nitric oxide contains an unpaired electron in a  $2p \pi^*$  orbital, which is degenerate in the free molecule. In order to obtain an e.s.r. spectrum such that  $g_{xx} \approx g_{yy}$ , close to free spin and  $g_{zz} \ll$  free spin, the nitric oxide must be trapped at a site with a crystal field strong enough to lift the degeneracy of the  $2p \pi^*$  orbitals. From the e.s.r. spectrum it is clear that there is only one trapping site for the nitric oxide and that this site exerts a crystal field of precise symmetry on the radical, so that one of the  $2p \pi^*$  orbitals ( $2p \pi_x^*$ , say) will have a lower energy than the other. We may represent the electronic configuration by the following diagram :

Figure 2.6



Thus we may say that the unpaired electron will be in the  $2p_{\pi x}^*$  level in the absence of any spin-orbit interaction. The low  $g$ -value will then arise when the field is along the  $z$ -direction (the N-O axis), where the ground state  $(2p_{\pi x}^*)^1$  mixes with the excited state  $\dots(2p_{\pi y}^*)^1$  via spin-orbit coupling.

The isotropic hyperfine coupling constant is calculated to be 6 gauss, using the values  $A_z = -10G.$ ,  $A_y = -3G.$  and  $A_x = +31G.$ , and the relationship  $A_{iso} = \frac{A_x + A_y + A_z}{3}$ . This value is in good agreement with the value of 8 gauss calculated for nitric oxide in the gas phase <sup>15</sup>.

However the anisotropic hyperfine tensor (25 -9 -16) is different from the tensor expected for an electron in a  $p_{\pi}$ -orbital, which should be of the form (2B -B -B). In principle such a discrepancy can be explained by a librational movement of the molecule. In general, if a molecule containing an unpaired electron in a  $p$ -type orbital having an anisotropic tensor of the form  $(A_x A_y A_z) = (2B -B -B)$  is rapidly rotating about one of

Table 2.3

E.S.R. Data for  $\delta$ -Irradiated Sodium Nitroprusside and for the  $\text{Fe}(\text{CN})_5\text{NO}^{3-}$  Ion.

Sample	g-tensor			$^{14}\text{N}$ Hyperfine tensor (gauss)			Ref.
	$g_{11}$	$g_{22}$	$g_{33}$	$A_{11}$	$A_{22}$	$A_{33}$	
Single crystal	2.0422	2.0377	2.0059	14.43	13.42	16.17	2
Hydrated powder	2.0409	2.0350	2.0050	15.5	14.6	16.5	2
Anhydrous powder <sup>a</sup>	2.0355	2.0355	2.0062	14.1	14.1	17.0	2
Anhydrous powder <sup>b</sup>	2.0376	2.0376	2.0069	14.7	14.7	16.3	d
Species C	2.040	2.035	2.006	14.9	14.2	17.0	This work
$\text{Fe}(\text{CN})_5\text{NO}^{3-}$ <sup>c</sup>	2.0313	2.0313	2.0059	14.75	14.75	17.1	1

a) powder  $\delta$  irradiated at 77K.

b) powder  $\delta$ -irradiated at room temperature.

c) polarographically reduced solution in D.M.F., glass at 77K.

d) B.A. Goodman, unpublished result.

its coordinate axes (y, say) then the principal values for the other two directions (x and z) become completely averaged, and the tensor becomes  $\left(\frac{1}{2}(A_x + A_z) \quad A_y \quad \frac{1}{2}(A_x + A_z)\right) = (B/2 \quad -B \quad B/2)$ .

If the molecule is librating about an axis (and not completely rotating) then the hyperfine values in the other two directions will not be completely averaged but will tend to move towards the average value. In the case of NO in question, neither libration about the x or y axes, nor a combination of the two will produce the values obtained experimentally. Starting with the anisotropic tensor predicted for NO in the gas phase,<sup>15</sup> (28 -14 -14), libration about the y - axis could produce the tensor (25 -14 -11) which is reasonably close to the experimental tensor, but not close enough for the conclusion to be drawn that librational motion is the only cause of the discrepancy. Nevertheless it could well be a major contribution. Any remaining discrepancy could be explained by some modification of the orbitals in NO by the trapping site itself, via some form of bonding between the two.

In common with trapped NO in other matrices the principal g-values are in agreement with the expected g-tensor for the NO molecule in a strong crystalline field where the splitting of the doublet  $\pi$ -antibonding level is large, and the unpaired electron is mainly confined to one level.

#### Identification of Species C.

Comparison of the e.s.r. parameters of this species (Table 2.3) with those of a species obtained by irradiating hydrated sodium

nitroprusside at room temperature<sup>1</sup> leaves little doubt that they are identical. The latter species has been interpreted as the  $d^7$  pentacyanonitrosyl iron (I) complex, where the unpaired electron density was shown to be located mainly on iron in a  $d_{z^2}$  orbital.<sup>1,2</sup> There has, however, been some controversy over the exact nature of the species. The problem will be briefly summarised here but will be dealt with again in the next chapter.

The controversy really centres on the structure of an analogous species formed in solution by chemical or polarographic reduction of sodium nitroprusside. McNeil, Raynor and Symons used the latter method of reduction in dimethylformamide<sup>2</sup> and assigned the species thus formed the structure  $[\text{Fe}(\text{CN})_5\text{NO}]^{3-}$ . Van Voorst and Hemmerich<sup>16</sup> obtained two species by reducing sodium nitroprusside with sodium dithionite at different solution pH values. One of which, formed at  $\text{pH} < 4$ , was identical to the above species, whereas the other had  $g$ -values less than free spin and was formed exclusively in the pH range 7 - 10. The low  $g$ -value species (I) could be converted into the high  $g$ -value species (II) by lowering the solution pH and the reverse reaction occurred on raising the pH. They also reduced a solution of anhydrous sodium nitroprusside in dimethylformamide with sodium metal, which exclusively produced species (I) which was converted into species (II) by one equivalent of acetic acid. From this they concluded that species (II) was protonated and that species (I) was in fact  $[\text{Fe}(\text{CN})_5\text{NO}]^{3-}$ .

Raynor and Symons<sup>17</sup> have postulated that the species formed in alkaline solution was  $[\text{Fe}(\text{CN})_5\text{NO}_2]^{5-}$  and that instead of a protonation/deprotonation reaction taking place on changing

the pH of the solution, the process was in fact the well established equilibrium reaction<sup>20</sup> :



This would certainly explain the results of van Voorst's work with aqueous solutions. However if species (I) were indeed  $\left[\text{Fe}(\text{CN})_5\text{NO}_2\right]^{5-}$  it is difficult to explain how it could be formed by the reduction of a solution of anhydrous nitroprusside in D.M.F. with metallic sodium.

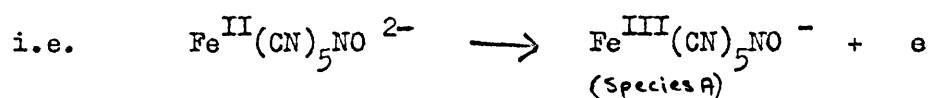
The settlement of the controversy is thus not aided by the existence of conflicting experimental results. However as far as the species formed in the solid state is concerned, all workers are agreed that the unpaired spin density is mainly concentrated on the iron atom<sup>1,2,16</sup>. The similarity of e.s.r. parameters of this species to those of the 'high g-value' species formed in solution would suggest that these species are identical. However in view of the different environments it would be surprising if the two species were alike in every respect. For example, the complex in solution will be solvated, thereby modifying the structure somewhat. In the solid state the structure will tend to be modified by the presence of neighbouring ions. We shall consider the various possibilities further in the next section.

#### Mechanism of Radiation Damage.

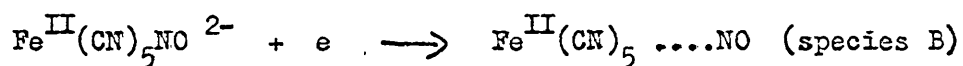
We shall first of all assume the truth of the above assignments, notwithstanding the controversy over species C, and propose a mechanism to accommodate the experimental facts, and then consider

some possible alternative mechanisms and show that these do not fit the experimental findings.

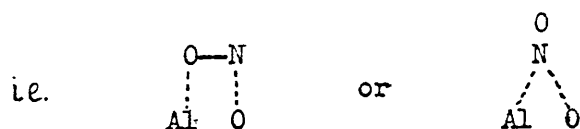
The primary process may be envisaged as the removal of an electron from the nitroprusside anion by means of the high energy radiation ,



thus forming an electron together with its corresponding hole centre, species A. The electron being mobile, migrates through the lattice and reduces a nitroprusside<sup>ion</sup> as follows :



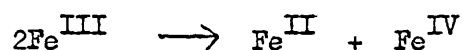
The nitroprusside anion may be considered to have a formal charge of +2 on the iron atom and a formal charge of +1 on the nitrosyl group. The 'free' electron may be thought of then, in crude terms, as neutralising the charge on the nitrosyl group and forming nitric oxide as an uncharged ligand. An alternative and strictly more accurate viewpoint is that the electron will go into the lowest lying unfilled energy level. According to Manoharan and Gray's energy level scheme<sup>8</sup> this is the 7e level, which is mainly  $\pi^*(\text{NO})$  in character. Thus the two viewpoints are essentially the same. The effect of the additional electron in the 7e level is to lengthen and hence weaken the Fe-N bond. The NO ligand, being only weakly bonded to iron will bear considerable resemblance to NO trapped in other matrices, where, for example, in alumina<sup>13</sup> the trapping of NO may be considered as a weak form of bonding at a surface site:



On warming the sample in a closed tube the hole centre rapidly disappears by means of an irreversible process forming diamagnetic products. We may safely assume this, since the disappearance of species A is not accompanied by the formation of any detectable paramagnetic products. One common mechanism for the formation of diamagnetic products from paramagnetic intermediates is that of disproportionation. For example, the well established<sup>18,19</sup> case of the  $\text{Cl}_2^-$  ion in a KCl lattice :



The analogous reaction in the case in question would be :



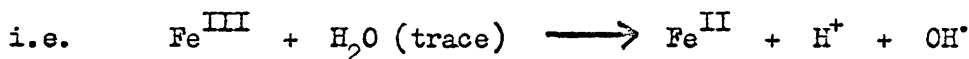
However the formation of an iron(IV) complex does not seem very likely since the pentacyanonitrosyl system would tend to stabilise low rather than high oxidation states of the metal by back bonding into empty  $\pi$ -antibonding orbitals. Another possibility is that the hole centre being mobile, migrates to the surface and reacts with oxygen to form diamagnetic products.

The electron excess centre species B, on the other hand is much more stable and decays slowly with the formation of species C. Now, since the latter is normally formed in the presence of water (as a product of radiation damaged  $\text{Na}_2\text{Fe}(\text{CN})_5\text{NO} \cdot 2\text{H}_2\text{O}$ ) one possibility is that traces of water still present in the powder are involved in the decay of species B into species C. One piece of

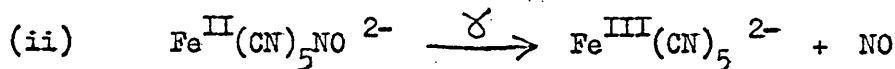
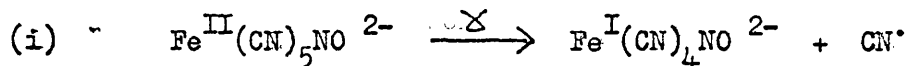


conclusion that water molecules (or protons, cf. van Voorst<sup>16</sup>) are tending to solvate and pull off the axial cyanide group. This is certainly possible in acid solution where protonation of the axial cyanide would tend to remove it as HCN. Protonation of a cyanide ligand will weaken the  $\sigma$ -bond between the ligand and the metal, but will increase the degree of  $\pi$ -bonding. Kinetic results for  $[\text{Cr}(\text{CN})_5\text{NO}]^{3-}$  indicate that  $\sigma$ -bond weakening is dominant<sup>21</sup>. Thus van Voorst's theory could be correct, although we stipulate that protonation will take place on the axial cyanide and not on the nitrosyl group as van Voorst seems to suggest.

In the solid state, following radiation damage of the 'anhydrous' powder, protons could be formed following the loss of the hole centre on annealing the sample at room temperature :



The  $\gamma$ -ray damage mechanism postulated above adequately explains the formation of the observed paramagnetic species, whereas the following possible alternative mechanisms do not. These possibilities involve homolytic bond fission and may be represented as follows :



Both these mechanisms result in pairwise trapping. However none of the spectra obtained showed the presence of any wing-lines characteristic of pairwise trapping. Moreover neither of the above processes can explain the observed sequence of events.

The mechanism of radiation damage in hydrated sodium nitroprusside will be discussed in the next chapter so we cannot fully compare mechanisms in the anhydrous and hydrated systems here. However, at this point we can say that the primary radiation damage process in the hydrated material is considered to be damage of water molecules, forming  $H^\bullet$  and  $OH^\bullet$  radicals, whereas in the anhydrous material the primary process is thought to be the ejection of an electron from the  $[Fe(CN)_5NO]^{2-}$  anion.

References for Chapter 2.

1. B.A. Goodman, D.A.C. McNeil, J.B. Raynor and M.C.R. Symons, J. Chem. Soc. (A), 1547, (1966).
2. D.A.C. McNeil, J.B. Raynor and M.C.R. Symons, J. Chem. Soc., 410, (1965).
3. B.A. Goodman, J.B. Raynor and M.C.R. Symons, J. Chem. Soc. (A), 994, (1966).
4. H.A. Kuska and M.T. Rogers, J. Chem. Phys., 42, 3034, (1965).
5. J.J. Fortman and R.G. Hayes, J. Chem. Phys., 43, 15 (1965).
6. B.R. McGarvey and J. Pearlman, J. Chem. Phys., 46, 4992, (1967).
7. P.T. Manoharan and H.B. Gray, Chem. Comm. 324 (1965).
8. P.T. Manoharan and H.B. Gray, Inorg. Chem., 5, 823 (1966).
9. B.A. Goodman, Ph.D. Thesis, (1968).
10. H. Ohigashi and Y. Kurita, J. Phys. Soc. Jap., 24, 654, (1968).
11. J.H. Lunsford, J. Chem. Phys., 46, 4347, (1967).
12. J.H. Lunsford, J. Phys. Chem., 72, 2141, (1968).
13. B.M. Hoffman and N.J. Nelson, J. Chem. Phys., 50, 2598, (1969).
14. P.H. Kasai and M. Ruta, unpublished result.
15. R.L. Brown and H.E. Radford, Phys. Rev., 147, 6, (1966).
16. J.D.W. van Voorst and P. Hemmerich, J. Chem. Phys., 45, 3194, (1966).
17. J.B. Raynor and M.C.R. Symons, J. Chem. Soc., (A), 339, (1970).
18. M.C.R. Symons, J. Chem Soc., 570, (1963).
19. T.G. Castner and W. Kanzig, J. Phys. Chem. Solids, 3, 178, (1957).
20. J.H. Swinehart and P.A. Rock, Inorg. Chem., 5, 573, (1966).
21. J. Burgess, B.A. Goodman and J.B. Raynor, J. Chem. Soc. (A), 501, (1968).

CHAPTER 3.

PARAMAGNETIC SPECIES OBTAINED FROM

SODIUM NITROPRUSSIDE DIHYDRATE.

### Introduction.

Prior to the commencement of this work a stable paramagnetic product derived from  $\text{Na}_2\text{Fe}(\text{CN})_5\text{NO}\cdot 2\text{H}_2\text{O}$  by  $\gamma$ -irradiation at room temperature has been reported<sup>1</sup>. The controversy over the structure of this species has been covered in the preceding chapter. By analogy with the work in chapter 2, it was thought that low-temperature irradiation of sodium nitroprusside would give rise to thermally unstable radicals which would decay on warming to give the particularly stable species reported. This theory was tested and found to be correct. However following the completion of the experimental work described in this chapter, van Voorst and Hemmerich<sup>2</sup> reported the principal values and directions of the  $g$ - and  $^{14}\text{N}$  hyperfine tensors of one of the low-temperature irradiated species studied here. There is, however, some doubt concerning the interpretation of some of their results and they have made no attempt to explain the unusual anisotropic  $A$ -tensor, which will be discussed in some detail in this chapter.

During the course of this work an additional species was found, which appears to be the precursor of all other paramagnetic species obtained in irradiated sodium nitroprusside dihydrate. This chapter also deals with a consideration of  $\gamma$ -ray damage mechanisms in the hydrated system.

### Experimental.

Reagent grade sodium nitroprusside was purified by recrystallisation from water. The dihydrate was then powdered .

and  $\gamma$ -irradiated at 77K for about twelve hours. The sample was then transferred to an e.s.r. Dewar vessel containing liquid nitrogen without allowing it to warm up. An e.s.r. spectrum at 77K was then obtained on a Varian E-3 X-band spectrometer. The sample was then warmed to room temperature for five seconds, recooled to 77K and a new spectrum obtained. This process of warming, recooling and re-running spectra was repeated until there was no further change in the spectrum; i.e. until lines of a decaying radical were no longer able to be detected. This occurred after about two hours at room temperature.

A polycrystalline sample was  $\gamma$ -irradiated at room temperature for approximately twenty-four hours and then immediately cooled to 77K. The spectrum of this sample showed the presence of two species, one of which was found to be decaying on warming. Accordingly the above annealing process was repeated until no further change in the spectrum was detected. E.s.r. spectra of microcrystalline samples  $\gamma$ -irradiated at 77K and at room temperature were also obtained at 298K.

To aid in the interpretation of the low temperature powder spectra and to obtain further information about the nature of the radicals involved, an e.s.r. study on a single crystal of sodium nitroprusside was performed. Crystals of sodium nitroprusside were grown from aqueous solution by slow evaporation over a period of seven to ten days. After drying in the air they were checked for flaws or twinning using a polarising microscope and a suitable single crystal chosen. The crystal was then  $\gamma$ -irradiated for approximately twelve hours at 77K, after which

it was quickly mounted on a goniometer and placed in the e.s.r. cavity, which was surrounded by a cooling bath containing liquid nitrogen. The base of the goniometer consisted of a perspex cube (illustrated in Figure 3.1) which was cut so that the crystal could be mounted on it and could be rotated about the a-, b- and c- axes of the unit cell of sodium nitroprusside. These directions (illustrated in Figure 3.2) were found in an X-ray analysis performed by Manoharan and Hamilton<sup>3</sup>. The crystal was rotated through  $180^\circ$  at  $5^\circ$  intervals for each of the a-, b- and c- axes and a calibrated spectrum was obtained for each orientation. The g-values were corrected by calibrating a spectrum of charred dextrose ( $g = 2.0023$ ) at the beginning and end of each experiment.

A crystal of sodium nitroprusside was also  $\gamma$ -irradiated for a period of twelve hours at 77K, but instead of being mounted on a goniometer it was placed in an e.s.r. Dewar containing liquid nitrogen. The time taken to transfer the crystal to the Dewar was very much less than the corresponding time taken for it to be mounted on the goniometer, thus minimising the risk of losing short-lived radicals by thermal decay. The crystal was aligned so that the magnetic field was approximately perpendicular to the needle axis. Spectra were then obtained for several different orientations of the crystal.

Where applicable S- and Q- band spectra were obtained to clarify the interpretation of the spectra of low-temperature irradiated polycrystalline samples. A spectrum of a polycrystalline sample  $\gamma$ -irradiated at 77K was also obtained at 19K using a Varian variable temperature assembly and liquid helium as coolant.

Mount for E.S.R. Study of Sodium Nitroprusside Single Crystal.

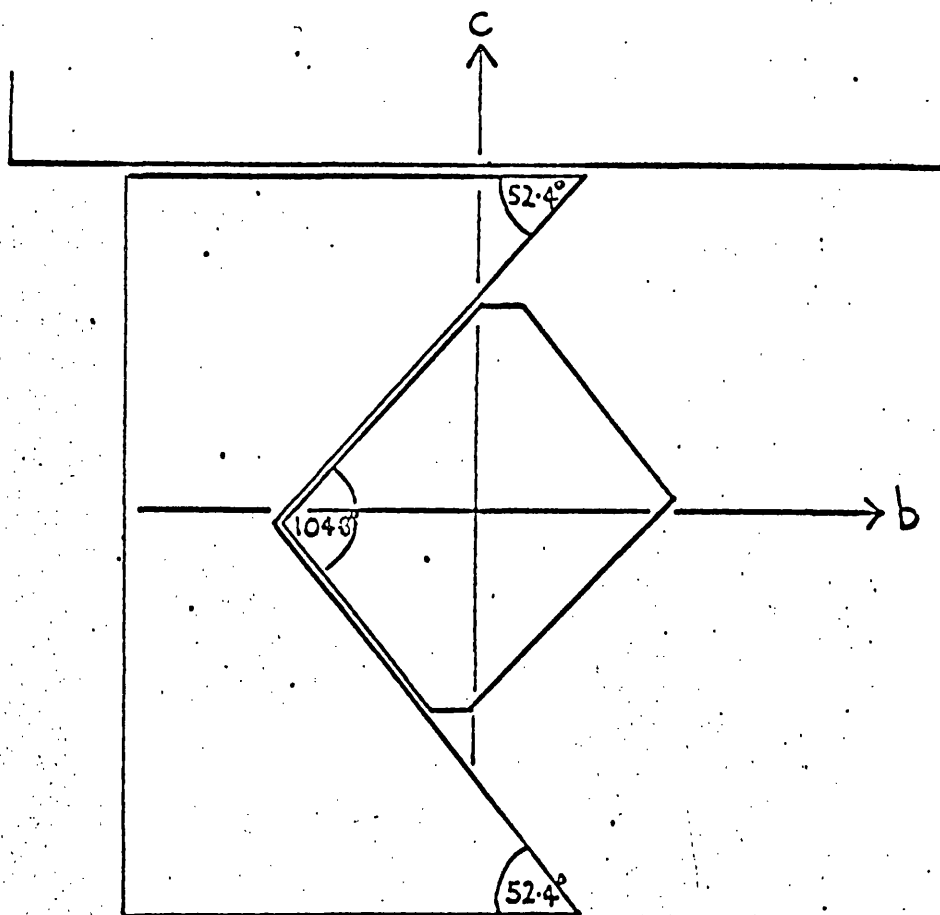


Figure 3.1

Crystal of Sodium Nitroprusside Showing Position of Unit Cell.

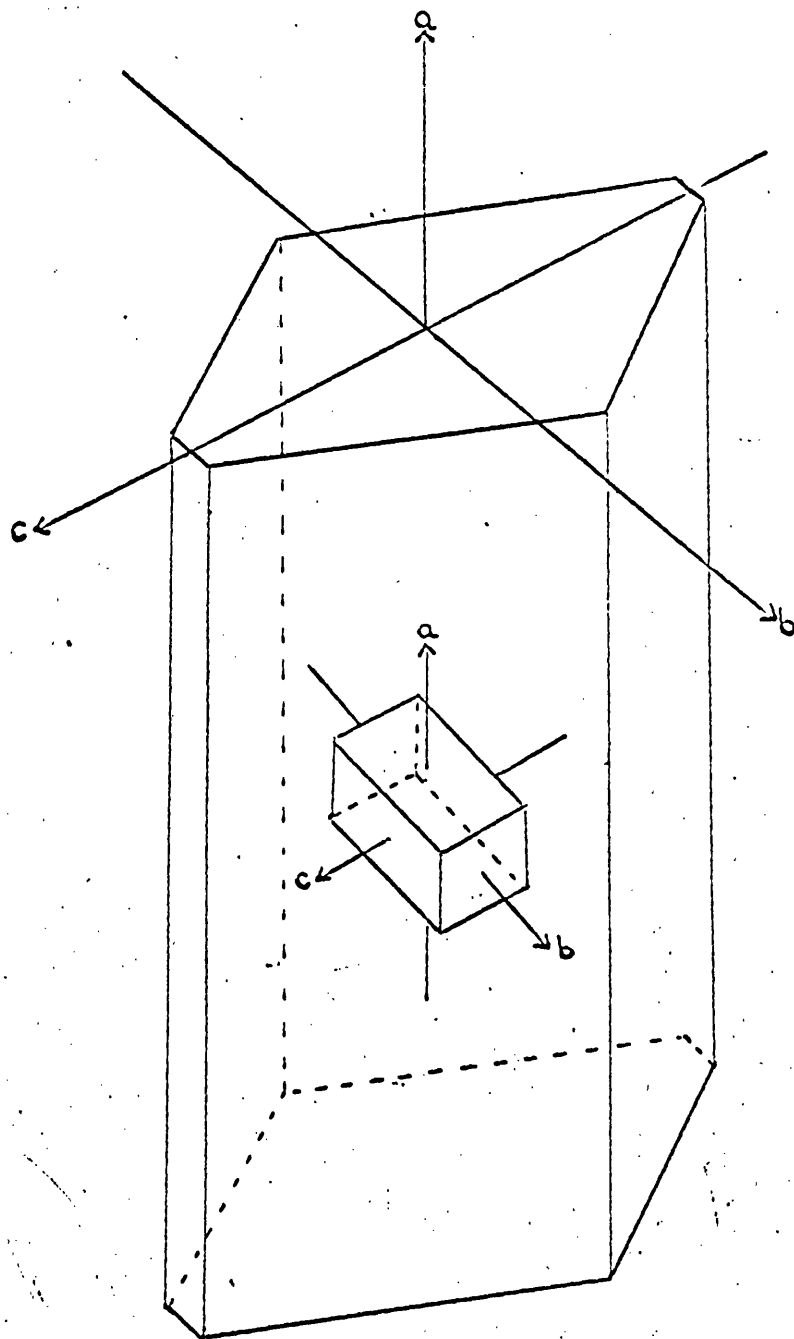


Figure 3.2(a)

Arrangement of  $[\text{Fe}(\text{CN})_5\text{NO}]^{2-}$  Molecules  
within the ab Plane of Sodium Nitroprusside.

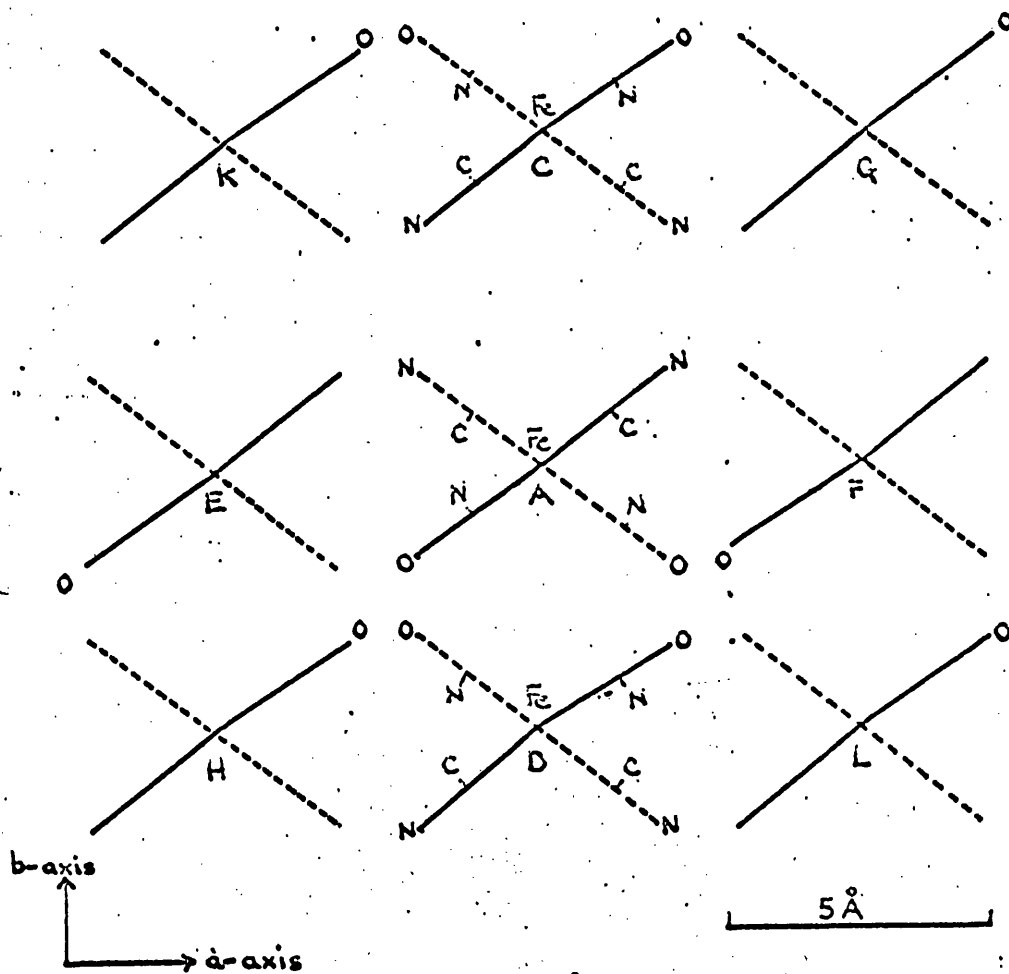


Figure 3.2(b)

By means of a rapid transfer technique, it was ensured that the temperature of the sample did not rise above 77K during the transfer procedure. It was intended to obtain a spectrum at 4.2 K using the Varian liquid helium accessory. However this was not performed as it would have entailed warming the sample to room temperature in order to transfer it to the apparatus. The temperature of 19K was the lowest that could be obtained using the variable temperature accessory.

### Results.

The e.s.r. parameters for the low-temperature irradiated polycrystalline samples of  $\text{Na}_2\text{Fe}(\text{CN})_5\text{NO}\cdot 2\text{H}_2\text{O}$  are set out in Table 3.1, together with the results of other workers for comparison purposes.

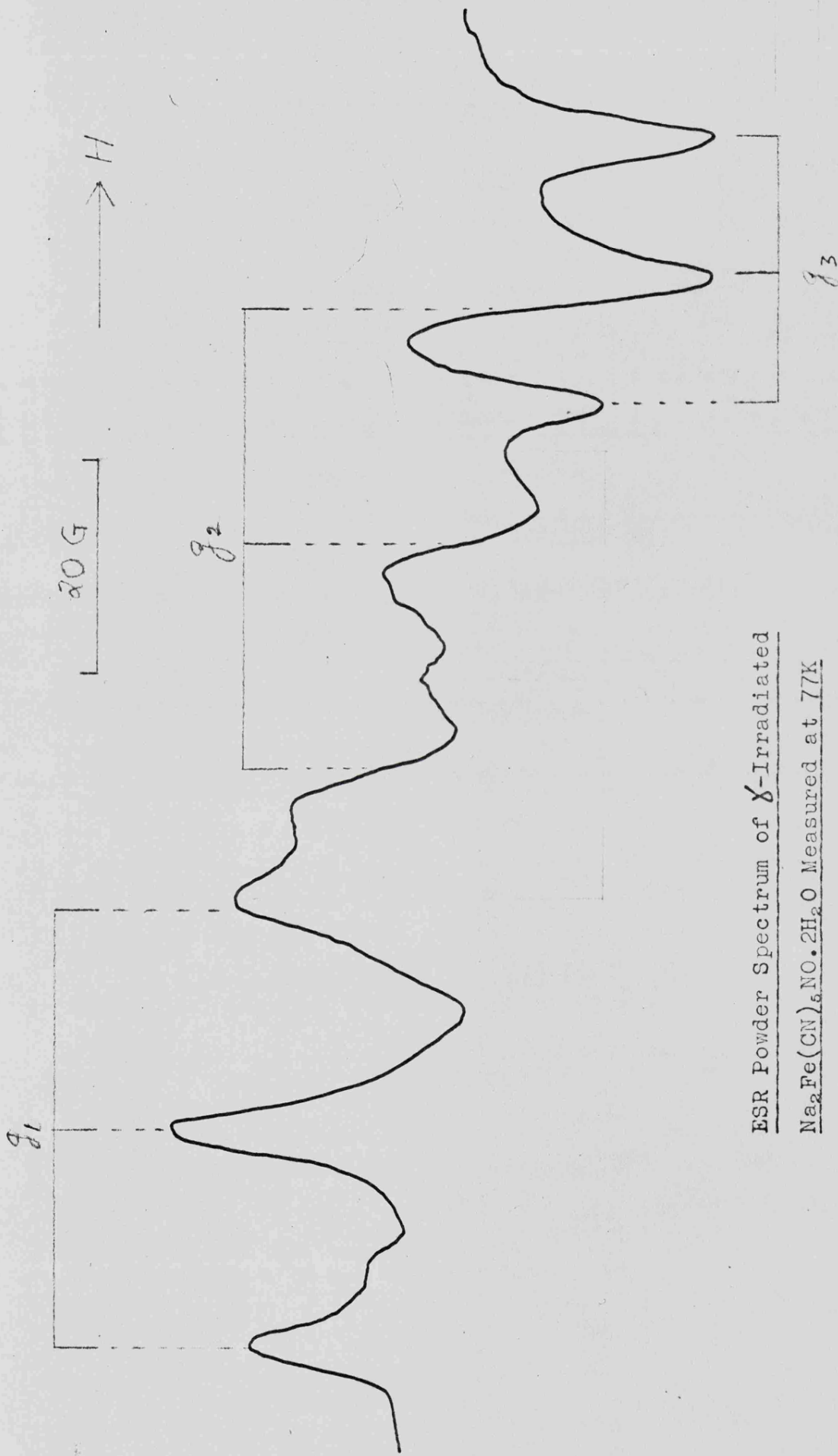
When the polycrystalline sample was irradiated for twelve hours at 77K, the e.s.r. spectrum (illustrated in figure 3.3) mainly consisted of nine lines; a triplet of triplets. All these lines had similar intensity-versus-microwave power characteristics so they may be interpreted as being associated with a single paramagnetic species, which we shall call species X. This has three g-values and hyperfine coupling lines characteristic of interaction of the unpaired electron with a nucleus of spin  $I = 1$ . Since there are no other elements present with a nuclear spin of unity we may assume that some of the unpaired spin density in this species is localised on nitrogen. In addition to these well-defined triplets, the spectrum reveals the presence of some weaker lines at a lower magnetic field position than the main lines.

TABLE 3.1 E.s.r. Data for Sodium Nitroprusside  
 $\gamma$ -irradiated at 77 K

Species and Direction		g		A( $^{14}\text{N}$ ) (gauss)		Reference
		19 K	77 K	77 K	19 K	
Species X	x	2.002	1.999	20.4	17.5	This work
	y	1.968	1.970	21.4	22.5	
	z	1.955	1.956	12.2	12.5	
Species X	x	2.000		21		5
	y	1.969		20		
	z	1.955		13		
Species Y	x	2.00		25 $\pm$ 2		This work †
	y	1.98		18 $\pm$ 2		
	z	1.95		10 $\pm$ 2		
Species Y	x	1.999		25.9		This work ‡
	y	1.984		18.2		
	z	1.951		8.1		
Species Y	x	2.00		25.9		2
	y	1.98		18.3		
	z	1.93		8.5		

† : polycrystalline sample measured at Q-band.

‡ : single crystal measured at X-band.



ESR Powder Spectrum of  $\gamma$ -Irradiated

$\text{Na}_2\text{Fe}(\text{CN})_6 \cdot \text{NO} \cdot 2\text{H}_2\text{O}$  Measured at 77K

Figure 3.3

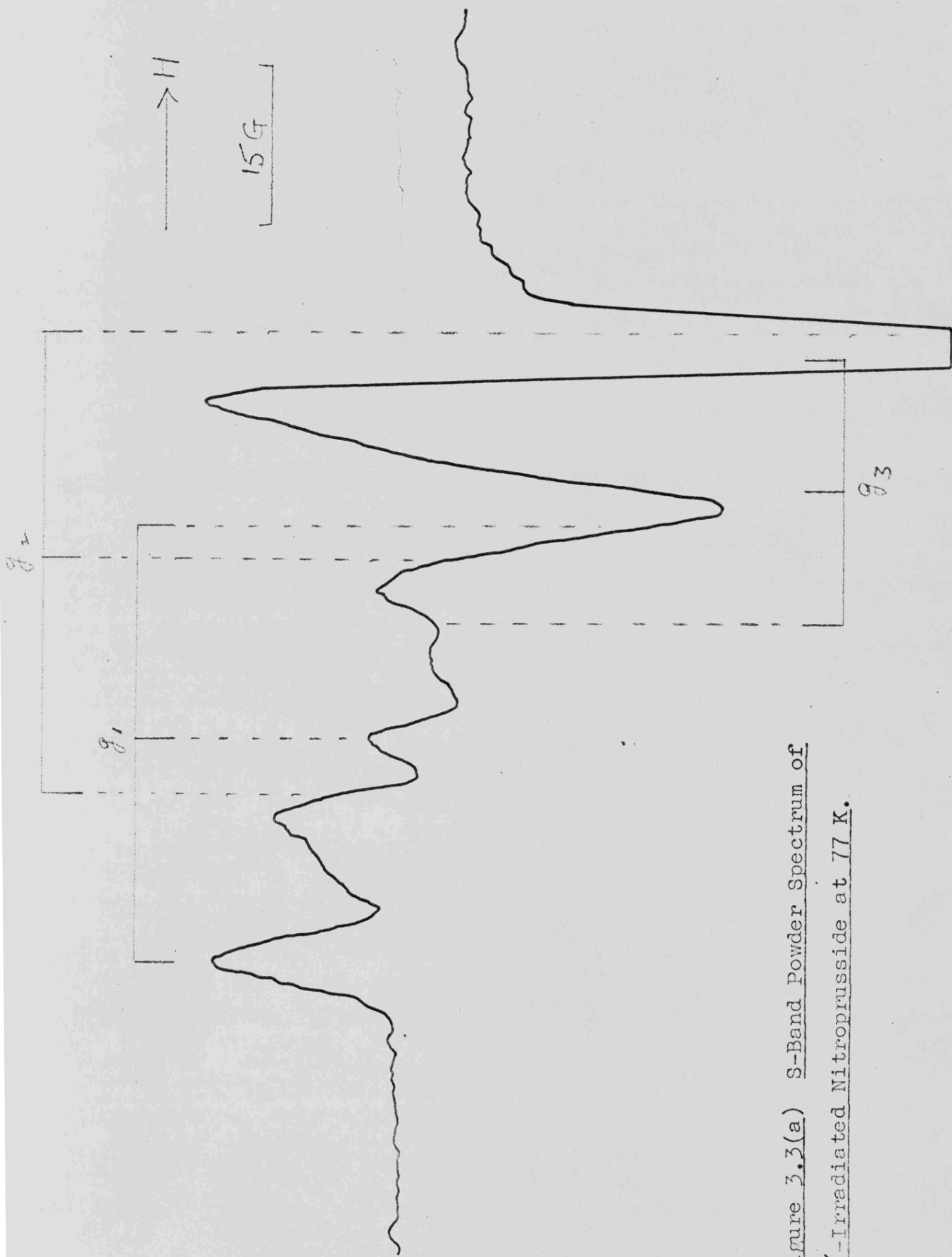


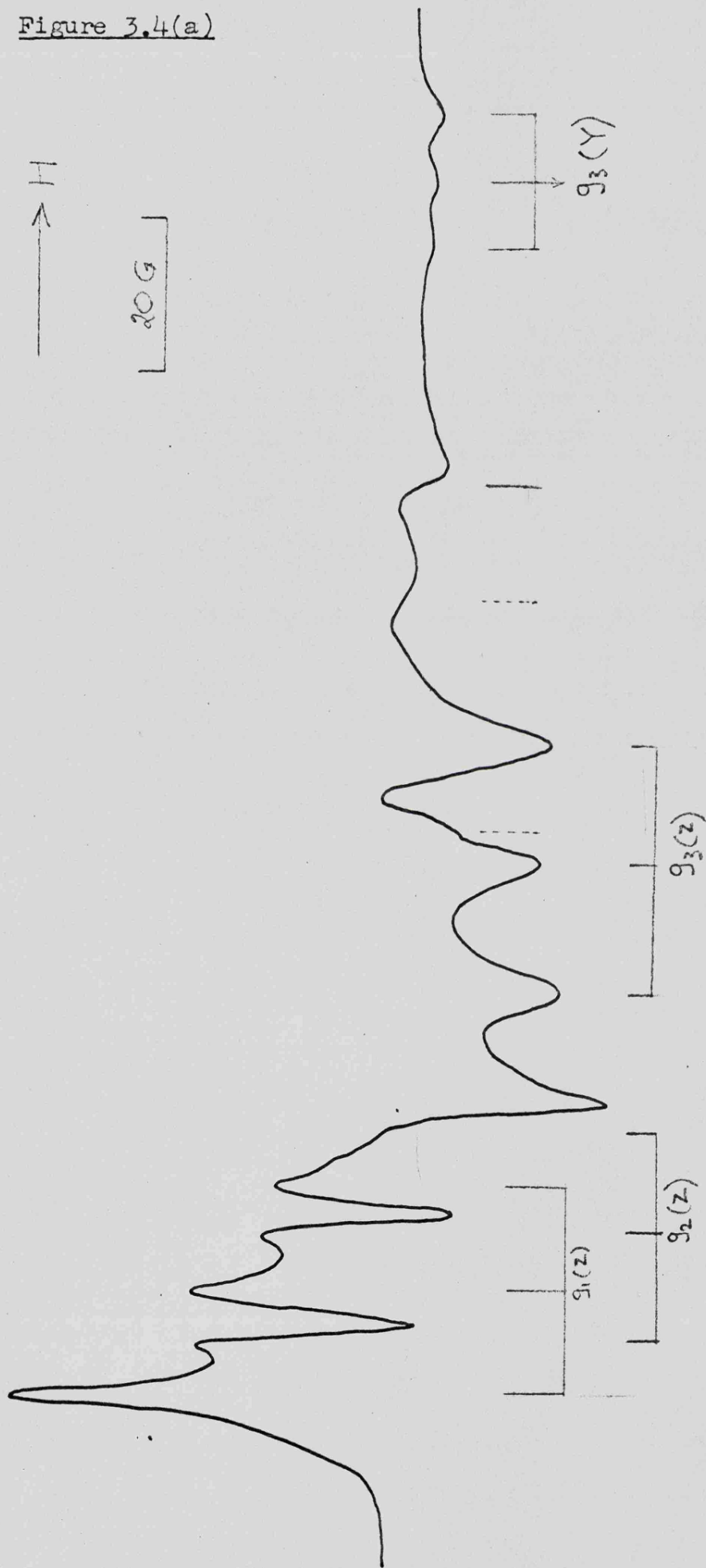
Figure 3.3(a) S-Band Powder Spectrum of  
 $\chi$ -Irradiated Nitroprusside at 77 K.

These lines can be attributed to a species in low abundance with axially symmetric  $g$ - and  $A$ - tensors, where the unpaired electron is interacting with a nitrogen nucleus. This species will be referred to as species Z.

On warming the sample to room temperature for approximately five seconds and recooling it to 77K, there was a significant change in the spectrum. (Illustrated in Figure 3.4). The lines attributed to species X completely disappeared, whilst those due to species Z increased slightly in intensity. In place of the lines attributed to species X, a new set of lines appeared. These lines were rather broad and some of the low-field features overlapped to some extent with lines attributed to species Z, however a triplet at high-field could be discerned quite easily. A spectrum was obtained at Q-band frequency in order to clarify the interpretation of the X-band spectrum. This spectrum showed, in addition to the lines due to species Z, the presence of nine lines, comprising three triplets. Thus the spectrum is similar to that of species X in that it may be attributed to a species with three  $g$ - and  $A$ - values and hyperfine features characteristic of the unpaired electron interacting with a nitrogen nucleus. We shall refer to this paramagnetic centre as species Y.

When the e.s.r. spectrum of a polycrystalline sample of sodium nitroprusside, which had been irradiated at room temperature for twenty-four hours, was recorded at 77K immediately after removal from the radiation source, it revealed the presence of species Y together with species Z. A comparison showed that this spectrum was almost identical to that obtained after warming

$\text{Na}_2\text{Fe}(\text{CN})_5 \cdot \text{NO} \cdot 2\text{H}_2\text{O}$  Powder  $\gamma$ -Irradiated for 12 hours at 77 K.



Sample Warmed to Room Temp. for 5 secs and Recooled to 77 K. Spectrum Measured at X-Band.

Na<sub>2</sub>Fe(CN)<sub>5</sub>NO·2H<sub>2</sub>O Powder  $\gamma$ -Irradiated for 12 hrs at 77 K.

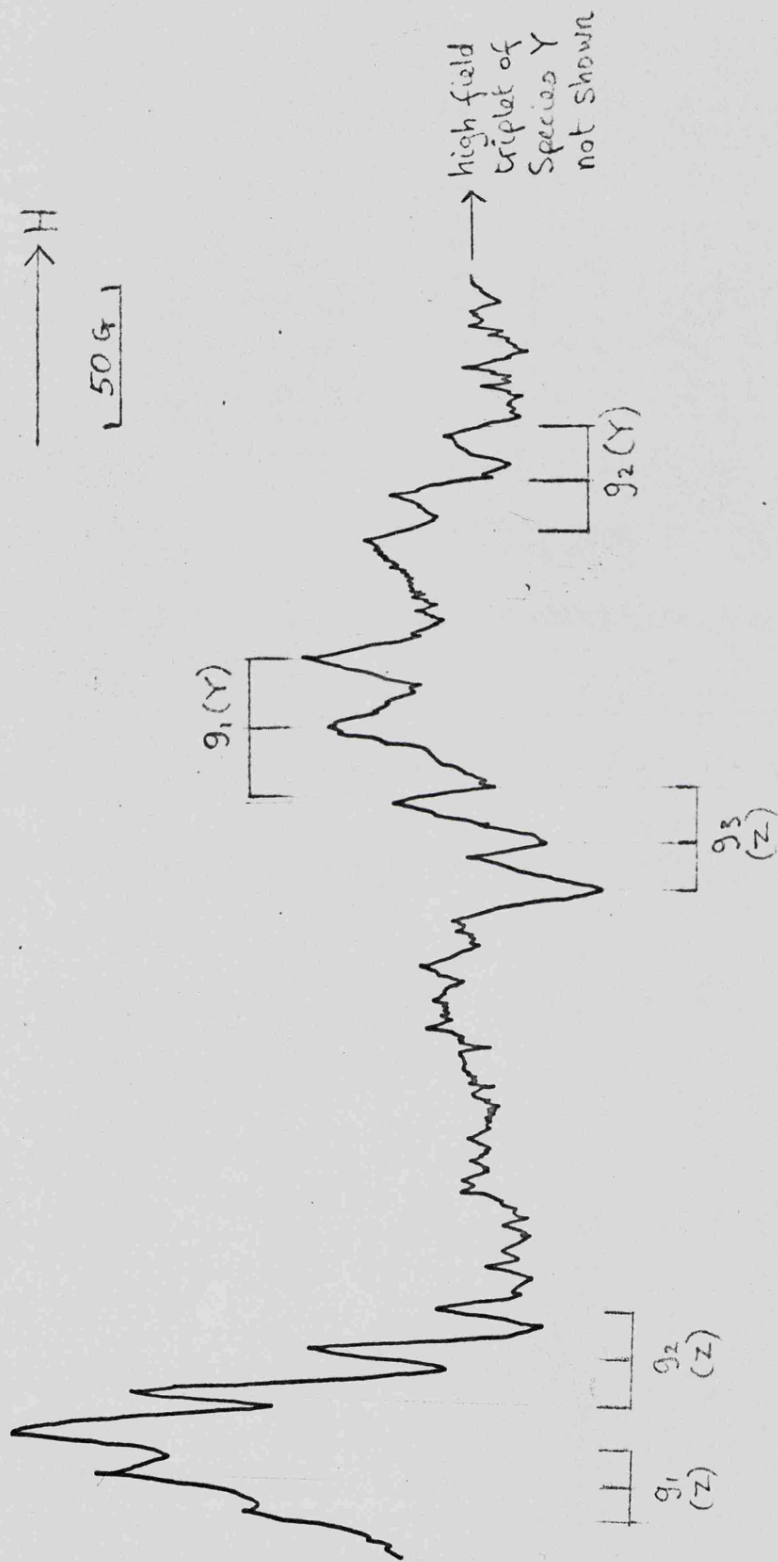


Figure 3.4(b)

Sample Warmed to Room Temp. for 5 secs and Recooled to 77 K. Spectrum Measured at Q-Band.

the low-temperature irradiated sample for a few minutes; the only difference being that the room-temperature irradiated sample contained a larger proportion of species Z.

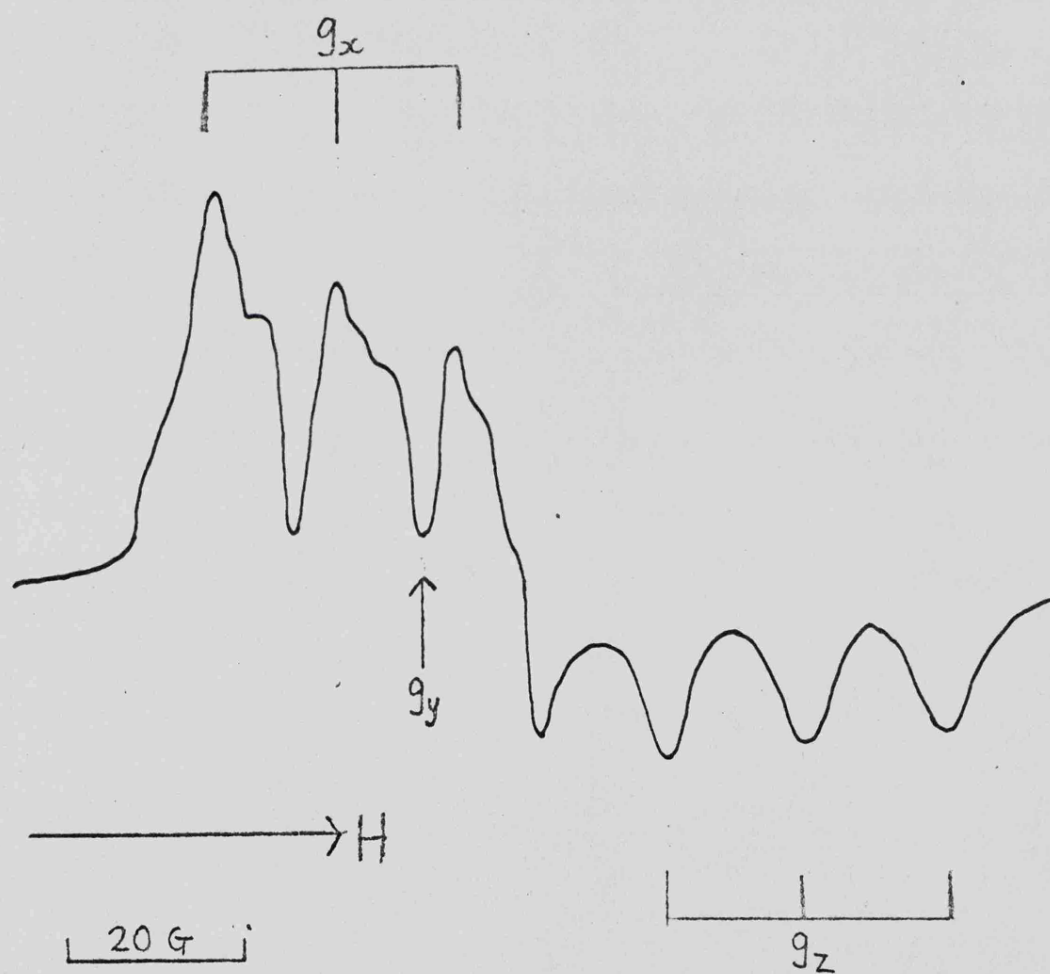
A variable-temperature study performed on the polycrystalline sample showed that the lines attributed to species Y broadened on warming and could not be detected above 240K. Spectra of powder samples irradiated at room temperature, which were recorded at the ambient temperature, showed only the presence of species Z (Figure 3.5), as did spectra of samples irradiated at 77K, in accordance with the findings of the variable-temperature study. In addition to the line-broadening effect observed, species Y was also found to be decaying on warming, with a concomitant increase in the concentration of species Z. After two hours at room temperature species Y had disappeared completely and a comparison of the areas under the lines of the e.s.r. spectra recorded at 77K, showed that species Y had completely decayed into species Z. The latter species is very stable indeed at ordinary temperatures.

The spectrum of the polycrystalline sample irradiated at 77K, which was recorded at 19K (Figure 3.6) without warming above 77K, was significantly different from the corresponding spectrum recorded at 77K. Lines attributed to species X together with weaker lines due to species Z were still present, however there was a small shift in the g- and A- values of the former. Moreover, there were additional lines in the spectrum which were apparently not related to any of the species observed at 77K. The most pronounced of these additional features observed was a triplet,

Figure 3.5

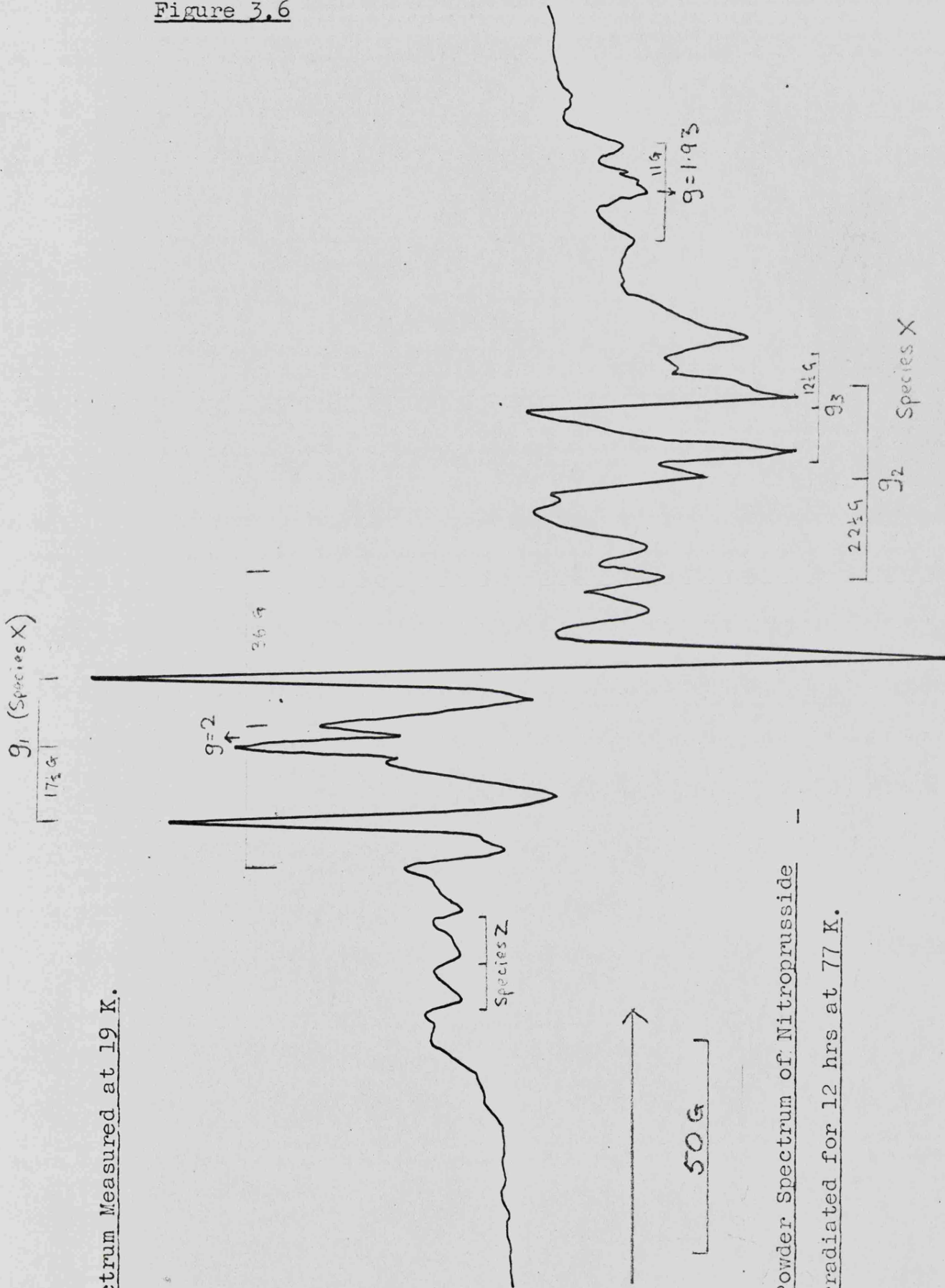
ESR Powder Spectrum of  $\text{Na}_2\text{Fe}(\text{CN})_5\text{NO}\cdot 2\text{H}_2\text{O}$   $\gamma$ -Irradiated

at Room Temperature.



Spectrum Measured at Room Temp. and X-Band Frequency.

Figure 3.6



Spectrum Measured at 19 K.

ESR Powder Spectrum of Nitroprusside

$\gamma$ -Irradiated for 12 hrs at 77 K.

whose  $g$ -value was close to the free-spin value and whose hyperfine coupling constant was approximately 36 gauss. Less well-defined features observed were a line at  $g = 2.003$  with no detectable hyperfine splitting, a broad triplet of approximately 11 gauss splitting at  $g = 1.928$  and a weak feature at  $g = 1.925$  which could just be resolved into a triplet of about 5 gauss splitting.

#### Results of Single Crystal Study.

After the crystal had been irradiated for twelve hours at 77K it was removed from liquid nitrogen for a few seconds in order to mount it on the specially cut perspex cube referred to in the experimental section, before being placed in the e.s.r. cavity at 77K. During this time, as indicated by the results obtained for the polycrystalline samples, species X would have decayed into species Y. Therefore all the e.s.r. parameters obtained from this single-crystal study refer to the latter species. It was originally intended to study species X in the single crystal, however it was found to be technically impossible to mount a crystal with any precision on a goniometer, while keeping it at 77K.

The e.s.r. spectrum of species Y consisted of two equally intense triplets which merged into a single triplet of twice the former intensity for certain orientations of the crystal. When the crystal was mounted with the crystallographic  $a$ - or needle axis vertical, (i.e. perpendicular to the magnetic field) the maximum separation of the two triplets was very small compared with the corresponding value for the other two axes;

Figure 3.7 Plots of  $g$ - and  $A(^{14}\text{N})$  against Angle of Rotation for Species Y in a Nitroprusside Crystal.

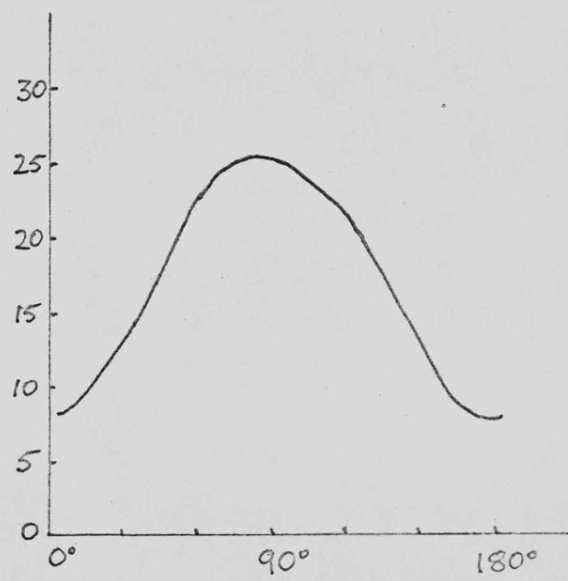
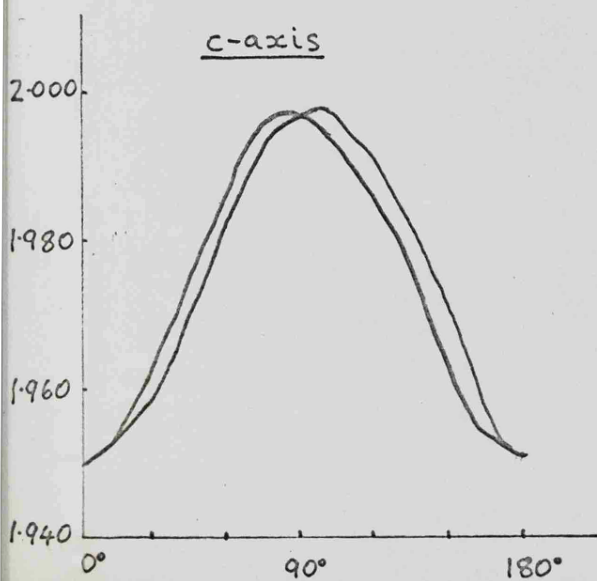
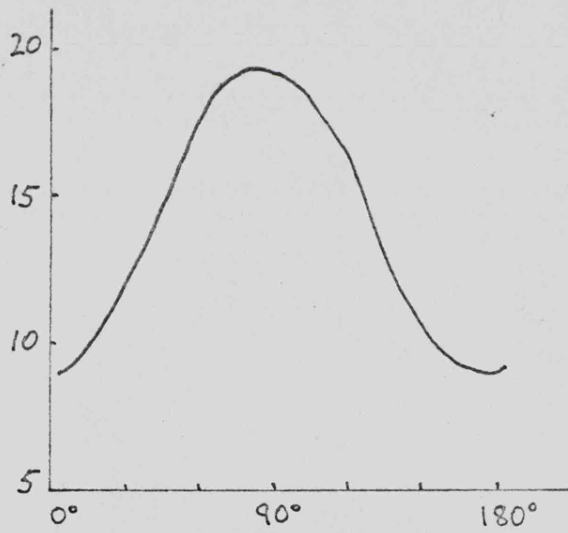
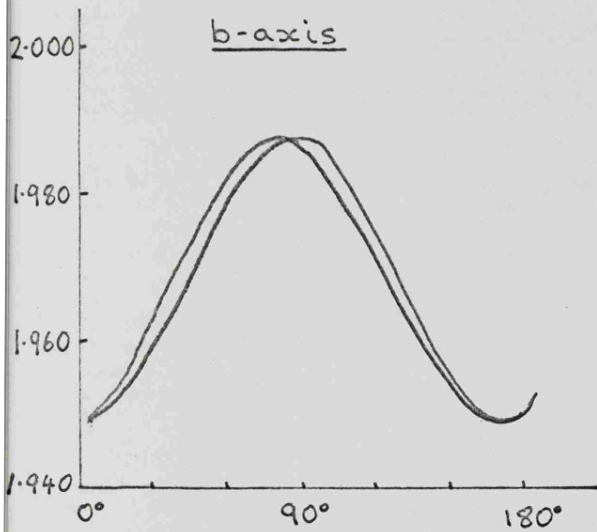
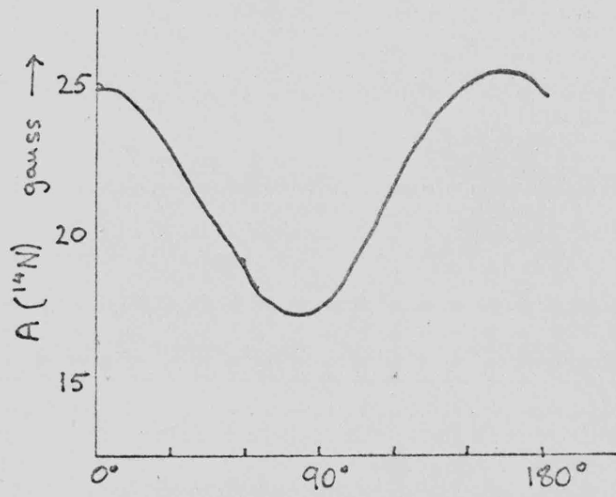
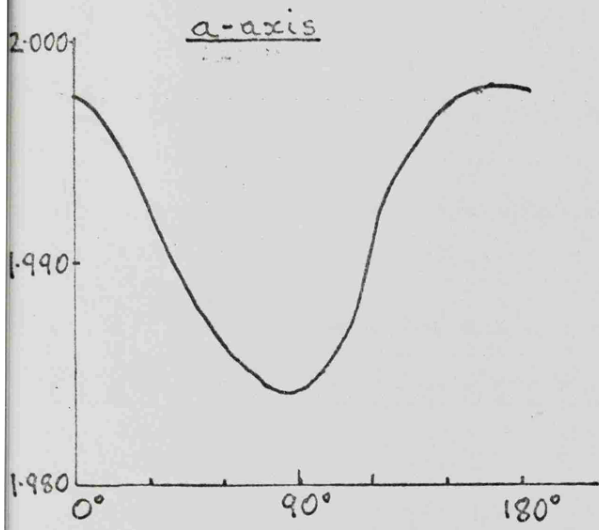


TABLE 3.2 Maximum and Minimum  $g$ - and  $A(^{14}\text{N})$  Values for Species Y  
in a Sodium Nitroprusside Crystal Rotated about Four Different Axes

Rotation Axis	$g_{\text{max}}$	$g_{\text{min}}$	$A_{\text{max}}$	$A_{\text{min}}$ (gauss)
a	1.9985	1.9842	25.85	17.90
b	1.9850	1.9511	18.55	8.05
c	1.9993	1.9506	25.67	8.82
c'	1.9975	1.9510	25.40	8.04

TABLE 3.3 Computed Principal g-values and  
Directions for Species Y

1st Set:

Principal Axis	Principal g-value	Crystal Axis	Direction Cosine	Acute Angle
x	1.9994	a	+0.1378	82° 5 <sup>1</sup>
		b	+0.9787	11° 53 <sup>1</sup>
		c	+0.1522	81° 15 <sup>1</sup>
y	1.9843	a	-0.0654	86° 15 <sup>1</sup>
		b	+0.1624	80° 39 <sup>1</sup>
		c	-0.9846	10° 6 <sup>1</sup>
z	1.9506	a	-0.9883	8° 44 <sup>1</sup>
		b	+0.1258	82° 44 <sup>1</sup>
		c	+0.0863	85° 3 <sup>1</sup>

2nd Set:

x	1.9992	a	+0.1226	82° 57 <sup>1</sup>
		b	+0.9875	9° 5 <sup>1</sup>
		c	+0.0995	84° 18 <sup>1</sup>
y	1.9846	a	+0.1124	83° 33 <sup>1</sup>
		b	+0.0859	85° 4 <sup>1</sup>
		c	-0.9899	8° 7 <sup>1</sup>
z	1.9505	a	-0.9861	9° 30 <sup>1</sup>
		b	+0.1326	82° 23 <sup>1</sup>
		c	-0.1004	84° 14 <sup>1</sup>

TABLE 3.3 (a) Computed Principal  $^{14}\text{N}$  Hyperfine Values and Directions for Species Y

1st Set:

Principal Axis	Principal A( $^{14}\text{N}$ ) Value (gauss)	Crystal Axis	Direction Cosine	Acute Angle
x	25.88	a	+0.0518	$87^\circ 2^1$
		b	+0.9828	$10^\circ 38^1$
		c	+0.1773	$79^\circ 47^1$
y	18.24	a	-0.2130	$77^\circ 42^1$
		b	+0.1844	$79^\circ 23^1$
		c	-0.9595	$16^\circ 22^1$
z	8.05	a	-0.9757	$12^\circ 41^1$
		b	+0.0119	$89^\circ 18^1$
		c	+0.2189	$77^\circ 21^1$

2nd Set:

x	25.86	a	+0.0169	$89^\circ 2^1$
		b	+0.9859	$9^\circ 38^1$
		c	+0.1663	$80^\circ 26^1$
y	18.32	a	+0.2371	$76^\circ 17^1$
		b	+0.1577	$80^\circ 56^1$
		c	-0.9586	$16^\circ 34^1$
z	7.94	a	-0.9713	$13^\circ 45^1$
		b	+0.0557	$86^\circ 48^1$
		c	-0.2312	$76^\circ 38^1$

the two orientations of the parent nitroprusside ion (Figure 3.2) being magnetically equivalent in this setting.

A plot of the  $g$ - and  $A$ - values of the triplets against the angle of rotation about the crystallographic  $a$ -,  $b$ - and  $c$ - axes is shown in Figure 3.7. A comparison of these plots shows that the principal directions of the  $g$ - and  $A$ - tensors differ by no more than  $5^\circ$ . Thus, within the limit of experimental error, the principal axes may be said to be co-directional. The maximum and minimum  $g$ - and  $A$ - values for each axis (Table 3.2) were processed by the method of Schonland<sup>4</sup> (see Appendix), to give the principal values of the  $g$ - and  $A$ - tensors together with their principal directions. However, this method always gives rise to an ambiguity of sign in one of the matrix elements in the tensor to be diagonalised. This leads to the computation of two alternative sets of principal  $g$ - and  $A$ - tensors and directions (Table 3.3). There is, however, a method of deciding which of the two sets of principal values is the correct one. This involves making  $g$ - and  $A$ - value measurements in a direction not included in the previous measurements and comparing these with the results predicted by the two possible sets of principal values. (see Appendix)

Accordingly, the crystal was rotated about a fourth axis, the  $c'$ - axis, making an angle of  $15^\circ$  with the  $c$ - axis, and a plot of  $g$ - and  $A$ - against angle of rotation was drawn. The maximum and minimum  $g$ - and  $A$ - values were found for the  $c'$ - axis and are included in Table 3.2. By using these values in the procedure outlined in the Appendix, it was ascertained that the first set of principal values was the correct one.

These values are very similar to those reported by van Voorst and Hemmerich<sup>2</sup> in their single crystal study of sodium nitroprusside X-irradiated at 77K. The e.s.r. parameters of species Y and van Voorst's species I are compared in Table 3.4.

Table 3.4

Comparison of e.s.r. parameters of species Y and species I.

<u>Radical</u>	<u>g-tensor</u>			<u><sup>14</sup>N Hyperfine tensor (gauss)</u>		
	$g_{11}$	$g_{22}$	$g_{33}$	$A_{11}$	$A_{22}$	$A_{33}$
Species Y	1.95	1.98	2.00	8.1	18.2	25.9
Species I	1.93	1.98	2.00	8.5	18.3	25.9

These values are in very good agreement, except that the lowest g-value of van Voorst's species I differs from the corresponding value for species Y by an amount larger than experimental error. There is also a small discrepancy in the lowest A-values but this is less than .5 gauss and therefore within the limit of experimental error.

Our computed results show the principal axes of the g- and <sup>14</sup>N hyperfine tensors are co-directional and inclined at 8° to the a-axis, 12° to the b-axis and 10° to the c-axis. This compares with the values of 10°, 10° and 0° respectively, which van Voorst and Hemmerich obtained. It may be assumed then, that the two sets of e.s.r. data refer essentially to the same species, however the difference in directions of the principal tensors implies that the two species possess a significantly different geometry. The discrepancy in the  $g_{11}$ -values may imply a more fundamental

difference in the nature of the two species.

In their paper, van Voorst and Hemmerich make no mention of having allowed the crystal to warm above 77K, but presumably they must have done so, since they have not reported seeing the paramagnetic centre referred to here as species X, whose thermal decay gives rise to species Y. Thus they are incorrect in their assumption that species Y ( species I in their nomenclature ) is the main product of irradiation at 77K.

If we denote the reference axes for the nitroprusside anion such that the z-axis is the axial N-C-Fe direction and the x- and y- axes pass through opposite pairs of equatorial cyanide ligands, then the directions of the computed g-tensor do not coincide with these at all. This indicates that the orbital containing the unpaired electron has a different direction from any of the parent nitroprusside orbitals. A calculation shows that the principal direction corresponding to the lowest g-value ( $g_{11} = 1.95$ ) makes an angle of  $28^\circ$  with the z-axis (so that we may alternatively refer to it as  $g_z$ ), and its projection onto the equatorial xy plane makes an angle of  $40 \pm 10^\circ$  with one of the equatorial cyanide ligands. (see Appendix for calculation) The implication of this will be discussed later.

Now, as mentioned earlier, a crystal irradiated at 77K was transferred (without raising its temperature) to an e.s.r. Dewar at 77K, so that its needle axis was approximately vertical. The crystal was rotated about the  $\alpha$ -axis and e.s.r. spectra for several orientations were obtained. Two of these are illustrated in Figure 3.8. For one orientation of the crystal the e.s.r.

Crystal Spectra of Nitroprusside  $\gamma$ -Irradiated at 77K

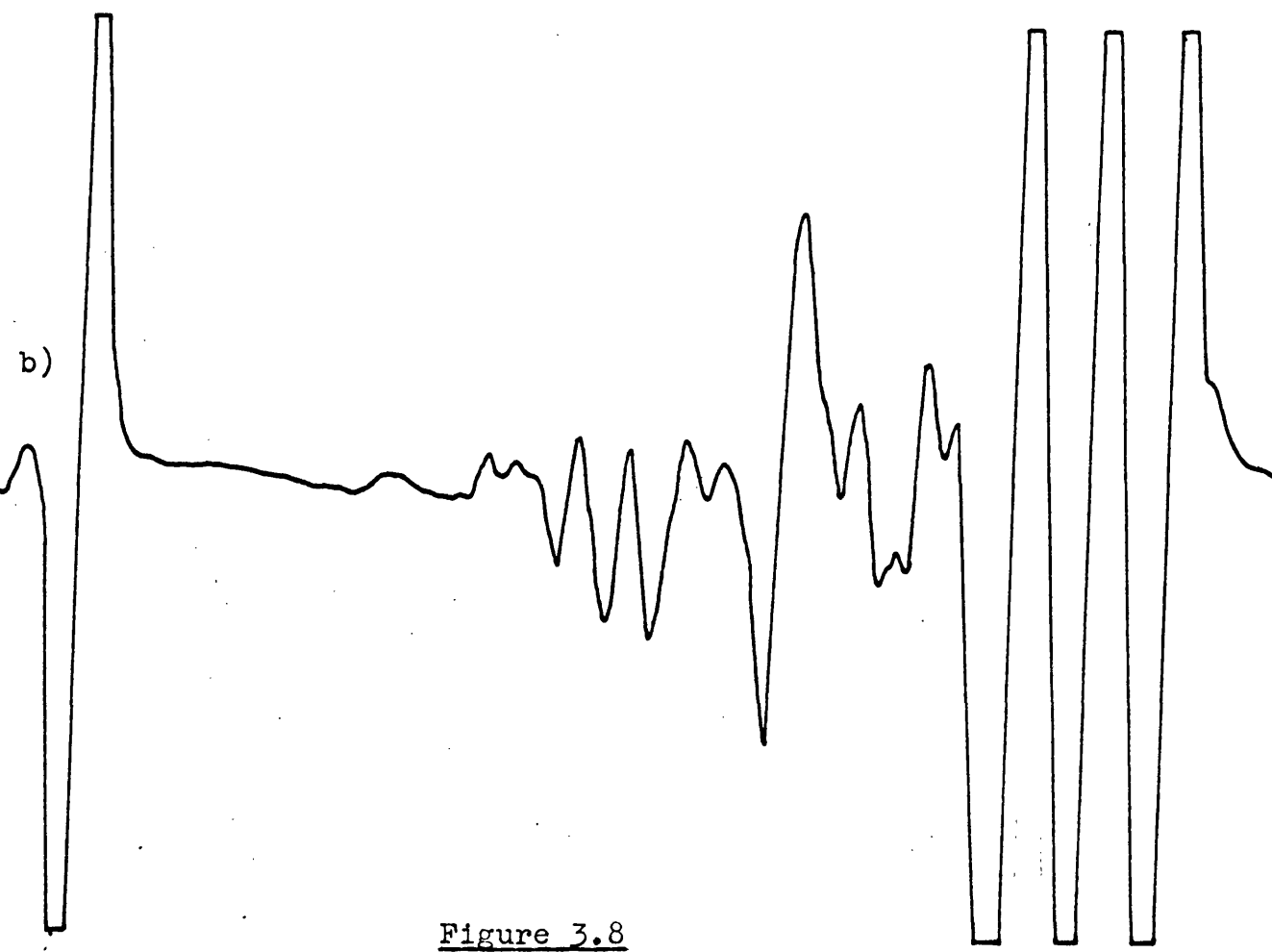
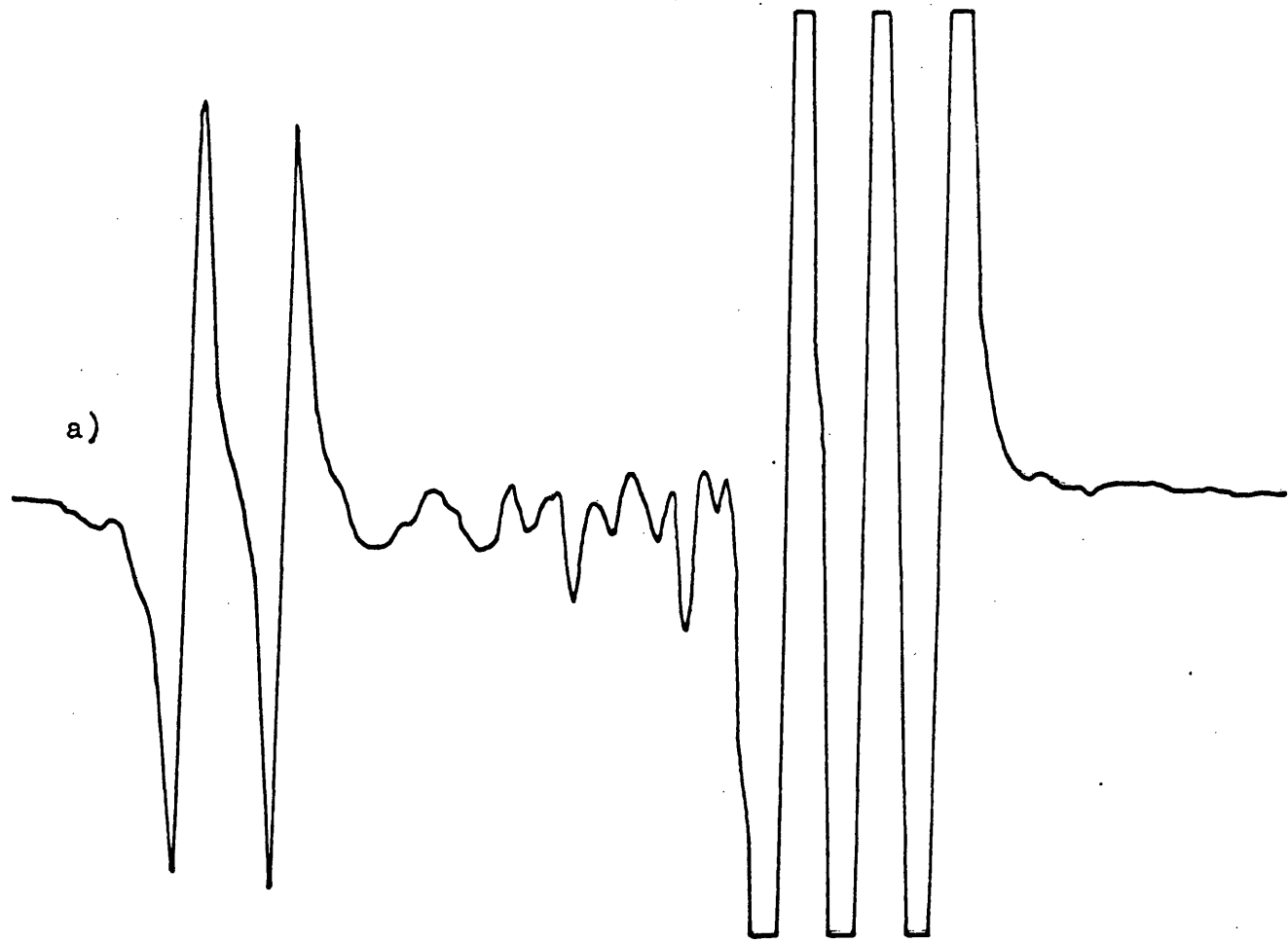


Figure 3.8

spectrum consisted of a very intense triplet at high field plus two single lines of equal intensity on the low field side of the spectrum together with a number of less intense lines. When the crystal was rotated through  $90^\circ$  the two single lines merged into a single line whose intensity was twice that of the former lines. This is characteristic of a paramagnetic species which exists in two magnetically inequivalent sites in the lattice which become equivalent at one particular orientation of the crystal. It should be noted that the crystal used in this (preliminary) study was large and thus permitted radicals to be seen which would not normally show up clearly in a powder spectrum. One such radical was the one giving the above singlet whose  $g_{\max}$  for rotation about the a-axis was approximately 2.14. This was only seen as a very weak bump in the e.s.r. spectrum of the irradiated polycrystalline sample. No hyperfine coupling whatsoever could be detected for this singlet. The maximum and minimum g- values of the e.s.r. triplet (for rotation about the a-axis) are 1.99 and 1.97 respectively. These values are compatible with the results obtained for species X in the corresponding powder spectrum. Since, for reasons previously mentioned, it was not feasible to perform a full single crystal study on the low-temperature irradiated crystal, we cannot obtain the principal directions of the g- and A- axes for species X. All we can say is that there appears to be only one magnetic site for the radical (or two sites which become equivalent) when the crystal is rotated about the needle axis.

Since it has only been possible to study species X and Y

in rigid media, no isotropic hyperfine coupling constant has been experimentally determined for either species. This means that there is some uncertainty in the signs of the  $^{14}\text{N}$  hyperfine tensors. There are eight different sign combinations for the A-tensors of species X and Y and hence eight possible values for each of their isotropic hyperfine coupling constants. These possibilities are illustrated in Table 3.5 and will be discussed in the next section.

#### Discussion.

(It will be borne in mind that species Z has been reported previously<sup>1</sup> and that it is identical to species C referred to in Chapter 2, where some aspects of its structure have been discussed.)

#### Identification of Species X and Species Y.

In view of the similarity in the form of the  $g$ - and  $A$ -tensors of species X and Y, they will be treated together. It is proposed, first of all, to demonstrate that they are most probably pentacyanonitrosyl  $\pi$ -complexes, in which the major portion of the spin-density of the unpaired electron is located

TABLE 3.5

Possible Sign Combinations of  $^{14}\text{N}$  Hyperfine  
Tensor for a) Species X and b) Species Y

	<u>Experimental A-tensor</u>				<u>Anisotropic A-tensor</u>		
	<u>A<sub>x</sub></u>	<u>A<sub>y</sub></u>	<u>A<sub>z</sub></u>	<u>Aiso</u>	<u>B<sub>x</sub></u>	<u>B<sub>y</sub></u>	<u>B<sub>z</sub></u>
a)	20.4	21.4	12.2				
	+	+	+	+18.0	2.4	3.4	-5.8
	+	+	-	+ 9.9	10.5	11.5	-22.1
	+	-	+	+ 3.7	16.7	-25.1	8.5
	-	+	+	+ 4.4	-24.8	17.0	7.8
	-	-	-	-18.0	- 2.4	- 3.4	5.8
	-	-	+	- 9.9	-10.5	-11.5	22.1
	-	+	-	- 3.7	-16.7	25.1	- 8.5
	+	-	-	- 4.4	24.8	-17.0	- 7.8
b)	25.9	18.2	8.1				
	+	+	+	+17.4	8.5	0.8	- 9.3
	+	+	-	+12.0	13.9	6.2	-20.1
	+	-	+	+ 5.2	20.7	-23.4	2.9
	-	+	+	+ 0.4	-26.3	17.8	7.7
	-	-	-	-17.4	- 8.5	- 0.8	9.3
	-	-	+	-12.0	-13.9	- 6.2	20.1
	-	+	-	- 5.2	-20.7	23.4	- 2.9
	+	-	-	- 0.4	26.3	-17.8	- 7.7

on the nitrogen of the nitrosyl group. The evidence for this is threefold : i.r., e.s.r. and mechanistic evidence.

(i) Infra-red Evidence

Danon et. al.<sup>5</sup> have performed some solid state infra-red studies on x-irradiated sodium nitroprusside. They obtained three lines in the N-O stretching frequency region corresponding to three nitrosyl species. One of which, with  $\nu(\text{NO}) = 1940\text{cm}^{-1}$  was attributed to sodium nitroprusside itself, while the other two lines at  $1850\text{cm}^{-1}$  and  $1720\text{cm}^{-1}$  were attributed to products of radiation damage in the nitroprusside ion. The line at  $1720\text{cm}^{-1}$  decayed at the same rate as the e.s.r. triplet which we have attributed to species Y, while the  $1850\text{cm}^{-1}$  line increased simultaneously at the same rate as the increase of the e.s.r. triplet attributed to species Z. They also found that samples examined a few days after irradiation gave only the line at  $1850\text{cm}^{-1}$ , which is in accordance with our e.s.r. evidence that only species Z is observed on examining the sample a few days after irradiation. (see also ref. 1) Species X was not observed in the infra-red spectra obtained by Danon et. al., presumably on account of its very short half-life. This infra-red study confirms our e.s.r. evidence that species Y decays into species Z.

The infra-red shifts to lower energy of the  $\nu(\text{NO})$  lines attributed to species Y and Z show that the N-O bond has been weakened. This indicates that the nitroprusside ion has been reduced in both cases. Now in the case of species Z, the unpaired electron is known to be mainly on iron<sup>1</sup> and therefore the effect of the additional electron is to reduce the iron from the +2

oxidation state to the +1 oxidation state. On the other hand, the N-O stretching frequency in species Y has been lowered by a further  $130\text{cm}^{-1}$ . This indicates that the N-O bond has been weakened further, most probably by direct reduction placing the unpaired electron into an antibonding  $\pi$ -orbital on the nitrosyl group itself. An alternative explanation, that the iron has been further reduced to the zero oxidation state, may be discounted since  $\text{Fe}^0$ , with eight d-electrons, is diamagnetic and our e.s.r. evidence is that species Y is definitely paramagnetic.

(ii) E.s.r. evidence.

The following e.s.r. evidence for species Y shows that the unpaired electron is mainly on the nitrosyl group and not on the iron atom nor on a cyanide ligand. Van Voorst and Hammerich<sup>2</sup> have substituted  $^{57}\text{Fe}$  ( $I = \frac{1}{2}$ ) for  $^{56}\text{Fe}$  ( $I = 0$ ) in  $\text{Na}_2\text{Fe}(\text{CN})_5\text{NO}\cdot 2\text{H}_2\text{O}$  and have found for species Y (species I in their nomenclature) only a small broadening of 1.5 gauss due to unresolved  $^{57}\text{Fe}$  hyperfine structure. However they obtained an isotropic splitting of 7.2 gauss due to  $^{57}\text{Fe}$  in species Z (species II in their nomenclature). From these results they calculated a spin density of about 80% of the unpaired electron on iron in species Z, compared with a value of less than 8% of the unpaired electron on iron in species Y.

Danon et. al.<sup>5</sup> have prepared sodium nitroprusside with  $^{13}\text{C}$  substituted for  $^{12}\text{C}$  in the cyanide ligands and have observed no hyperfine structure due to  $^{13}\text{C}$  in species Y. This proves that there is no unpaired spin density on the cyanide ligands. Danon et. al.<sup>6</sup> have, on the other hand, reported hyperfine coupling

to  $^{13}\text{C}$  of the cyanide ligands in species Z, however their report of seeing an equal and isotropic interaction with both equatorial and axial cyanides is in conflict with the results of other workers<sup>7,8</sup>. This will be discussed later.

This is fairly conclusive evidence that species Y has the major portion of its unpaired spin density on the nitrogen of the nitrosyl group. Additional but indirect evidence for this is to be found in the results of our single-crystal study. The fact that the g- and A- tensors are coaxial, coupled with the fact that their mutual axes are quite a large extent removed from the axes of the parent nitroprusside ion implies that the unpaired electron is not in an iron orbital. If there were significant unpaired spin density on iron then the g- and A- tensors would not be coaxial; the g-tensor being determined by iron orbitals and the  $^{14}\text{N}$  hyperfine tensor determined by orbitals on nitrogen. For example, the computed results<sup>1</sup> for species Z show that the principal directions of the g-tensor coincide with the reference axes while the A-tensor is directed at an angle of  $10^\circ$  to the g-tensor. This has been interpreted in terms of a bending of the Fe-N-O bond by  $10^\circ$  from linearity<sup>1</sup>. In species Y, however, the g- and A- tensors are both determined by orbitals having the same axes i.e. nitrogen orbitals.

(iii) Mechanistic Evidence.

From our e.s.r. results we may deduce that the following sequence of events takes place following irradiation of sodium nitroprusside. The paramagnetic centre initially formed, species X, decays on warming into species Y which subsequently decays forming

species Z. Now species Z has been previously characterised<sup>1</sup> and is known to be a nitrosyl complex, therefore the inference must plainly be drawn that species X and Y are also nitrosyl complexes, particularly in the light of the evidence mentioned in (i) and (ii).

Having established that species X and Y are most probably nitrosyl radicals we can now look at the nature of their g- and A- tensors and consider the probable structure of the species.

#### The g-tensor.

There are certain similarities between species X and Y and the trapped NO centre, species B, described in Chapter 2. In a nitrosyl radical the unpaired electron will be found in the lowest lying empty molecular orbital. In free nitric oxide this level comprises the degenerate  $2p_{\pi}$ \* pair of orbitals. (see Chapter 2) Now in order to observe an e.s.r. spectrum, the NO must be trapped or bonded in such a way that this degeneracy is lifted. Accordingly, one of the  $2p_{\pi}$ \* -orbitals will have a lower energy than the other. (see Figure 2.6)\* The lowest g-value (1.956 for species X and 1.951 for species Y) will then arise from a mixing of the  $2p_{\pi_x}$ \* -orbital containing the unpaired electron with the other, empty  $2p_{\pi_y}$ \* -orbital via spin-orbit coupling. This will occur when the applied field is along the N-O bond direction (the z'-axis).

The single crystal results for species Y show that the N-O bond (actually the principal direction of  $g_z$ ), is directed at an angle of  $27^\circ$  away from the axial N-C-Fe direction and points approximately midway between one pair of equatorial cyanide ligands.

\* page 27.

Now in the absence of perturbations (such as bending the N-O group) which would tend to lower the symmetry of the M.O.'s involving the N-O group, the other two g-values ( $g_x$ , and  $g_y$ ,) would be expected to be close to the free-spin value, since in unperturbed NO there are no orbitals of the required symmetry available for spin-orbit coupling with the  $2p_{\pi^*}$ -orbital when the applied field is along the perpendicular (x' and y') directions. In species X and Y, however, the  $g_x$ - and  $g_y$ - values are both less than free-spin, although in each case one of the g-values is quite close to free-spin (1.999 and 2.000 respectively) while the other is appreciably removed from the free-spin value (1.969 and 1.984 respectively). It is difficult to envisage how bending of the N-O group could in fact bring into existence an empty orbital with the symmetry required for coupling with the  $2p_{\pi^*}$ -orbital under consideration. Neither can we explain the g-tensor in terms of spin-orbit coupling on iron, since we have stressed that, because the g- and A- tensors are coaxial, the g-tensor is not governed by orbitals on the central metal ion even though there may be a small spin-density on iron. Therefore we must turn our attention to the theory, put forward in Chapter 2, that the N-O group is librating or wagging. Librational motion, it should be noted, will tend to mix the g-values as well as the A-values. If we make the assumption that the g- tensor for non-librating NO is of the form :

$$\begin{pmatrix} g_{xx} & & \\ & g_{yy} & \\ & & g_{zz} \end{pmatrix} \equiv (\sim \text{f.s.} \quad \sim \text{f.s.} \quad \ll \text{f.s.})$$

(where f.s. stands for free-spin)

then we can explain the form of the measured g-tensors :

Species X : (1.999 1.969 1.956) — tensor 1

Species Y : (2.000 1.984 1.951) — tensor 2

by postulating libration of the N-O group about the x and y axes. Furthermore, if this hypothesis is correct then we can say that the N-O group in species X is librating more strongly than in species Y, since it would require more libration of the N-O to obtain tensor 1 than it would to obtain tensor 2. A further consideration of the effect of libration will be given below.

#### The A-tensor.

The difficulty in interpreting the  $^{14}\text{N}$  hyperfine tensor is that  $A_{\text{iso}}$  is unknown, and hence the signs of the tensor components are unknown. Now as Table 3.5\* shows there are eight computed values of  $A_{\text{iso}}$  for species X and Y; four positive and four negative values. All the experimental evidence suggests that there is positive spin-density on the nitrogen atom therefore we can fairly confidently eliminate the negative values of  $A_{\text{iso}}$ .

Comparing the values of  $A_{\text{iso}}$  for species X and Y with the value of 8G. calculated for NO in the gas phase<sup>9</sup>, we find that the value 9.9G. for species X taking the sign combination ( + + - ) is the closest to this value; whereas for species Y, two values of  $A_{\text{iso}}$  12.4 and 5.2 taking sign combinations ( + + - ) and ( + - + ) respectively, are almost equally as close. However none of the anisotropic A-tensors corresponding to these values of  $A_{\text{iso}}$  is of the form ( 2B, -B -B ) expected

\* following p. 48

for an electron in a  $p_{\pi}$ -orbital so we must again consider the effect of librating the N-O group being the probable cause of the discrepancy. Now the form of the measured  $^{14}\text{N}$  hyperfine tensors (and also the g-tensors - vide supra) suggests that species X is librating more strongly than species Y, therefore if the difference between them was purely a matter of the degree of libration, then by librating the N-O group in species Y further we ought to be able to transpose its tensor into that of species X.

$$\text{Species X : } A_{\text{iso}} = 9.9\text{G} \quad A_{\text{aniso}} = \begin{pmatrix} x & y & z \\ 10.5 & 11.5 & -22.1 \end{pmatrix} \text{ G.}$$

$$\text{Species Y : } A_{\text{iso}} = 12.0\text{G} \quad A_{\text{aniso}} = \begin{pmatrix} 13.9 & 6.2 & -20.1 \end{pmatrix} \text{ G.}$$

$$A_{\text{iso}} = 5.2\text{G} \quad A_{\text{aniso}} = \begin{pmatrix} 20.7 & -23.4 & 2.9 \end{pmatrix} \text{ G.}$$

The effect of libration on the tensor  $(20.7 \ -23.4 \ 2.9)$  cannot give  $(10.5 \ 11.5 \ -22.1)$  under any circumstances, since libration can only have the effect of shifting two tensor components towards their average value, the latter being the limit for complete rotation. So we may tentatively discard the former tensor. On the other hand, the effect of librating the N-O group (in the xy plane) on the tensor  $(13.9 \ 6.2 \ -20.1)$  will give the tensor  $(10.0 \ 9.2 \ -20.1)$ , which is still not close enough to  $(10.5 \ 11.5 \ -22.2)$  to be really satisfactory. Furthermore none of these anisotropic tensors can be derived (by libration) from the tensor  $(28 \ -14 \ -14)$  calculated for NO in the gas-phase<sup>9</sup>, so this fact would tend to eliminate them, notwithstanding the agreement in  $A_{\text{iso}}$ . If the N-O group is bonded to iron, however, we would not really expect good

agreement of the isotropic coupling constants of species X and Y with  $A_{\text{iso}}$  for free NO. Spin polarisation, for example, would tend to increase the value of  $A_{\text{iso}}$  while having little effect on the anisotropic hyperfine tensor. If we now take an all-positive sign combination of the measured A-tensors for species X and Y we obtain the values for  $A_{\text{iso}}$  of 18.4G. and 17.0G. respectively, which are reasonable for bonded N-O. If we consider the effect of librating the N-O group of species Y on its anisotropic tensor we find that we can exactly transpose this tensor into that of species X.

$$Y \equiv (8.5 \quad 0.8 \quad -9.3) \xrightarrow{\text{z-axis}} (5.9 \quad 3.4 \quad -9.3) \xrightarrow{\text{y-axis}} (2.4 \quad 3.4 \quad -5.8) \equiv X$$

This libration involves partial rotation about the y- and z- axes. Moreover both of these anisotropic tensors can be derived (to a good approximation) from the tensor (28 -14 -14) for nitric oxide. However we should not look at the analogy with trapped nitric oxide too closely as some measure of bonding with iron will modify the  $\pi$ -orbitals on nitrogen and hence modify the anisotropic tensor somewhat, depending on the degree of bonding involved.

It was hoped to be able to obtain a spectrum of species X at 4.2K in order to test the libration theory, however for reasons previously mentioned, this was not possible and the lowest temperature obtainable was 19K. We would expect that the libration of the N-O group would be completely quenched at 4.2K and that the g- and A- values measured at this temperature would be the

'true' values. The results at 19K however are inconclusive and neither prove nor disprove the libration theory. There certainly has been some shift in  $g$ - and  $A$ - values but these shifts are very small. (see Table 3.1)\* This result could, however, indicate that the N-O group is librating but that the libration is only slightly quenched at 19K. It is encouraging though, that some dependence of  $g$ - and  $A$ - values on temperature has been observed.

Additional lines in the 19K spectrum, not observed at 77K, may be attributed to a species in low abundance having the following  $g$ - and  $^{14}\text{N}$  hyperfine tensors : (2.000 2.003 1.925) and (36 5 5)G. respectively. This could be due to a small percentage of "free" NO which resulted from Fe-N-O bond homolysis in the nitroprusside ion on irradiation. Since it is not observed at liquid nitrogen temperature, the free NO must be sufficiently mobile at 77K that it does not remain at a site with a crystal field able to lift the degeneracy of the two  $\pi^*$ -orbitals for long enough to enable the e.s.r. spectrum to be recorded. Lowering the temperature must reduce the mobility of the free NO so that at 19K it does remain trapped at such a site.

It was also intended to study species Y at the lower temperature, however the liquid helium did not become available until the termination of experimental work and did not last long enough for a spectrum of the annealed sample to be obtained. Therefore the e.s.r. spectrum of species Y has not been observed at 19K.

Thus, although we cannot place any emphasis on any of the values computed for  $A_{\text{iso}}$  for species X and Y, we can say that the

\* following p. 40

all-positive sign combinations of the  $^{14}\text{N}$  hyperfine tensors, giving the highest values of  $A_{\text{iso}}$ , do give the most satisfactory results compatible with the libration theory.

At this point it is relevant to mention an iron nitrosyl compound with a  $^{14}\text{N}$  hyperfine tensor almost identical to that of species Y. Chien<sup>10</sup> has reported single-crystal e.s.r. results for nitrosylhaemoglobin (HbNO). The  $^{14}\text{N}$  hyperfine tensor computed for HbNO is (26.4 19.0 6.5)G compared with (25.9 18.2 8.1)G. for species Y. These tensors are remarkably similar and indicate a similar interaction of the unpaired electron with nitrogen in the two cases. Furthermore, nitrosylhaemoglobin gives an e.s.r. spectrum at room temperature<sup>11</sup> and the isotropic hyperfine coupling constant has been determined and found to be 17.3 gauss, showing that the all-positive sign combination is correct. However, this is where the similarity ends. A large Mössbauer hyperfine structure has been observed for HbNO<sup>12</sup>, which indicates a significant unpaired electron density on the iron atom. The results of this study indicate a spin-density of up to 30% of the unpaired electron on the iron atom, which is at considerable variance with the result found for species Y of less than 8% of the unpaired electron on iron<sup>2</sup>. Accordingly the g-tensor of HbNO (2.082 2.0254 1.991) is quite different from that of species Y (2.000 1.984 1.951). Furthermore, the principal directions of the g- and A- tensors of HbNO differ considerably; this result being interpreted in terms of a bent Fe-N-O bond angle of  $110^\circ$ . Thus, while the A-tensor is determined by molecular orbitals on nitrogen, the g-tensor is mainly determined by the metal, since spin-orbit coupling on iron

will be dominant (in view of its higher spin-orbit coupling constant). The larger spin-density on iron in nitrosylhaemoglobin could indicate that in HbNO the Fe-N bond distance is shorter than it is in species Y.

We can account for the relatively high values of  $A_{iso}$  in species X and Y (and nitrosylhaemoglobin) by an alternative mechanism, analogous to that used in bent  $AB_2$  triatomic molecules such as  $NO_2$ ,<sup>13</sup> containing a single electron in a  $\pi$ -type antibonding molecular orbital, using the fact that they all have bent Fe-N-O bonds. The mechanism whereby ligands acquire spin-density (the pseudo  $\pi$  mechanism) has been discussed by Walsh<sup>14</sup> and can be depicted in terms of atomic orbitals as shown in Figure 3.9. The pseudo  $\pi$  orbital shown stems from the formally degenerate  $\pi^*$  level of the linear molecule and tends towards an orbital localised entirely on A as the bending increases. This is because the atomic s-character on A increases and also because the effective overlap with the orbitals on B decreases as the radical bends.

This analogy is useful in explaining the comparatively high s-character of the unpaired electron and its degree of localisation on nitrogen, but in view of the more complex nature of the systems studied here, it is probably not strictly accurate.

Chien has followed the method of van Voorst and Hemmerich in interpreting the anisotropy of the  $^{14}N$  hyperfine tensor, where the unpaired electron density on nitrogen was determined using the following expressions<sup>2,10,15</sup>:

(see over)

The Pseudo- $\pi$  Orbital in Bent  $AB_2$  Molecules.

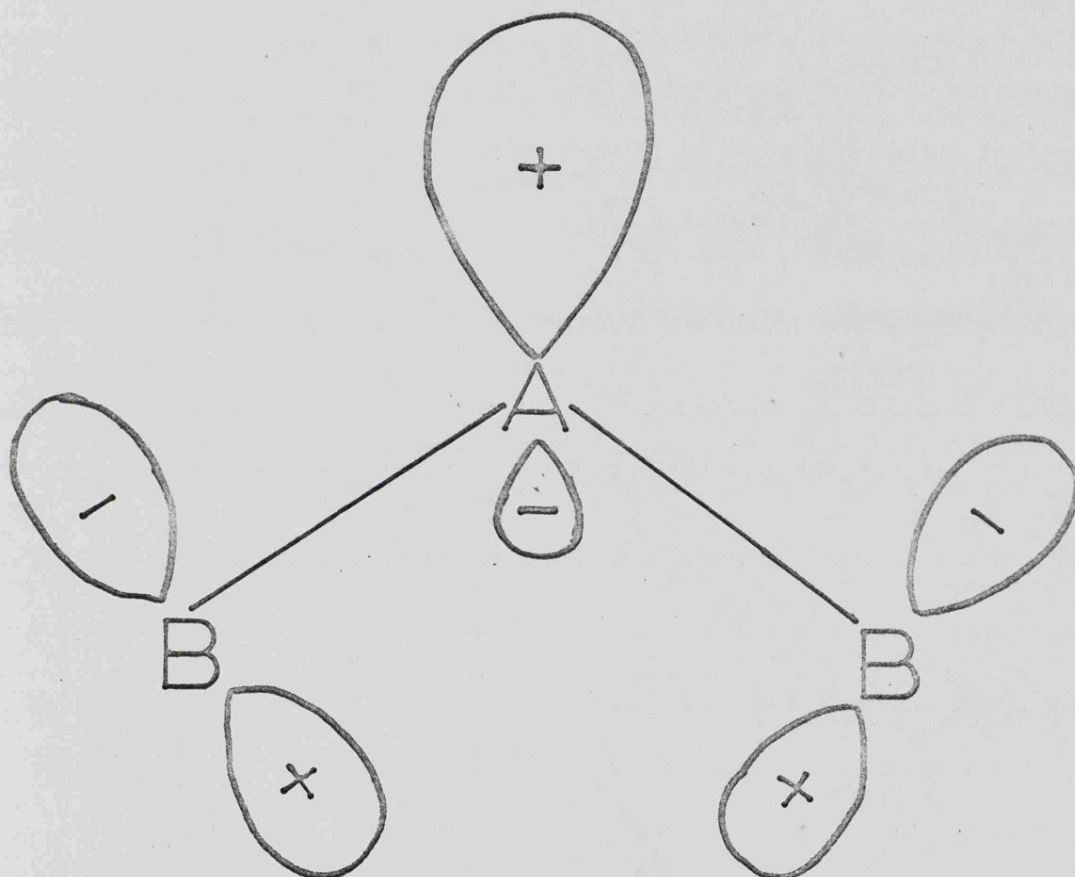


Figure 3.9

$$A_{zz'} = A_s c_s^2 + A_p (2c_{z'}^2 - c_{x'}^2 - c_{y'}^2)$$

$$A_{yy'} = A_s c_s^2 + A_p (2c_{y'}^2 - c_{x'}^2 - c_{z'}^2)$$

$$A_{xx'} = A_s c_s^2 + A_p (2c_{x'}^2 - c_{y'}^2 - c_{z'}^2)$$

$A_{xx'}$ ,  $A_{yy'}$ , and  $A_{zz'}$  are the measured hyperfine coupling constants along the three principal axes.  $A_s$  and  $2A_p$  are the coupling constants for a pure s orbital and for a pure p orbital on a nitrogen atom, 550G and 34G,<sup>16</sup> respectively.  $c_s^2$ ,  $c_{x'}^2$ ,  $c_{y'}^2$  and  $c_{z'}^2$  are, respectively, the coefficients of the pure s,  $p_{x'}$ ,  $p_{y'}$  and  $p_{z'}$  nitrogen orbitals in the M.O. of the unpaired electron. Using this method, taking the all-positive sign combination of the  $^{14}\text{N}$  hyperfine tensor, they each find a value for  $c_s^2$  of approximately 0.03, which we would not dispute. However, the values of  $c_{x'}^2$ ,  $c_{y'}^2$  and  $c_{z'}^2$  cannot be solved simultaneously from these equations, so they have put the value of  $c_{z'}^2$ , the  $p_{\pi}$  population in the N-O bond direction, equal to zero on the grounds that the nitrogen is primarily sp hybridised. They then calculate an almost equal population of the  $p_{x'}$  and  $p_{y'}$  levels on nitrogen; e.g. van Voorst calculates a value of  $c_{x'}^2 = 0.324$  and  $c_{y'}^2 = 0.202$  for species Y, resulting in a spin density on nitrogen of about 50%. This method has been criticised by Hayes<sup>17</sup> who states that "van Voorst's results predict a considerable orbital angular momentum, which implies a large orbital hyperfine term, which means the calculated spin distribution no longer produces the observed coupling constants." Hayes has modified van Voorst's results to take orbital momentum into account and, (using the same assumption that  $c_{z'}^2 = 0$ ) has arrived at a value for the total spin-density in nitrosyl  $\pi^*$  orbitals of 27%.

However, we believe this interpretation is still unsatisfactory because it does not take into account the fact that the spin-orbit coupling required for approximately equal population of the two  $\Pi^*$  levels would bring down the lowest g-value ( $g_z$ ) well below the 1.93 observed by van Voorst and Hemmerich. Accordingly, we hesitate to place any reliance on any numbers obtained in such a spin-population analysis of the anisotropic tensors.

We stress that the libration theory is the only one which can satisfactorily account for the form of both the g- and A-tensors.

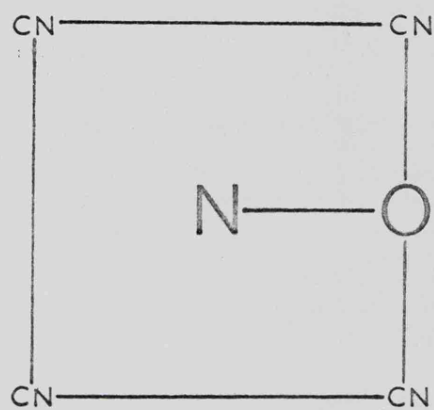
#### The Structure of Species X and Y.

We have fairly conclusively established that species X and Y are pentacyanonitrosyl complexes with the unpaired electron mainly localised on a librating nitrosyl group. The result computed for the Fe-N-O bond angle of  $152^\circ$  in species Y must refer to the mean position of the librating N-O group (see Figure 3.10). The mean position of the nitrosyl group also corresponds to its pointing midway between a pair of adjacent cyanide ligands (vide supra). The situation in reality could be explained in terms of the nitrosyl group librating in the xz plane so that its extreme positions coincided with its being directly over the two adjacent cyanide ligands (Figure 3.10).

The preliminary single-crystal e.s.r. results for species X suggest that the N-O bond may be bent further away from the  $\text{Fe}(\text{CN})_5$  pyramid than it is in species Y. The fact that the  $^{14}\text{N}$  hyperfine tensors of species X and Y can be interconverted by

Plan View of Librating N-O Group.

a) Mean Position



b) Extreme Positions.

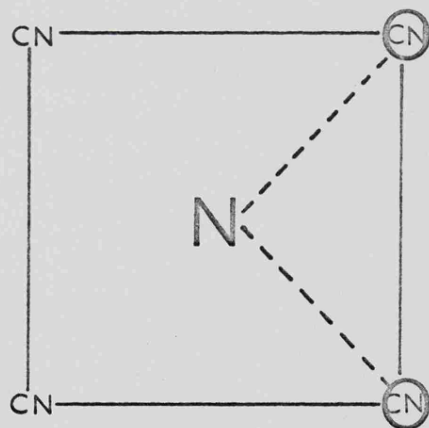


Figure 3.10

the effect of librating the N-O group suggests that there is only a subtle difference between the structures of the two species. One possibility is that the former has a longer Fe-N bond which could allow a stronger libration of the N-O group. The conversion of species X into species Y on warming will be discussed in the section dealing with the mechanism of  $\gamma$  damage.

#### Identification of Species Z.

This species has been reported previously by workers in this laboratory<sup>1</sup>, where it was formed by the  $\gamma$ -radiolysis of sodium nitroprusside at room temperature. The controversy over the structure of this species has been discussed in Chapter 2, where it was shown that it was derived from a product of radiation-damaged anhydrous nitroprusside (species B) by the addition of water. Early on, there was also a controversy over the ordering of the energy levels in this species. This controversy has been discussed elsewhere<sup>18,19</sup>, but it will be briefly summarised here insofar as it is relevant to the understanding of the present problem. For the purpose of this discussion we will assume that the species formed by the electrolytic reduction of sodium nitroprusside in D.M.F. is identical with species Z. (see Chapter 2 however) The e.s.r. results obtained for this species by several workers are illustrated in Table 3.6.

McNeil, Raynor and Symons<sup>20,21</sup> polarographically reduced sodium nitroprusside in D.M.F. and deduced an energy level scheme (Figure 3.11) from their e.s.r. results obtained at room

TABLE 3.6 E.s.r. Data for Room Temperature Irradiated Sodium Nitroprusside and for the  $(\text{Fe}(\text{CN})_5\text{NO})^{3-}$  Ion

<u>Sample and Direction</u>	g	$A(^{14}\text{N})$ (gauss)	Ref.
$(\text{Fe}(\text{CN})_5\text{NO})^{3-}$			21
Solution	2.0231	15.5	
Glass $\perp$	2.0313	14.8	
//	2.0059	17.1	
Single Crystal			1
x	2.0422	14.4	
y	2.0370	13.4	
z	2.0059	16.2	
average	2.0284	14.6	
Powder			1,20,21
$\perp$	( 2.0409	15.5	
	( 2.0350	14.6	
//	2.0050	16.5	
Powder			5
$\perp$	2.0374	14.6	
//	2.0069	16.3	
Powder			This work
(Species Z)			
$\perp$	2.0360	14.4	
//	2.0054	17.2	

The McNeil, Raynor and Symons M.O. Diagram for  
Polarographically Reduced Sodium Nitroprusside

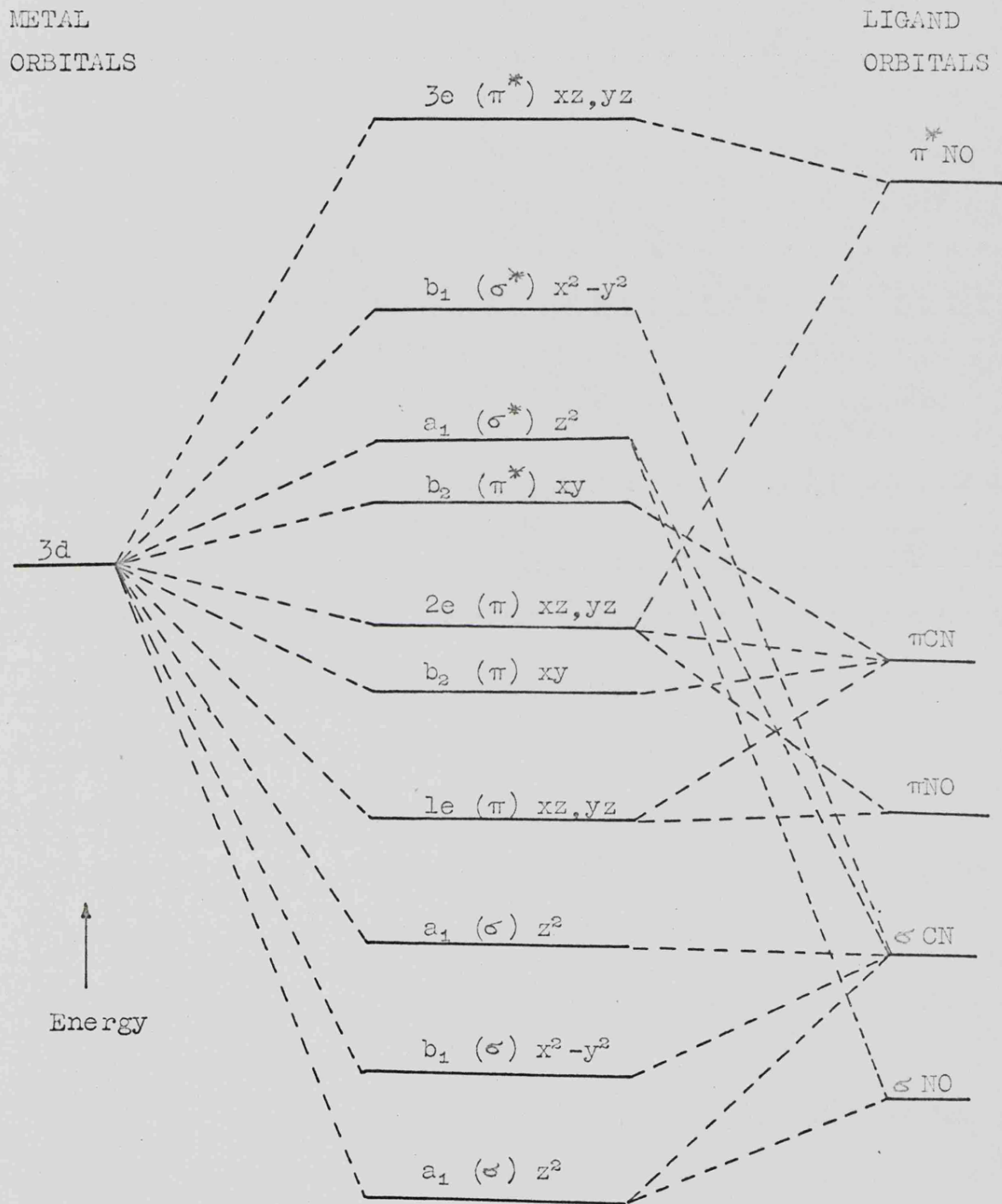


Figure 3.11

temperature and at 77K. Analysis of their  $^{14}\text{N}$  hyperfine data gave a total unpaired spin-density on nitrogen of 7.4% and a p:s ratio of 1.6. They concluded that the unpaired electron was in the  $\underline{5a_1}(d_z^2)$  orbital since  $\pi$ -interaction of the unpaired electron with nitrogen could not give rise to such a low p:s ratio. Further, the large coupling to nitrogen ( $A_{\text{iso}}=15.5\text{G}$ ) made it unlikely that the electron was in the  $\underline{3b_1}(d_{x^2-y^2})$  level particularly in view of the small coupling to nitrogen ( $A_{\text{iso}}(^{14}\text{N})=3.8\text{G}$ ) in  $\text{Mn}^{\text{II}}(\text{CN})_5\text{NO}^{2-}$  where the electron is known to be in the  $\underline{2b_2}(d_{xy})$  orbital.<sup>21,22,23</sup> The most conclusive evidence was that the observed g-tensor was in accord with the result theoretically predicted for an electron in a  $d_z^2$  orbital i.e.  $g_{\parallel}$  close to free-spin since spin-orbit coupling is not possible in this orientation ;  $g_{\perp} \gg$  free-spin by mixing  $d_z^2$  with  $d_{xz,yz}$  via spin-orbit coupling. Accordingly, these authors placed the  $\underline{5a_1}$  level below the  $\underline{3b_1}$  level in contrast to other schemes (vide infra).

Hockings and Bernal<sup>24,25</sup> examined the e.s.r. spectra of fluid solutions of electrolytically reduced sodium nitroprusside enriched with  $^{13}\text{C}$ . They found that each line of the original nitrogen triplet was split into five super-hyperfine lines ( $A_{\text{iso}}(^{13}\text{C})=4.6\text{G}$ ) due to four equivalent cyanide ligands. No axial component was observed in any of their spectra. These results suggested to them that the ground-state orbital was  $d_{x^2-y^2}$  and not  $d_z^2$  unless the axial cyanide ligand leaves the complex on reduction. Although admitting this last possibility, they preferred to conclude that the unpaired electron was in

the  $d_{x^2-y^2}$  orbital in spite of the fact that the large coupling to the nitrogen of the nitrosyl group suggested otherwise (vide supra).

There has, however, been conflicting evidence reported for the magnitude of the  $^{13}\text{C}$  hyperfine coupling. Kuska and Rogers<sup>7</sup> have reported a value of  $10.0 \pm 0.2$  gauss for  $A_{\text{iso}}(^{13}\text{C})$  but they do not state whether this interaction involves all five carbon atoms or just the equatorial ligands. Danon et al<sup>6</sup> have irradiated a single crystal of sodium nitroprusside enriched to 20% with  $^{13}\text{C}$  and their spectra indicate that the unpaired electron is interacting almost equally with all five carbon atoms ( $A(^{13}\text{C})$  varies between 9.0 and 10.1 gauss) in conflict with Hockings and Bernal's result.

Leaving aside the question of the actual magnitude of the  $^{13}\text{C}$  coupling, Hockings and Bernal's observation that the unpaired electron interacts only with the equatorial cyanides is in accord with our assertion (Chapter 2) that the process of removing (or partially removing) the axial cyanide is the only conceivable means of explaining why the  $5a_1(d_{z^2})$  level should be depressed below the  $7e(\pi^*\text{NO})$  level (vide infra) on reduction of the nitroprusside ion. The results of Danon et al can then be reconciled with those of Hockings and Bernal, since they were studying reduced nitroprusside in different media. Thus, in solution the axial cyanide ligand could be completely removed in the form of HCN by scavenging protons, while in the solid state the movement of the axial cyanide is limited by the constraints of the crystal lattice. Therefore, in the latter case the axial cyanide would

move only a short distance from the iron atom — long enough to depress  $\underline{5a_1}$  below  $\underline{7e}$  but short enough for  $^{13}\text{C}$  super-hyperfine splittings to be observed.

Manoharan and Gray<sup>23,26</sup> studied the optical spectra of the diamagnetic  $d^6$  ion  $\text{Fe}(\text{CN})_5\text{NO}^{2-}$  and, in conjunction with detailed S.C.C.C.-M.O. (self-consistent charge and configuration-molecular orbital) calculations for this ion, derived an energy level scheme which gave the following ordering of the electronic levels :

$$\underline{6e}(d_{xz,yz}) < \underline{2b_2}(d_{xy}) < \underline{7e}(\pi^*\text{NO}) < \underline{3b_1}(d_{x^2-y^2}) < \underline{5a_1}(d_{z^2})$$

Their calculation predicted a net axial destabilisation of the  $\underline{5a_1}(d_{z^2})$  orbital resulting in its being higher in energy than the  $\underline{3b_1}(d_{x^2-y^2})$  orbital. However, they stress that the  $\underline{5a_1}$  and  $\underline{3b_1}$  levels are not substantially different in energy. Manoharan and Gray also correlated the observed optical spectra with the predicted energies of the electronic transitions (Table 3.7). It will be noted that their assignment of the energies of the transitions  $\underline{6e} \rightarrow \underline{5a_1}$  and  $\underline{6e} \rightarrow \underline{3b_1}$  contradicts their energy level scheme and would put the  $\underline{3b_1}$  level below the  $\underline{5a_1}$  level. The new and most interesting result of their SCCC-MO calculations was the fact that the  $\underline{7e}$  orbital, derived mainly from  $\pi^*\text{NO}$  was situated between the  $\underline{2b_2}(d_{xy})$  and  $\underline{3b_1}(d_{x^2-y^2})$  orbitals. The ground state, according to this scheme was  $\dots(\underline{6e})^4(\underline{2b_2})^2 = {}^1A_{1g}$ ; the diamagnetic  $d^6$  ion formally comprising  $\text{Fe}(\text{II})$  and  $\text{NO}^+$ . The calculated final charge distribution in the molecule was in fact :

$$\left[ \text{Fe}^{+0.3166}(\text{CN})_4^{-2.2000}(\text{CN})^{-0.5809}(\text{NO})^{+0.4643} \right].$$

Table 3.7 Electronic Spectral Parameters for  $[\text{Fe}(\text{CN})_5\text{NO}]^{2-}$

Observed Maxima $\text{cm}^{-1}$	$\zeta_{\text{max}}$	Calculated Energies $\text{cm}^{-1}$	Band Assignments
20,080	~8	20,540	${}^1\text{A}_1 \rightarrow {}^1\text{E}$ ( $2b_2 \rightarrow 7e$ )
25,380	25	25,090	${}^1\text{A}_1 \rightarrow {}^1\text{A}_1$ ( $6e \rightarrow 7e$ )
30,300	40	30,770	${}^1\text{A}_1 \rightarrow {}^1\text{A}_2$ ( $2b_2 \rightarrow 3b_1$ )
37,800	900	37,750	${}^1\text{A}_1 \rightarrow {}^1\text{E}$ ( $6e \rightarrow 5a_1$ )
42,000	700	40,900	${}^1\text{A}_1 \rightarrow {}^1\text{E}$ ( $6e \rightarrow 3b_1$ )
50,000	24,000	49,900	${}^1\text{A}_1 \rightarrow {}^1\text{E}$ ( $2b_2 \rightarrow 8e$ )

Taken from Reference 26

Manoharan and Gray then went on to extend their treatment of the diamagnetic  $\text{Fe}(\text{CN})_5\text{NO}^{2-}$  ion to cover the case of the reduced nitroprusside ion  $\text{Fe}(\text{CN})_5\text{NO}^{3-}$ . According to their energy level scheme, the ground state of the latter ion was the configuration  $\dots(6e)^4(2b_2)^2(7e)^1$ , placing the unpaired electron in the  $7e$  ( $\pi^*\text{NO}$ ) orbital. Population analysis showed this level to be 72.5%  $\pi^*\text{NO}$  with some  $d_{\pi}$ ,  $\sigma\text{CN}$ ,  $\pi\text{CN}$  and  $\pi^*\text{CN}$  contributions. From interelectronic-repulsion considerations they suggested that all metal nitrosyls with one or more electrons in molecular orbitals will have a bent M-N-O system. This last statement is, of course, in accord with our results for species X and Y, which show that the electron is indeed in the  $\pi^*\text{NO}$  level. However, these authors were not aware at the time that there was any form of reduced nitroprusside other than species Z. Their assignment of a  $(\pi^*\text{NO})^1$  ground state for species Z was totally incompatible with the experimentally observed g-tensor and could not conceivably account for the positive  $g_{\perp}$  shift obtained. As strong evidence against a  $(d_{z^2})^1$  assignment, they quoted Hockings and Bernal's result of seeing only the equatorial  $^{13}\text{CN}$  splitting and, without giving any mention to the possibility of losing the axial cyanide ligand, dismissed the scheme of McNeil, Raynor and Symons as 'appearing to be without justification'.

Undaunted by this scurrilous attack on their reputation by the Americans, the gallant British team comprising McNeil, Raynor and Symons,<sup>27</sup> later joined by Goodman,<sup>1</sup> soon were able to provide fresh evidence which showed unequivocally that the unpaired electron was located mainly on the iron atom. They found that, on

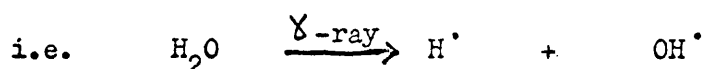
prolonged irradiation of sodium nitroprusside at room temperature, the concentration of radicals was sufficient to cause an interaction between adjacent pairs (pairwise trapping). From the directions and magnitude of the spin-spin interaction tensors the radical pairs were assigned in terms of their position in the host lattice. The separations between magnetic centres and their directions deduced from the interaction tensors showed without doubt that the interacting centres were the iron atoms and not the nitrosyl groups.

This result was later corroborated by van Voorst and Hemmerich's  $^{57}\text{Fe}$  isotopic substitution experiment<sup>2</sup> (vide supra) which showed the unpaired spin-density on iron in species Z to be 80%, thus confirming what McNeil, Raynor and Symons had postulated right from the start — that the unpaired electron was in the  $5a_1(d_{z^2})$  orbital.

We are indebted to Manoharan and Gray, however, for their S.C.C.C.-M.O. calculations which lend support to our assignment of the ground state of species X and Y being  $\dots(\pi^*NO)^1$ .

Mechanism of Radiation Damage.

We postulate that the radiation damage mechanism in hydrated sodium nitroprusside involves initial dissociative electron capture by water molecules.



However, we do not have any direct evidence to confirm this; i.e. we have not been able to detect any hydrogen or hydroxyl radicals formed on low-temperature irradiation. Nevertheless, the fact that completely different products are formed on irradiation of the anhydrous material (Chapter 2) strongly suggests that water is involved in the radiation damage mechanism in the dihydrate. Either a hydrogen atom or a hydroxyl radical (or both) could attack the nitroprusside anion to give  $[\text{Fe}(\text{CN})_4(\text{CNH})(\text{NO})]^{2-}$  and/or  $[\text{Fe}(\text{CN})_4(\text{CNOH})(\text{NO})]^{2-}$  respectively. We would expect the equatorial cyanides to be attacked preferentially because of the proximity of the water molecules in the lattice<sup>3</sup> (water molecules occupy bridging positions between sets of two equatorial cyanides belonging to two adjacent nitroprusside anions)<sup>3</sup> and the statistical factor of four.

We then envisage the unpaired electron going into the lowest lying unfilled level, i.e.  $\pi^*(\text{NO})$ , with a concomitant increase in length of the Fe-N bond, the N-O bond simultaneously bending to relieve the antibonding character of the unpaired electron on the nitrosyl group. The possibility that a hydrogen atom or a hydroxyl radical directly attacked the NO group can be discounted since there was no evidence for any proton hyperfine splitting on the nitrogen triplets of species X.

The decay of species X into species Y is thought to involve a subtle change in the direction of the N-O axis and is definitely not a true 'chemical' change since the activation energy for the process is rather low - only 5kcal/mol.<sup>28</sup> In contrast the activation energy for the formation of species Z from species Y is markedly higher - 30kcal/mol.<sup>28</sup> This indicates that a more substantial change has taken place and accords with our suggestion that the NO group 'recombines' with the  $[\text{Fe}(\text{CN})_5^-]$  pyramid and that the axial cyanide may be concurrently pulled off (or partially pulled off) by a proton (vide supra). In view of the lack of axial symmetry of species Z (vide supra) we may best regard it as having the structure  $[\text{Fe}(\text{CN})_3(\text{CNR})(\text{CNH})(\text{NO})]^{2-}$ , where R is H or OH, attached to an equatorial cyanide. The corresponding species formed by addition of water to the  $\gamma$ -irradiated anhydrous nitroprusside (see Chapter 2) may then be formulated  $[\text{Fe}(\text{CN})_4(\text{CNH})(\text{NO})]^{2-}$ . The protonation of the axial cyanide only, accords with our observation that this species does possess axial symmetry unlike species Z.

Thus the protonation mechanism which we have proposed, appears to be a tenable theory since it is able to accommodate all the experimental facts.

References for Chapter 3.

1. B.A. Goodman, D.A.C. McNeil, J.B. Raynor and M.C.R. Symons, J. Chem. Soc.(A), 1547, (1966).
2. J.D.W. van Voorst and P. Hemmerich, J. Chem. Phys., 45, 3194, (1966).
3. P.T. Manoharan and W.C. Hamilton, Inorg. Chem., 2, 1043, (1963).
4. D.S. Schonland, Proc. Phys. Soc., 73, 788, (1959).
5. L. Tosi and J. Danon, Compt. Rend. Acad. Sci. Paris, 263B, 970, (1966).
- 5' J. Danon, R.P.A. Muniz and A.O. Caride, unpublished result.
6. J. Danon, R.P.A. Muniz and A.O. Caride, J. Chem. Phys., 46, 1210, (1967).
7. H.A. Kuska and M.T. Rogers, J. Chem. Phys., 42, 3034, (1965).
8. E.F. Hockings and I. Bernal, J. Chem. Soc., 5029, (1964).
9. R.L. Brown and H.E. Radford, Phys. Rev., 147, 6, (1966).
10. J.C.W. Chien, J. Chem. Phys., 51, 4220, (1969).
11. J.C.W. Chien, J. Am. Chem. Soc., 91, 2166, (1969).
12. G. Lang and W. Marshall, J. Mol. Biol., 18, 385, (1966).
13. P.W. Atkins and M.C.R. Symons, " The Structure of Inorganic Radicals," Elsevier, (1967).
14. A.D. Walsh, J. Chem. Soc., 2266, (1953).
15. W. Marshall and R. Stuart, Phys. Rev., 117, 1222, (1960).
16. M.C.R. Symons, Advan. Phys. Org. Chem., 1, 332, (1963).
17. R.G. Hayes, J. Chem. Phys., 48, 4806, (1968).
18. D.A.C. McNeil, Ph.D. Thesis, (1966).
19. B.A. Goodman, Ph.D. Thesis, (1968).

References (cont.)

20. D.A.C. McNeil, J.B. Raynor and M.C.R. Symons, Proc. Chem. Soc., 364, (1964).
21. D.A.C. McNeil, J.B. Raynor and M.C.R. Symons, J. Chem. Soc., 410, (1965).
22. P.T. Manoharan and H.B. Gray, Chem. Comm., 324, (1965).
23. P.T. Manoharan and H.B. Gray, Inorg. Chem., 5, 823, (1966).
24. I. Bernal and E.F. Hockings, Proc. Chem. Soc., 361, (1962).
25. E.F. Hockings and I. Bernal, J. Chem. Soc., 5029, (1964).
26. P.T. Manoharan and H.B. Gray, J. Am. Chem. Soc., 87, 3340, (1965).
27. D.A.C. McNeil, J.B. Raynor and M.C.R. Symons, Mol. Phys., 10, 297, (1966).
28. J. Danon, A.O. Caride and R.P.A. Muniz, unpublished result.

CHAPTER 4

SPECTROSCOPIC STUDIES ON CHROMIUM AND MANGANESE

PENTACYANONITROSYLS IN ALKALI HALIDE LATTICES.

### Introduction.

In Chapter 2 we discussed the trends in the g- and  $^{14}\text{N}$  hyperfine tensors for the isoelectronic series of  $d^5$  pentacyano-nitrosyl ions : chromium(I), manganese(II) and iron(III). Now, the only  $d^7$  pentacyanonitrosyl ion which has been reported is that of iron(I). (see Refs. 1 & 2 in Chapter 2) Those of chromium(-I) and manganese(0) have hitherto not been prepared, presumably because of the difficulty in stabilising the very low oxidation states required.

The work described in this chapter was undertaken in order to prepare and study these unstable complexes by a method first outlined by Root<sup>1</sup>, who used it in the study of complex cyanides. The technique consisted of incorporating transition metal hexacyanides into alkali halide lattices, followed by  $\gamma$ -irradiation. Subsequent infra-red and e.s.r. measurements revealed that the metal ions were reduced to a lower oxidation state by the action of radiolysis. The basic theory behind this method was that  $\text{M}(\text{CN})_6^{n-}$  ions ( $n = 3,4$ ) were incorporated into a potassium chloride lattice by replacing a  $[\text{KCl}_6]^{5-}$  unit. Electronic spectra showed that F-band formation was depressed on  $\gamma$ -irradiation, which indicated that the complex was acting as an electron trap - thus tending to attain charge balance within the lattice.

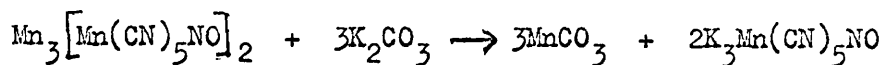
This method seemed ideally suited for the attempted preparation of the  $d^7$  pentacyanonitrosyl ions of chromium and manganese via the  $d^5$  and  $d^6$  pentacyanonitrosyl ions  $\text{Cr}^{\text{I}}(\text{CN})_5\text{NO}^{3-}$  and  $\text{Mn}^{\text{I}}(\text{CN})_5\text{NO}^{3-}$  respectively, which could be readily synthesised.

The case of manganese seemed to be the most promising, since only a one-electron reduction step was required to form the  $d^7$  complex, whereas in the case of chromium a two-electron step involving a diamagnetic intermediate would be required. However, it was thought that some success in the latter case might be merited, since the desired product would have a five-negative charge and would not therefore require charge compensation within the lattice. This would serve to make it very stable in the alkali halide lattice.

#### Experimental.

Potassium pentacyanonitrosyl chromate(I),  $K_3Cr(CN)_5NO \cdot H_2O$ , was prepared<sup>2</sup> by treating chromium trioxide with hydroxylamine in basic solution containing an excess of cyanide ions. The complex was isolated by precipitation with ethanol and purified by dissolving in the minimum quantity of water and reprecipitating with 95% ethanol.

Potassium pentacyanonitrosyl manganate(I),  $K_3Mn(CN)_5NO \cdot 2H_2O$ , was prepared by the method described by Cotton et al.<sup>3</sup> This method involved the initial preparation of  $K_4Mn(CN)_6$  from  $MnCO_3$  and KCN, which was oxidised in situ with a current of air to form  $K_3Mn(CN)_6$ . The hexacyanomanganate(III) was treated with a basic solution of hydroxylamine containing an excess of cyanide ions. The mixture was acidified with glacial acetic acid and a saturated solution of manganous acetate was added to precipitate  $Mn_3[Mn(CN)_5NO]_2$ . This was digested with a solution of potassium carbonate, whereupon the desired product was formed according to the equation :



The complex was isolated by precipitation with ethanol and purified by dissolving in water and reprecipitating with ethanol. The anhydrous complex was made by leaving the dihydrate overnight in a desiccator over  $P_2O_5$  in vacuo.

The chromium and manganese pentacyanonitrosyls were incorporated into potassium chloride and potassium bromide crystals by allowing an aqueous solution containing less than one per cent of the complex to evaporate over a period of several days. The solutions were not allowed to evaporate to dryness but were filtered as soon as a reasonable crop of crystals had grown. Microcrystalline samples of the doped alkali halides were prepared by rapid evaporation of aqueous solutions under reduced pressure, and by precipitation from aqueous solutions with ethanol. After drying over  $P_2O_5$  in vacuo, the doped halides were thoroughly ground and made into pressed discs of varying thickness (usually 1 - 2mm.). Mixtures made by grinding the complexes with dry KCl (or KBr) were also made into pressed discs. The infra-red spectra of all the pressed discs were recorded on a Perkin Elmer 225 double beam instrument. Since it was known that  $K_3Mn(CN)_6$  was a common impurity in  $K_3Mn(CN)_5NO$ , the former complex was also incorporated into a KCl lattice and an i.r. spectrum of the sample in the form of a pressed <sup>disc</sup> was recorded.

In order to check on the presence of any paramagnetic impurities, e.s.r. spectra of the manganese-doped halides were recorded at room temperature and at 77K on a Varian E-3 spectrometer.

The doped halides, in the form of pressed discs, were exposed to  $^{60}Co$   $\gamma$ -irradiation at room temperature for various periods of time ranging from one hour to several days and their i.r. spectra

recorded. A low temperature attachment of the cold finger type<sup>4</sup> was used to record spectra down to about 100K. In most cases an e.s.r. spectrum of the crushed disc was recorded at X-band frequency at room temperature and at 77K. In addition, e.s.r. spectra were obtained for  $\gamma$ -irradiated powders and single crystals containing various concentrations of incorporated pentacyanonitrosyl ions.

Single crystals of the doped halides were also irradiated at liquid nitrogen temperature and transferred without warming to the e.s.r. cavity and their spectra recorded at 77K. They were then removed from the cavity, allowed to warm up for a few seconds to anneal the  $V_k$  centre ( $Cl_2^-$ ) and returned to the cavity for a new spectrum to be obtained. The crystals were not accurately mounted on a goniometer but were placed in an e.s.r. Dewar containing liquid nitrogen so that they could be rotated approximately about one of the unit cell axes (viz. an axis passing through the centres of opposite faces of the KCl cube.) The e.s.r. spectrum of the manganese-doped halide crystal was of sufficient complexity that a complete single-crystal<sup>study</sup> was not performed. However e.s.r. spectra were recorded for a number of different orientations of the crystal.

Attempts were made to dope sodium nitroprusside ions into various alkali halide lattices (viz. KCl, KBr, KI and NaCl) but it was found that the nitroprusside ion, having only a 2-negative charge, did not incorporate very easily into these lattices. Very small amounts went into the potassium halide lattices, however a more appreciable amount did incorporate into a sodium chloride lattice. In order to prepare a pressed disc of this material, it was ground up with an equal amount of potassium chloride, since

discs made from sodium chloride alone tended to crumble. The i.r. spectrum of the pressed disc was obtained prior to and after  $\gamma$ -irradiation.

The doped halides were also exposed to u.v. radiation for various periods of time and their i.r. and e.s.r. spectra recorded.

### Results.

#### a) Before $\gamma$ -irradiation

##### (i) I.R. Results

Table 4.1 shows the main i.r. bands in the solution grown doped halides prior to  $\gamma$ -irradiation. The i.r. spectra of the samples produced by rapid evaporation from aqueous solution are similar to those of samples grown over a period of days by slow evaporation. However, the samples prepared by precipitation with ethanol and those obtained merely by grinding the complex with alkali halide prior to preparing the pressed discs are different. The former show multiplet splittings at the  $\nu(\text{CN})$  and  $\nu(\text{NO})$  stretching frequencies, whereas the latter exhibit only single broad lines at these frequencies. After prolonged grinding, however, other peaks can be observed, which on further grinding become well-resolved and are very similar to those obtained for the solution grown samples.

Figures 4.1 - 4.3 show the i.r. spectra of solution grown pressed discs containing chromium, manganese and iron pentacyano-nitrosyls. The i.r. spectra of KCl doped samples were better resolved than those of samples prepared using KBr.

Table 4.1

Infra-red Absorptions of Complex Ions in KCl Lattices.

i) The Cyanide Stretching Region.

<u>[Mn(CN)<sub>5</sub>NO]<sup>3-</sup></u>	<u>[Cr(CN)<sub>5</sub>NO]<sup>3-</sup></u>	<u>[Fe(CN)<sub>5</sub>NO]<sup>2-†</sup></u>	<u>[Mn(CN)<sub>6</sub>]<sup>3-</sup></u>
2105 m	2120 sh	2170 s	2120 sh
2095 w	2111 s	2164 m	2111 s
2091 w	2107 sh	2154 m	2107 sh
	2104 s	2141 s	2104 s
2087 s			
2083 s	2085 w		2085 w
2075 s	2060 w		2060 w
2069 w	2035 w		2035 w
2067 w	2030 w		2030 w
2060 w			
2033 w			
2029 w			

ii) The Nitrosyl Stretching Region.

1830 w	1710 sh	1940 vs
1820 w	1690 s	
1805 sh	1660 s	
1795 sh	1645 s	
1776 vs	1640 sh	
1755 s		
1736 m		
1730 sh		

All frequencies in cm<sup>-1</sup>

† : [Fe(CN)<sub>5</sub>NO]<sup>2-</sup> in an NaCl lattice with added KCl.

Figure 4.1 I.R. Spectrum of  $[\text{Cr}(\text{CN})_5\text{NO}]^{3-}$  in KCl.

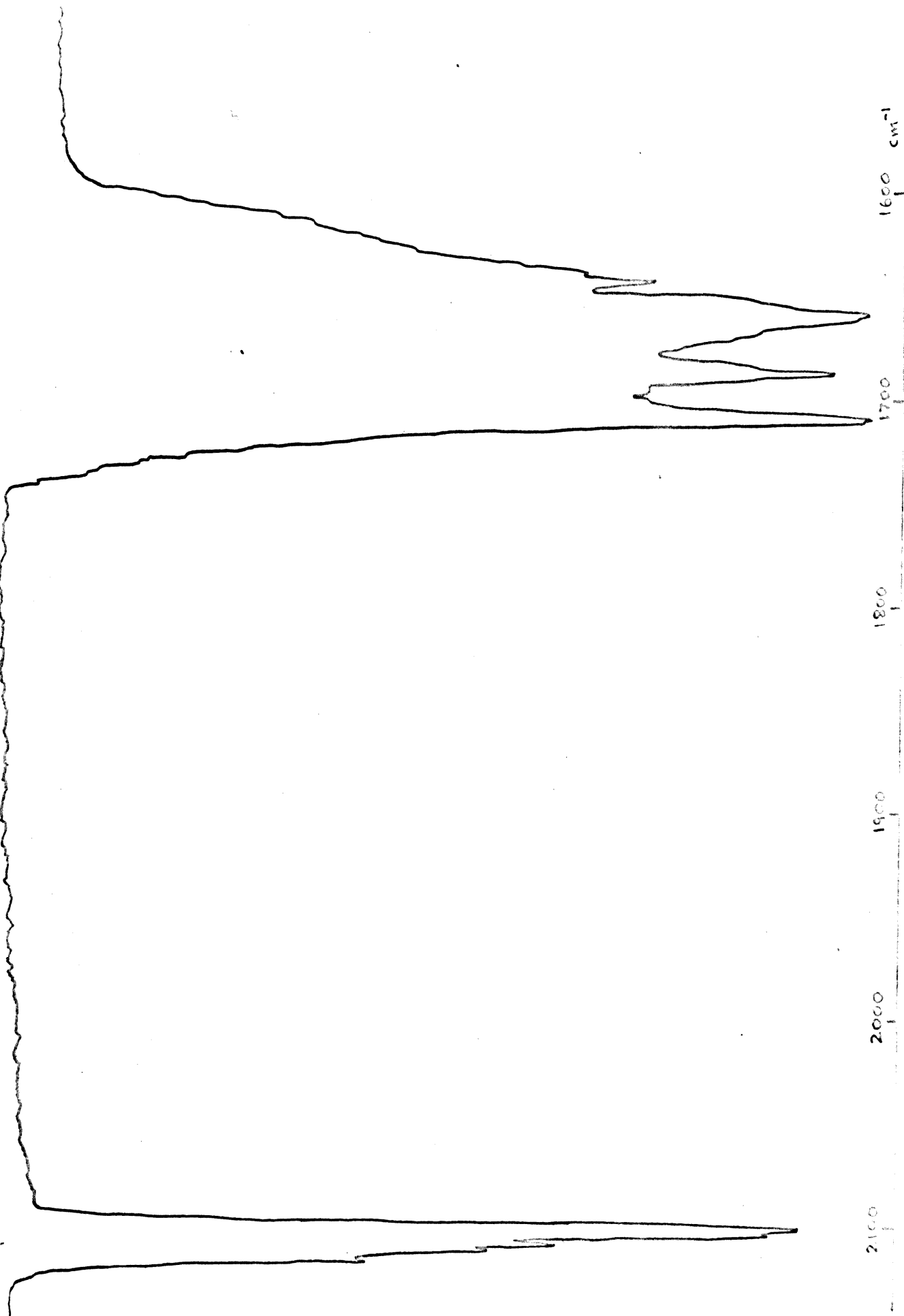


Figure 4.2 I.R. Spectrum of  $[\text{Mn}(\text{CN})_5\text{NO}]^{3-}$  in KCl.

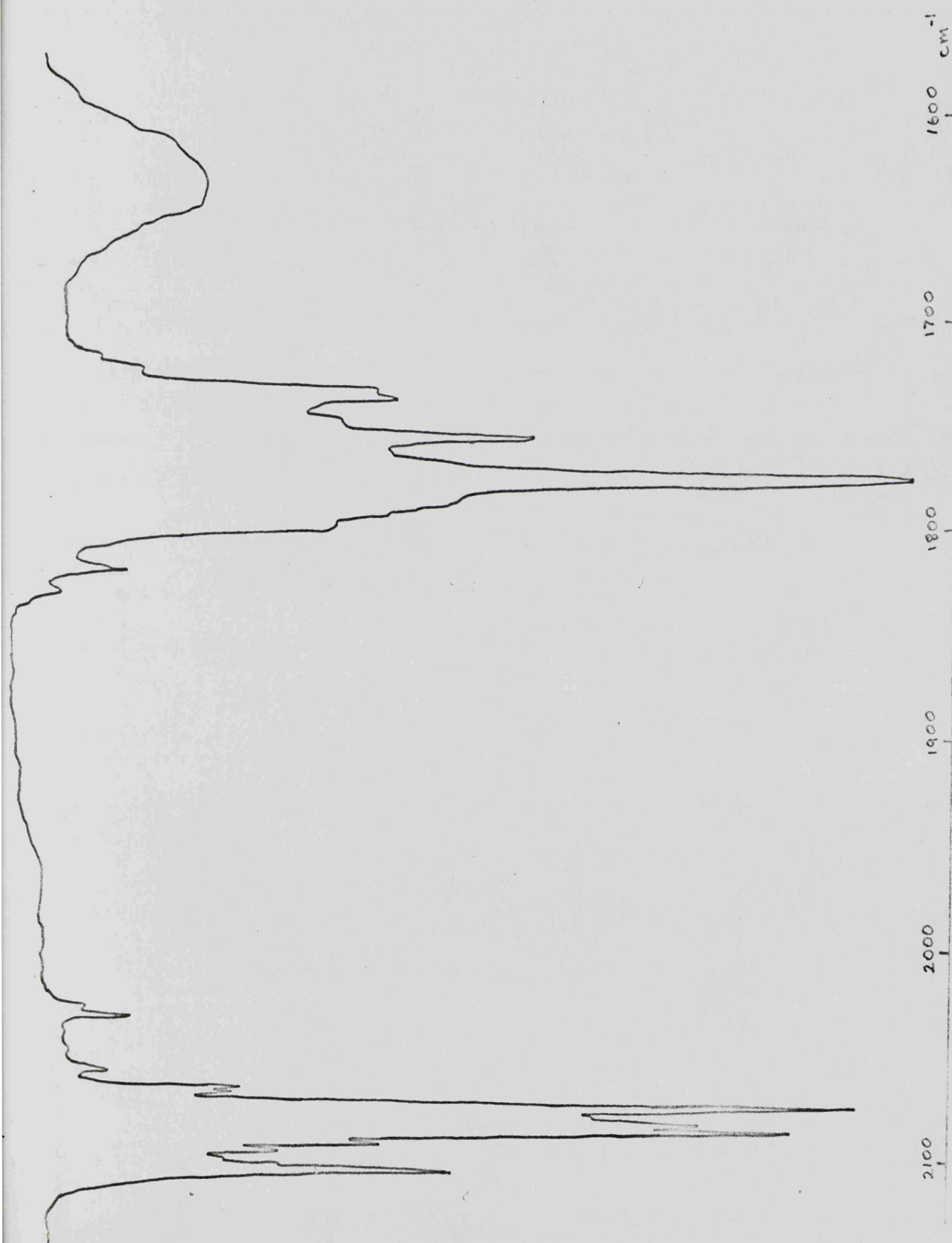
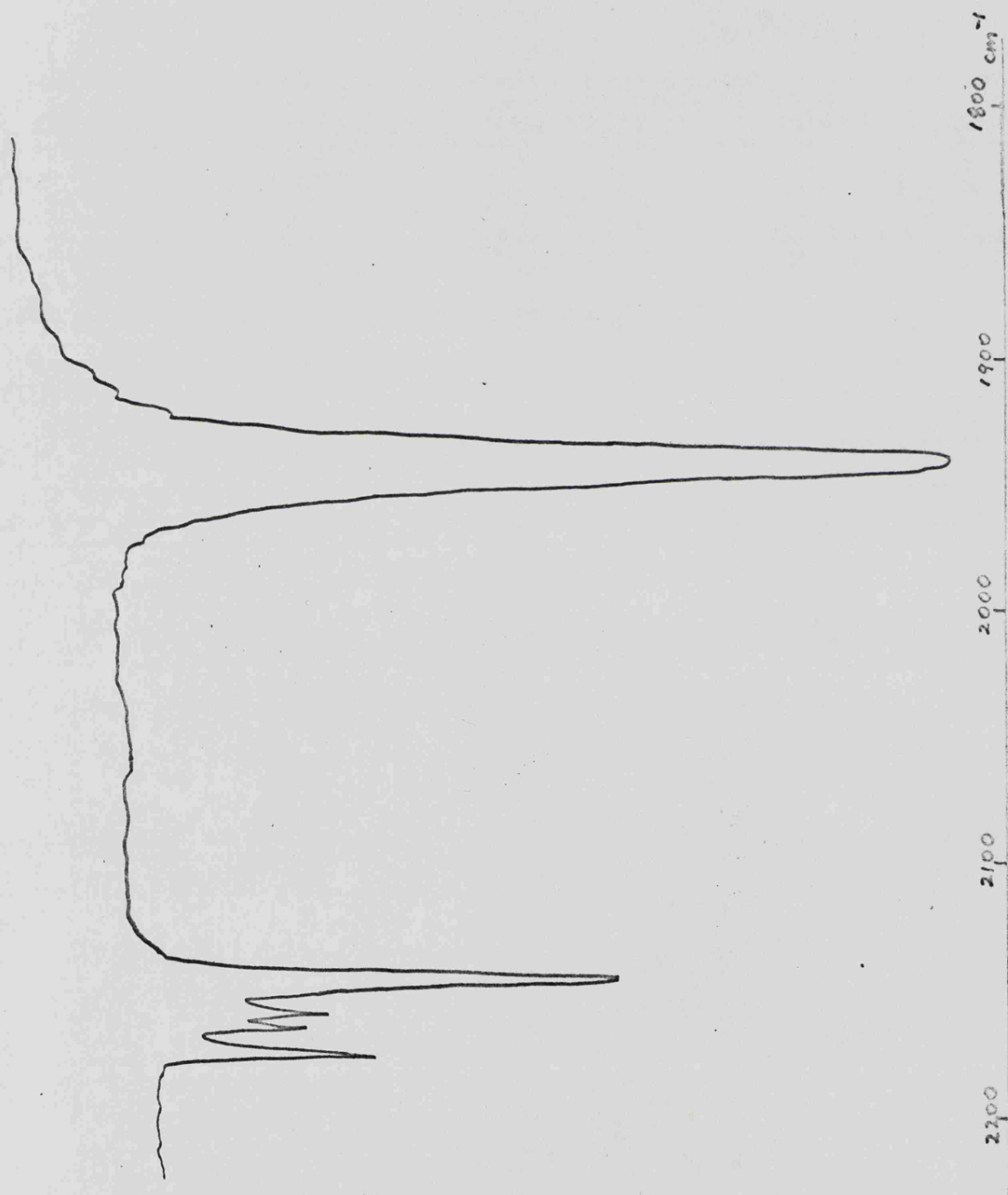


Figure 4.3

I.R. Spectrum of  $[\text{Fe}(\text{CN})_5\text{NO}]^{2-}$  in NaCl/KCl.



The spectra of pressed discs containing  $[\text{Mn}(\text{CN})_5\text{NO}]^{3-}$  showed the presence of small amounts of  $[\text{Mn}(\text{CN})_6]^{3-}$  as impurity. In addition the i.r. spectra of all the pressed discs showed that water was present in varying amounts in the alkali halide lattices.

(ii) E.S.R. Results

The e.s.r. spectra of a single crystal and a polycrystalline sample of KCl doped with  $[\text{Cr}(\text{CN})_5\text{NO}]^{3-}$  are illustrated in Figure 4.4<sup>19\*</sup>. This ion is well characterised and has been reported in a KCl lattice by Kuska and Rogers.<sup>5</sup>

The e.s.r. spectra of KCl samples doped with  $[\text{Mn}(\text{CN})_5\text{NO}]^{3-}$  and  $[\text{Mn}(\text{CN})_6]^{3-}$  did not reveal the presence of any paramagnetic impurities at normal receiver gain. At very high receiver gain and using high modulation however, broad poorly resolved features were observed showing that very small amounts of paramagnetic impurity were present. In view of their exceedingly low concentration these were not investigated further. E.s.r. examination of samples doped with sodium nitroprusside showed them to be free from paramagnetic impurities.

b) After Irradiation.

(i) I.R. Results

When the pressed discs were  $\gamma$ -irradiated at room temperature for a few hours, new bands appeared in their i.r. spectra on the low energy side of the main cyanide and nitrosyl stretching bands, with a concomitant decrease in intensity of these original bands. Figures 4.4 - 4.6 show the i.r. bands which appeared in KCl and KBr

\* following p 85

Figure 4.4 I.R. Spectrum of  $[\text{Mn}(\text{CN})_5\text{NO}]^{3-}/\text{KCl}$   
After 12 hours  $\gamma$ -Irradiation.

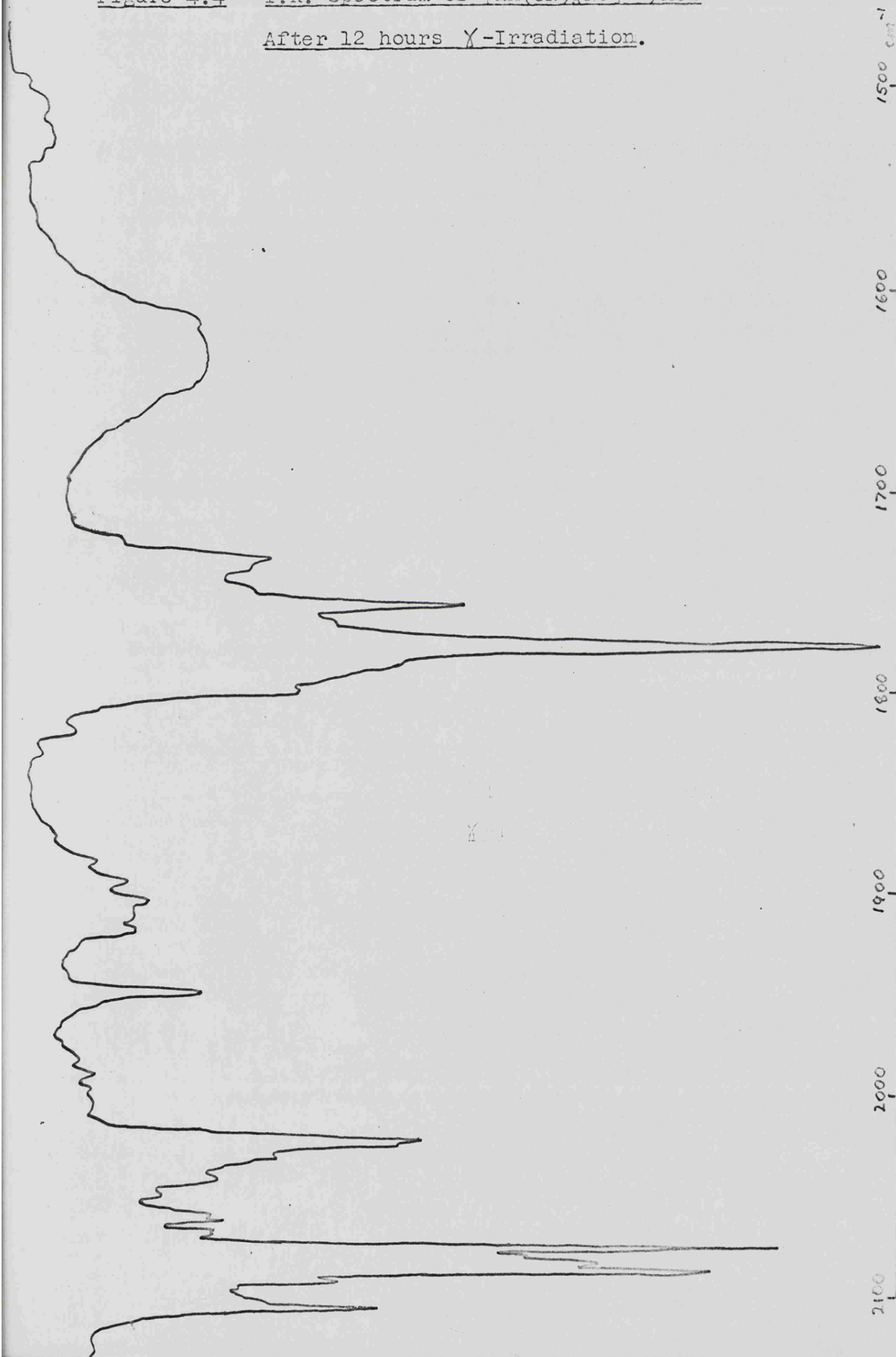
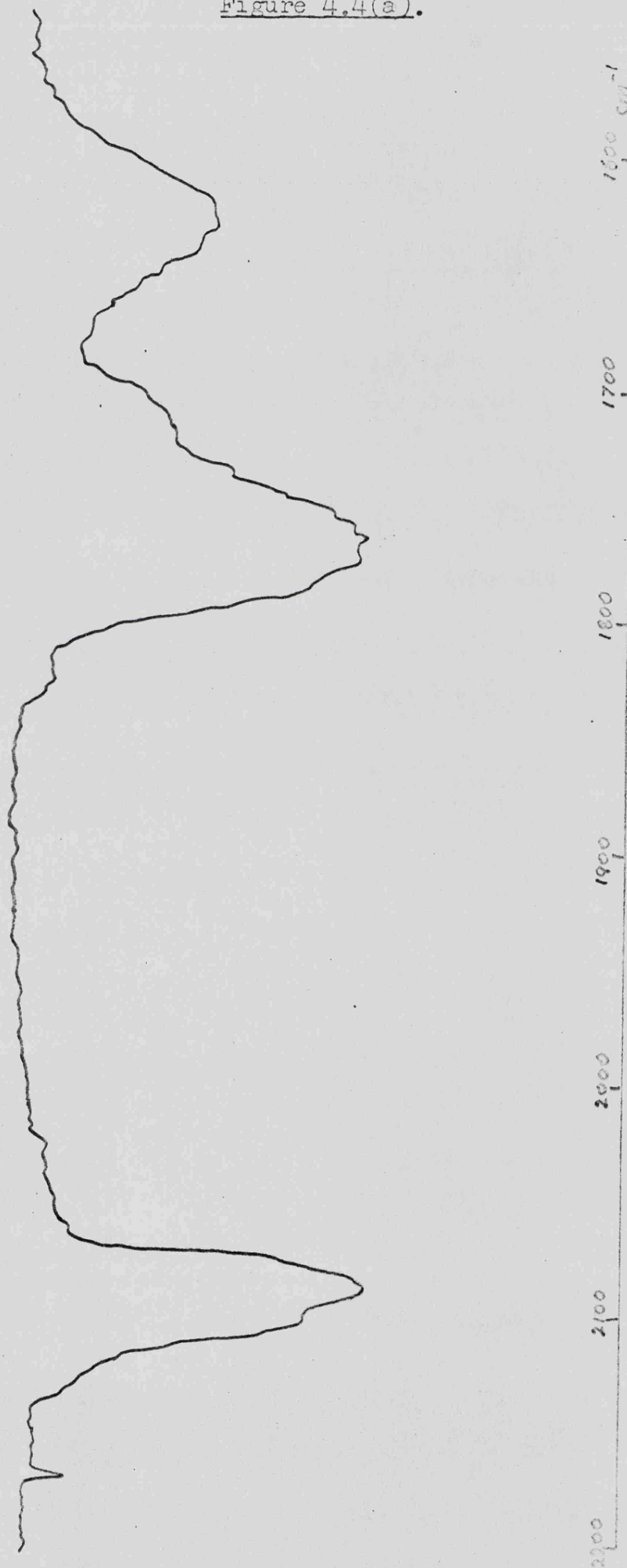


Figure 4.4(a).



I.R. Spectrum of  $[\text{Mn}(\text{CN})_5\text{NO}]^{3-}$  /KBr After 12 hours  $\gamma$ -Irradiation.

Figure 4.5

I.R. Spectrum of  $[\text{Mn}(\text{CN})_6]^{3-}$  in KCl.



Figure 4.5(a) I.R. Spectrum of  $[\text{Mn}(\text{CN})_6]^{3-}/\text{KCl}$   
After 12 hours  $\gamma$ -Irradiation.

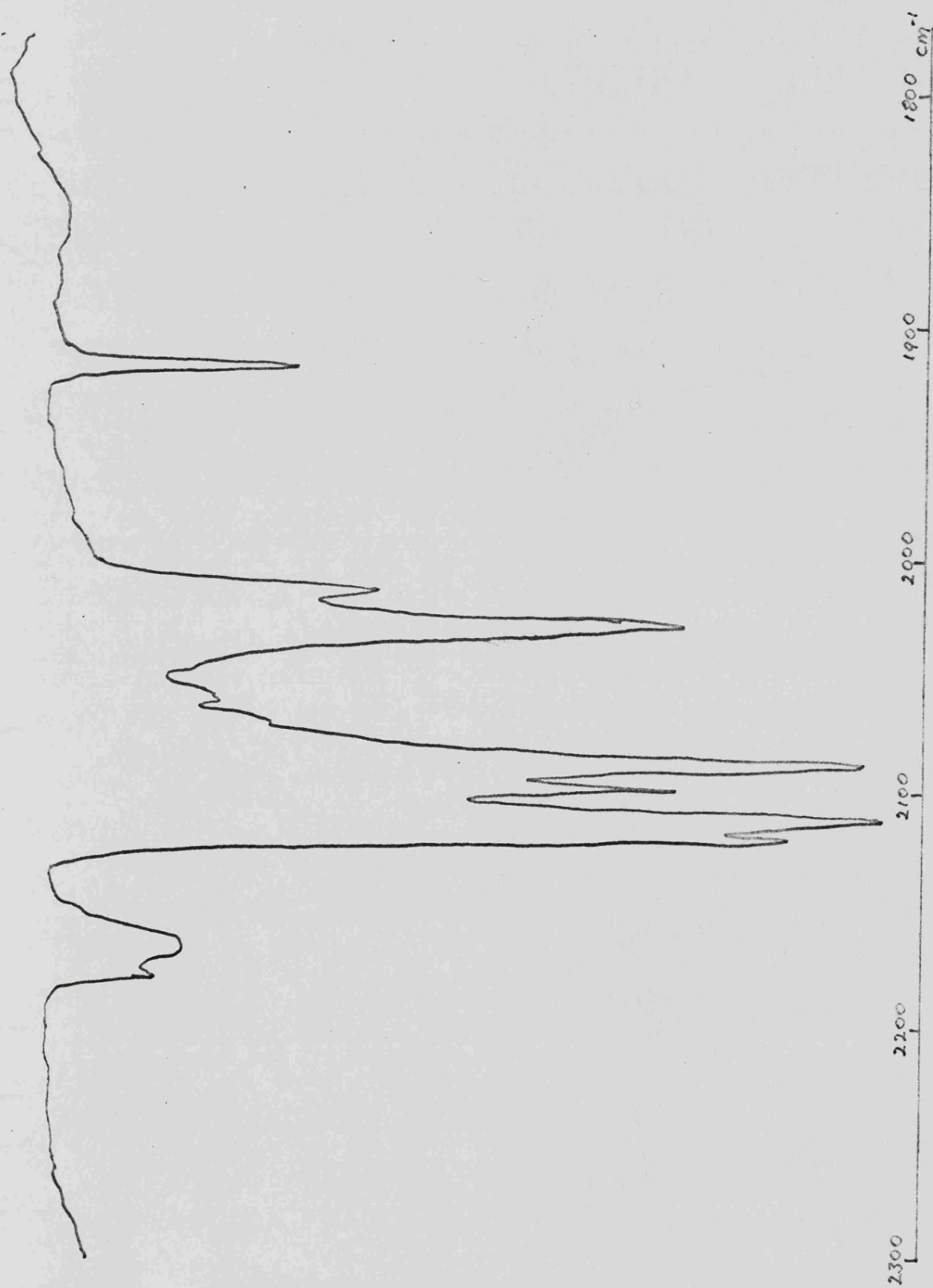
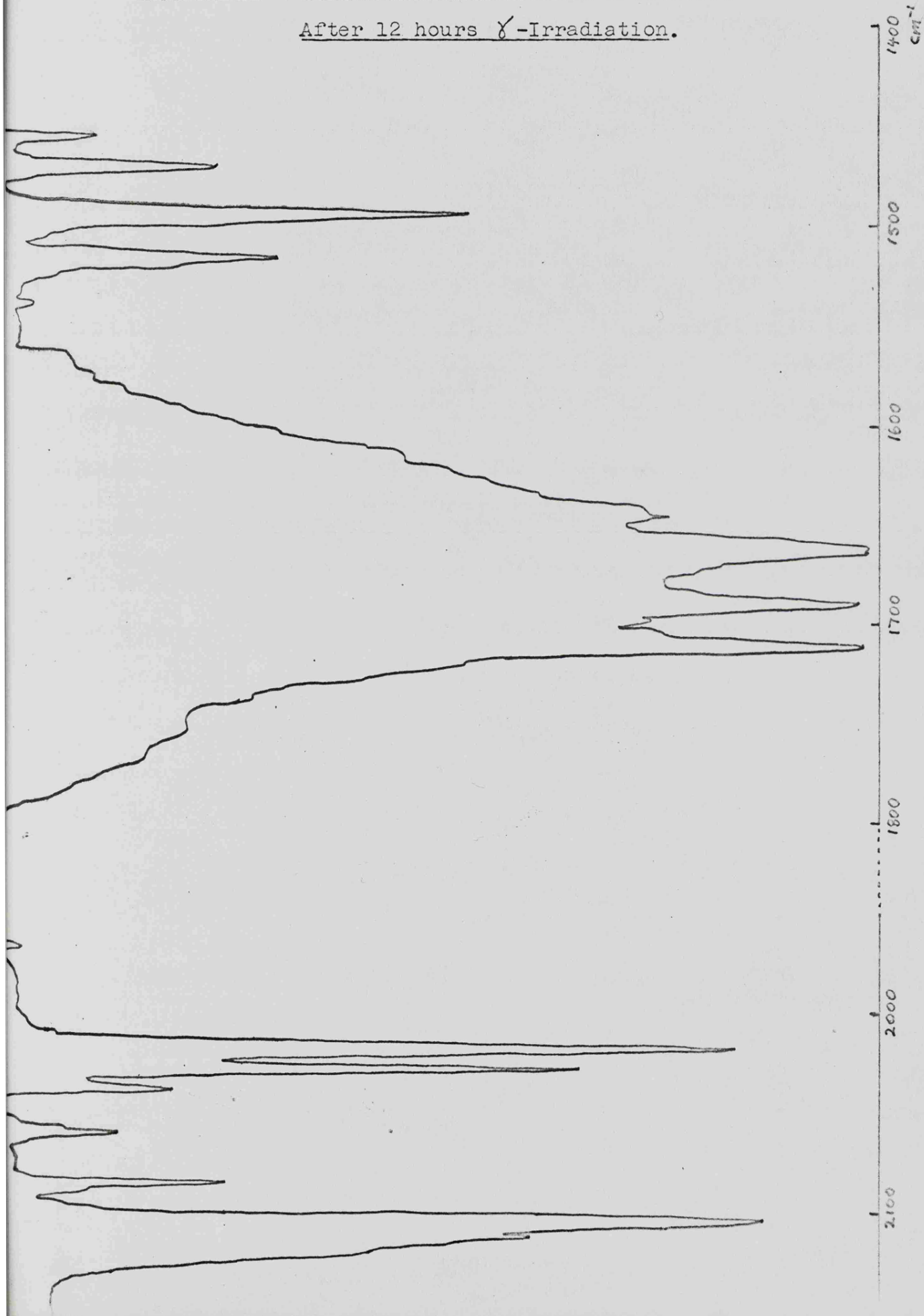


Figure 4.6 I.R. Spectrum of  $[\text{Cr}(\text{CN})_5\text{NO}]^{3-}/\text{KCl}$   
After 12 hours  $\gamma$ -Irradiation.

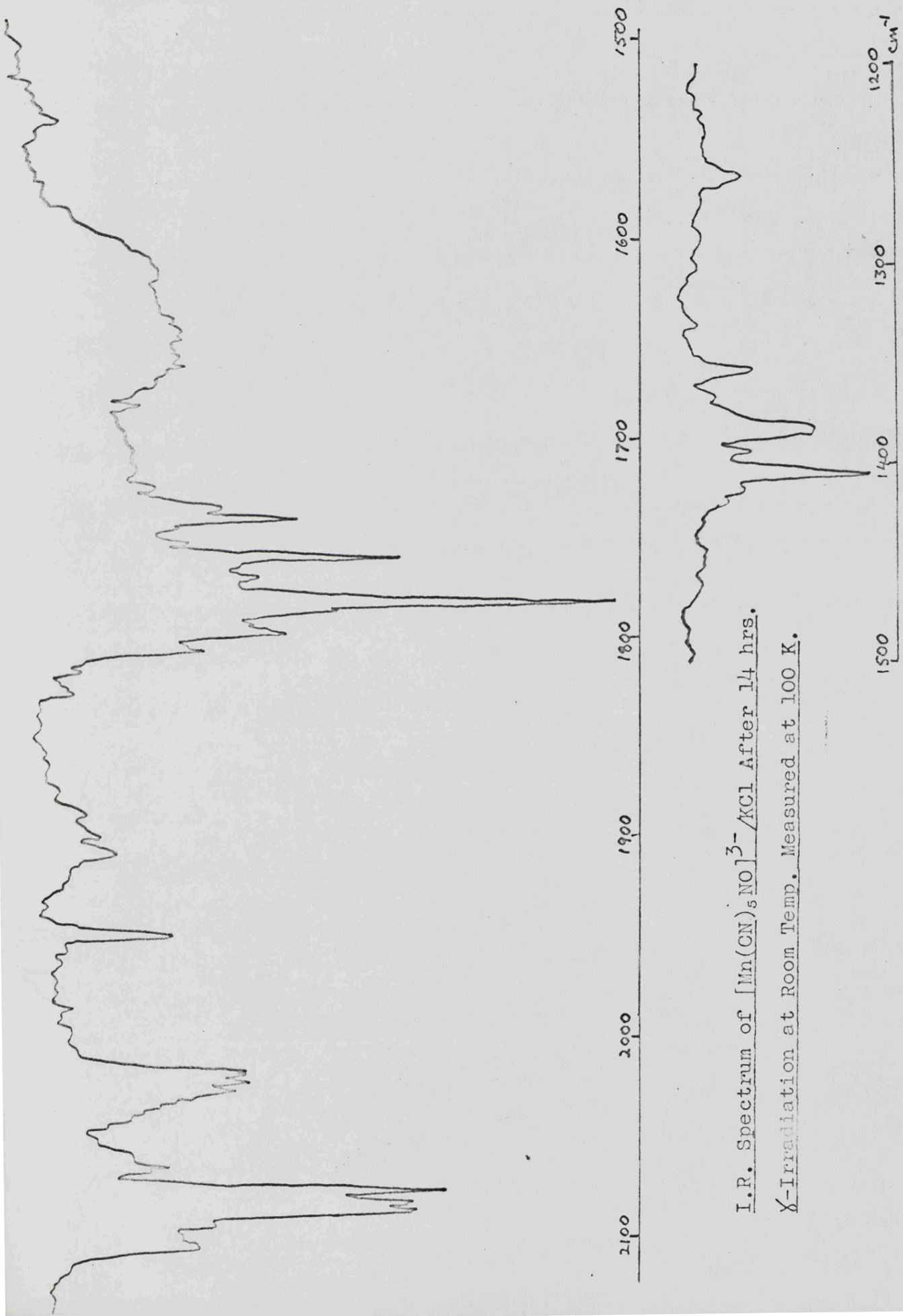


discs containing  $[\text{Mn}(\text{CN})_5\text{NO}]^{3-}$ ,  $[\text{Mn}(\text{CN})_6]^{3-}$  and  $[\text{Cr}(\text{CN})_5\text{NO}]^{3-}$  after approximately 12 hours irradiation. Figures 4.7 and 4.8 show the low temperature i.r. spectra (measured at 100 K) of KCl discs containing  $[\text{Mn}(\text{CN})_5\text{NO}]^{3-}$  and  $[\text{Cr}(\text{CN})_5\text{NO}]^{3-}$  which were irradiated at room temperature for 14 hours. Figure 4.9 shows the spectrum of a disc containing sodium nitroprusside incorporated into NaCl, after 24 hours irradiation. The positions of the radiation-induced i.r. bands are given in Table 4.2.

In the case of  $[\text{Cr}(\text{CN})_5\text{NO}]^{3-}$  in KCl, the radiation-induced bands in the cyanide and nitrosyl stretching region were most intense; the new  $\nu(\text{CN})$  band after 12 hours irradiation being of comparable intensity and sharpness to the original  $\nu(\text{CN})$  band, which only imperceptibly decreased in intensity. The original  $\nu(\text{NO})$  band, however, overlapped with a broad, lattice-water band and was hence broadened itself. Because of this we cannot, therefore, compare intensities of the original and new  $\nu(\text{NO})$  bands. After 48 hours the new  $\nu(\text{CN})$  band was slightly more intense than the original band, which now showed definite signs of weakening. The new  $\nu(\text{NO})$  band was now of comparable intensity to the original  $\nu(\text{NO})$  plus  $\delta(\text{H-O-H})$  bands. The rate of formation of new cyanide and nitrosyl bands "tailed off" after about 48 hours irradiation time.

In the case of  $[\text{Mn}(\text{CN})_5\text{NO}]^{3-}$  in KCl, the radiation-induced bands were less intense than those produced in the irradiated chromium complex; the new  $\nu(\text{CN})$  band never reaching the intensity of the original band even after several days irradiation. There is some ambiguity over the assignment of the radiation-induced  $\nu(\text{NO})$  band, since there happens to be a broad, lattice-water band in the probable vicinity of the expected  $\nu(\text{NO})$  band (around  $1630\text{cm}^{-1}$ ).

Figure 4.7



I.R. Spectrum of  $[\text{Mn}(\text{CN})_5\text{NO}]^{3-}/\text{KCl}$  After 14 hrs.

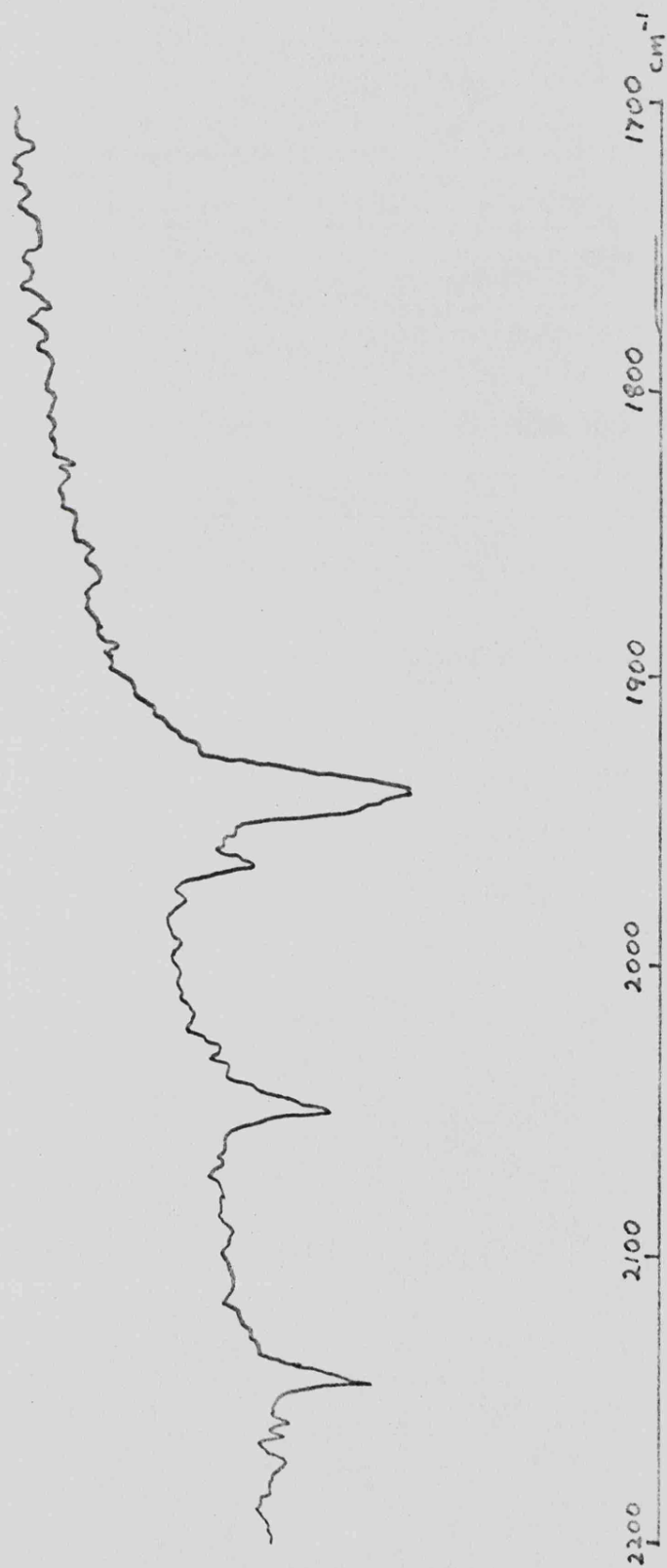
X-Irradiation at Room Temp. Measured at 100 K.

Figure 4.8 I.R. Spectrum of  $[\text{Cr}(\text{CN})_5\text{NO}]^{3-}$  After 14 hrs.

$\gamma$ -Irradiation at Room Temp. Measured at 100 K.



Figure 4.9



I.R. Spectrum of  $[\text{Fe}(\text{CN})_5\text{NO}]^{2-} \text{NaCl}$  After 24 hours  $\gamma$ -Irradiation.

Table 4.2

Positions of Radiation-Induced Infra-red Bands  
for Complex Ions in KCl Lattices.

<u>[Mn(CN)<sub>5</sub>NO]<sup>3-</sup></u>	<u>[Cr(CN)<sub>5</sub>NO]<sup>3-</sup></u>	<u>[Fe(CN)<sub>5</sub>NO]<sup>2-</sup></u>	<u>[Mn(CN)<sub>6</sub>]<sup>3-</sup></u>
2050 w	2085 m	2050 m	1920 m
2040 w	2056 m	1965 m	
2030 m			
2020 sh	2040 m		
2017 s	2035 s		
	2025 s		
1950 m	2016 sh		
1920 w	1965 w		
1905 w			
1895 w	1535 w		
1883 w	1520 m		
	1492 s		
1620 w	1470 m		
1525 w	1454 m		
1405 w	1405 w		
1395 w	1395 w		
1380 w	1385 w		
	1257 w		

After 48 hrs  $\gamma$ -irradiation all complexes yielded peaks at 2182 and 2170  $\text{cm}^{-1}$  in KCl lattices.

However, there is also a band at approximately  $1525\text{cm}^{-1}$ , which, although rather weak, could be a new  $\nu(\text{NO})$  band. The rate of formation of new cyanide and nitrosyl bands appeared to tail off after about 24 hours irradiation time.

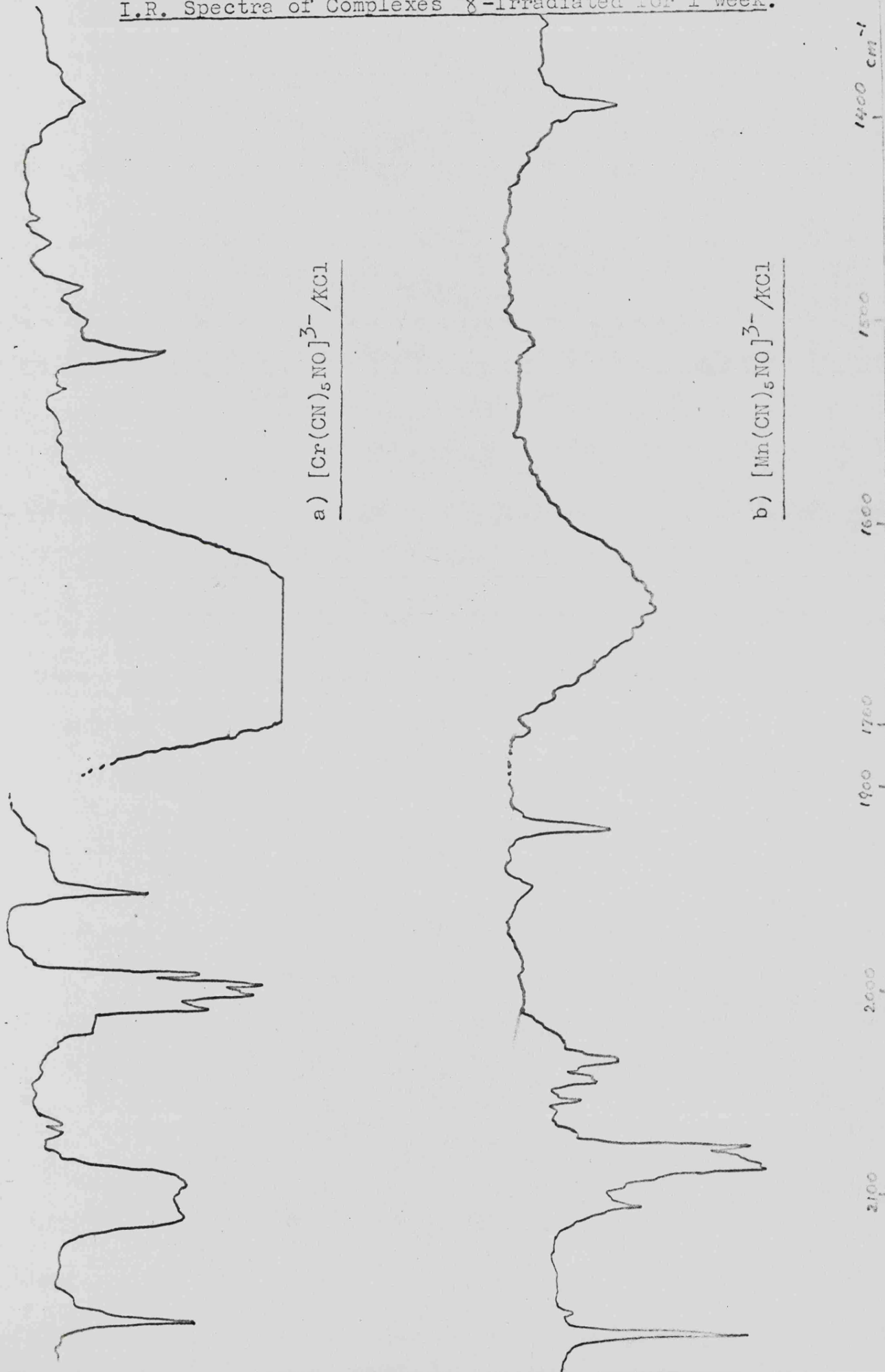
In the case of  $[\text{Fe}(\text{CN})_5\text{NO}]^{2-}$  in NaCl, the i.r. spectrum showed a sharp new band in the cyanide stretching region after twenty-four hours irradiation, but new bands in the nitrosyl stretching region could not be detected even after several days irradiation.

After prolonged irradiation further lines appeared in the i.r. spectrum of the doped halides, notably one at  $2182\text{cm}^{-1}$  in KCl discs and at  $2170\text{cm}^{-1}$  in KBr discs. This shift is characteristic of an isolated cyanate ion in alkali halide lattices<sup>6</sup>. In addition, a broad peak centred around  $1400\text{cm}^{-1}$  appeared after several days  $\gamma$ -irradiation in discs containing all three pentacyanonitrosyl anions. Figure 4.10 shows the i.r. spectra of discs which had been irradiated for approximately one week.

In the particular case of  $[\text{Mn}(\text{CN})_5\text{NO}]^{3-}$  in KCl, some additional unexplained lines were observed in the i.r. spectrum of the irradiated sample. For example, a line at  $1950\text{cm}^{-1}$  was quite intense after about 12 hours irradiation, but on prolonged irradiation it gradually decayed until it could no longer be detected after about 10 days irradiation. On the other hand, a band at  $1920\text{cm}^{-1}$ , which was weak initially, continued to grow on prolonged irradiation, while the band at  $2185\text{cm}^{-1}$ , attributed to the cyanate ion simultaneously grew and reached a higher intensity in a shorter time than it did in the other irradiated complexes. This indicates that there may be a line underneath the latter band which could accompany the line at  $1920\text{cm}^{-1}$ .

Figure 4.10

I.R. Spectra of Complexes  $\gamma$ -Irradiated for 1 week.



The spectrum of an irradiated KBr disc containing  $[\text{Mn}(\text{CN})_5\text{NO}]^{3-}$  was quite different from that obtained using KCl. There were no new bands in the cyanide or nitrosyl stretching region even after several days irradiation. The only new features observed were a sharp peak at  $2170 \text{ cm}^{-1}$  attributed to  $\text{CNO}^-$  and a weak, broad peak centred around  $1390 \text{ cm}^{-1}$ .

The spectra of irradiated KBr discs containing  $[\text{Cr}(\text{CN})_5\text{NO}]^{3-}$  were similar to those obtained using KCl, although the lines were shifted slightly due to lattice effects. The fundamental difference between the spectra in KCl and KBr discs concerns a line at approximately  $1960 \text{ cm}^{-1}$ . In KCl this line is at  $1965 \text{ cm}^{-1}$  and is seen as a weak feature after about 12 hours irradiation but grows on continued irradiation. In KBr, however, this line is at  $1961 \text{ cm}^{-1}$  and is quite intense after about 12 hours irradiation and does not continue to grow on prolonged irradiation.

Ultra-violet irradiation of KCl discs produced similar peaks to those observed after  $\gamma$ -irradiation. However no band at  $2182 \text{ cm}^{-1}$  appeared even after several days of irradiation. The effect of  $\gamma$ -irradiation on the three pentacyanonitrosyl ions, measured by the formation of new i.r. bands, increased in the order  $\text{Fe} < \text{Mn} < \text{Cr}$ . This is in contrast with the effect of u.v. radiation where the rate of formation of new i.r. bands increased in the converse order i.e.  $\text{Cr} < \text{Mn} < \text{Fe}$ .

(ii) E.S.R. Results.

1. Manganese: When a polycrystalline sample of KCl containing 0.05%  $[\text{Mn}(\text{CN})_5\text{NO}]^{3-}$  was  $\gamma$ -irradiated at room temperature for 24 hours the e.s.r. spectrum recorded at X-band frequency at 298 K showed the presence of two species (A and B), both of

which had isotropic hyperfine lines characteristic of the unpaired electron interacting with a nucleus of spin  $I = 5/2$ . One set of six lines (corresponding to species A) was broad and reached its maximum intensity after approximately 48 hours irradiation, whereafter it steadily diminished in intensity on further irradiation. The second set of six lines (corresponding to species B) was somewhat sharper and continued to grow on prolonged irradiation at the expense of the first set. The e.s.r. parameters for these two species and other radiation-induced paramagnetic centres are set out in Table 4.3.

When a polycrystalline sample of KCl containing 0.01%  $[\text{Mn}(\text{CN})_5\text{NO}]^{3-}$  was  $\gamma$ -irradiated for approximately 2 weeks the e.s.r. spectrum showed only the presence of species B.

In addition to species A and B, e.s.r. spectra of the irradiated polycrystalline samples showed the presence of two radicals which did not appear to be interacting with a metal nucleus :

When a polycrystalline sample of KCl containing approximately 0.01% dopant was irradiated for one week, the e.s.r. spectrum, recorded at room temperature, showed the presence of an isotropic triplet of lines ( $g \doteq 2$ ,  $A = 21\text{G}$ ), attributed to a species, (C), where the unpaired electron is interacting with a single nucleus of spin  $I = 1$ .

When a powder sample containing approximately 0.05% dopant was irradiated for a similar period of time, the e.s.r. spectrum showed, in addition to species A and B, a quintet of lines ( $g \doteq 2$ ,  $A = 12.5\text{G}$ ) whose intensities were approximately in the ratio 1:2:3:2:1. This is characteristic of an unpaired electron

Table 4.3 ESR Parameters for Species Formed in Irradiated, Manganese-doped Alkali Halides, and the Mn<sup>2+</sup> Ion.

<u>Radical (Ion)</u>	<u>g<sub>iso</sub></u>	<u>A<sub>iso</sub>(<sup>55</sup>Mn)</u>	<u>A<sub>iso</sub>(<sup>14</sup>N)</u>	<u>Ref.</u>
Species A	2.000	105.5 G	-	a
Species B	2.004	95.5 G	-	a
[Mn(H <sub>2</sub> O) <sub>6</sub> ] <sup>2+</sup>	2.004	95.2 G	-	a
Mn <sup>2+</sup> /NaF	2.002	95.0 G	-	20-24
Mn <sup>2+</sup> /LiF	2.000	90.0 G	-	20-24
Species C	2.006	-	21.5 G	a
Species D	2.003	-	12.5 G	a
Species E	g <sub>1</sub> = 2.1112	A <sub>1</sub> = (unresolved)		
	g <sub>2</sub> = 2.0106	A <sub>2</sub> = 12 G		b
	g <sub>3</sub> = 2.0028	A <sub>3</sub> = 12 G		

a. This work      γ-irradiated [Mn(CN)<sub>5</sub>NO]<sup>3-</sup>/KCl

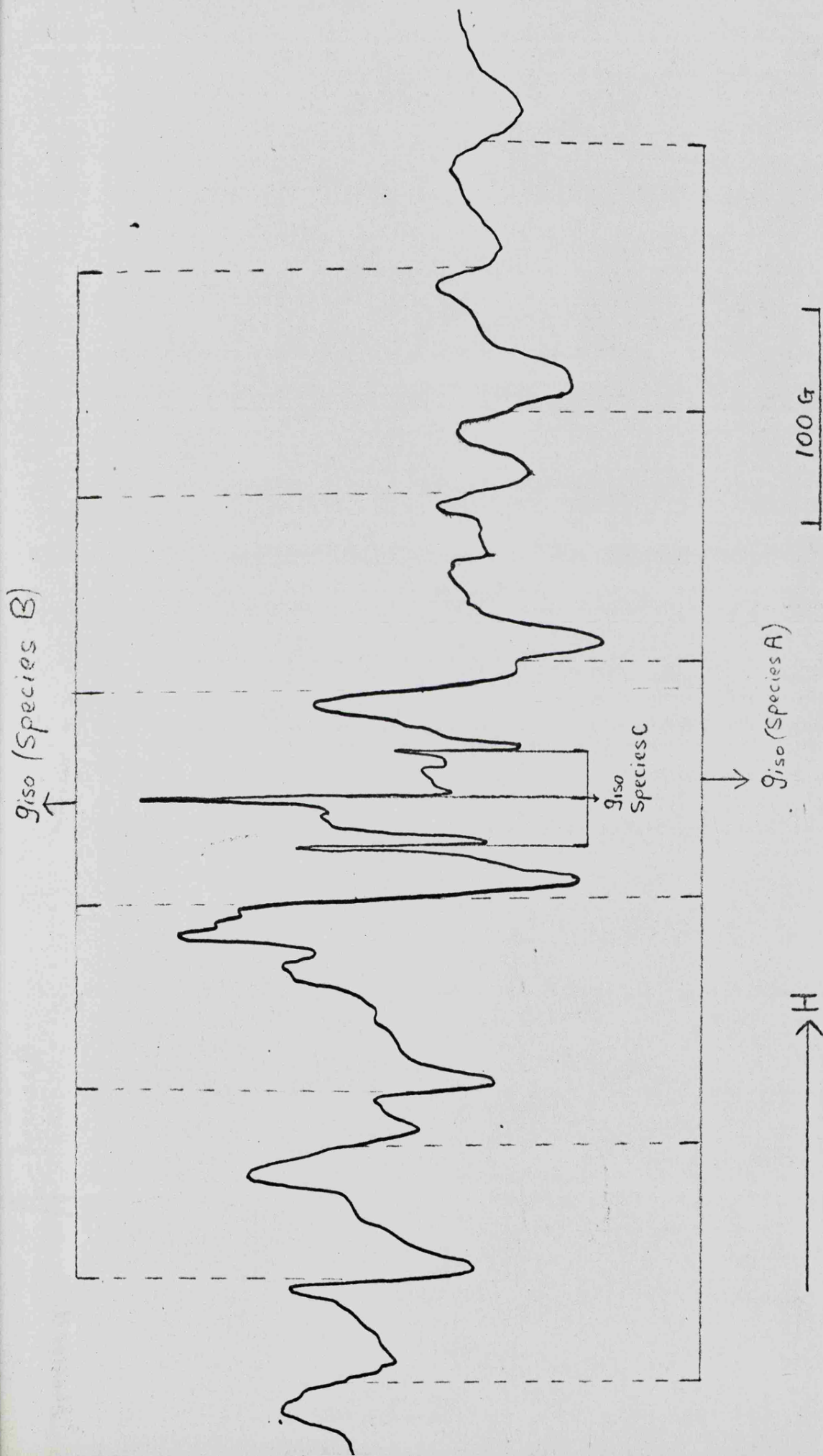
b. This work      γ-irradiated [Mn(CN)<sub>6</sub>]<sup>3-</sup>/KCl

interacting with two equivalent nuclei of spin  $I = 1$ . These lines were sharp and appeared to be the parallel features of a species with axial symmetry (species D). However, measurements on a single crystal irradiated for a few days at room temperature, showed that these lines were completely isotropic.

The e.s.r. spectra of 0.01% and 0.05% doped polycrystalline samples of  $[\text{Mn}(\text{CN})_5\text{NO}]^{3-}$  in KCl,  $\gamma$ -irradiated for one week at room temperature, are shown in Figure 4.11.

When a single crystal of KCl doped with approximately 0.05%  $\text{Mn}(\text{CN})_5\text{NO}^{3-}$  was irradiated at room temperature for twelve hours, the e.s.r. spectrum showed the presence of a species with axial symmetry and hyperfine coupling characteristic of an unpaired electron interacting with manganese, whose nuclear spin equals  $5/2$ . The e.s.r. parameters for this species are similar to those reported<sup>7,8,9</sup> for the  $d^5$  ion  $[\text{Mn}(\text{CN})_5\text{NO}]^{2-}$ , (see Table 4.4), which we shall refer to simply as 'the  $d^5$  ion'. On further irradiation the lines due to this species decayed somewhat, with the simultaneous appearance of the isotropic lines due to species A and B. These isotropic lines completely dominated the spectrum, recorded at room temperature, after approximately four days irradiation. The spectrum of the  $d^5$  ion, although observed in the crystal, was not observed in the polycrystalline sample irradiated at room temperature since the concentration of radicals was too low. (Whereas a low concentration of radicals may be readily seen in the single crystal, the effect of grinding it into a powder is to smear out the spectrum so that the signal to noise ratio may be sufficiently reduced, as appears to be the case here, that the spectrum cannot be detected above the noise.) The e.s.r. spectra of

Figure 4.11



ESR Powder Spectrum of 0.01% Doped  $[\text{Mn}(\text{CN})_6]^{3-}$  in KCl X-Irradiated for

Approximately 7 days at Room Temperature.

Figure 4.11(a)

Powder Spectrum of 0.05% Doped  $[\text{Mn}(\text{CN})_5\text{NO}]^{3-}/\text{KCl}$   
 $\gamma$ -Irradiated for 7 days at Room Temperature.

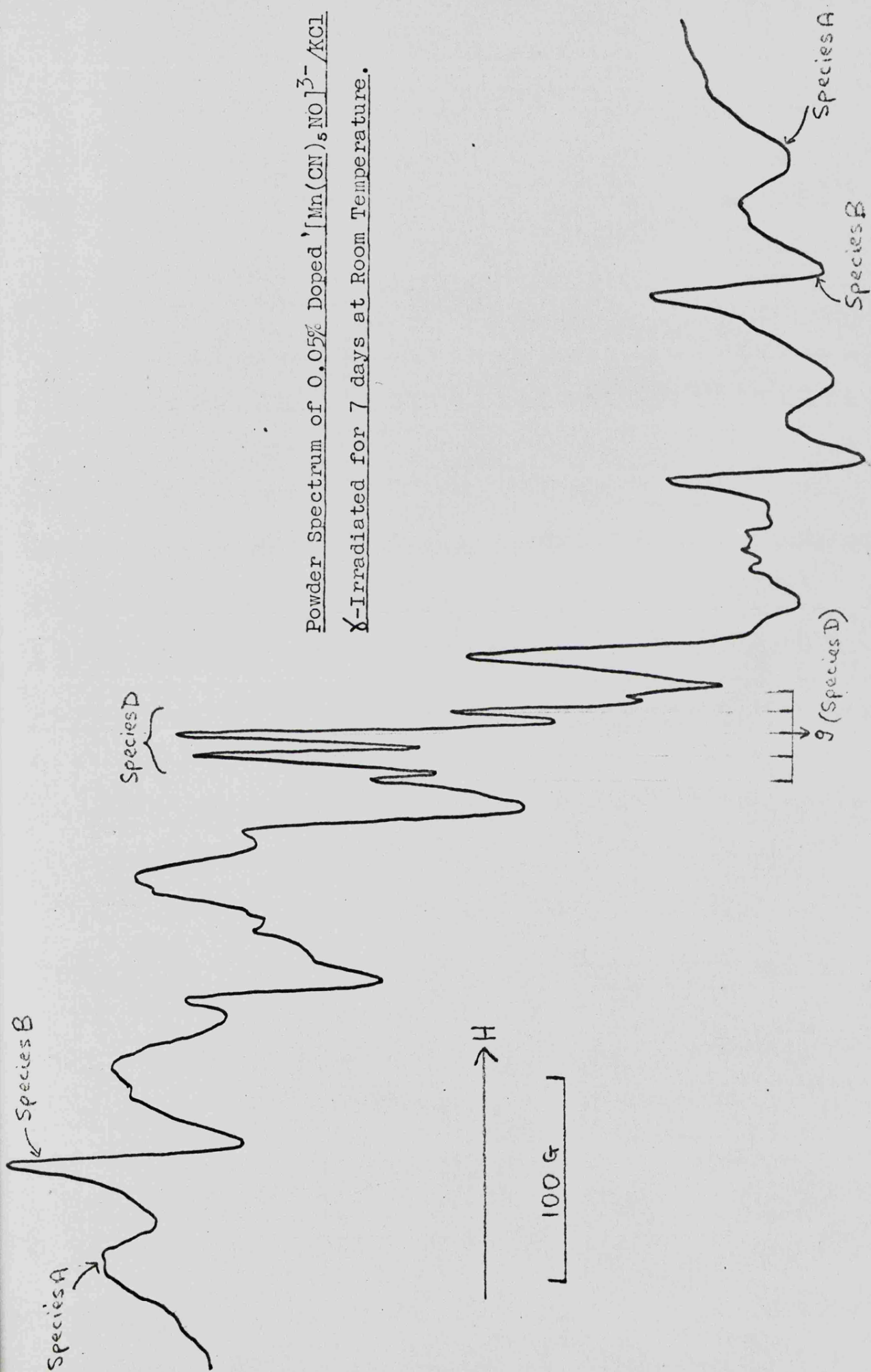


Table 4.4 ESR Data for the  $d^5$   $[\text{Mn}(\text{CN})_5\text{NO}]^{2-}$  Ion.

	$g_{\parallel}$	$g_{\perp}$	$A_{\parallel}(\text{}^{55}\text{Mn})$	$A_{\perp}(\text{}^{55}\text{Mn})$	$A_{\parallel}(\text{}^{14}\text{N})$	$A_{\perp}(\text{}^{14}\text{N})$	Reference
Powder	1.9873	2.0279	164.2	34.0	-	-	7
Crystal	1.9922	2.0311	160.0	36.6	1.9	4.8	8
Crystal	1.9892	2.0265	162.2	38.3	1	4.4	9
Powder	1.989	2.027	164	37			This work

All hyperfine values in gauss

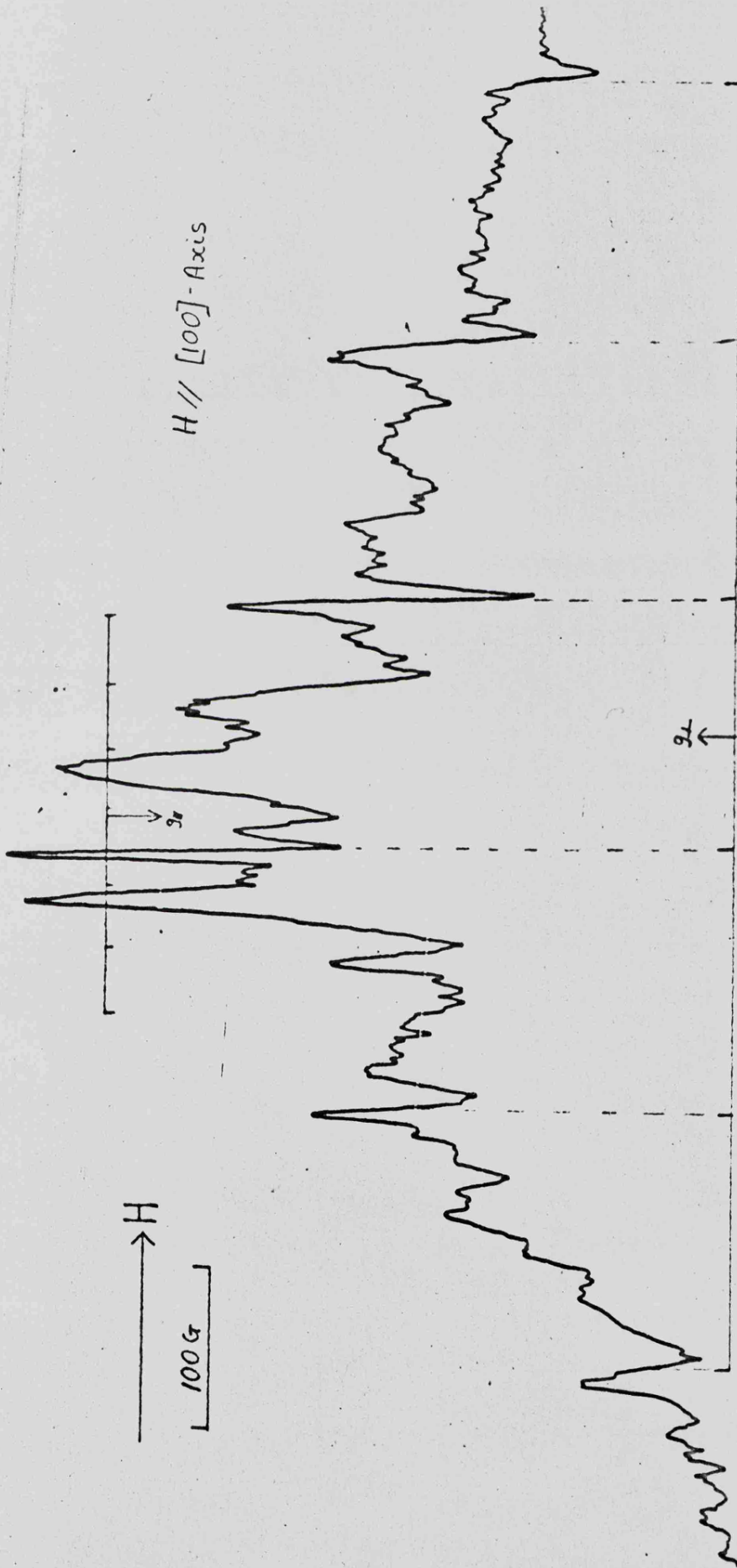
a single crystal irradiated at room temperature for 12 hours and 4 days are shown in Figure 4.12.

When a single crystal of KCl containing  $[\text{Mn}(\text{CN})_5\text{NO}]^{3-}$  was irradiated at liquid nitrogen temperature for approximately 48 hours, the e.s.r. spectrum of the unwarmed sample, measured at 77K, comprised a very large number of lines. (Figure 4.13). The species responsible for these lines is the  $V_k$  centre ( $\text{Cl}_2^-$ ) which has been reported previously in a potassium chloride lattice<sup>10</sup>.

In view of the difficulty in precisely mounting the crystal at 77 K on a goniometer, the experimental axis of rotation did not exactly coincide with the intended  $[100]$ -axis. As a result of this approximate setting, the complexity of the spectrum increased considerably, thus making it virtually impossible to analyse the spectrum for the presence of any underlying features which might have been attributed to a manganese ion for example. However the e.s.r. spectrum of an unwarmed polycrystalline sample, recorded at 77 K, was greatly simplified and therefore much easier to interpret. This spectrum (Figure 4.14) showed sets of axially symmetric septets, the most prominent of which had hyperfine coupling parameters (to the  $^{35}\text{Cl}$  nucleus), which agreed well with the values of  $A_{\parallel} = 101$  G and  $A_{\perp} = 12.5$  G reported by Castner and Kanzig<sup>10</sup> for the  $V_k$  centre. There did not appear to be any features which could be assigned to a manganese complex in this spectrum. However, since this spectrum was of a polycrystalline sample, any lines due to a paramagnetic manganese species in low concentration may have been obscured by noise.

When the single crystal was warmed to room temperature for a few seconds, the intense violet colour of the crystal was visibly

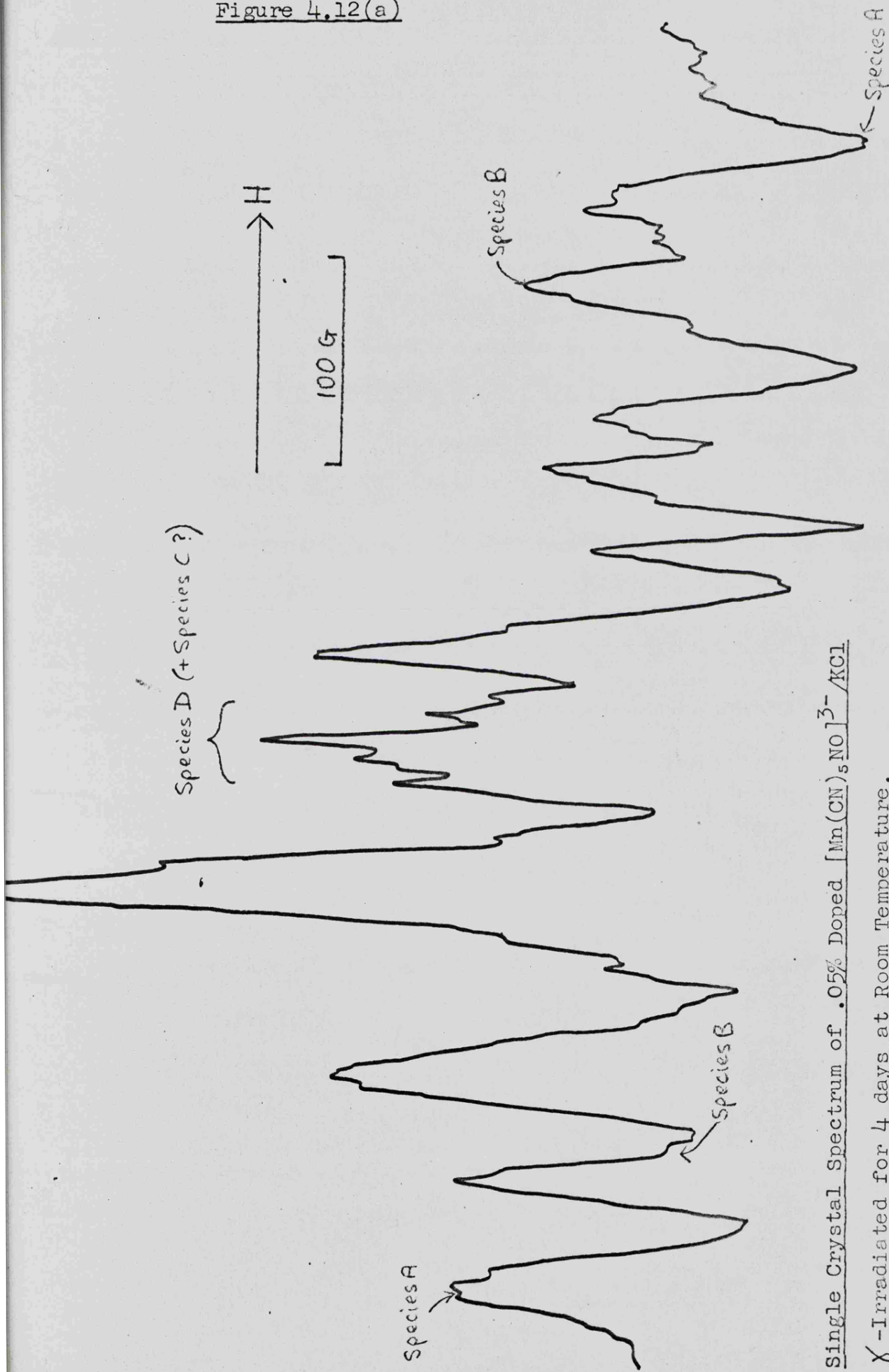
Figure 4.12



Single Crystal Spectrum of 0.05% Doped  $[\text{Mn}(\text{CN})_5\text{NO}]^{3-}/\text{KCl}$

$\chi$ -Irradiated for 12 hrs at Room Temperature.

Figure 4.12(a)



Single Crystal Spectrum of .05% Doped  $[\text{Mn}(\text{CN})_5\text{NO}]^{3-}/\text{KCl}$

X-Irradiated for 4 days at Room Temperature.

Figure 4.13

ESR Spectra of  $[\text{Mn}(\text{CN})_5\text{NO}]^{3-}/\text{KCl}$   $\gamma$ -Irradiated 48 hrs.  
at 77K. Measured at 77K.

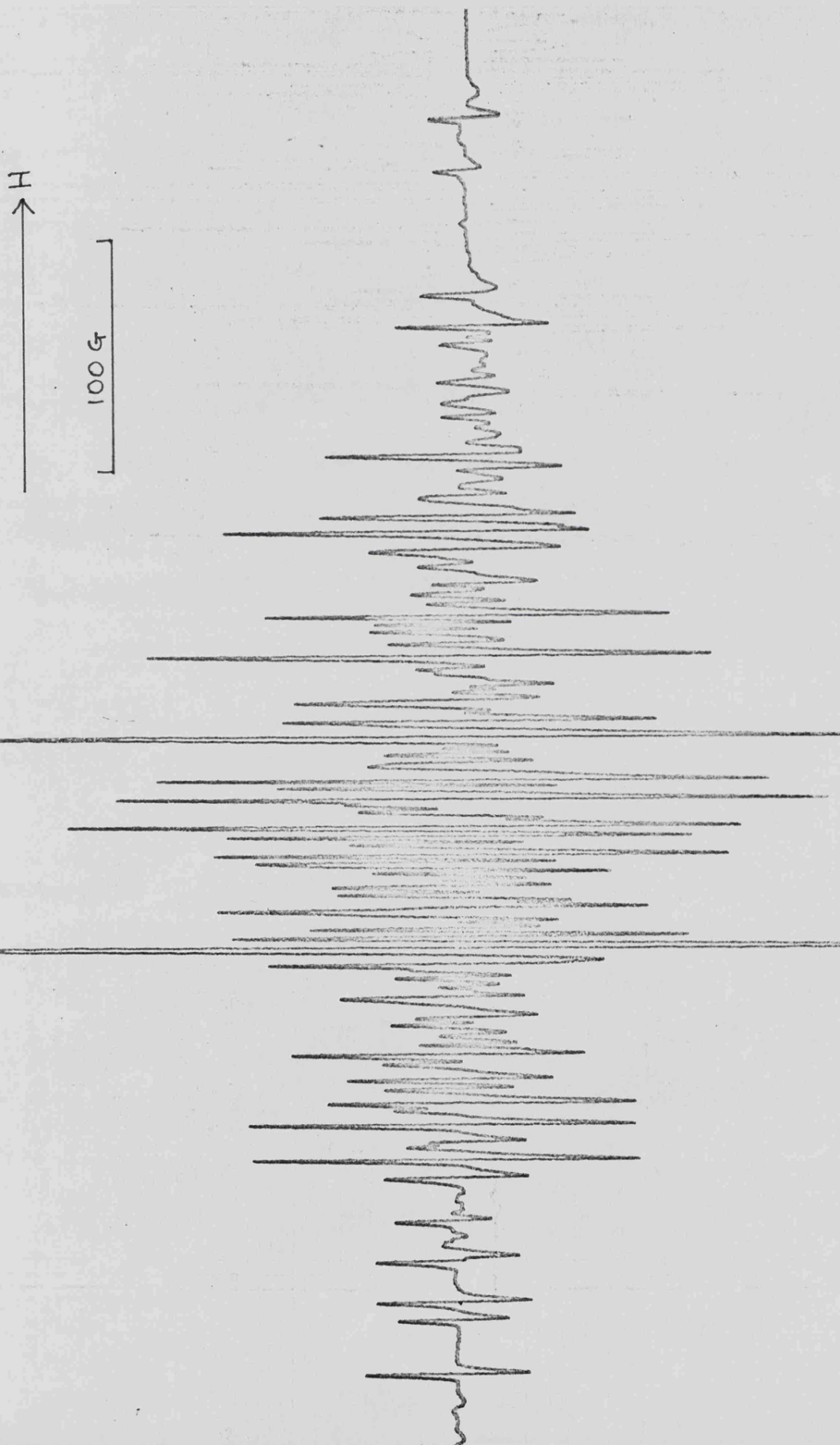
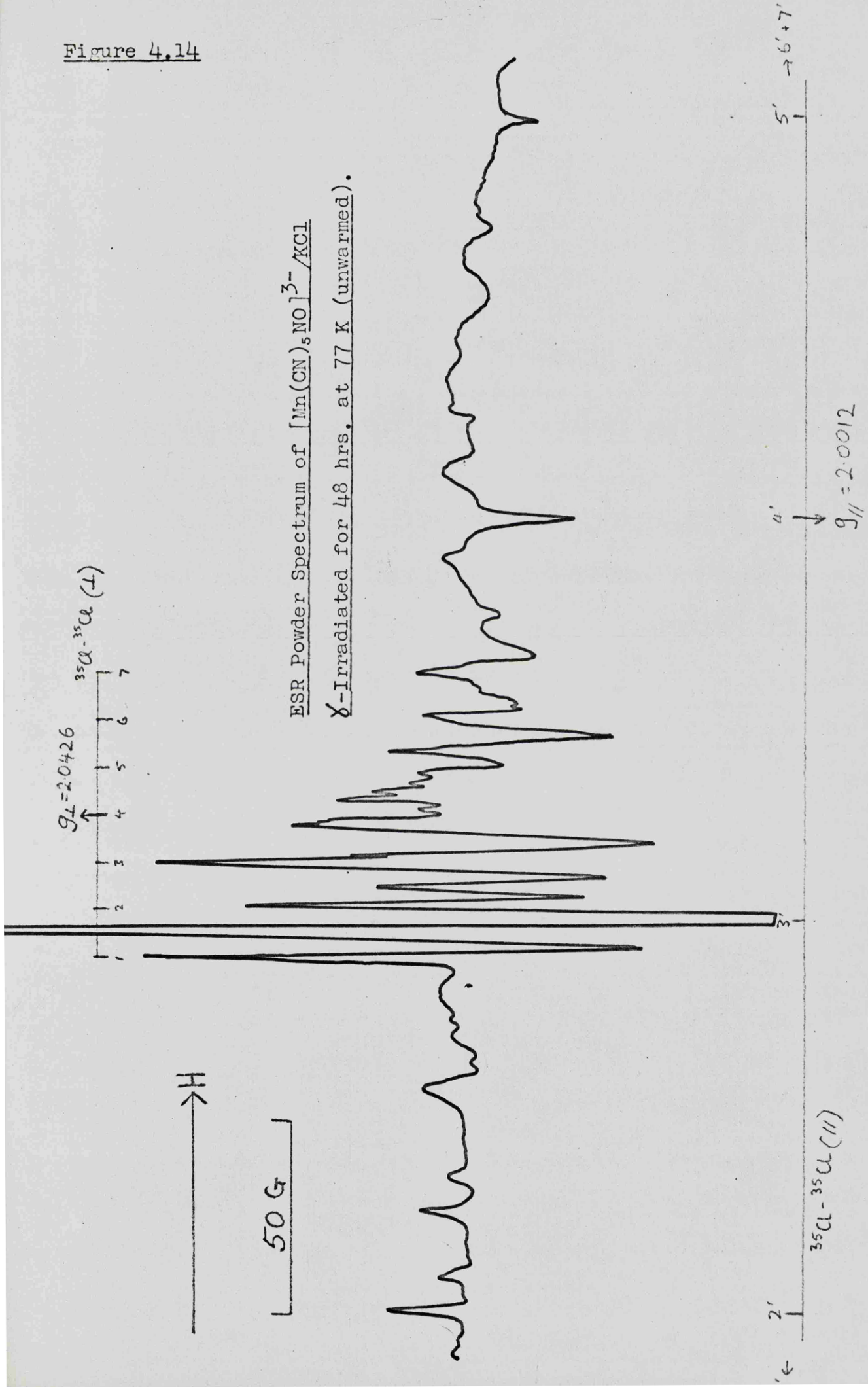


Figure 4.14

ESR Powder Spectrum of  $[\text{Mn}(\text{CN})_5\text{NO}]^{3-}/\text{KCl}$   
 $\chi$ -Irradiated for 48 hrs. at 77 K (unwarmed).



seen to decay. When the sample was recooled to 77 K the e.s.r. spectrum had changed completely. The lines due to the  $V_k$  centre had disappeared, while several features appeared, which were apparently not in the spectrum of the unwarmed crystal. These lines appear to be due to the well characterised  $d^5$  ion  $[\text{Mn}(\text{CN})_5\text{NO}]^{2-}$  in several different orientations. The largest splitting corresponds well with the reported<sup>7</sup> value of  $A_{\parallel} = 164$  G,  $g_{\parallel} = 1.987$  for the  $d^5$  ion. These lines also show the superhyperfine nitrogen splitting of approximately 4 G reported by Manoharan and Gray<sup>8</sup> and by Fortman and Hayes<sup>9</sup>. Figure 4.15 shows the e.s.r. spectrum of an irradiated single crystal which had been warmed for 30 seconds and recooled to 77 K. The corresponding spectrum of the polycrystalline sample (Figure 4.16) was much simplified and showed only the presence of the axially symmetric  $d^5$  ion.

When a single crystal of potassium bromide containing approximately 0.1%  $[\text{Mn}(\text{CN})_5\text{NO}]^{3-}$  was irradiated at room temperature for twenty-four hours, the e.s.r. spectrum, recorded at 298 K, showed only an isotropic triplet of lines whose intensities were roughly equal. (Figure 4.17). These lines are thus characteristic of an unpaired electron interacting with a single nucleus of spin  $I = 1$ . The experimental e.s.r. parameters for this species were as follows:  $g_{\text{iso}} = 2.0059$ ,  $A_{\text{iso}} = 21.5$  G. These parameters are identical to those attributed to species C, which was seen in an irradiated potassium chloride sample in addition to the lines due to the (manganese) species A and B. However, no lines attributable to manganese hyperfine coupling were seen in the spectrum of the potassium bromide sample, except at very high receiver gain and only after several days irradiation at room temperature. These weak

Figure 4.15

$[\text{Mn}(\text{CN})_5\text{NO}]^{3-}/\text{KCl}$   $\gamma$ -Irradiated for 48 hrs at 77 K

Single Crystal Spectrum of Sample Warmed to Room Temp. for 30 secs and Recooled to 77 K.

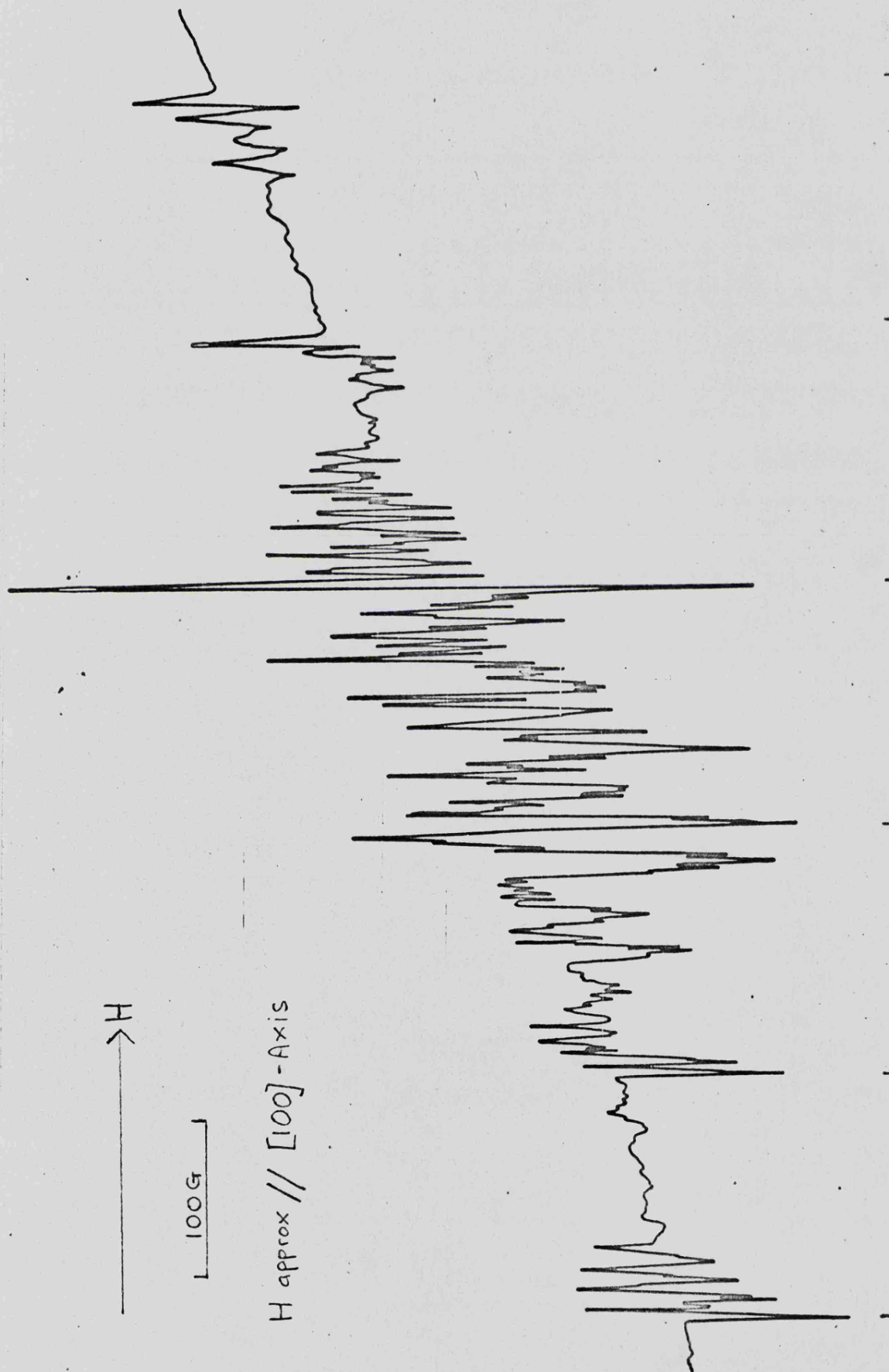
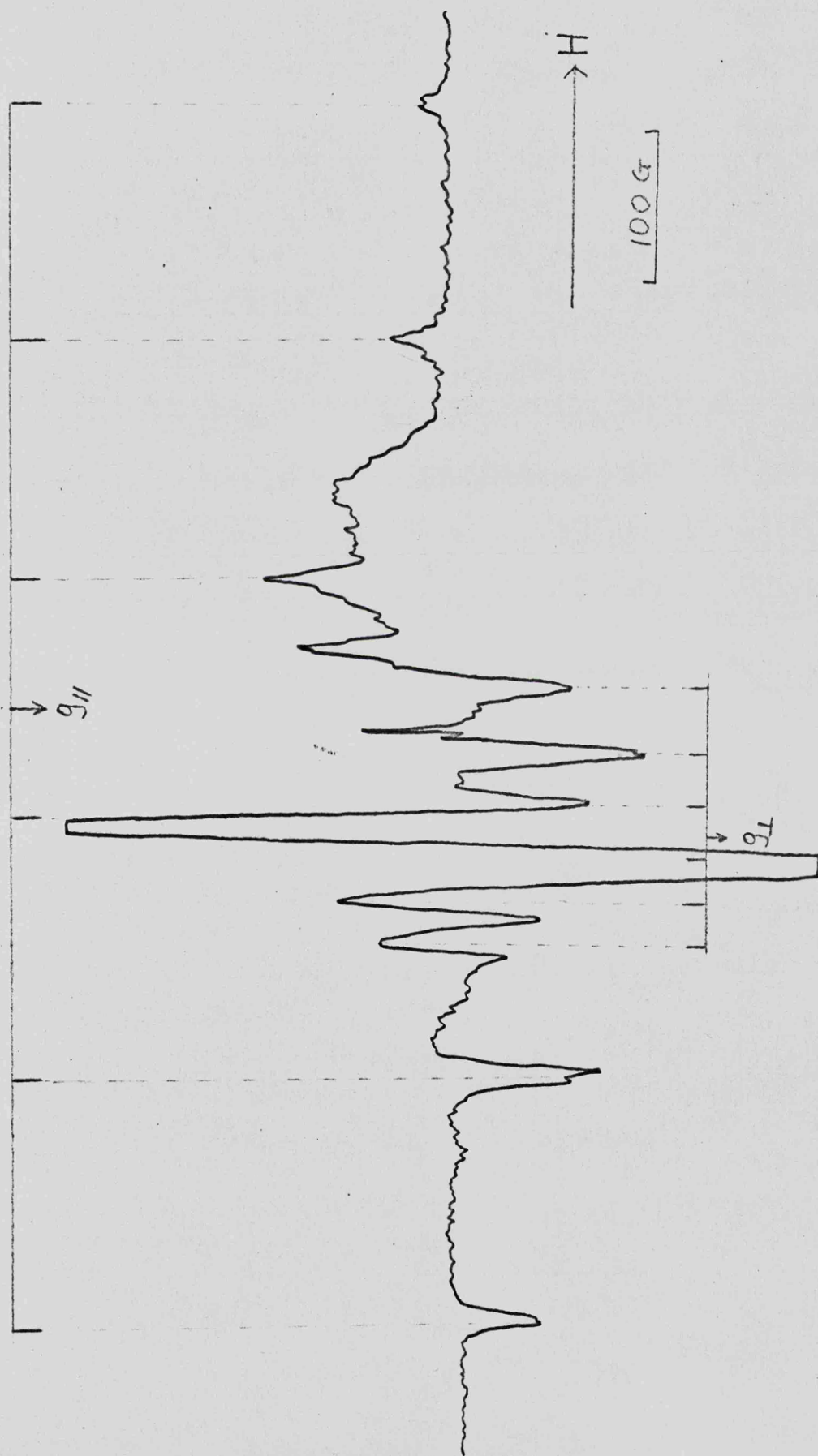


Figure 4.16

$[\text{Mn}(\text{CN})_5\text{NO}]^{3-}/\text{KCl}$  X-Irradiated for 48 hours at 77 K.

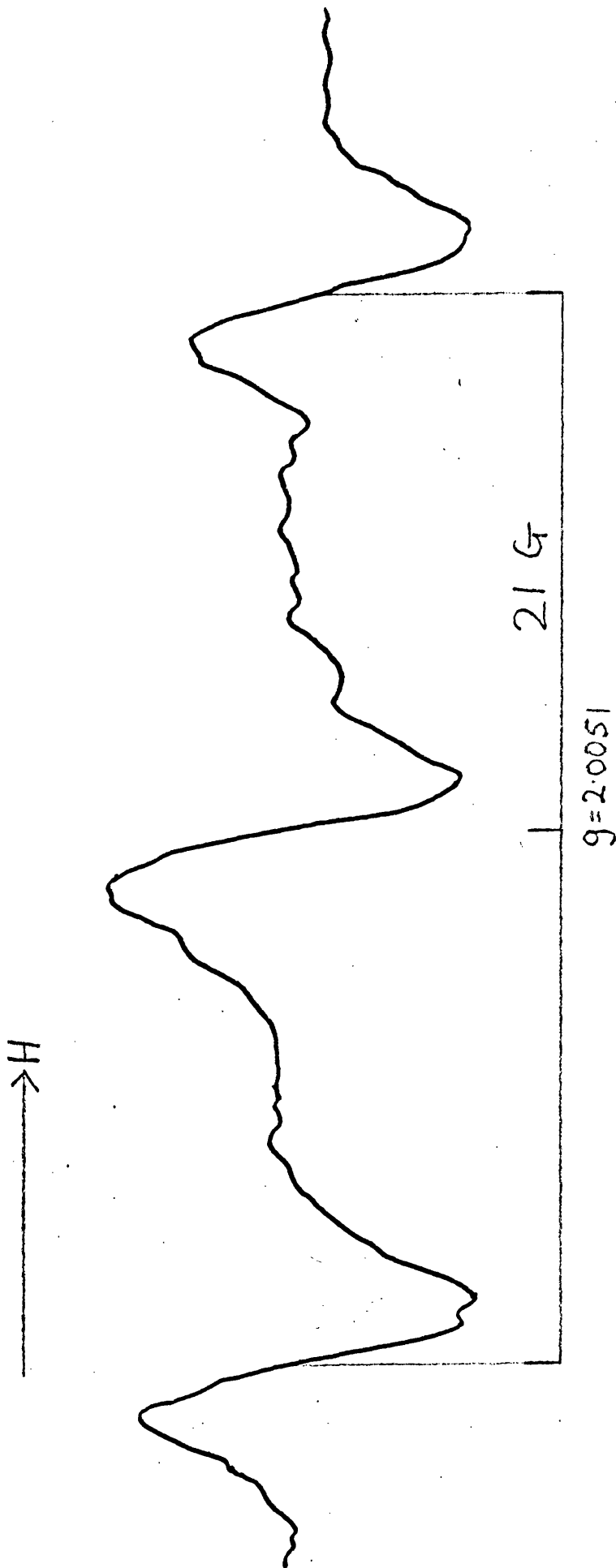


ESR Powder Spectrum of Sample Warmed for 30 seconds and Recooled to 77 K.

Figure 4.17

Single Crystal ESR Spectrum of  $[\text{Mn}(\text{CN})_5\text{NO}]^{3-}/\text{KBr}$

$\gamma$ -Irradiated for 24 hrs. at Room Temperature.



lines had similar e.s.r. parameters to those of the second (manganese) species observed in an irradiated KCl sample, i.e. species B.

When a polycrystalline sample of KCl doped with potassium hexacyanomanganate,  $[\text{Mn}(\text{CN})_6]^{3-}$ , together with some free cyanide ions, was irradiated at room temperature for one week, the e.s.r. spectrum comprised three very broad features (line-width  $\approx 75$  G). These lines may be attributed to a species with rhombic symmetry, (species E). Superimposed on two of the features appeared to be a quintet of lines with hyperfine coupling similar to species D, (A = 12.5 G) which was observed in a polycrystalline sample of KCl containing  $[\text{Mn}(\text{CN})_5\text{NO}]^{3-}$ , irradiated for a similar period of time. No hyperfine structure could be resolved on the third line. The e.s.r. spectrum of the hexacyanomanganate-doped potassium chloride sample is illustrated in Figure 4.18. The e.s.r. data for all the species formed in  $\gamma$ -irradiated alkali halides doped with manganese complexes are summarised in Table 4.3.\*

2. Chromium: The room temperature e.s.r. spectra of a single crystal and a polycrystalline sample of potassium chloride containing approximately 0.05%  $[\text{Cr}(\text{CN})_5\text{NO}]^{3-}$  are shown in Figure 4.19. The only effects on the e.s.r. spectrum when the sample was irradiated, was a broadening of the lines and a decrease in their intensity. There was no evidence for the formation of any new paramagnetic species even after samples had been irradiated for several weeks. Figure 4.20 illustrates the e.s.r. spectrum of a polycrystalline sample of KCl containing  $[\text{Cr}(\text{CN})_5\text{NO}]^{3-}$  after 4 weeks irradiation.

\* following p. 81

Figure 4.18

ESR Powder Spectrum of  $[\text{Mn}(\text{CN})_6]^{3-}/\text{KCl}$

$\gamma$ -Irradiated for 7 days at Room Temp.

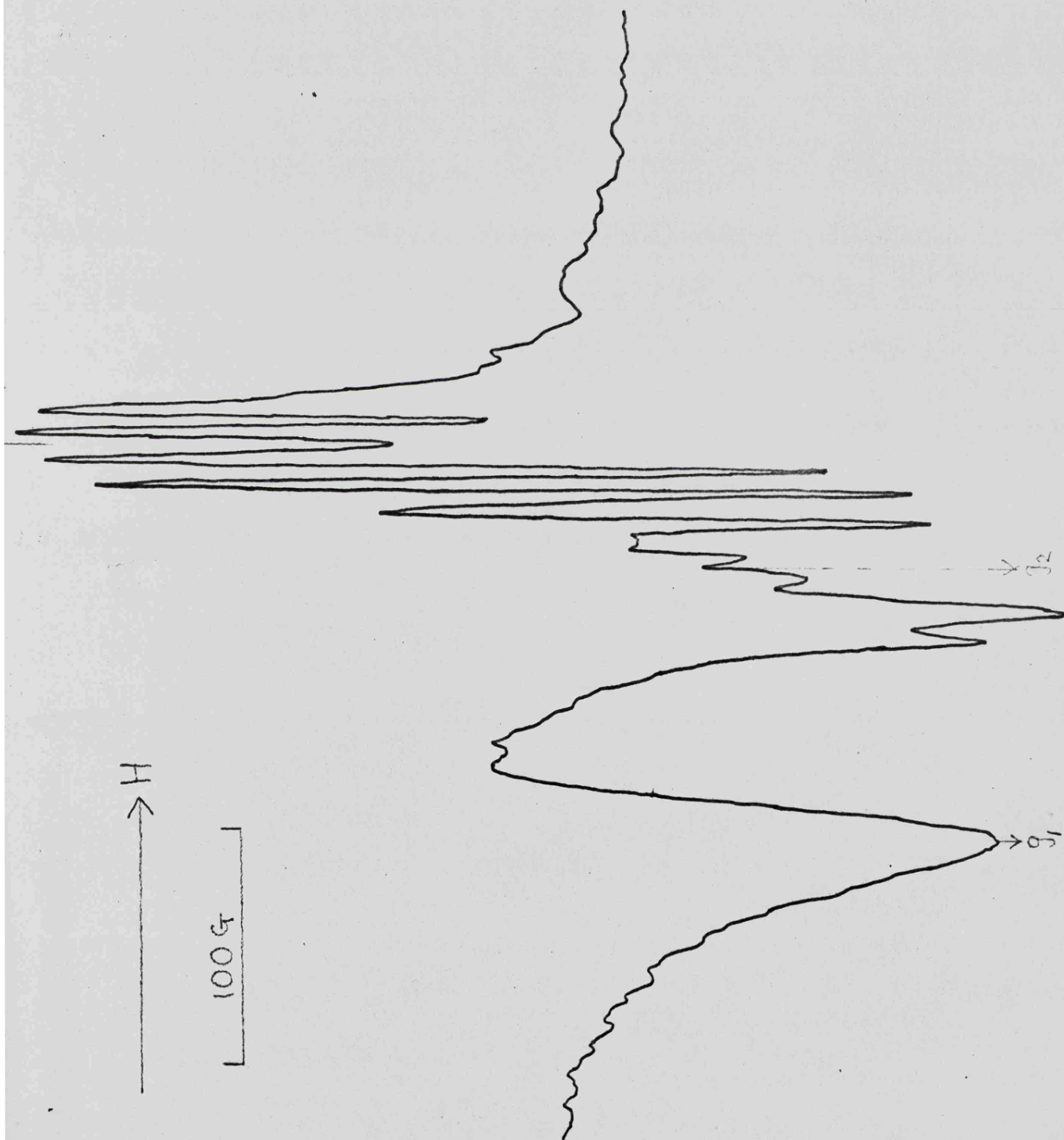
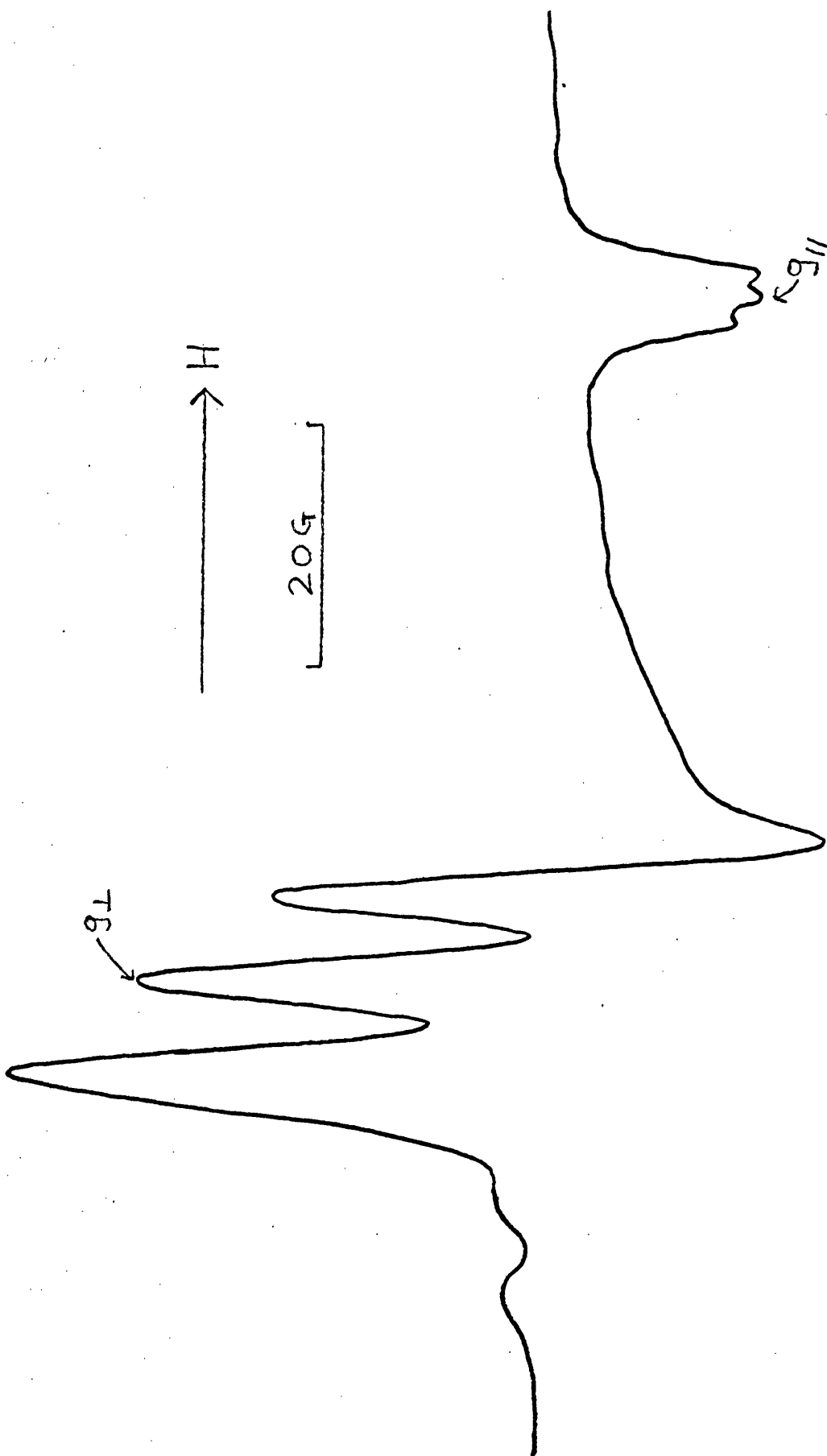


Figure 4.19



ESR Powder Spectrum of  $[\text{Cr}(\text{CN})_5\text{NO}]^{3-} / \text{KCl}$  Measured at Room Temperature. (Unirradiated)

Figure 4.19(a)

Room Temp. Single Crystal  
Spectrum of  $[\text{Cr}(\text{CN})_5\text{NO}]^{3-}/\text{KCl}$

(Random Orientation)

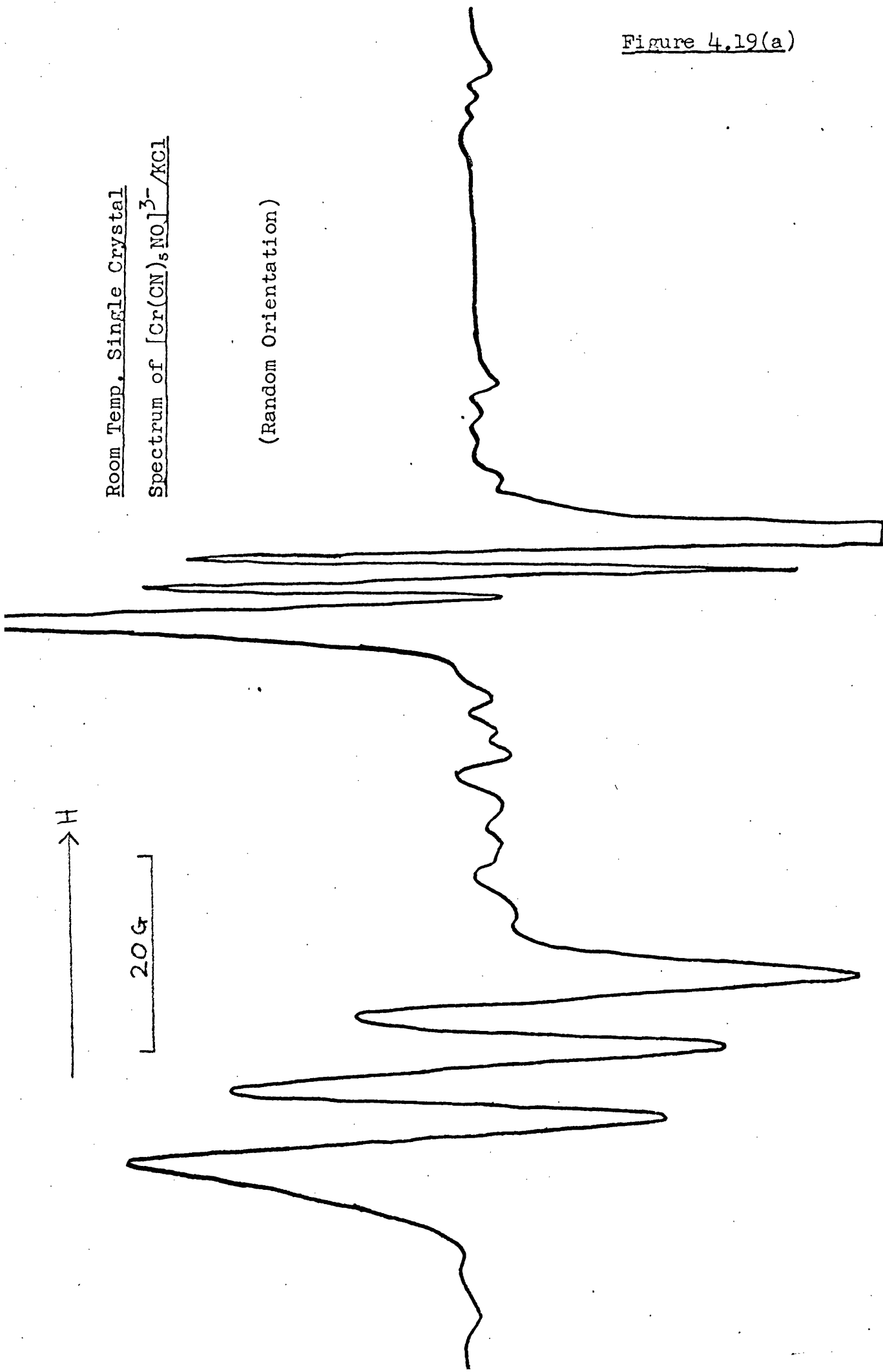
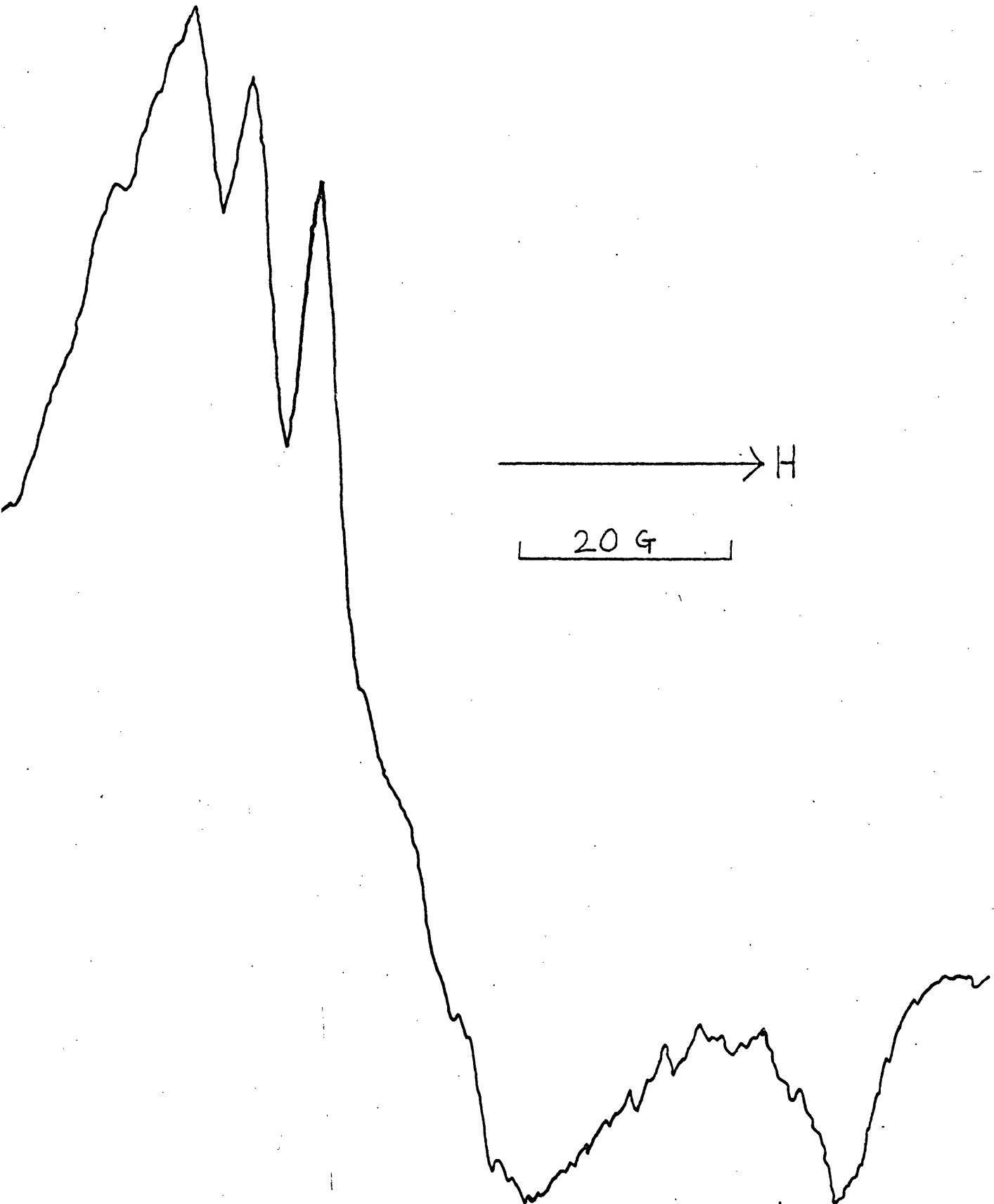


Figure 4.20

ESR Powder Spectrum of  $[\text{Cr}(\text{CN})_5\text{NO}]^{3-}/\text{KCl}$

$\gamma$ -Irradiated for 4 weeks at Room Temp.



3. Iron: When a polycrystalline sample of KCl containing less than 0.01% of sodium nitroprusside was  $\gamma$ -irradiated at room temperature for periods of time ranging from one hour to several days, the e.s.r. spectrum consisted only of broad, weak, poorly resolved lines. However, when the sample was irradiated with ultraviolet light for four hours a much higher concentration of radicals was produced. The e.s.r. spectrum, illustrated in Figure 4.21, consisted of broad features, of which only one could be resolved into a triplet of lines. The latter lines appeared to be the perpendicular features of an axially symmetric species. The measured e.s.r. parameters of this species were  $g_{\perp} = 2.031$  and  $A_{\perp} = 16$  G, which corresponds well with the perpendicular values reported for the  $d^7$  ion  $[\text{Fe}(\text{CN})_5\text{NO}]^{3-}$  (see Refs. in Chapters 2 & 3). A similar result was obtained when the sample was irradiated at liquid nitrogen temperature and the spectrum recorded at 77 K.

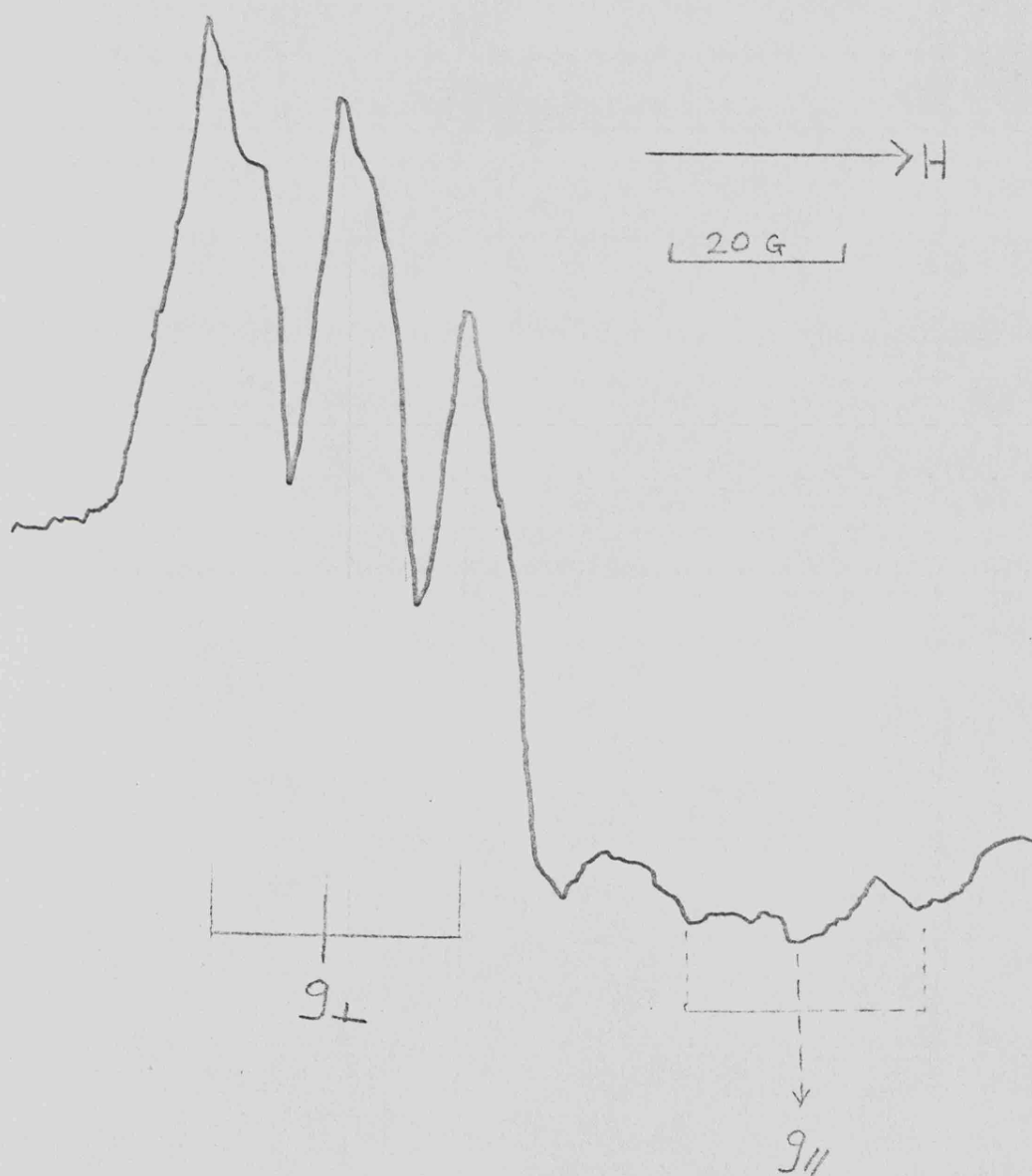
#### Discussion.

##### Incorporation of Complex Ions into Alkali Halide Lattices.

It was suggested by Root and Symons<sup>1,11</sup> that octahedral  $[\text{M}(\text{CN})_6]^{n-}$  ions could be incorporated into an alkali halide lattice by replacing a  $[\text{M}(\text{Hal})_6]^{5-}$  unit. If the complex has five negative charges there will be complete charge balance, and the ion should be easily incorporated into the lattice. The ease of incorporation into the lattice was found to be markedly dependant on the charge of the complex ion. It was found that the greater the difference in charge on the ion from five, the greater the difficulty of incorporation into the lattice.

Figure 4.21

ESR Spectrum of a Polycrystalline Sample of  $[\text{Fe}(\text{CN})_5\text{NO}]^{2-}$   
in NaCl/KCl, Irradiated with Ultra-violet Light.

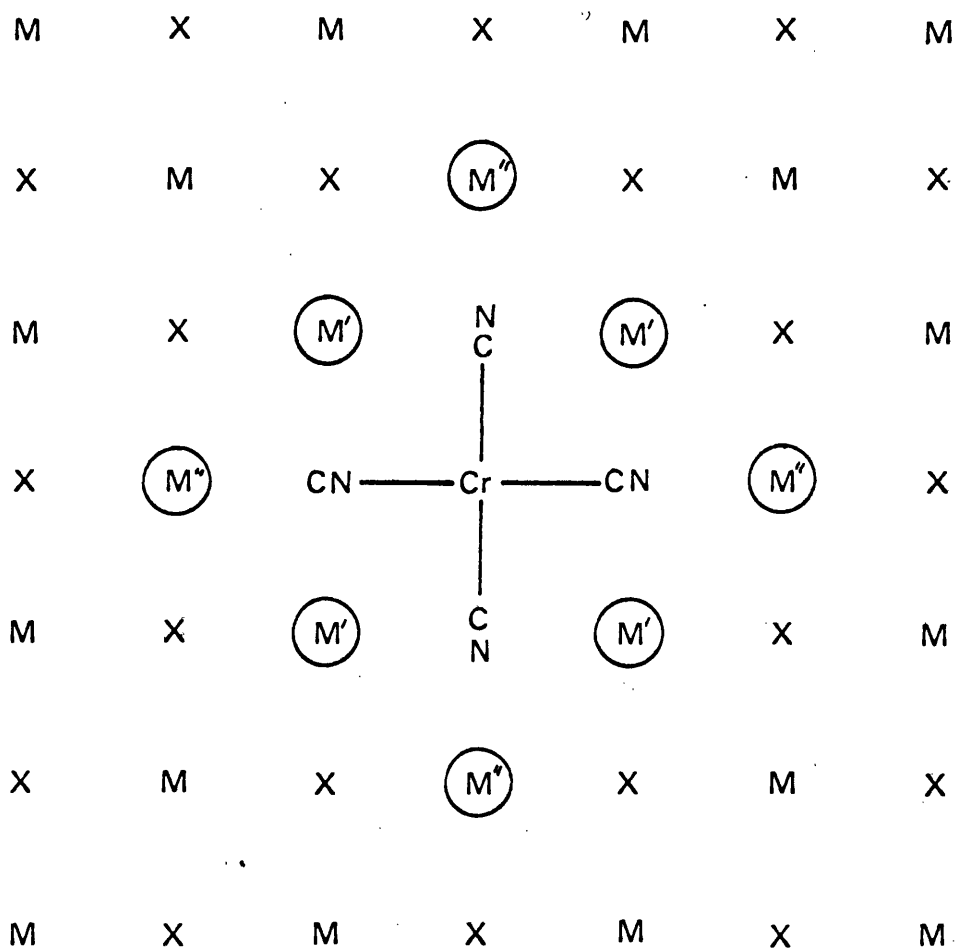


Additional weight may be lent to this argument by considering the dimensions of the ions involved. If we include the van der Waals radii of the nitrogen atoms, the linear distance across an N-C-M-C-N group is about 9.7 Å and that across an N-C-M-N-O group about 9.5 Å. (where M = Mn<sup>I</sup>, Cr<sup>I</sup>). Including the van der Waals radii for the Hal<sup>-</sup> ions, the distance across Cl-K-Cl is about 9.9 Å and that across Br-K-Br about 10.2 Å. Clearly, the ions  $[\text{Cr}(\text{CN})_5\text{NO}]^{3-}$  and  $[\text{Mn}(\text{CN})_5\text{NO}]^{3-}$  are able to replace an octahedral  $[\text{K}(\text{Hal})_6]^{5-}$  group without distorting the lattice. From a consideration of size alone, potassium chloride would seem to be the most suitable host lattice since the dimensions of the  $[\text{M}(\text{CN})_5\text{NO}]^{3-}$  ions and the  $[\text{KCl}_6]^{5-}$  group are the most consistent with a perfect fit. However, since we are incorporating ions with only 3 negative charges into the lattice, two neighbouring K<sup>+</sup> ions must be removed from the lattice to achieve electrical neutrality. From a consideration of the electrostatic interactions in the lattice we would expect these cation vacancies to be adjacent to the  $[\text{M}(\text{CN})_5\text{NO}]^{3-}$  ion for minimum energy. Furthermore they will have the highest probability of being found in the first shell of cations surrounding the incorporated complex ion (those marked M' in Figure 4.22). Since the probability of finding cation vacancies in a given shell surrounding the complex anion decreases as the square of the distance involved, the probability of cation vacancies being found beyond the second shell of surrounding cations should be very small indeed. Now these cation vacancies will have a profound effect on the i.r. spectra of the pentacyanonitrosyl complexes; the most noticeable and most easily monitored effect being on the N-O stretching band. If we assume that a pentacyanonitrosyl complex

Figure 4.22

Plan View of Ions in the [100] Plane in an Alkali Halide Lattice.

(1<sup>st</sup> and 2<sup>nd</sup> shells of K<sup>+</sup> ions surrounding the complex are circled).



M' = 1<sup>st</sup> Shell

M'' = 2<sup>nd</sup> Shell

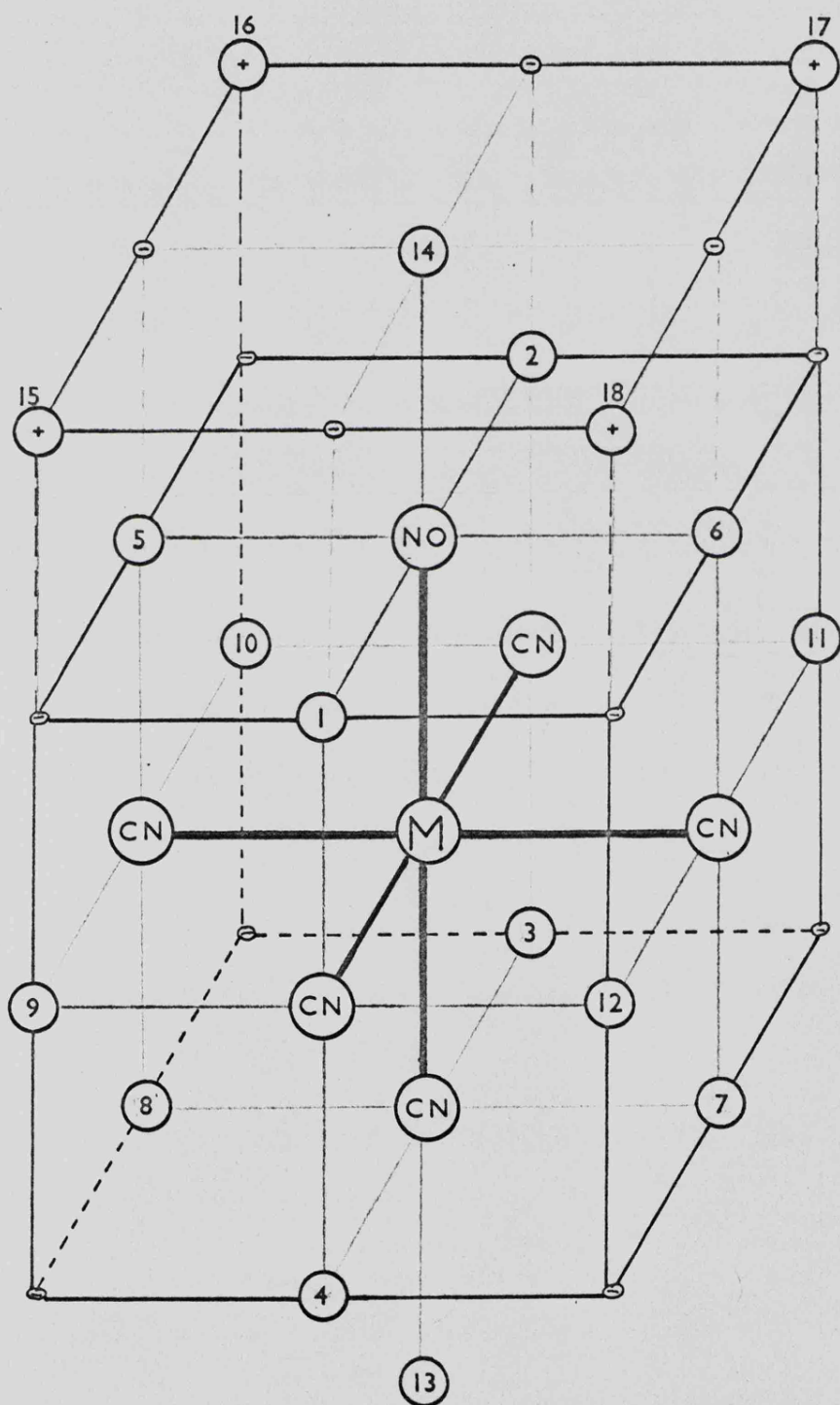
$[\text{M}(\text{CN})_5\text{NO}]^{n-}$  belongs to the point group  $C_{4v}$ , it could be shown<sup>12</sup> that this symmetry demands three  $\text{C}\equiv\text{N}$  stretching modes (Two  $A_1$  and one  $E$ ), and one  $\text{N}=\text{O}$  stretching fundamental which are active in the infra-red. The actual frequency of the latter will depend on the local environment of the  $\text{N}-\text{O}$  group, and is therefore a good monitor of the presence of neighbouring cation vacancies. Thus, in an alkali halide lattice the nitrosyl group will have a different stretching frequency depending on the configuration of neighbouring cation vacancies; the intensity and the degree that the band has been shifted (from that in the pure complex) will depend on a statistical factor and the proximity (and hence the strength of interaction) of the cation vacancies to the nitrosyl group. For example, if both cation vacancies were close to the nitrosyl group, the strength of interaction would be high and hence the band would be shifted to a marked extent. However, the statistical probability (and also the electrostatic feasibility) of this situation occurring is low, therefore the intensity of the band caused by this configuration would be low.

We will now analyse the i.r. spectra for the chromium and manganese complexes in a potassium chloride lattice, with special reference to the  $\text{N}-\text{O}$  stretching bands, in terms of the different possible "hole" configurations. In a perfectly cubic environment the  $[\text{M}(\text{CN})_5\text{NO}]^{n-}$  ion will belong to the point group  $C_{4v}$ . However, the close proximity of the two cation vacancies will lower this symmetry. In fact, depending on the position of the vacancies the complex ion will have  $C_{4v}$ ,  $C_{2v}$ ,  $C_s$  or  $C_1$  symmetry. Figure 4.23(a) shows the  $[\text{M}(\text{CN})_5\text{NO}]^{n-}$  ion in  $\text{KCl}$ . The numbered circles correspond to the first shell of potassium ions surrounding the

Figure 4.23(a)

Showing the  $[M(CN)_5NO]^{n-}$  Ion in a KCl Lattice.

(Neighbouring  $K^+$  Cation Sites are Numbered).

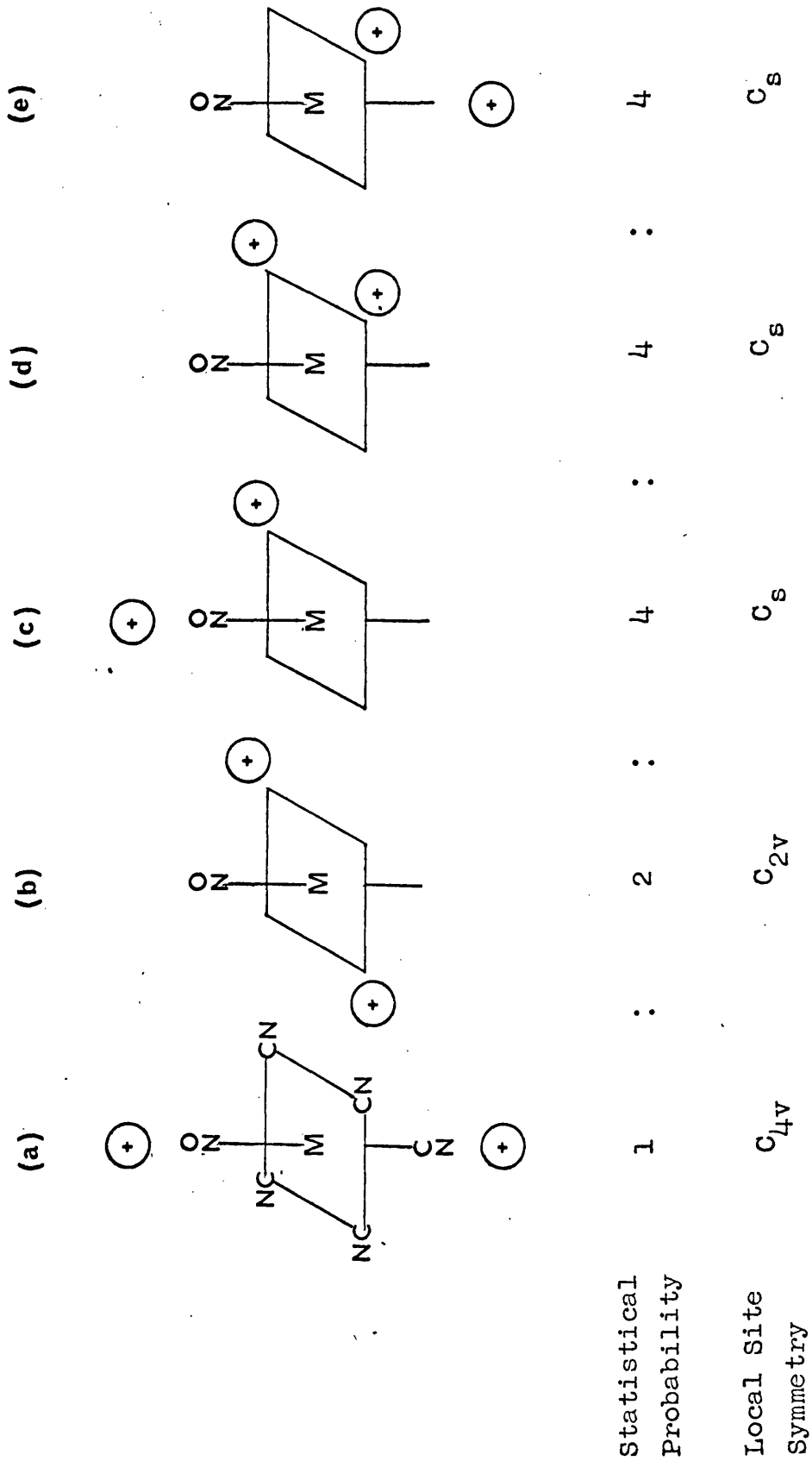


complex. Figure 4.23(b) illustrates the different possible configurations if two cations ( $K^+$ ) are removed from the second shell surrounding the complex. Now, in practice two cations may be removed from the first shell, the second shell or one from each, (or indeed from neither shell). The most symmetrical arrangement of holes surrounding the complex will be most favoured on electrostatic grounds, particularly when the configuration allows the vacancies to be situated as far apart from each other as possible. Referring to Figure 4.23(a), this situation occurs when "trans" cations are removed from the lattice, e.g. when pairs (1 & 3), (2 & 4), (5 & 7), (6 & 8); (9 & 11) and (10 & 12) are removed. Only the removal of the first four pairs of cations will directly affect the N-O stretching frequency, since each of these configurations places a vacancy close to the nitrosyl group. Jones<sup>13</sup> has postulated that the above configurations should be the most favourable on energy minimisation grounds, when  $[\text{Co}(\text{CN})_6]^{3-}$  is incorporated into KCl; this reduces the  $O_h$  symmetry to  $D_{2h}$ . If we consider the  $\text{Co}(\text{CN})_6$  octahedron as inscribed in a cube with the six CN groups at the centres of the six faces, the  $D_{2h}$  model will have cation vacancies at the centre of two opposite edges of the cube. The correlation rules show that reduction to  $D_{2h}$  symmetry should result in a splitting of the triply degenerate infra-red active CN stretching vibrations into three non-degenerate infra-red active vibrations. Three intense CN stretching peaks are in fact observed<sup>13</sup> in dilute solid solutions of  $[\text{Co}(\text{CN})_6]^{3-}$  in KCl, thus giving credence to this argument.

Now the low temperature, high resolution i.r. spectrum of

Different Possible Configurations in the Case Where Two Cations are Removed from the Second Shell of Potassium Ions Surrounding the  $[M(CN)_5NO]^{n-}$  Complex.

Figure 4.23(b)



$[\text{Mn}(\text{CN})_5\text{NO}]^{3-}$  in KCl (Figure 4.7)\* shows at least eight bands in the N-O stretching region, whose intensities are approximately in the ratio 1: 2: 4: 1: 2:  $\frac{1}{2}$ : 1: 1. Table 4.6 illustrates the various possible hole configurations which are likely to influence the N-O stretching frequency. It can be seen that there are around eight sets of equivalent hole configurations which are most likely to affect the nitrosyl group. Thus we appear to be able to predict the number of bands observed by this method. The most intense band almost certainly corresponds to a situation (of highest statistical probability) where there are no cation vacancies close to the nitrosyl group. It must be stressed though, that this is a non-rigorous treatment and we are not attempting to assign a particular infra-red band to a particular hole configuration. Moreover, we would not expect a simple correlation between the intensity of a band and the statistical probability of its corresponding hole configuration. This is because those configurations which may have a high statistical probability, may also have a high electrostatic repulsion energy, which would clearly make them improbable from the point of view of energy minimisation. So although we cannot assign each band to a particular environment of the nitrosyl group, we can at least account for the number of bands observed in the N-O stretching region in terms of the number of possible configurations of cation vacancies close to the nitrosyl group.

We would again predict about eight bands in the N-O stretching region for  $[\text{Cr}(\text{CN})_5\text{NO}]^{3-}$  in KCl, since this ion also has three negative charges and therefore requires two charge compensating cation vacancies. However, in this case the N-O band overlaps to

\* following p. 78

Table 4.6

Possible Configurations of Cation Vacancies Likely to  
Influence the N-O Stretching Frequency.\*

<u>Configuration</u>	<u>No. of Holes Close to NO</u>	<u>Statistical Probability</u>	<u>Electrostatic Stability</u>
1. (1,3);(2,4);(5,7);(6,8)	1	4	high
2. (1,4);(2,3);(5,8);(6,7)	1	4	high
3. (1,5);(1,6);(2,5);(2,6)	2	4	low
4. (13,14)	1	1	high
5. (1,2);(5,6)	2	2	low
6. (15,17);(16,18)	2	2	low
7. (14,-)	1	>4	-
8. (-,-)	0	>4	-

\* with reference to Figure 4.23(a)

some extent with a nearby water band and hence the N-O band is considerably broadened. Nevertheless, the i.r. spectrum (Figure 4.1) reveals the presence of four clearly defined lines of roughly equal intensity plus a number of non-resolved shoulders.

We may also account for the number of bands in the C-N stretching region using a similar argument to that outlined above. However, the actual point group of the molecule plus immediate environment is now important in determining how the CN bands are split out under different site symmetries. Now the CN band is spread over a narrower range of wave-numbers than the NO band, indicating that the strength of interaction of the cation vacancies with the cyanide ligands is less than that with the nitrosyl ligand. This indicates that any additional splitting of the band is due to a site symmetry effect rather than direct interaction.

Now, under the original  $C_{4v}$  symmetry of the pentacyanonitrosyl complexes we expect four C-N stretching modes, two  $A_1$  and one E, the latter being split out under high resolution into two equally intense bands. When the site symmetry of the complex has been reduced to lower symmetries such as  $C_{2v}$ ,  $C_s$  and  $C_1$ , we would expect to see several additional bands. In experimental reality, however, there may be a sufficiently large number of lines which overlap to make the spectrum appear 'blurred'. For example, in each spectrum of  $[\text{Cr}(\text{CN})_5\text{NO}]^{3-}$  in KCl, the original cyanide band appears as a single, broad line — however there are indications of an indefinite number of unresolved lines within the main band. The i.r. spectra of  $[\text{Mn}(\text{CN})_5\text{NO}]^{3-}$  in KCl are rather better resolved and show up to ten lines in the cyanide stretching region, although some of these may

be due to the presence of impurities such as the  $[\text{Mn}(\text{CN})_6]^{3-}$  ion or to free cyanide ions, which absorb in this region.

It should be noted that all the i.r. spectra of the pentacyanonitrosyl complexes in potassium bromide lattices are poorly resolved. This may be due to the fact that the  $[\text{KBr}_6]^{5-}$  unit is larger than the  $[\text{KCl}_6]^{5-}$  unit and therefore the complexes only fit 'loosely' in the lattice of potassium bromide. Thus they will not be affected so strongly by neighbouring cation vacancies nor will they have such a precise site symmetry in a KBr lattice.

To summarise then: the number of clearly defined bands in the nitrosyl stretching region may be explained in terms of the interaction of the nitrosyl group with one or both of two neighbouring cation vacancies. Since only one N-O stretching band is observed in the spectrum of the pure pentacyanonitrosyl complexes (or of discs prepared by grinding the pure complex with KCl), the presence of these extra bands confirms that the complex ions have been incorporated into the alkali halide lattices substitutionally and not in clusters.

#### Effect of $\gamma$ -Irradiation on the Infra-red Spectra.

In view of the well known correlation between the wave number of an absorption band of a ligand in a metal complex and the oxidation state of the metal, the formation of new bands on the low energy side of the original cyanide and nitrosyl bands indicates that the irradiated complexes have been reduced. The effect of adding an extra electron to a metal complex is to lower the charge on the metal, which allows the electrons to be delocalised onto the

ligands. Thus, reduction of the pentacyanonitrosyl complexes places additional electron density into  $\pi^*$ -antibonding molecular orbitals on the cyanide and nitrosyl ligands and thereby weakens the C-N and N-O bonds, while simultaneously strengthening the M-C and M-N bonds. This decreases the C-N and N-O stretching frequencies (and is confirmed by observation), and should increase the M-C and M-N stretching frequencies. However, no bands which could be attributed to metal-carbon or metal-nitrogen stretching modes were observed in any of the spectra.

Table 4.7 gives the central positions of the original and radiation-induced cyanide and nitrosyl bands for the  $[\text{Cr}(\text{CN})_5\text{NO}]^{3-}$  and  $[\text{Mn}(\text{CN})_5\text{NO}]^{3-}$  ions in KCl, and the  $[\text{Fe}(\text{CN})_5\text{NO}]^{2-}$  ion in NaCl. Included in the Table are published i.r. data for pentacyanonitrosyl- and hexacyano- complexes of chromium, manganese and iron in various oxidation states. From the Table we obtain the following "red shifts" for the  $\nu(\text{CN})$  and  $\nu(\text{NO})$  bands in the pentacyanonitrosyl- complexes.

	<u>Cyanide Shift</u>	<u>Nitrosyl Shift</u>
$\text{Cr}(\text{I}) \rightarrow \text{Cr}(\text{O})$ $d^5 \quad d^6$	70 $\text{cm}^{-1}$	190 $\text{cm}^{-1}$
$\text{Mn}(\text{I}) \rightarrow \text{Mn}(\text{O})$ $d^6 \quad d^7$	50 $\text{cm}^{-1}$	155 $\text{cm}^{-1}$ and/or 250 $\text{cm}^{-1}$
$\text{Fe}(\text{II}) \rightarrow \text{Fe}(\text{I})$ $d^6 \quad d^7$	95 $\text{cm}^{-1}$	90 $\text{cm}^{-1}$ and 220 $\text{cm}^{-1}$
		(from Ref. 14)

Table 4.8

\*\* \* \*\* \*\* \*

It can be seen from the magnitudes of the i.r. shifts that the  $\nu(\text{NO})$  band is much more sensitive to the effect of the charge on the metal

Table 4.7(a) Central Positions of Original and Radiation-Induced I.R. Bands in Cr, Mn and Fe Pentacyanonitrosyl Complexes in Potassium Chloride.

		<u>Chromium</u>	<u>Manganese</u>	<u>Iron</u>
ν (CN)	d <sup>5</sup>	2105	2185	-
	d <sup>6</sup>	2035	2080	2145
	d <sup>7</sup>	-	2030	2050
ν (NO)	d <sup>5</sup>	1675	1920	-
	d <sup>6</sup>	1485	1775	1940
	d <sup>7</sup>	-	1620	1850
			or 1525	and 1720

Table 4.7(b) Literature Values of I.R. Bands in Pentacyanonitrosyl and Hexacyano- Complexes of Cr, Mn and Fe.

<u>Complex</u>	<u>ν (CN)</u>	<u>ν(NO)</u>	<u>Reference</u>
K <sub>3</sub> [Cr(CN) <sub>5</sub> NO]	2125	1640	19
K <sub>4</sub> [Cr(CN) <sub>5</sub> NO].2H <sub>2</sub> O	-	1515	15
K <sub>3</sub> [Mn(CN) <sub>5</sub> NO]	2135	1713	3
	2100	1693	
	2080		
K <sub>3</sub> [Mn(CN) <sub>5</sub> NO]	2093	1730	19
Zn[Mn(CN) <sub>5</sub> NO]	2193	1900	19
Zn[Mn(CN) <sub>5</sub> NO]	2195	1885	3
	2150		
Na <sub>2</sub> [Fe(CN) <sub>5</sub> NO].2H <sub>2</sub> O	2173	1939	12
	2161		
	2157		
	2143		

Table 4.7(b)      (cont)

<u>Complex</u>	<u><math>\nu(\text{CN})</math></u>	<u>Reference</u>
$\text{K}_3 [\text{Cr}(\text{CN})_6]$	2132	a, b
$\text{K}_3 [\text{Mn}(\text{CN})_6]$	2120	a, b
$\text{K}_4 [\text{Mn}(\text{CN})_6]$	2060	a, b
$\text{K}_3 [\text{Fe}(\text{CN})_6]$	2110	a, b
$\text{K}_4 [\text{Fe}(\text{CN})_6]$	2050	a, b

- a. A.Hidalgo and J.P.Mathieu, Compt. Rend. 249, 233, (1959)  
b. V.Cagliotti, G.Sartori and M.Scrocco,  
J. Inorg. Nuclear Chem., 8, 87, (1958)

All frequencies in  $\text{cm}^{-1}$

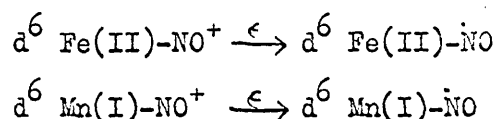
than is the  $\nu(\text{CN})$  band. This is to be expected, since the  $\pi$ -acceptor properties of the nitrosyl group are greater than those of the cyanide group, i.e. the nitrosyl group will take a greater share of the extra delocalised electron into its  $\pi$ -antibonding M.O.'s than the cyanide group.

Now in the case of the pentacyanonitrosyl-chromate(I) in KCl, the positions of the new cyanide and nitrosyl bands compare favourably with those reported<sup>15</sup> for  $\text{K}_4\text{Cr}(\text{CN})_5\text{NO}$  in nujol, allowing for shifts due to lattice effects. We shall now attempt to assign the radiation-induced bands (in  $[\text{Cr}(\text{CN})_5\text{NO}]^{3-}/\text{KCl}$ ) which have so far not been assigned. A sharp band at  $2085 \text{ cm}^{-1}$  is most probably free  $\text{CN}^-$  which usually absorbs at around  $2080 \text{ cm}^{-1}$  in a KCl lattice. A band at  $1966 \text{ cm}^{-1}$  and one at  $1295 \text{ cm}^{-1}$  could possibly correspond with the  $\nu(\text{CN})$  and  $\nu(\text{NO})$  bands respectively, of the further-reduced  $d^7$  chromium(-I) complex. Assuming that the reduction  $\text{Cr(0)} \rightarrow \text{Cr(-I)}$  does take place, the corresponding i.r. shifts for the  $\nu(\text{CN})$  and  $\nu(\text{NO})$  bands are  $75 \text{ cm}^{-1}$  and  $190 \text{ cm}^{-1}$  respectively; these are of the same order as the corresponding shifts of  $70 \text{ cm}^{-1}$  and  $195 \text{ cm}^{-1}$  respectively, for the reduction  $\text{Cr(I)} \rightarrow \text{Cr(0)}$ . However, this is only a tentative assignment and is by no means proven. A band at  $2060 \text{ cm}^{-1}$ , close to the Cr(I) cyanide band could correspond to the  $\nu(\text{NC})$  band in  $[\text{Cr}(\text{CN})_4(\text{NC})\text{NO}]^{4-}$ , where one (or more) of the cyanides has "flipped round" on irradiation. This phenomenon has been previously seen in  $\gamma$ -irradiated KCl lattices containing  $[\text{Fe}(\text{CN})_6]^{4-}$ , where one cyanide ligand is postulated<sup>1,11,16</sup> to have flipped round; and also in high-energy electron-irradiated  $[\text{Co}(\text{CN})_6]^{3-}$  in KCl, where two cyanides are postulated<sup>17,18</sup> to have turned round. This phenomenon will be discussed further in the e.s.r. section.

Now, in the case of the pentacyanonitrosyl-manganate(I) ion in KCl, although we can positively assign a new  $\nu(\text{CN})$  band corresponding to the  $d^7$  manganate(0) ion, there is some ambiguity concerning the new  $\nu(\text{NO})$  band. This may absorb at  $1620 \text{ cm}^{-1}$  (where it would be obscured by a lattice-water band) or at  $1525 \text{ cm}^{-1}$ ; the corresponding "red shifts" being  $155 \text{ cm}^{-1}$  and  $250 \text{ cm}^{-1}$  from the original  $\nu(\text{NO})$  band. It is possible that they might both correspond to  $\nu(\text{NO})$  bands in two types of reduced manganese(0) complex. This is quite likely since, as we have seen in Chapter 3, there are at least three types of reduced iron-nitrosyl species in irradiated sodium nitroprusside. Two of these reduced species have been studied<sup>14</sup> by i.r. spectroscopy. These have  $\nu(\text{NO})$  bands at  $1850 \text{ cm}^{-1}$  and at  $1720 \text{ cm}^{-1}$ , corresponding to red shifts of  $90 \text{ cm}^{-1}$  and  $220 \text{ cm}^{-1}$  respectively. The species responsible for the former band is a  $d^7$  ion with the unpaired electron mainly in a  $d_{z^2}$  orbital on iron; while the latter band is attributed to a species where the unpaired electron is mainly in a  $\pi$ -antibonding orbital on the nitrosyl group. (see Chapter 3).

It is conceivable then, that there could be two manganese-nitrosyl species similar to the above iron-nitrosyl species. However, in the case of the manganese complex, the  $d^7$  ion would have zero charge on the metal; such a low oxidation state would necessitate extensive delocalisation onto the ligands with probably less than 50% of the unpaired electron density on the manganese, compared with about 80% on the metal in the corresponding iron complex. These two cases are certainly comparable in that they each involve the addition of an electron to a  $d^6$  ion giving a  $d^7$  species. If we represent the reduction giving the 'iron'  $\nu(\text{NO})$  band shifted by  $90 \text{ cm}^{-1}$  by:

$d^6 \text{Fe(II)} \rightarrow d^7 \text{Fe(I)}$ , then the 'manganese'  $\nu(\text{NO})$  band shifted by  $155 \text{ cm}^{-1}$  could correspond to the reduction:  $d^6 \text{Mn(I)} \rightarrow d^7 \text{Mn(0)}$ ; the larger shift being due to the greater delocalisation into  $\pi$ -antibonding nitrosyl orbitals in the latter case. Similarly we could represent the reduction processes giving the  $155 \text{ cm}^{-1}$  and  $250 \text{ cm}^{-1}$  shifted bands in the iron and manganese complexes respectively, by the following:



where the unpaired electron is largely (i.e.  $\gg 50\%$ ) on the nitrosyl group. (in  $\pi$ -antibonding M.O.'s). We must stress that we can only make tentative assignments of this sort using i.r. data alone, and such arguments need to be backed up by confirmatory e.s.r. results before they can be seriously considered as proven.

Now, two lines which appear to grow simultaneously in irradiated  $[\text{Mn}(\text{CN})_5\text{NO}]^{3-}/\text{KCl}$  are a band at  $2185 \text{ cm}^{-1}$  (overlapping with the  $\text{CNO}^-$  band) and one at  $1920 \text{ cm}^{-1}$ . These lines are in the right region to correspond with the  $\nu(\text{CN})$  and  $\nu(\text{NO})$  bands respectively, of the  $d^5$  ion,  $[\text{Mn}(\text{CN})_5\text{NO}]^{2-}$ , which could be formed by the oxidation of the  $d^6$  ion. Their observed positions compare favourably with the reported<sup>3</sup> values of  $2193 \text{ cm}^{-1}$  and  $1930 \text{ cm}^{-1}$  for the  $d^5$  ion in a  $\text{Zn Mn}(\text{CN})_5\text{NO}$  lattice.

One line, so far unassigned in irradiated  $[\text{Mn}(\text{CN})_5\text{NO}]^{3-}/\text{KCl}$ , is a feature at  $1950 \text{ cm}^{-1}$ , which reaches its maximum intensity after 12 hours irradiation and which decays on further irradiation. It is not clear what this band is due to, but it may well have some connection with Species A, which was responsible for an isotropic

e.s.r. sextet of lines which decayed on prolonged irradiation. Another unexplained band which is observed in all three pentacyanonitrosyls is at  $1400\text{ cm}^{-1}$ ; this remains unassigned at the present time.

In the i.r. spectra of  $\gamma$ -irradiated  $[\text{Mn}(\text{CN})_5\text{NO}]^{3-}$  in KBr, it is not immediately clear why there are no new bands in the cyanide and nitrosyl stretching regions — i.e. why the complex in KBr is not reduced on irradiation. One reason could be that, due to the increased size of the  $\text{Br}^-$  ion, the complex only fits "loosely" in the lattice, and therefore does not act as an efficient electron trap; the source of electrons on irradiation being the F-centre.<sup>1,11</sup>

If we compare the i.r. spectra of  $\gamma$ -irradiated  $[\text{Cr}(\text{CN})_5\text{NO}]^{3-}$  and  $[\text{Mn}(\text{CN})_5\text{NO}]^{3-}$  in KCl lattices, it is apparent that the  $d^6$  chromium(0) complex is formed more readily than the  $d^7$  manganese(0) complex. This is not unexpected, since it is easier to add an extra electron to a non-bonding ' $t_{2g}$ -type' metal orbital than (it is) to an essentially antibonding ' $e_g$ -type' metal orbital or  $\pi$ -antibonding ligand orbital.

Now, returning to the theme of charge-compensating cation vacancies; when the Cr(I) and Mn(I) pentacyanonitrosyl ions are reduced, the resulting complexes will have four negative charges and therefore will only require one cation vacancy for charge compensation. This means that one neighbouring cation vacancy will be rendered redundant and therefore will migrate to some other position in the lattice. This could explain why the radiation-induced  $\nu(\text{CN})$  and  $\nu(\text{NO})$  bands comprise fewer lines than the original  $\nu(\text{CN})$  and  $\nu(\text{NO})$  bands.

Effect of  $\gamma$ -irradiation on E.S.R. Spectra.

1) Manganese.

a) Species formed after room-temperature irradiation.

Identification of Species A and B.

Now although the infra-red spectra of the room-temperature irradiated samples suggested that the pentacyanonitrosyl manganate(I) complex had been reduced, none of the e.s.r. spectra of similar samples appeared to substantiate this hypothesis. (of course we do not actually know what the e.s.r. spectrum of the reduced species would look like; the reduced complex could be like any of the three reduced nitroprusside species - see Chapter 3 and below)

Of the three manganese species seen by e.s.r. in room-temperature irradiated  $[\text{Mn}(\text{CN})_5\text{NO}]^{3-}/\text{KCl}$ , only one can be positively identified. This is the oxidised species (the  $d^5$  ion) which is formed before the other two species are clearly seen. The latter both give isotropic lines whose hyperfine coupling constants ( $A(^{55}\text{Mn}) = 95\text{G}$  and  $105\text{G}$  for species B and A, respectively) are of the same order as  $\text{Mn}^{2+}$  observed in several alkali halide lattices.<sup>20-24</sup> Thus species B and A would appear to be two forms of high spin  $d^5$  manganese(II), the former resembling  $[\text{Mn}(\text{H}_2\text{O})_6]^{2+}$  ( $g = 2.0038$ ,  $A = 95.2\text{G}$ ) most closely. Furthermore the absence of zero-field splitting lines requires a highly symmetrical ligand environment and a weak ligand field. So far no good explanation has been found for the formation of such species.

We can say unequivocally that species A and B are products

of irradiation damage since the e.s.r. spectra of unirradiated samples showed little or no paramagnetic content. This discounts the theory that  $[\text{Mn}(\text{CN})_5\text{NO}]^{3-}$  had hydrolysed and had been oxidised by the air giving  $[\text{Mn}(\text{H}_2\text{O})_6]^{2+}$  during the process of slow evaporation. It is possible that 'partial' hydrolysis had taken place giving  $[\text{Mn}(\text{CN})_n(\text{H}_2\text{O})_{5-n}\text{NO}]^{(n-2)-}$  for example, but this would not produce the highly symmetrical environment required.

Although the  $d^5$  ion is seen before species A and B, an examination of the e.s.r. spectra does not indicate that the lines due to species A and B grow at the expense of the lines attributed to the  $d^5$  ion. So the  $d^5$  ion does not appear to be the precursor of species A and B.

There appears to be no satisfactory explanation how  $[\text{Mn}(\text{CN})_5\text{NO}]^{3-}$  could lose all its ligands and end up in a perfectly symmetrical environment purely by the action of  $\gamma$ -irradiation. Ligand exchange is a possibility (vide infra) but it would seem highly improbable that five cyanide ligands and the nitrosyl group should all exchange with  $\text{Cl}^-$  in the KCl lattice on irradiation. There is, in fact, e.s.r. evidence for ligand exchange in complex ions in KCl following high-energy irradiation. Danon et al.<sup>25</sup> irradiated the system  $[\text{Rh}(\text{CN})_6]^{3-}/\text{KCl}$  and found hyperfine interaction with two equivalent chlorine atoms and concluded that two (trans) cyanide ligands had exchanged with two lattice chloride ions.

So at the present moment in time the nature of species A and B, and the mechanism whereby  $[\text{Mn}(\text{CN})_5\text{NO}]^{3-}$  appears to be stripped of its ligands on  $\gamma$ -irradiation must remain as unanswered questions.

#### Identification of Species C and D.

Species C. This species was observed when  $[\text{Mn}(\text{CN})_5\text{NO}]^{3-}$  doped into

KCl (and KBr) was irradiated at room temperature and gives an isotropic triplet ( $A(^{14}\text{N}) = 21\text{G}$ ,  $g = 2.005$ ) even when cooled to 77 K. A very similar triplet is observed<sup>26</sup> when KCl and KCN are fused together in a silica crucible for 10 minutes, cooled to room temperature and  $\gamma$ -irradiated for one hour. However it has not been assigned a structure. Its e.s.r. parameters are unlike those of any nitrogen containing radicals hitherto characterised. The radical probably contains carbon, but this has not been directly verified, since it has proved impossible to detect  $^{13}\text{C}$  splittings due to the presence of other e.s.r. lines in the free-spin region of the spectrum. A useful experiment would be to cool the sample to liquid-helium temperature to determine whether the isotropy is due to the radical tumbling rapidly in an interstice in the lattice. Without further information it would be unwise to draw any conclusions concerning the nature of this radical.

Species D. This species is produced in room-temperature irradiated samples of  $[\text{Mn}(\text{CN})_5\text{NO}]^{3-}$  in KCl, when in higher concentration. Like species C, it too gives an isotropic spectrum even at 77 K. ( $A(^{14}\text{N}) = 12.5\text{G}$ ,  $g = 2.003$ ). It is not absolutely certain that it is a 1:2:3:2:1 quintet, since the lines overlap with a much broader feature. If it is, then we may interpret it in terms of a species with two equivalent nitrogen atoms. Again it is impossible to detect  $^{13}\text{C}$  hyperfine splitting due to the presence of other lines in the spectrum. The radical  $(\text{CN})_2$  has been observed<sup>27</sup> in irradiated cyanide-doped potassium chloride, but does not tumble in the lattice. Moreover it has an  $A_{\text{iso}}(^{14}\text{N})$  value much lower (5.9G) than that of species E.

An alternative interpretation is that species D contains

hydrogen so that the quintet could be made up of two triplets in which the last line of one overlaps with the first line of the other giving five lines of intensity ratio 1:1:2:1:1. This would leave the value of  $A(^{14}\text{N})$  unaltered (12.5G) and would mean that the hyperfine splitting to hydrogen would be 25 gauss. A similar 'quintet' where  $A(^{14}\text{N}) = 17\text{G}$ ;  $A(^1\text{H}) = 34\text{G}$ , has been observed by Root<sup>1</sup> in KCl doped with cyanide ions prepared from aqueous solutions,  $\gamma$ -irradiated at room temperature. Addition of hydroxide ion impurity into the crystal lattice increased the yield of this species, which has been tentatively assigned to  $\text{HON}^+$ . Species D may well be a similar type of radical but it would be unwise to draw any definite conclusions without further evidence.

Species formed in  $\gamma$ -irradiated  $[\text{Mn}(\text{CN})_6]^{3-}/\text{KCl}$ .

This spectrum, which is illustrated in Figure 4.18,\* may be interpreted in terms of three broad g-features with h.f.s. of about 12G on two of the lines; any h.f.s. on the third line being unresolved. The interpretation of this spectrum is complicated by the fact that two of the g-features are close together, so that overlap makes it difficult to determine unambiguously whether there are five or six hyperfine lines. A spectrum obtained at Q-band frequency should resolve this difficulty. This spectrum could well be due to some impurity in the lattice since it is quite unlike the spectrum expected for the reduced complex  $[\text{Mn}(\text{CN})_6]^{4-}$ . This  $d^5$  species, if distorted from octahedral symmetry, should have a large manganese h.f.s. ( $A_{\text{iso}}(^{55}\text{Mn})$  should be of the order 70-80 gauss for an electron in a  $d_{xy}$  orbital on manganese, cf.  $[\text{Mn}(\text{CN})_5\text{NO}]^{2-}$ ). The species responsible for this spectrum will not be discussed further.

\* following p 85

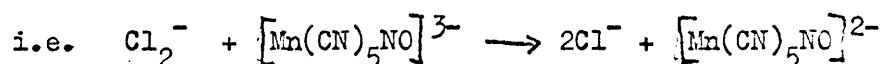
At this point it is instructive to mention the e.s.r. results obtained for some other irradiated hexacyano- complexes in alkali halide lattices. When the  $d^6$  ions  $[\text{Fe}(\text{CN})_6]^{4-}$  and  $[\text{Co}(\text{CN})_6]^{3-}$  incorporated into KCl lattices were  $\gamma$ -irradiated, the e.s.r. spectra showed hyperfine interaction with one and two nitrogen nuclei, respectively.<sup>11,17,18</sup> These spectra have been interpreted in terms of a flipping of one cyanide or two axial cyanides, respectively, forming isocyanide bonds. Since the nitrogen end of the cyanide has a ligand-field strength much lower than the carbon end,<sup>28,29</sup> the effect of forming isocyanide bonds is to make the metal  $d_{z^2}$  orbital less antibonding. Furthermore the number of cyanides which flip in each complex accords with the number of cation vacancies required for charge compensation in each case; one in the case of the iron complex and two in the cobalt case. These vacancies may be involved in the mechanism of flipping the CN group and may be partly responsible for the stabilisation of the isocyanide bonds which are closest to them.

b) Species formed after low-temperature irradiation.

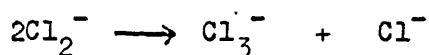
When  $[\text{Mn}(\text{CN})_5\text{NO}]^{3-}/\text{KCl}$  is irradiated at 77 K, the e.s.r. spectra of unwarmed samples apparently show only the presence of the  $V_K$  centre ( $\text{Cl}_2^-$ ). Now since this is a hole-centre one would expect to see an excess centre at the same time. The question is: do the 'free' electrons stay in a conduction band (as the F-centre) or are they trapped at some potential well? If some electrons are trapped then the most likely place would be at a complex ion site. However, if a  $d^7$  manganese(0) species is formed then it must be in a sufficiently low concentration so as not to be detected in the

powder spectrum. Furthermore, due to the complexity of the single crystal spectra, it has not proved possible to assign lines in the spectra unambiguously to a manganese species. However, further work on a crystal accurately mounted along a known axis should resolve the problem: subtracting out the lines due to the  $V_k$  centre should give the spectrum of any electron excess centre present.

When the sample is warmed to room temperature the  $V_k$  centre decays while the  $d^5$  ion  $[\text{Mn}(\text{CN})_5\text{NO}]^{2-}$  is formed simultaneously. The most likely mechanism for this is a simple electron-transfer process:



Some of the  $V_k$  centres may however, decay giving diamagnetic products:



It should be noted that, unlike the case of sodium nitroprusside,  $\gamma$ -irradiation of the pure potassium pentacyanonitrosyl-manganate(I) results in the oxidation of the  $d^6$  complex ion forming a  $d^5$  species rather than reduction giving a  $d^7$  ion. It is clear then that the  $d^7$  manganese(0) complex is not readily formed and must be a good deal more unstable than the corresponding  $d^7$  iron(I) complex.

We shall conclude this section by briefly considering a few possible structures for a pentacyanonitrosyl-manganate(0) complex. Now according to Manoharan and Gray's M.O. energy level scheme<sup>30</sup> (see also Chapters 2 and 3) we would expect the extra electron to go initially into the  $7e \pi^*(\text{NO})$  level. Due to the lower oxidation state on the metal, the additional electron would have less tendency to go onto the metal than in the nitroprusside case. Thus the radical

could resemble a trapped NO species (similar to those found in low-temperature irradiated nitroprusside) with very little manganese hyperfine interaction, depending on how close the NO was trapped to manganese.

Now if there were two cation vacancies, one situated above and the other below the axial ligands, then the latter could elongate into the vacancies, thus lowering the energy of the  $d_z^2$  orbital on manganese. In this case the electron could be said to be formally in an  $a_1$  ( $d_z^2$ ) metal orbital, but with extensive delocalisation onto the ligands. By analogy with the hexacyano-complexes of iron<sup>11</sup> and cobalt,<sup>17,18</sup> one might expect the axial cyanide to form an isocyanide bond. This would also tend to lower the energy of the  $d_z^2$  metal orbital.<sup>28</sup> Moreover, the very low oxidation state of the metal itself would tend to lower the ligand field splitting energy and hence lower the energy of the antibonding  $d_z^2$  and  $d_{x^2-y^2}$  orbitals.

Finally, we shall mention one manganese(0) complex which has been reported.<sup>31</sup> This is the species  $[(CO)_3(SPh)Mn]_2$ , whose e.s.r. spectrum shows two equivalent manganese atoms with the remarkably small h.f.s. of 14 gauss showing that the additional electron is delocalised very considerably.

## 2) Chromium.

The e.s.r. results indicated that the  $d^5$ , chromium(I) ion  $[Cr(CN)_5NO]^{3-}$  is reduced to the diamagnetic  $d^6$ , chromium(0) ion  $[Cr(CN)_5NO]^{4-}$  by the action of  $\gamma$ -irradiation on the KCl host lattice. This is confirmed by the infra-red results. There is no e.s.r. evidence for the formation of a  $d^7$  chromium(-I) ion. This is

not altogether unexpected in view of the manganese results and the fact that a two-electron reduction is not particularly favoured.

### 3) Iron.

Following  $\gamma$ -irradiation the species formed is identical to that formed on irradiating pure sodium nitroprusside at room temperature. It is highly probable that the nitroprusside ion was not incorporated into the alkali halide lattice in the same way as the chromium and manganese complexes, but was incorporated in clusters. This being so, no new information has been obtained from this particular study.

-----

In conclusion, although we have not achieved our original objective of preparing the  $\text{Mn}(0)$  and  $\text{Cr}(-I)$  complexes and correlating e.s.r. data for the isoelectronic series of  $d^7$  pentacyanonitrosyl ions, ( $\text{Fe}^I$ ,  $\text{Mn}^0$  and  $\text{Cr}^{-I}$ ), this study has not proved entirely fruitless. The infra-red work has shown that the complexes have been reduced following  $\gamma$ -irradiation and i.r. results have furnished evidence of interaction of the NO group with cation vacancies. The e.s.r. work on manganese complexes has posed many fascinating questions and it is to be hoped that further work may soon uncover some of the answers.

References for Chapter 4.

1. K.D.J. Root, Ph.D. Thesis, Leicester, (1967).
2. W.P. Griffith, J. Lewis and G. Wilkinson, J. Chem. Soc., 872, (1959).
3. F.A. Cotton, R.R. Monchamp, R.J.M. Henry and R.G. Young, J. Inorg. Nucl. Chem., 10, 28, (1959).
4. R.G.J. Miller (Ed.), "Laboratory Methods in I.R. Spectra," Heydon and Son Ltd., London, (1965).
5. H.A. Kuska and M.T. Rogers, J. Chem. Phys., 42, 3034, (1965).
6. W.C. Price, W.F. Sherman and G.R. Wilkinson, Spectrochim. Acta, 16, 663, (1960).
7. D.A.C. McNeil, J.B. Raynor and M.C.R. Symons, J. Chem. Soc., 410, (1965).
8. P.T. Manoharan and H.B. Gray, Inorg. Chem., 5, 823, (1966).
9. J.J. Fortman and R.G. Hayes, J. Chem. Phys., 43, 15, (1965).
10. T.G. Castner and W. Kanzig, J. Phys. Chem. Solids, 19, 139, (1961).
11. K.D.J. Root and M.C.R. Symons, J. Chem. Soc. (A), 2366, (1968).
12. G. Bor, Acta. Phys. Chem. Szeged (Suppl.), 4, 44, (1958).
13. L.H. Jones, J. Chem. Phys., 36, 1400, (1962).
14. J. Danon, R.P.A. Muniz and A.O. Caride, unpublished result.
15. W.P. Griffith, J. Chem. Soc., 3286, (1963).
16. S.I. Zanette, Ph.D. Thesis, Brazil, (1968).

17. J. Danon, R.P.A. Muniz, A.O. Caride and I. Wolfson, J. Mol. Struct., 1, 127, (1968).
18. A.O. Caride, S.I. Zanette and J. Danon, J. Chem. Phys., 52, 4911, (1970).
19. B. Jezowska-Trzebiatowska and J. Ziolkowski, Bull. Acad. polon. Sci., Ser. Sci. chim., geog., geol., 12, 503, (1964).
20. T.P.P. Hall, W. Hayes, R.W.H. Stevenson and J. Wilkens, J. Chem. Phys., 38, 1977, (1963).
21. T.P.P. Hall, W. Hayes, R.W.H. Stevenson and J. Wilkens, J. Chem. Phys., 39, 35, (1963).
22. W. Hayes and D.A. Jones, Proc. Phys. Soc., 71, 503, (1958).
23. T.T. Chang, W.H. Tantilla and J.S. Wells, J. Chem. Phys., 39, 2453, (1963).
24. K.K. Chan and L. Shields, J. Chem. Soc. (A), 3114, (1968).
25. J. Danon, A.O. Caride and R.P.A. Muniz, to be published.
26. K.D.J. Root, Private Communication.
27. K.D.J. Root and M.C.R. Symons, J. Chem. Soc.(A), 21, (1968).
28. D.F. Shriver, S.A. Shriver and S.E. Anderson, Inorg. Chem., 4, 725, (1965).
29. D.F. Shriver, "The Ambident Nature of Cyanide" in Structure and Bonding, Vol.1, Springer-Verlag, Berlin (1966).
30. P.T. Manoharan and H.B. Gray, Inorg. Chem., 5, 823, (1966).
31. R.E. Dessy, R. Kornmann, C. Smith and R. Hayter, J. Amer. Chem. Soc., 90, 2001, (1968).

PART II

STABILISED RADICALS IN PRECIPITATED POWDERS.

## INTRODUCTION TO PART II.

In Part II of this thesis we report the preparation of some interesting inorganic radicals by  $\gamma$ -irradiation of polycrystalline matrices containing impurity ions. These doped powders were produced by coprecipitating the microcomponent with a large excess of a suitable host material, particularly barium sulphate. An e.s.r. study of such radicals was used both as an aid to their identification and as a probe into their electronic structure and geometry.

The initial step in the radiation damage of inorganic diamagnetic solids is commonly electron ejection. If the ejected 'conduction' electron is trapped in some manner at a distance from the parent ion, and if the latter distorts to inhibit hole migration, then paramagnetic species result and can often be studied by e.s.r. In general these paramagnetic centres are stable only at low temperatures and readily decompose when the substrate is annealed. In the absence of impurity or defect sites the electron and the hole-centre may recombine to form an excited parent molecule which often decomposes before it has had time to drop to the ground state. A suitable impurity ion at a lattice site in the solid can act as a competing trapping site for the electron, and the resulting radical may have a high thermal stability. This stability will be enhanced if the configuration and charge of the paramagnetic impurity centre are compatible. For example, as we shall see later, the most stable oxyanion radicals trapped in an  $M^{II}XO_4$  lattice are almost certain to have the  $XO_4^{2-}$  structure.

The coprecipitation technique has several major advantages over conventional methods of obtaining dilute solid solutions of impurity ions in ionic crystals. In particular, one can often

coprecipitate either salts that do not form mixed crystals with the host when grown by slow evaporation from solution, or salts that decompose at elevated temperatures thus precluding melt-growth techniques. A fundamental understanding of the coprecipitation phenomenon is necessary before it is possible to anticipate which impurity ions will be incorporated into a particular precipitated matrix. We begin, therefore, with a brief review of those factors which influence this process.

#### Coprecipitation.

Coprecipitation of an impurity with the host material probably occurs either by the adsorption of the micro-component onto the host or by the formation of a solid solution. The concentration of the microcomponent is determined by:

- a) The relative sizes and charges of the coprecipitant and host lattice ions: A low concentration of coprecipitant ions will occur if their inclusion in the host lattice necessitates a significant lattice distortion. This distortion may be relieved however, if the impurity ions aggregate to form neutral molecules or clusters within the matrix.
- b) The structural relationship between the host lattice and the coprecipitant salt: The highest concentration of impurity ions are obtained when the materials are isomorphous. This seems to indicate that molecular units rather than individual ions are incorporated into the host lattice.

The rapid direct mixing of reagents in high concentration to form precipitates is the least reproducible method of inducing coprecipitation. However, this method does have the advantage that it often leads to a loss of selectivity by the host, and a concomitant increase in concentration of impurity ions. The solid state diffusion process may then be sufficiently rapid to render the solid phase homogeneous; the rate of diffusion increasing markedly when the precipitate is annealed close to its melting point. When the substrate forms as a colloidal precipitate, impurity ions in the solution can be adsorbed onto the solid surface. These foreign ions may then be incorporated into the substrate lattice, mainly as the 'inner' surface of each precipitate particle. This mechanism is particularly important since coprecipitation may occur with the formation of an adsorption compound even though the microcomponent ions are structurally incompatible with the host lattice.

There is no apparent reason why liquids should not be coprecipitated with solids, and indeed, solvent molecules have been found in close association with the host lattice (a) as part of the solvation structure in the normal crystal lattice, (b) as part of the crystal structure, (c) incorporated with the coprecipitated foreign ions, and (d) occluded and entrapped at microscopic sites.

We have used barium sulphate extensively as the host matrix for the coprecipitation of impurity ions for the following reasons:

- a) Barium sulphate forms as a colloidal precipitate from aqueous media at temperatures close to the boiling points of the solutions. Thus impurity ions whose structure may not be compatible with this lattice may still be coprecipitated as adsorption compounds. If the powders are then

annealed at high temperatures, ion diffusion occurs, rendering the solid phase homogeneous.

b) It does not contain abundant magnetic nuclei so that there is no line broadening in the e.s.r. spectrum of trapped radicals through superhyperfine interactions with the matrix.

c) It is highly insoluble in water.

d) The e.s.r. spectra of radicals formed by the  $\gamma$ -irradiation of pure  $\text{BaSO}_4$  are relatively simple, consisting of broad featureless absorptions centred close to the free-spin  $g$ -factor. Consequently, they do not complicate the analysis of e.s.r. spectra arising from trapped radicals.

Bibliography: A.G. Walton, "The Formation and Properties of Precipitates," Interscience, New York, (1967).

CHAPTER 5

INTERACTION OF TRAPPED HYDROGEN ATOMS WITH ALKALI  
METAL IONS IN BARIUM SULPHATE.

## Introduction.

Hydrogen atoms have been extensively studied by e.s.r. in a wide variety of solid matrices.<sup>1</sup> In several instances extra features have been observed in the vicinity of the expected isotropic low- and high-field lines. Thus in aqueous acid media, satellites were detected flanking the main lines, whose relative intensity increased as the microwave power was increased.<sup>2</sup> These lines are caused by nuclear transitions of neighbouring protons, and are not normal hyperfine features. Jen and co-workers<sup>3</sup> detected a hyperfine interaction to neighbouring xenon nuclei when hydrogen atoms were trapped in a xenon matrix, and strong coupling to surrounding fluoride ions was detected for hydrogen atoms trapped interstitially in calcium fluoride crystals.<sup>4</sup>

In the present work, the exposure of precipitated barium sulphate (also strontium sulphate and barium phosphate) to  $\gamma$ -rays led to the formation of hydrogen atoms which were subsequently trapped at a variety of sites in the host lattice.<sup>5,6</sup> In each case one such trapped hydrogen atom centre, stable at 77 K, exhibited hyperfine coupling to a second nucleus.

## Experimental.

All reagents used were of AnalaR grade purified further by recrystallisation from aqueous solution prior to use. Barium sulphate was precipitated from aqueous solutions of barium chloride containing approximately 10% of required impurity ions by slow addition of aqueous sodium sulphate at 370 K. Strontium sulphate powders were prepared similarly using aqueous solutions of

strontium chloride, while barium phosphate powders were prepared using aqueous solutions of barium chloride and tri-sodium orthophosphate. The resulting suspensions were digested at about 340 K for several hours, filtered and dried at about 350 K for two hours prior to exposure to  $^{60}\text{Co}$   $\gamma$ -rays at 77 K or room temperature. Radiation doses varied from about 0.5 to 30 Mrad. E.s.r. spectra were measured at 77 K or room temperature with Varian E3 or V4502 high-resolution spectrometers, the latter being calibrated with a proton resonance probe.

### Results.

When a sample of barium sulphate, which had been precipitated from aqueous <sup>solution</sup> containing sodium ions, was  $\gamma$ -irradiated at 77 K its e.s.r. spectrum measured at this temperature and a microwave power level of 10 mW showed the presence of three discrete paramagnetic species. (Figure 5.1). The most abundant radical, characterised by an intense single absorption line centred close to the free-spin  $g$ -factor, also resulted when fused barium sulphate was  $\gamma$ -irradiated at 77 K. This centre probably originated from the radiation damage of sulphate anions. However, we were unable to detect hyperfine interactions involving  $^{33}\text{S}$  ( $I = 3/2$ , 0.74% isotopic abundance) and therefore, could not unambiguously identify this species. For the purposes of the present account we shall label this centre the "sulphate" radical.

At 77 K and a microwave power level of 100 mW, features from the "sulphate" radical and the second paramagnetic centre, labelled Radical B in Figure 5.1, were almost completely saturated

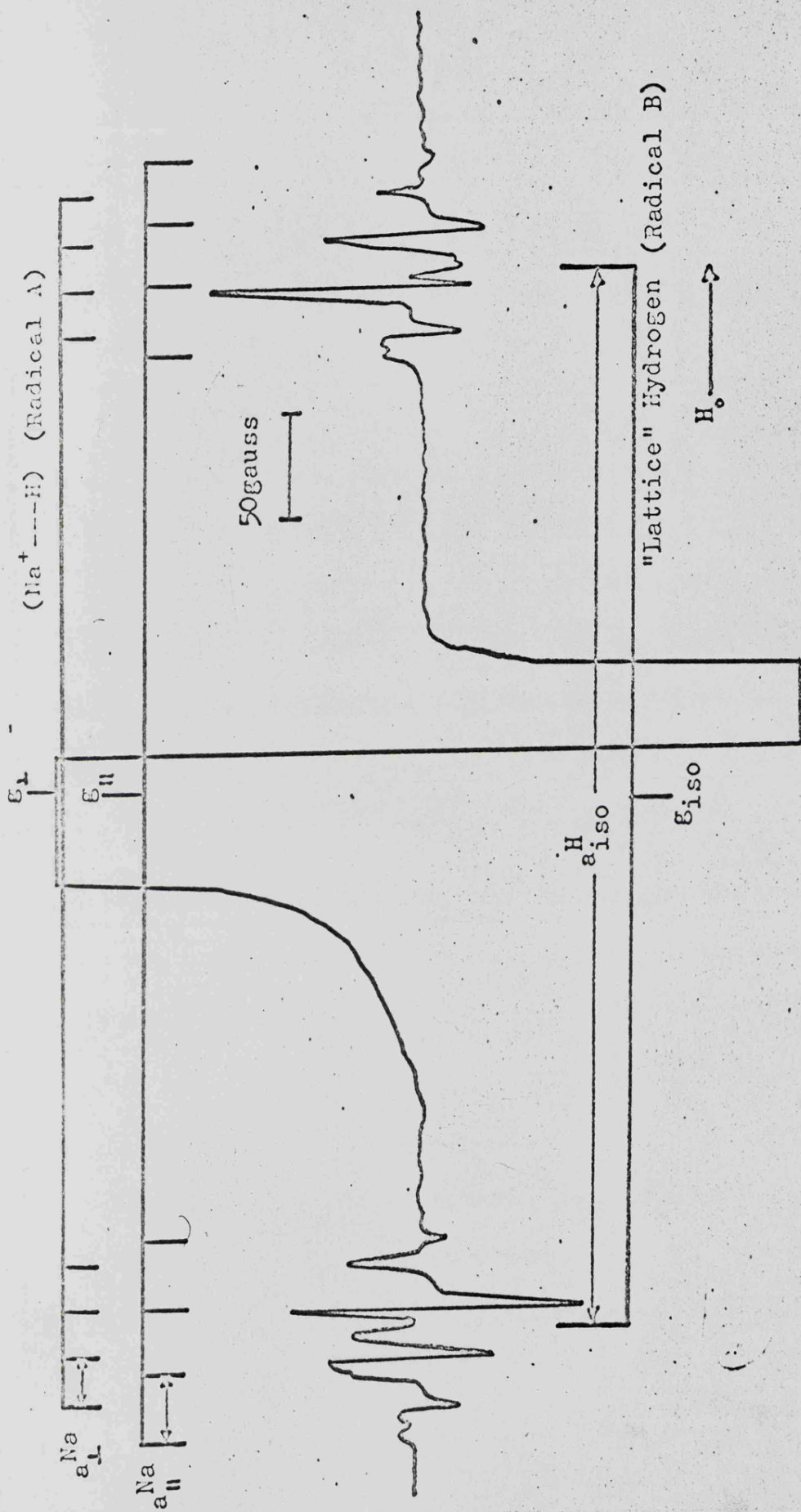


Figure 5.1 The ESR spectrum of irradiated, precipitated  $\text{BaSO}_4$  measured

at 77 K.

whilst those of Radical A, a pair of axially symmetric quartets (Figure 5.2) separated by approximately 511 gauss, had increased both in resolution and intensity. When singly charged anions such as nitrate, chlorate or perchlorate were added as the sodium salts to the solution prior to precipitation, the quartets due to Radical A were greatly enhanced relative to the lines due to Radical B.

When potassium ions were incorporated into the barium sulphate lattice an analogous species to Radical A was formed, but the hyperfine quartet features from this centre were less well resolved and it was only possible to obtain the perpendicular hyperfine splitting constants from the outermost features of the quartets. (Figure 5.3).

When a sample of barium sulphate, which had been precipitated using  $H_2O$ -free reagents in a solution of  $D_2O$ , was  $\gamma$ -irradiated at liquid-nitrogen temperature, its e.s.r. spectrum at 77 K and 100 mW showed that the original principal doublet splitting of 511 gauss of Radical A had collapsed to a triplet of approximately 79 gauss separation. (Figure 5.4). These deuterium hyperfine triplets still showed the quartet splittings associated with Radical A.

Features from Radical A decayed irreversibly when the sample was annealed to about 220 K and there was a concomitant increase in intensity of the e.s.r. signal from Radical B.

Figures 5.5 and 5.6\* show the e.s.r. spectra, measured at 77 K and a microwave power level of 10 mW, of low-temperature irradiated strontium sulphate doped with sodium perchlorate and barium phosphate doped with sodium selenate, respectively. The

\* following pp 120, 121.

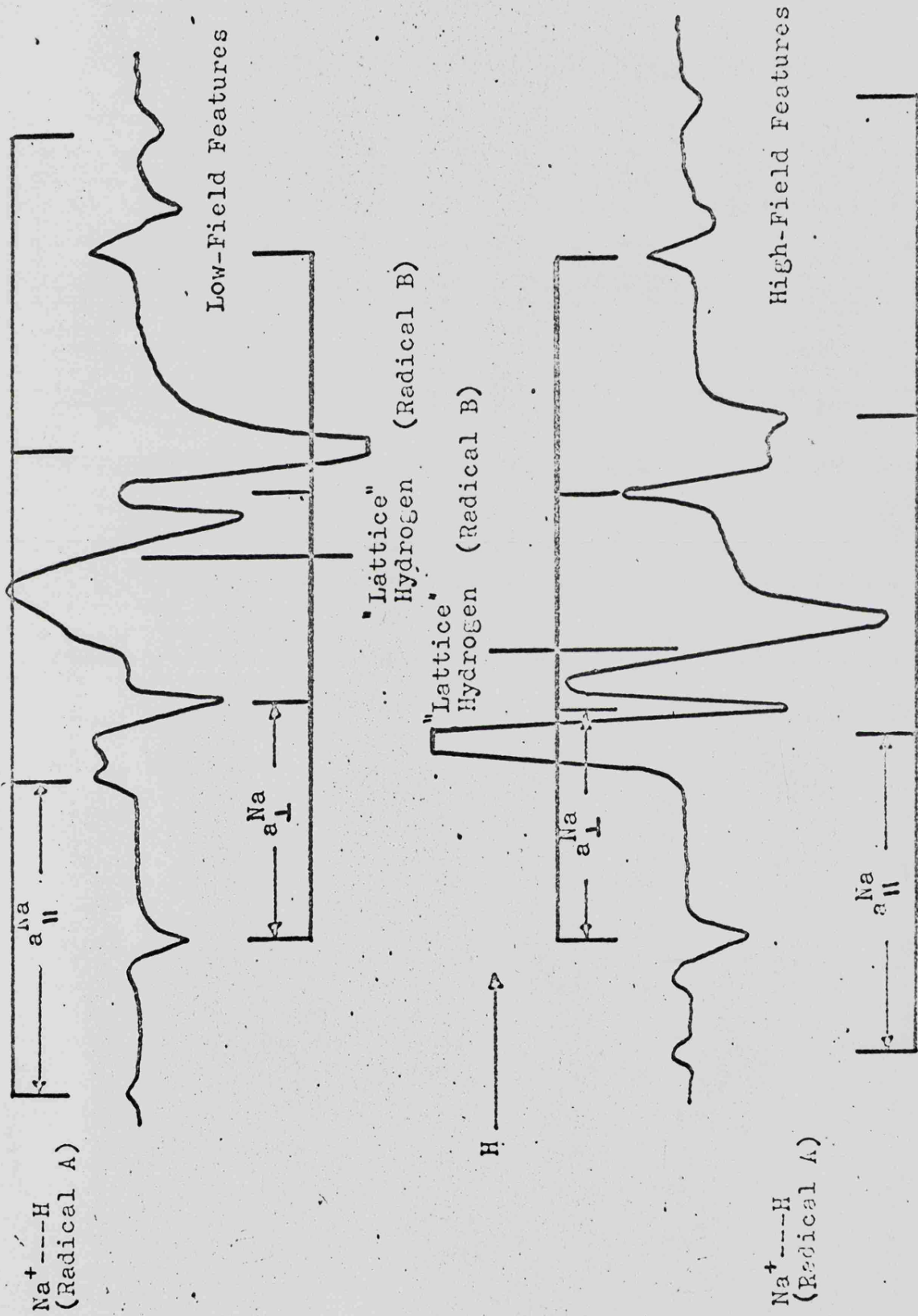


Figure 5.2 The Low-field and High-field Components of the  $\text{NaH}^+$  and Lattice Hydrogen ESR Spectra in  $\text{BaSO}_4$ . Measured at 77 K.

→ H

30 G

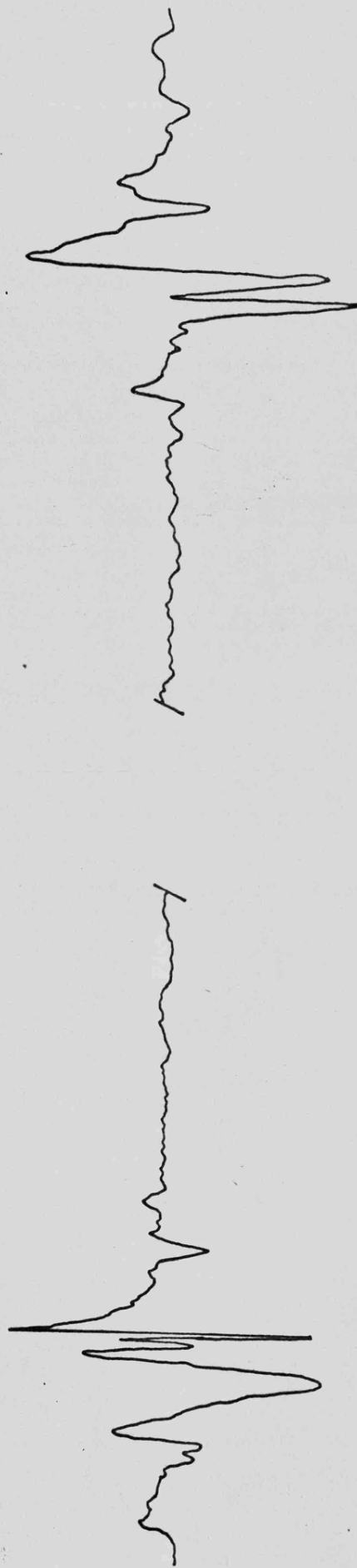
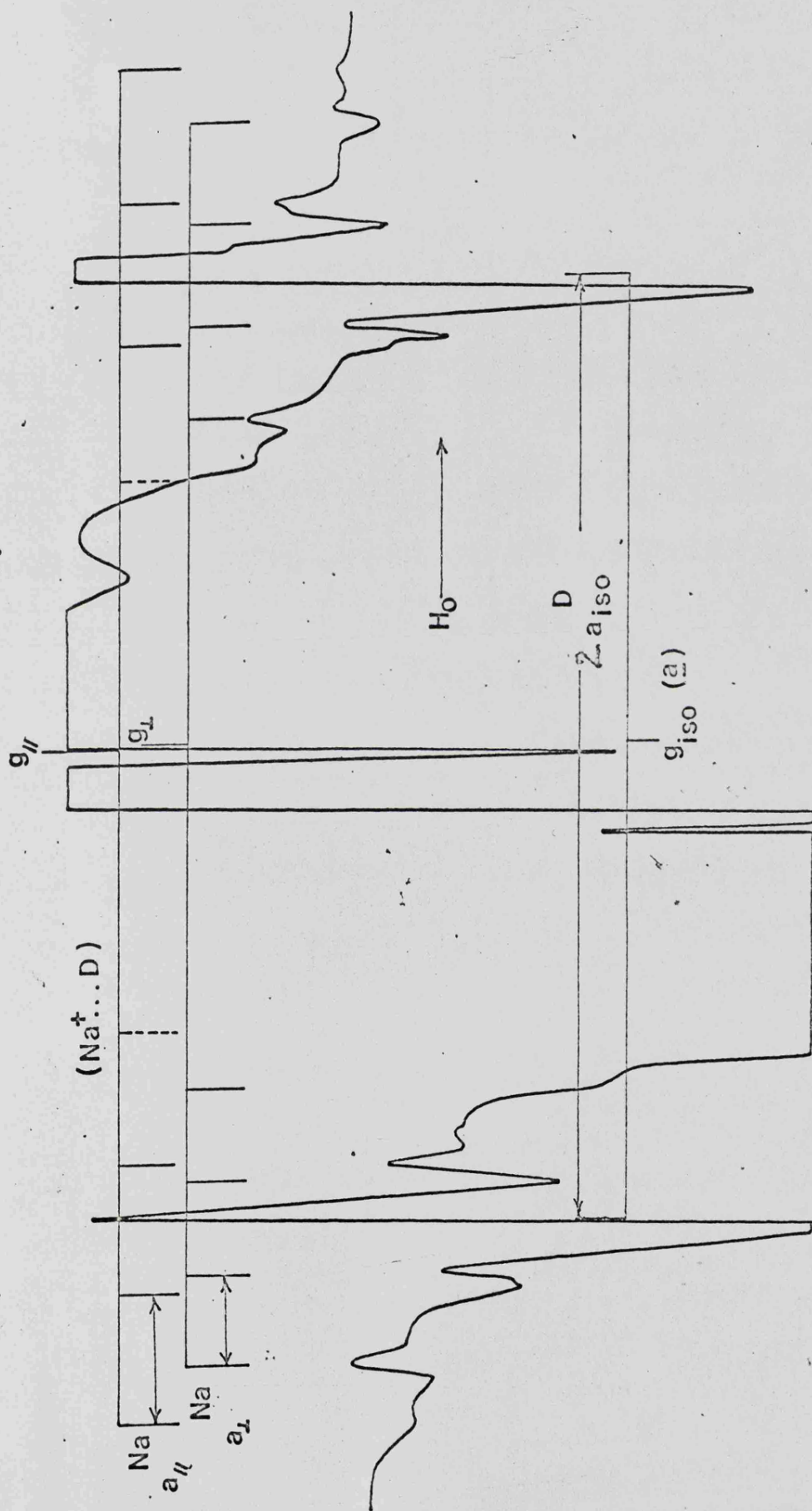


Figure 5.3 ESR Spectrum of BaSO<sub>4</sub> Containing K<sup>+</sup> Ions  $\gamma$ -Irradiated at 77 K.

Figure 5.4



ESR Spectrum of  $\text{BaSO}_4$  Precipitated from  $\text{D}_2\text{O}$

$\chi$ -Irradiated at 77 K.

multi-line features in the 'hydrogen atom' regions of these spectra also decay irreversibly on warming.

### Discussion.

#### Identification of Radical A.

We have assigned Radical A the structure  $\text{NaH}^{\cdot}$  for the following reasons:

- a) The major doublet splitting of 511 gauss must arise from the interaction of the unpaired electron with a single proton ( $I = \frac{1}{2}$ ). Deuterium substitution resulted in the expected major triplet splitting of 79 gauss arising from the coupling of the unpaired electron with the  $^2\text{H}$  nucleus ( $I = 1$ ).<sup>1</sup>
- b) The secondary, axially symmetric quartet splitting arises through hyperfine coupling to a sodium nucleus ( $I = 3/2$ ). A marked reduction in this subsidiary splitting occurred when potassium ions ( $^{39}\text{K}$ ;  $I = 3/2$ , 93.08% isotopic abundance) replaced sodium ions in the sulphate lattice. This is to be expected in view of the smaller magnetic moment of potassium compared to sodium.<sup>1</sup> We have ruled out the possibility that this splitting arises through coupling to a  $^{35}\text{Cl}$  nucleus ( $I = 3/2$ ; 74.6% isotopic abundance) of a chloride ion for two reasons. Firstly, we were unable to detect features arising from the corresponding  $^{37}\text{Cl}$  nucleus ( $I = 3/2$ , 24.6% isotopic abundance) and secondly, we obtained exactly the same e.s.r. spectrum from an irradiated sample of barium sulphate precipitated from a solution of barium

nitrate, in the complete absence of chloride. The low natural abundance of the magnetic  $^{135}\text{Ba}$  and  $^{137}\text{Ba}$  nuclei ( $I = 3/2$ ; 6.6 and 11.3% isotopic abundance, respectively) makes it unlikely that these isotopes are responsible for this subsidiary interaction.

c) The intensity of the e.s.r. signal for this radical increased markedly when the barium sulphate was precipitated in the presence of singly charged anions such as  $\text{NO}_3^-$ ,  $\text{ClO}_3^-$  and  $\text{ClO}_4^-$ . The reason for this is that in order to maintain charge neutrality in the sulphate lattice, the inclusion of singly charged anions requires a concomitant increase in the concentration of impurity sodium ions. Although we formulate the species as  $\text{NaH}^+$  (and  $\text{KH}^+$ ), this is not meant to imply the complete absence of other atoms with non-magnetic nuclei in the overall unit.

#### Identification of Radical B.

The e.s.r. spectrum of radical B is completely isotropic and is characteristic of a species containing a single magnetic nucleus of spin:  $I = \frac{1}{2}$ . We may confidently assume that this species is a hydrogen atom trapped near a barium or sulphate ion site in the lattice, since the spin-resonance parameters of this centre are similar to those reported for hydrogen atoms trapped in a wide variety of matrices<sup>1</sup> and also to hydrogen atoms studied in the gas phase.<sup>1,7,8</sup> When the host lattice was precipitated from  $\text{D}_2\text{O}$ , radiation damage resulted in the formation of the predicted, corresponding deuterium atom centre.

The e.s.r. results obtained for Radicals A and B are included in Table 5.1.

Structure of the Alkali Metal Ion-Hydrogen Atom Centre.

Approximate spin-densities have been calculated as indicated in Table 5.1. The anisotropic hyperfine tensor representing the interaction of the unpaired electron with the sodium nucleus has the form  $(2B, -B, -B)$ . This anisotropic coupling to sodium can be entirely explained in terms of an indirect dipolar interaction from spin on hydrogen, there being no need to invoke 3p-orbital participation in the Na-H  $\sigma$ -bond. Using a simple point-dipole calculation we obtain a sodium-hydrogen bond length of  $1.5\text{\AA}$ . This can be compared with the value of  $1.8\text{\AA}$  obtained for sodium hydride in the gas phase.<sup>8</sup> A somewhat more refined calculation, in which the electron in the hydrogen 1s orbital was treated as being distributed octahedrally about the nucleus at a distance equal to the Bohr radius (see Appendix II), gave a value of the sodium-hydrogen bond length of  $1.8\text{\AA}$ .

Since the anisotropic coupling is necessarily positive, the isotropic coupling to  $^{23}\text{Na}$  must also be positive and almost certainly results from the direct delocalisation of the unpaired electron into the sodium 3s-orbital, giving a spin-density of 0.054. In that case, the proton coupling is unexpectedly large, being, in fact, slightly greater than that of hydrogen atoms in the gas phase.<sup>7,8</sup> This increase may be interpreted in terms of a slight orbital contraction for the 1s orbital on hydrogen, caused by a partial transfer of positive charge (or in other terms,

TABLE 5.1. Electron Spin Resonance Parameters for the (Na<sup>+</sup>---H) Centre and Related Species.

Radical	$g$ -tensor <sup>a</sup>	$\epsilon_{\parallel}$	$\epsilon_{av}$	$B_{\parallel}$	$B_{\perp}$	$A_{iso}$	$B_{\parallel}$	$B_{\perp}$	$A_{iso}$	Hydrogen Hyperfine Splittings (in gauss)	Hydrogen Hyperfine Splittings (in gauss)	$a_s^2$ on metal	Ref.
H atoms in the gas phase			2.00226										1,7,8
B "Lattice" Hydrogen centre in BaSO <sub>4</sub>			2.0015										c
A (Na <sup>+</sup> ---H)	2.0012	2.0013	2.0013	4.2	-2.1	17.2	+1.7	-0.8	511.5	0.054			c
(K <sup>+</sup> ---H) b.	2.0016					4.0					$a_{\perp}^D \approx$	500	~0.05 c
(Na <sup>+</sup> ---D) b.	2.0032					16.2					$a_{\perp}^D \approx$	79	c

a. Corrected to 2nd-order by application of the Breit-Rabi equation.<sup>22</sup>

b. Only the perpendicular features have been resolved.

c. This work.

a small increase in the effective nuclear charge on hydrogen, induced by the neighbouring cation).<sup>9</sup> Proton hyperfine coupling is particularly sensitive to small changes in this term, and a very small change would readily accommodate the present data.<sup>6</sup> However, an unrestricted Hartree-Fock (UHF) calculation actually gave a  $^1\text{H}$  coupling slightly greater than that for the free atom,<sup>10</sup> so this concept of orbital contraction is not necessarily required to explain these results.

An alternative mechanism to explain the increase in the proton hyperfine coupling is the theory proposed by Adrian,<sup>11</sup> and later developed by Jen and co-workers,<sup>12</sup> to account for the effect of the matrix upon the wave-functions of trapped atoms. They suggest that the perturbation of the trapped atom's wave-function by the matrix can be envisaged as the sum of several opposing effects, principally:

- a) The van der Waal's (dispersion) forces between two interacting particles, which will tend to maximise the interaction energy by expanding the wave-functions of the particles.
- b) Pauli exclusion forces, which operate when the particle separation is small, and which effectively result in a shrinking of the wave-functions of the interacting particles away from each other. This interaction will also admix some of the wave-functions of the matrix particles with those of the trapped atom.

Hence, for  $\text{NaH}^+$ , mechanism a) would lead to an overall reduction in the proton hyperfine coupling from the free atom value,

whilst mechanism b) would give rise to an increased proton coupling and superhyperfine splitting from the 'matrix' sodium ion. If this theory is correct then our experimental results clearly indicate that the effects of mechanism b) predominate over those of mechanism a). The theoretical UHF calculations<sup>10</sup> also suggested that there was no bonding between the hydrogen atoms and sodium ions, although the species detected is clearly well defined. It is, of course, possible that the actual trapping does not involve sodium ions, which just happen to be close to effective trapping sites: this point is considered later.

#### The Structure of the "Lattice" Hydrogen Centre.

The  $\text{NaH}^+$  centre was irreversibly converted to "lattice" hydrogen when the barium sulphate host lattice was annealed at 220 K, indicating the higher thermal stability of the latter centre. By analogy with the bonding scheme proposed for hydrogen atoms trapped at basic anion sites in a variety of irradiated phosphates,<sup>13,14</sup> we suggest that the proton of the "lattice" hydrogen centre forms a  $\sigma$ -bond to a basic oxygen of the sulphate anion. The extra electron is then accommodated in the corresponding  $\sigma^*$ -level. Since the  $\sigma$ -level is concentrated primarily on oxygen, the  $\sigma^*$ -level is mainly on hydrogen and therefore, the spin-resonance parameters for this centre closely resemble those of a free hydrogen atom.

#### Mechanism of Formation and Trapping.

Since there is no apparent reason why sodium ions should intrinsically favour hydrogen atom trapping in barium sulphate,

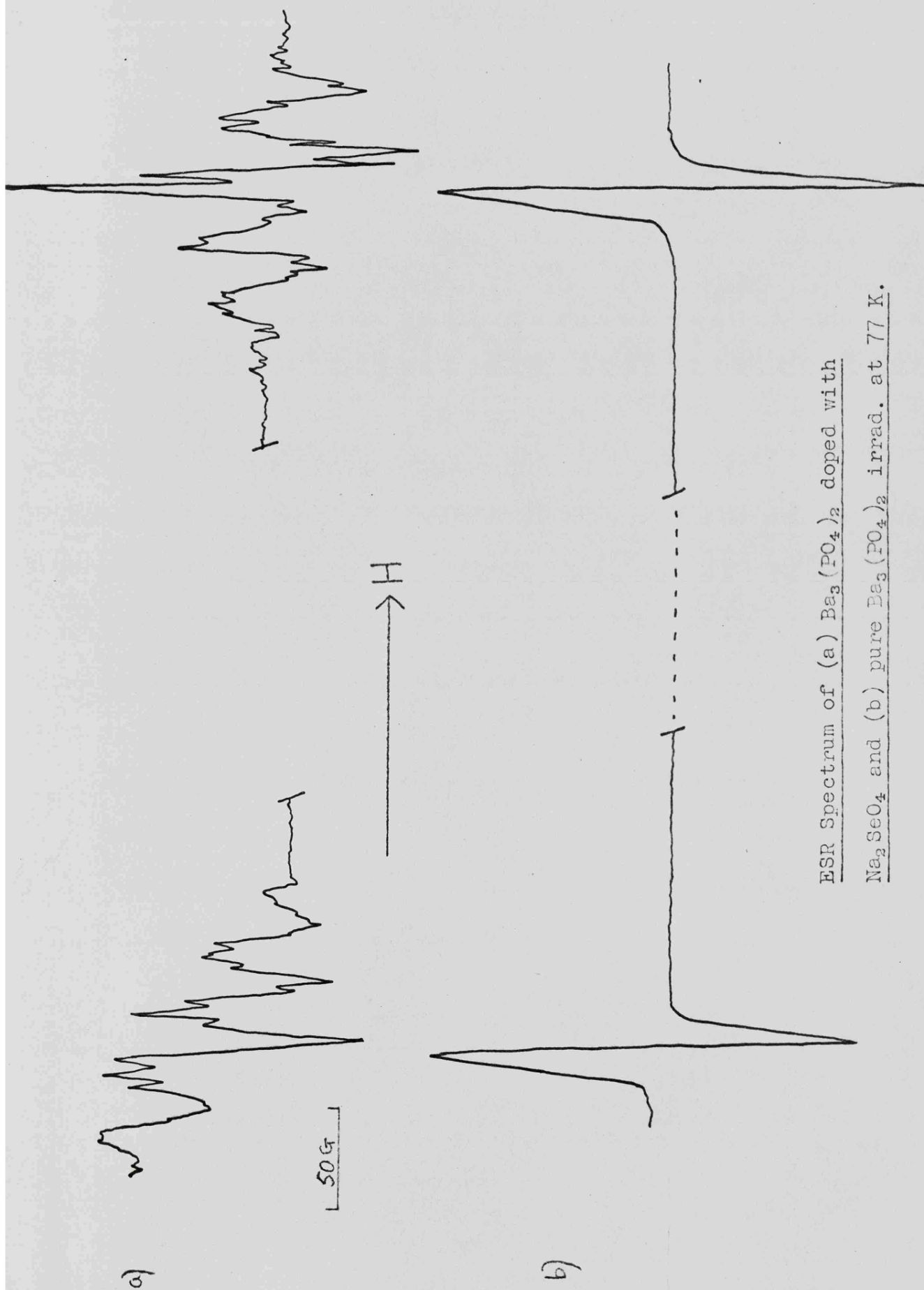
we need to find some other explanation for the high percentage of the  $\text{NaH}^+$  species in material containing only trace quantities of sodium ions. We propose the existence of two distinct and competing trapping sites in the sulphate lattice. X-ray studies of barium sulphate precipitated from aqueous solution have suggested that water coprecipitates with the salt and exists as a solid solution in the lattice; a group of three water molecules replacing a  $\text{BaSO}_4$  unit.<sup>15</sup> In an analogous manner, alkali metal ions and solvent molecules may be simultaneously coprecipitated if the size of the combined unit is appropriate. The lithium ion is known to carry one molecule of water into the precipitated sulphate lattice.<sup>16</sup>

If conduction electrons resulting from the radiation damage of the host lattice are subsequently trapped at defect sites containing an alkali metal ion and a water molecule, then there is a high probability that hydrogen atoms, formed by dissociative electron capture by  $\text{H}_2\text{O}$ , will be trapped near an alkali metal site (and remain trapped close to sodium). Alternatively, if these generated electrons are trapped at defect sites containing only coprecipitated solvent, then the resulting hydrogen atoms may be trapped at a sulphate anion site.

#### Related Systems.

Of the range of other host lattices and additives studied, only a few gave any clear indication of comparable trapping sites. One of the more interesting results was obtained in the case of barium phosphate doped with sodium selenate. When the polycrystalline sample was irradiated at 77 K, the e.s.r. spectrum measured at 77 K (Figure 5.6) showed four broad lines flanking the normal "lattice" hydrogen atom

Figure 5.6

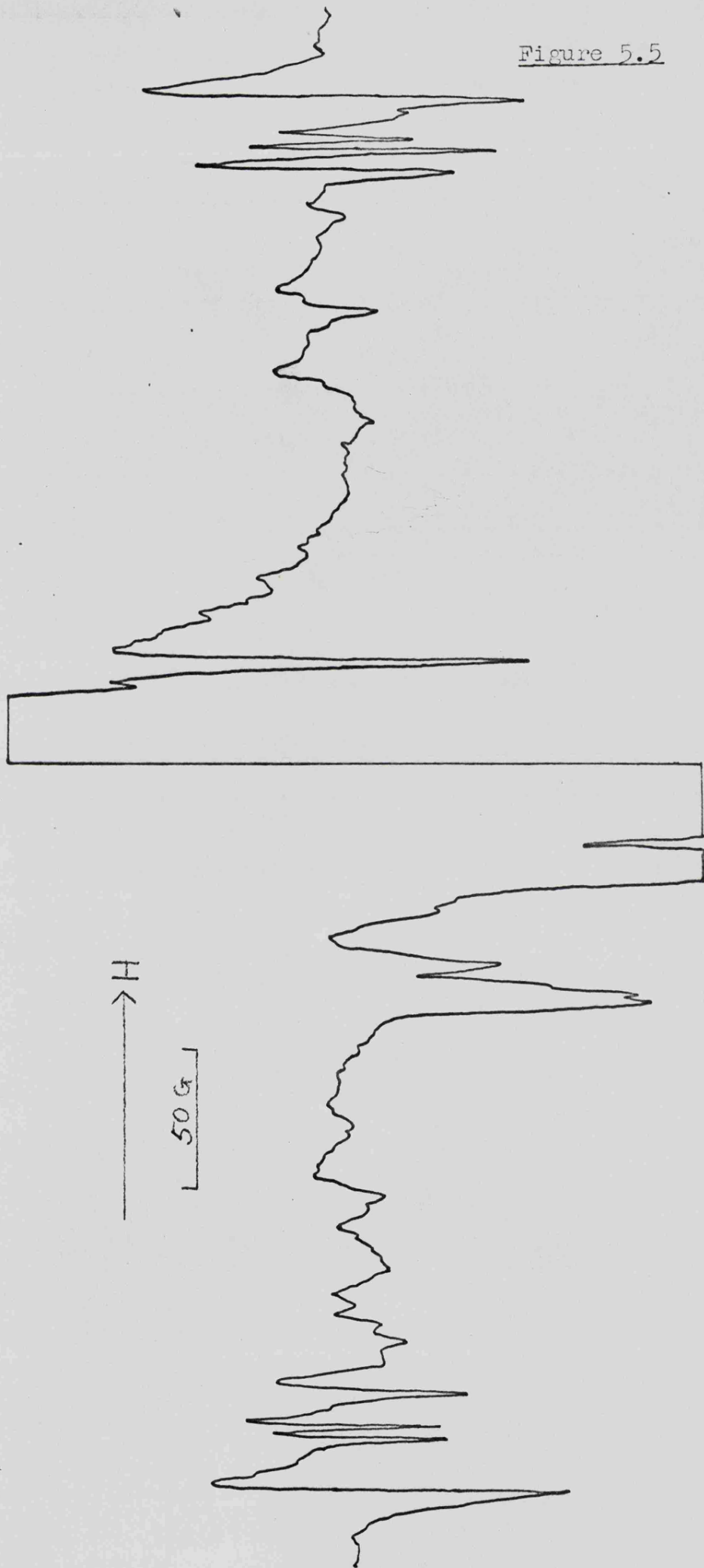


ESR Spectrum of (a)  $\text{Ba}_3(\text{PO}_4)_2$  doped with  $\text{Na}_2\text{SeO}_4$  and (b) pure  $\text{Ba}_3(\text{PO}_4)_2$  irradiated at 77 K.

lines, whose hyperfine coupling constants were approximately 30 G and 503 G respectively. In addition, several of these lines showed an extra 'triplet' splitting of about 5 G. The quartet features suggested a hyperfine coupling to  $^{23}\text{Na}$  ( $\sim 30$  G), and if these lines consist of parallel and perpendicular features as for the  $\text{NaH}^+$  centre in barium sulphate (Figure 5.2), then the extra coupling could be interpreted in terms of an isotropic doublet splitting of 5 G. One possible source of this coupling is interaction with a  $^{31}\text{P}$  nucleus in the  $\text{PO}_4^{3-}$  anion ( $^{31}\text{P}$ ;  $I = \frac{1}{2}$ , 100% isotopic abundance). If this were correct, it would support the suggestion of Atkins *et al*<sup>17</sup> that the major stabilising force for trapping in such environments is weak bonding to the anions, since there seemed to be some correlation with anion basicity.<sup>17</sup> This reasoning has been extended to successfully explain the ultraviolet absorption assigned to hydrogen atoms in aqueous solution.<sup>18</sup> To substantiate this theory, we have irradiated 'pure' barium phosphate (containing only traces of water as impurity) at 77 K, and the e.s.r. spectrum measured at 77 K (Figure 5.6), shows two broad hydrogen atom lines with definite signs of an unresolved doublet splitting of about 5 G; thus giving further support to the view that anion interaction is important in these centres.

When a sample of strontium sulphate doped with sodium perchlorate was irradiated at 77 K, the e.s.r. spectrum measured at 77 K (Figure 5.5) showed, in addition to the lattice hydrogen atom lines ( $A = 503$  G), a multiline pattern within these broad lattice hydrogen lines and not flanking them. Thus, the spectrum is quite unlike any of the other hydrogen atom centres previously seen, and could consist of a number of overlapping lines making interpretation difficult. For technical reasons it was not possible to obtain a spectrum at Q-band frequency, which could have resolved the difficulty. However, whatever the nature of this

Figure 5.5



ESR Spectrum of  $\text{SrSO}_4$  Doped with  $\text{NaClO}_4$   $\gamma$ -Irradiated at 77 K.

centre, there does appear to be a marked degree of delocalisation of the hydrogen atom's unpaired electron density onto some other atom(s) in view of the proton hyperfine coupling constant being reduced from its free atom value of 507 G to approximately 460 G. It is possible that there may be more than one hydrogen atom centre producing this spectrum, since there is no clear hyperfine splitting to a single magnetic nucleus; coupling to  $^{87}\text{Sr}$  being very unlikely ( $^{87}\text{Sr}$ ;  $I = 9/2$ , 7.02% isotopic abundance).

Other Systems: Experimental Evidence for the  $\text{H}_2^-$  and  $\text{H}_2^+$  Radical Ions.

Introduction.

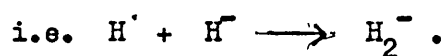
In order to explain the magnitude of the proton hyperfine coupling in  $\text{NaH}^+$  (511.5 G), which is even greater than the gas-phase value, we invoked the excess charge theory (vide supra) first proposed by Symons<sup>9</sup> to explain the effect of excess charge on the magnitude of proton coupling constants in various organic and inorganic radical ions. The basic concept is simply that the effective radius of the hydrogen 1s atomic orbital should be allowed to change systematically with the excess charge, or, in other terms, that the effective nuclear charge on the proton should be thought of as deviating from unity. This effect is not of great importance for most atoms in molecules, since the fractional change in nuclear charge ( $Z$ ) is relatively small and the effect is buffered by the remaining electrons. For protons, however, a small change in the effective nuclear charge ( $Z_{\text{H}}$ ) can make a large difference to the coupling constant, which will be proportional to  $Z_{\text{H}}^3$ . The theory has been used successfully to explain the magnitude of the proton hyperfine splitting in cations and anions of aromatic hydrocarbons such as anthracene,<sup>19</sup> and also in the series of isoelectronic planar radicals,  $\text{BH}_3^-$ ,  $\text{CH}_3$  and

$\text{NH}_3^+$ . Typical changes in  $Z_{\text{H}}$ , calculated from the observed coupling constants are included in Table 5.2. In the case of  $\text{NaH}^+$ , the increase in the proton hyperfine coupling constant over the expected value can be readily accommodated on this theory if there is a small increase in the effective nuclear charge on H ( $Z_{\text{H}} = 1.024$ ), induced by the neighbouring sodium ion. (Table 5.2).

One prediction that can be drawn from this theory is that the overall hyperfine coupling (2A) for  $\text{H}_2^-$  may be very much less than the value of about 500 G normally expected, whereas that of  $\text{H}_2^+$  could be quite a large amount in excess of this value. It was in order to test this prediction that attempts were made to prepare the ions  $\text{H}_2^-$  and  $\text{H}_2^+$  and to study their e.s.r. spectra.

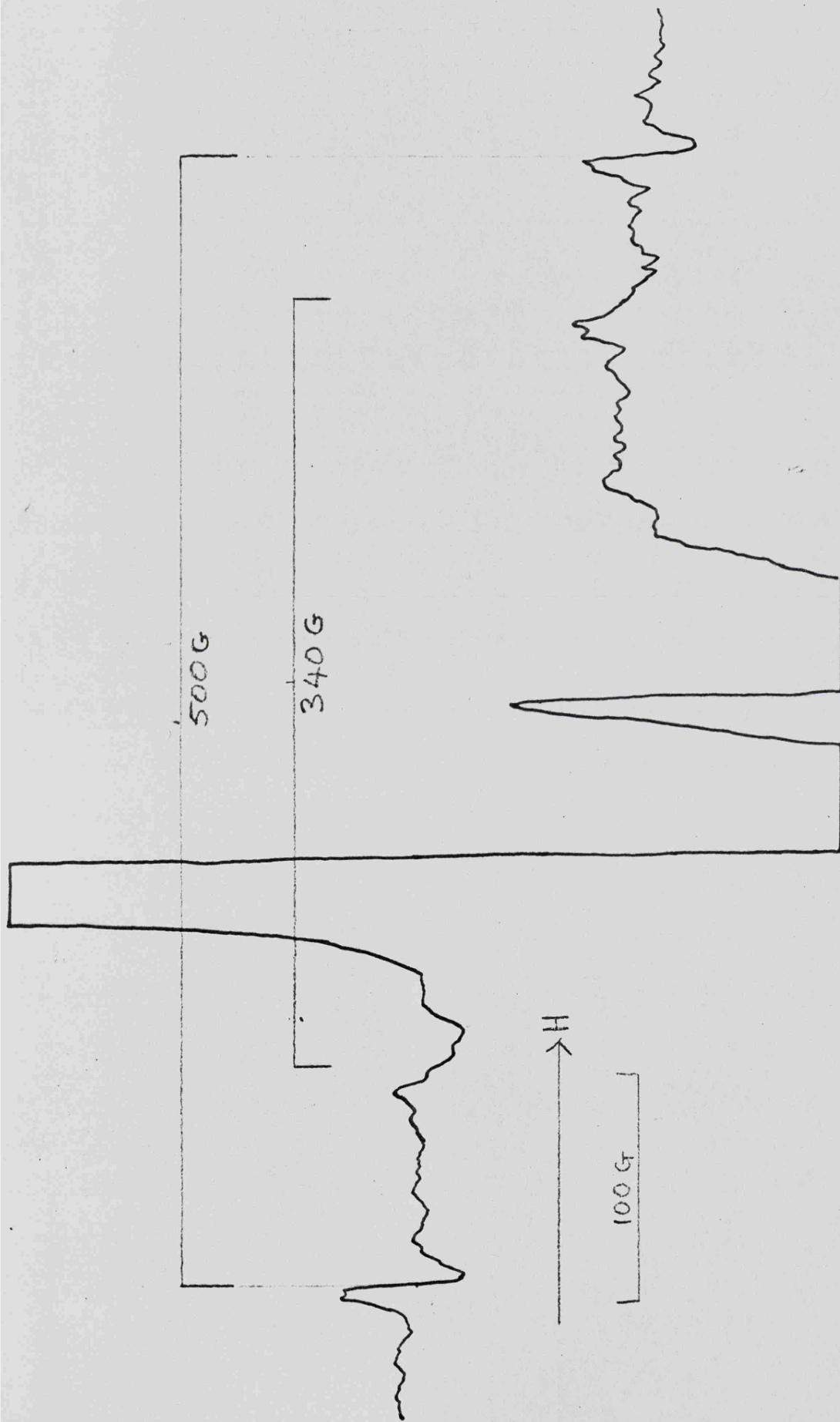
i) The Radical-Ion  $\text{H}_2^-$ .

Attempts were made to produce this centre by  $\gamma$ -irradiating a number of alkali metal and alkaline earth hydrides at 77 K; the idea being that hydrogen atoms might be trapped at hydride ion sites forming the required centre:



However, it was only in the case of irradiated lithium hydride that there was any indication of the formation of any other hydrogen atom centre apart from the 'normal' hydrogen atom centre of splitting  $\sim 500$  G. The e.s.r. spectrum of a polycrystalline sample of LiH  $\gamma$ -irradiated at 77 K (Figure 5.7) shows the presence of three paramagnetic centres; one of which gives a broad parallel and perpendicular feature centred around the free spin region of the spectrum, the second gives a doublet splitting of about 500 G corresponding to a 'normal' trapped hydrogen atom centre, whilst the third centre apparently consists of a broad doublet

Figure 5.7



ESR Spectrum of Lithium Hydride  $\gamma$ -Irradiated at 77 K.

Table 5.2 Proton Hyperfine Parameters for Various Radical Cations and Anions.

<u>Radical Ion</u>	<u><math>a_H</math> (gauss)</u>	<u><math>Z_{eff}</math></u>	<u>Reference</u>
Anthracene <sup>+</sup> (9H)	6.7	1.03	19
Anthracene <sup>-</sup> (9H)	5.6	0.97	19
BH <sub>3</sub> <sup>-</sup>	16.5	0.90	20
CH <sub>3</sub>	22.5	1.00	21
NH <sub>3</sub> <sup>+</sup>	27.0	1.06	21
NaH <sup>+</sup>	511.2	1.02	This work
H <sub>2</sub> <sup>-</sup>	340	0.87	This work
H <sub>2</sub> <sup>-</sup>	348	0.87	a
H <sub>3</sub> <sup>+</sup>	630	1.08	This work
H <sub>2</sub> <sup>+</sup>	660	1.09	a

a. values predicted by Dr. T.A. Claxton  
(Nature, 226, 1242, (1970))

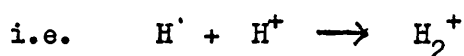
whose splitting is approximately 340 G. In view of the excess charge effect (vide supra), these lines could be the outermost features of  $\text{H}_2^-$ , the innermost features not being detected due to the intense, broad features in the centre of the spectrum. Coupling to two equivalent nuclei of spin,  $I = \frac{1}{2}$  is expected to give three lines of intensity ratio 1:2:1. However, the large hyperfine splitting in the present case indicates a considerable second order field effect of the Breit-Rabi type,<sup>22</sup> so that the centre line is split out into two lines giving a four line spectrum overall.

The  $\text{H}_2^-$  ion could be trapped near a lithium ion, and, if so, the broad outermost features could hide unresolved lithium hyperfine splitting ( $^7\text{Li}$ ;  $I = 3/2$ , 92.57% isotopic abundance).

A more satisfactory method of obtaining this radical in higher concentration might be hydrogen atom bombardment of saline hydrides; where hydrogen atoms formed from gaseous hydrogen by electrical discharge are passed over the powdered hydride at various temperatures and pressures. This method could have a higher success rate in trapping hydrogen atoms at hydride ion sites in the crystal lattice.

## ii) The $\text{H}_2^+$ Radical Ion.

One likely method of producing this radical seemed to be the formation of hydrogen atoms in situ in a strongly acidic medium, where, under suitable conditions, the hydrogen atoms could be trapped near protons, or in effect protonated:



Now, hydrogen atoms have been formed in frozen acids, namely perchloric, phosphoric and sulphuric acids, which were  $\gamma$ -irradiated at 77 K.<sup>23</sup> However, no evidence was found for protonated hydrogen atoms ( $\text{H}_2^+$ ) in

these acids. In view of this, we decided to use one of the most strongly ionizing and acidic media known to chemists,<sup>24</sup> namely the system  $\text{FSO}_3\text{H} - \text{SbF}_5$ , which is sometimes termed "magic acid." This combination of fluorsulphonic acid and antimony pentafluoride is an exceedingly powerful protonating agent, and as such should be able to protonate trapped hydrogen atoms more easily than conventional acids.

A sample of  $\text{FSO}_3\text{H} - \text{SbF}_5$  was prepared using high vacuum techniques by Dr. T.P. Sleight, and was  $\gamma$ -irradiated at 77 K in a sealed quartz tube. Its e.s.r. spectrum, measured at 77 K, showed the presence of at least three radicals (Figure 5.8); the spectrum of one was centred close to the free spin region and comprised three broad lines; the spectrum of 'normal' trapped hydrogen atoms was recognised and identified by its expected doublet splitting of approximately 500 G. The spectrum of the third paramagnetic species consisted, as far as could be seen, of a doublet of lines separated by approximately 630 G, whose intensity was about one-fiftieth of the intensity of the normal hydrogen atom lines.

Now, since the 'magic acid' was irradiated in the form of a frozen glassy matrix, the quartz tube could not be annealed in the normal way (see Chapter 1 - Experimental Section) without warming the acid to above its melting point. This means that the observed hydrogen atoms may be trapped in the quartz rather than in the acid itself; hydrogen being a characteristic impurity of most synthetic quartz crystals<sup>25</sup> and hydrogen atoms are known to be formed in quartz irradiated at 77 K.<sup>26</sup> The e.s.r. signals from these trapped atoms disappear after a subsequent warmup to temperatures in excess of 100 K.<sup>26</sup> Thus, if we assign the 500 G doublet (Figure 5.8) to hydrogen atoms trapped in quartz, the 630 G doublet could be the outermost features of  $\text{H}_2^+$ , trapped on the surface of the quartz. Again the innermost lines in the spectrum (assuming our assignment is correct) are not seen due to the intense, broad features in the central

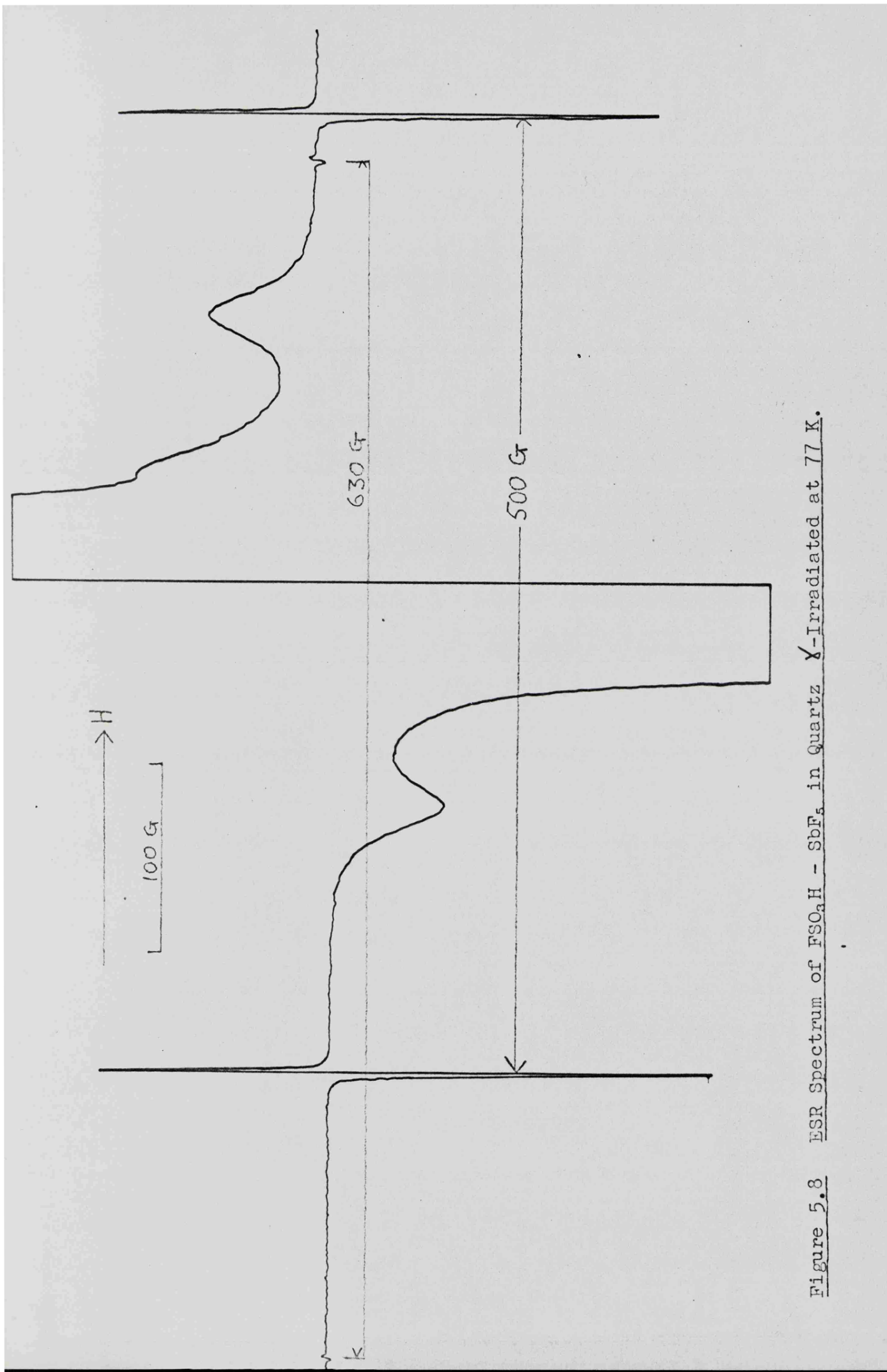


Figure 5.8 ESR Spectrum of  $\text{FSO}_3\text{H} - \text{SbF}_5$  in Quartz  $\times$ -Irradiated at 77 K.

portion of the spectrum.

When the sample was warmed above 100 K for a few seconds and then recooled to 77 K, the spectrum changed to that shown in Figure 5.9, where the normal hydrogen atom lines have decayed somewhat with the concomitant increase in intensity of the 630 G doublet. On further annealing the normal hydrogen atoms decayed completely, whereas the latter centre was relatively stable at room temperature, taking several hours to decay completely.

Now, in order to test whether these radicals were formed in the 'bulk acid' or on the surface of the quartz, the experiment was repeated using a quartz tube whose inner surface had just been moistened with the 'magic acid' prior to irradiation. The e.s.r. spectrum of this sample, measured at 77 K (Figure 5.10), showed a much higher proportion of the species giving the 630 G doublet, compared to the normal hydrogen atom species. This gave definite indication that it was closely connected with the quartz medium, and the quartz surface in particular, since irradiation of a pure quartz sample gave normal trapped hydrogen atoms only. When the sample was warmed to room temperature for a few seconds and recooled to 77 K, the spectrum showed that the normal hydrogen atoms had decayed completely whilst the central portion of the spectrum had increased in complexity quite markedly (Figure 5.11). There are several narrow lines in the spectrum of comparable intensity to the 630 G doublet, two of which could be the expected innermost features of  $H_2^+$ , if, indeed, this is formed. Some of these lines may be due to molecular oxygen, the presence of which was confirmed by measuring the spectrum at high field (5000 - 7000 G), and comparing it with the known spectrum of molecular oxygen,<sup>27,28</sup> the lines in this region of the spectrum being quite intense and well documented.<sup>27,28</sup> The lines in the free spin

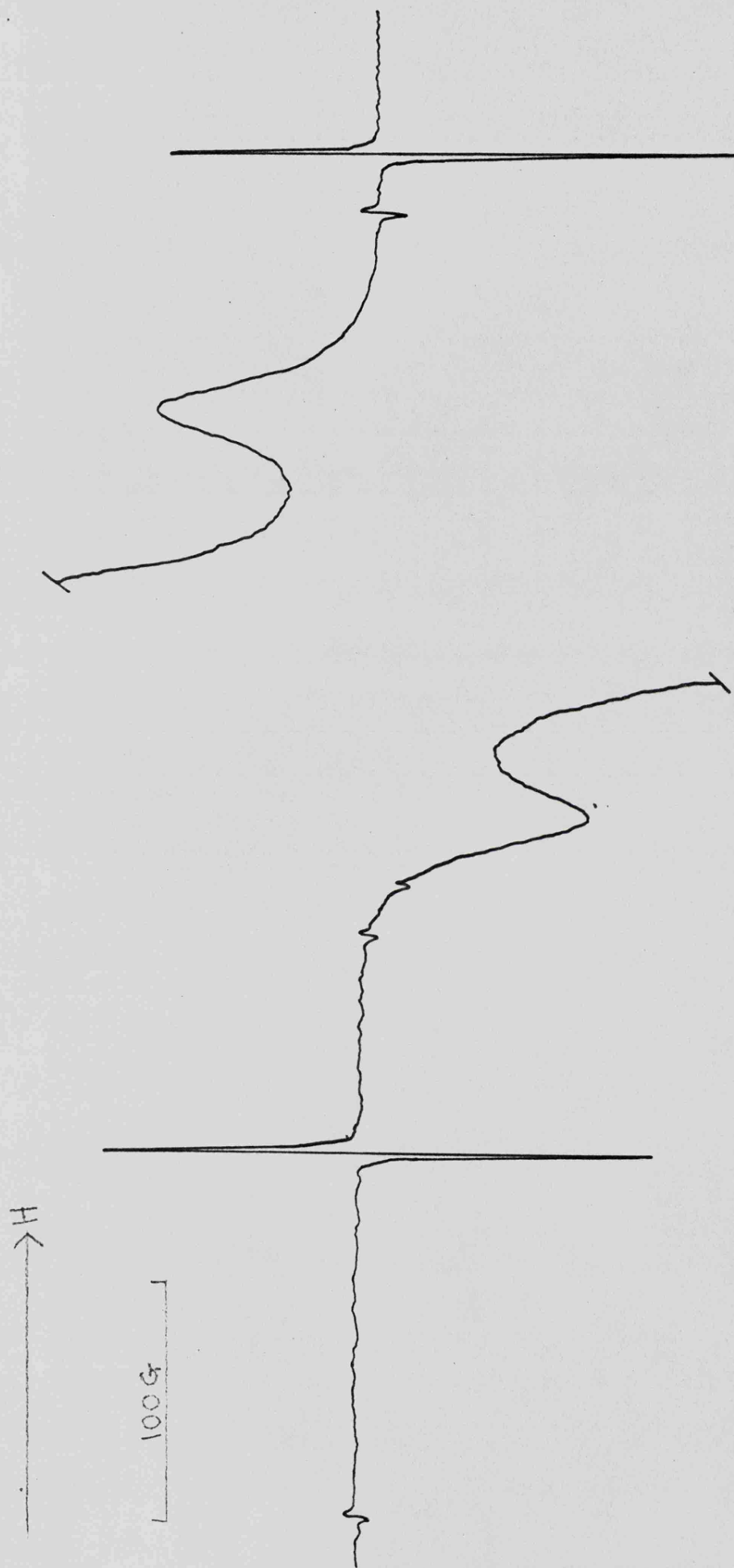


Figure 5.9 ESR Spectrum of Sample (asin Fig 5.8) Warmed for 10 secs and Recoiled to 77 K.

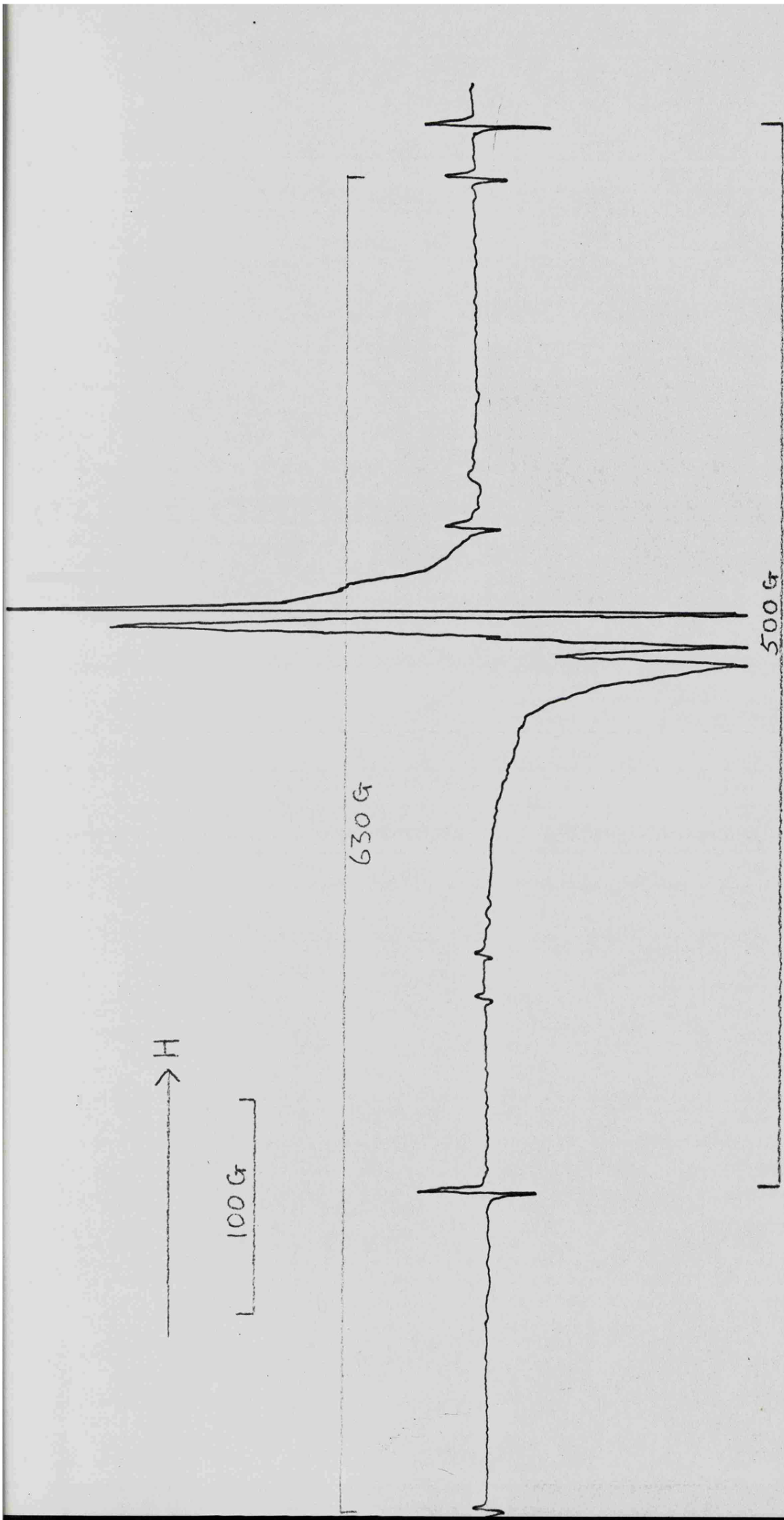


Figure 5.10 ESR Spectrum of a Quartz Tube Moistened with Magic Acid  $\chi$ -Irradiated at 77 K.

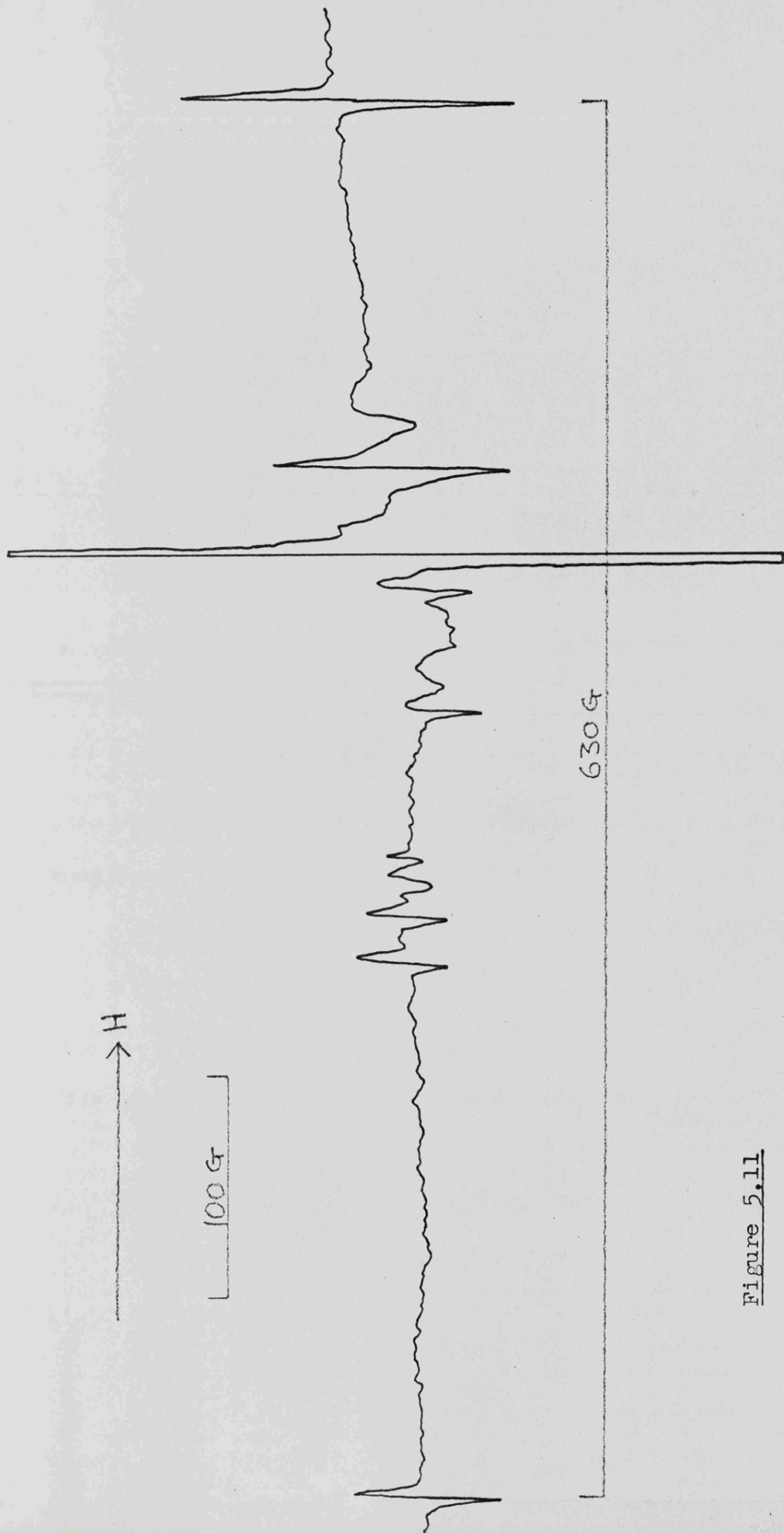


Figure 5.11

ESR Spectrum of Sample (as in Fig 5.10) Warmed to 300 K for 30 secs and Recooled to 77 K.

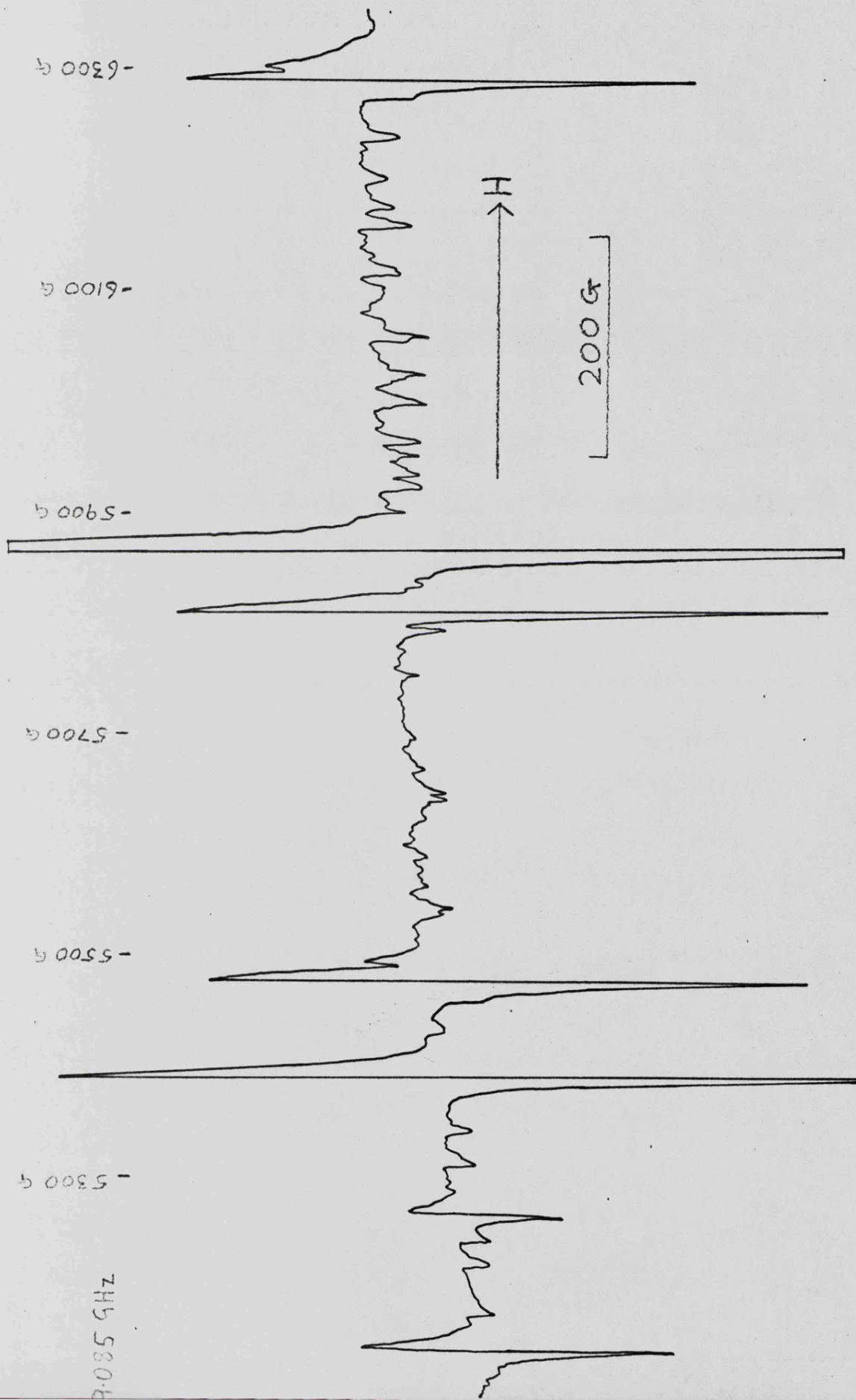


Figure 5.12 ESR Spectrum of Quartz/Magic Acid/Oxygen Measured at 77 K.

region, however, are much less intense (the weakest observable lines being over a thousandfold weaker than the strongest lines of the spectrum at 77 K)<sup>28</sup> and there is some uncertainty in their positions. It was hoped that the problem could be resolved by obtaining a spectrum of molecular oxygen in an uncontaminated quartz tube at 77 K. Unfortunately however, reproducible spectra of this type have not yet been obtained in this laboratory, and consequently we are not able to conclude anything about a possible relationship between the narrow features in the free spin region. So the possibility still remains that the 630 G features are a property of  $H_2^+$ , but in the absence of unambiguous experimental evidence nothing further can be concluded.

References for Chapter 5.

1. P.W. Atkins and M.C.R. Symons, The Structure of Inorganic Radicals, Elsevier, Amsterdam, (1967).
2. G.T. Tramell, H. Zeldes, and R. Livingston, Phys. Rev., 110, 630, (1958).
3. C.K. Jen, S.N. Foner, E.L. Cochran and V.A. Bowers, Phys. Rev., 112, 1169, (1958).
4. J.L. Hall and R.T. Schumacher, Phys. Rev., 127, 1892, (1962).
5. M.B.D. Bloom, R.S. Eachus and M.C.R. Symons, Chem. Comm., 1495, (1968).
6. M.B.D. Bloom, R.S. Eachus and M.C.R. Symons, J. Chem. Soc.(A), (1971).
7. P. Kusch, Phys. Rev., 100, 1188, (1955).
8. R. Berringer and M.A.S. Heald, Phys. Rev., 95, 1474, (1954).
9. M.C.R. Symons, Nature, 224, 686, (1969).
10. T.A. Claxton and D. McWilliams, Trans. Faraday Soc., 66, 513, (1970).
11. F.J. Adrian, J. Chem. Phys., 32, 972, (1960).
12. C.K. Jen, V.A. Bowers, E.L. Cochran and S.N. Foner, Phys. Rev., 126, 1749, (1962).
13. P.W. Atkins, Ph.D. Thesis, Leicester, (1964).

14. H.W. Wardale, Ph.D. Thesis, Leicester, (1967).
15. G. Walton and G.H. Waldon, J. Amer. Chem. Soc., 68, 1750, (1946).
16. G. Walton and G.H. Waldon, J. Amer. Chem. Soc., 68, 1742, (1946).
17. P.W. Atkins, N. Keen, M.C.R. Symons and H.W. Wardale, J. Chem. Soc., 5594, (1963).
18. T.A. Claxton and M.C.R. Symons, Chem. Comm., 379, (1970).
19. A. Carrington, F. Dravnick and M.C.R. Symons, J. Chem. Soc., 947, (1959).
20. M.C.R. Symons and H.W. Wardale, Chem. Comm., 758, (1967).
21. P.B. Ayscough, "Electron Spin Resonance in Chemistry," Methuen, London, (1968).
22. G. Breit and I. Rabi, Phys. Rev., 38, 2082, (1931).
23. S.A. Marshall, J.R. Gabriel and R.A. Serway, J. Chem. Phys., 45, 192, (1966).
24. see for example G.A. Olah and M.B. Comisarow, J. Amer. Chem. Soc., 90, 5033, (1968).
25. A. Kats, Philips Res. Rept., 17, 201, (1962).
26. R.A. Weeks and M. Abraham, J. Chem. Phys., 42, 68, (1965).
27. R. Beringer and J.G. Castle, Phys. Rev., 81, 82, (1951).
28. M. Tinkham and M.P.W. Strandberg, Phys. Rev., 97, 951, (1955).

CHAPTER 6

THE 33 VALENCE-ELECTRON  $\text{ClO}_4^{2-}$  ANION AND RELATED SPECIES.

## Introduction.

Morton<sup>1</sup> has detected two paramagnetic centres in potassium perchlorate crystals  $\gamma$ -irradiated at 77 K, which he suggested might be  $\text{ClO}_4$  radicals trapped in two magnetically distinct sites. However, their magnetic properties, given for comparison purposes with those assigned to  $\text{PO}_4^{2-}$  (ref. 2) and  $\text{SO}_4^-$  (ref. 3) in Table 6.1, did not seem to be very reasonable for the chlorine tetroxide radical with 31 valence electrons since both the total chlorine 3s-character and the p/s ratio are larger than expected. In addition the form of the g-tensor is different from that of the other radicals. Furthermore, we would not expect the same radical occupying two different lattice sites to have such dissimilar hyperfine parameters.

A possible alternative that has recently been proposed<sup>4</sup> for one of these radicals (labelled (I) in Table 6.1) is the peroxy-chlorine species  $\text{O}_2\text{ClOO}$ , and, in view of the results reported<sup>5</sup> for the electron-excess species  $\text{ClO}_3^{2-}$ , we feel that the other radical prepared by Morton is probably  $\text{ClO}_4^{2-}$ . In view of the previous successes reported from this laboratory,<sup>5,6,7</sup> in specifically preparing electron-excess species by doping the parent ion into a suitable host crystal, we attempted to form  $\text{ClO}_4^{2-}$  by irradiation of barium sulphate which contained a trace of perchlorate impurity.

In this chapter we compare and contrast the spin-resonance and molecular parameters obtained for this centre with those of Morton's radical (II) and the recently reported isostructural tetroxide species  $\text{AsO}_4^{4-}$  (or  $\text{As}(\text{OH})_4$ ),<sup>8</sup> formed by the interaction of  $\gamma$ -rays with  $\text{KH}_2\text{AsO}_4$  at 77 K, and the isostructural halides  $\text{PF}_4$ ,<sup>9,10</sup>  $\text{PCl}_4$ ,<sup>11</sup> and  $\text{SF}_4^+$ .<sup>12</sup>

Table 6.1 ESR Data for the  $\text{ClO}_4^{2-}$  and  $\text{ClO}_3$  Radicals in  $\text{BaSO}_4$  and Related Radicals.

Radical	Matrix	g-tensor			Hyperfine Tensor (G)				Ref.
		$g_{11}$	$g_{33}$	$g_{av}$	$B_{11}$	$B_{22}$	$B_{33}$	$A_{iso}$	
$\text{ClO}_4$ (I)	$\text{KClO}_4$ 77 K	2.0024	2.0548	2.0375	0	0	0	57.2	1
$\text{ClO}_4$ (II)		2.0050	2.0360	2.0260	-5.3	-3.3	8.7	74.3	1
$\text{ClO}_4^{2-}$ (A)	$\text{BaSO}_4$ 77 K	2.0021	2.0249	2.0325	0	3.3	-3.3	76.8	a
	$\text{BaSO}_4$ 300 K	2.0020	2.0255	2.0325	0	2.9	-2.9	74.6	a
$\text{PO}_4^{2-}$	$\text{CaSO}_4$	2.0072	2.0033	2.0122	-0.3	1.0	-0.5	19.1	2
$\text{SO}_4^-$	$\text{K}_2\text{SO}_4$	2.0082	2.0037	2.0486					3
$\text{ClO}_3$ (B)	$\text{BaSO}_4$ 77 K	2.0068	2.0147	2.0147	35.4	-16.7	-16.7	129.8	a
$\text{ClO}_3$	$\text{KClO}_3$ 77 K	2.0030	2.0083	2.0083	36	-18	-18	140	7
$\text{ClO}_3$	$\text{KClO}_4$ 300 K	2.0066	2.0132	2.0132	29	-15	-15	122	b

a. This work

b. P.W. Atkins, J.A. Brivati, N. Keen, M.C.R. Symons and P.A. Trevalion, J. Chem. Soc., 4785, (1962)

Table 6.1(a) Molecular Parameters for the  $\text{ClO}_4^{2-}$  and  $\text{ClO}_3$  Radicals

in  $\text{BaSO}_4$ , and Related Radicals.

Radical	$a_s^2$	$a_p^2$	$a_s^2 + a_p^2$	$a_p^2/a_s^2$	Reference
$\text{ClO}_4$ (I)	0.034	0.0	0.034		1
$\text{ClO}_4$ (II)	0.044	0.09	0.134	2.0	1
$\text{ClO}_4^{2-}$ (A)	300 K 0.044	$\sim 0.03$	$\sim 0.07$	$\sim 0.7$	This work
	77 K 0.046				
$\text{PO}_4^{2-}$	0.005	0.004	0.009	0.76	2
$\text{ClO}_3$	0.074	0.354	0.428	4.78	This work
$\text{ClO}_3$	0.083	0.36	0.44	4.4	7

### Experimental.

All reagents used were AnalaR grade purified further by recrystallisation from aqueous solution. Samples of barium sulphate doped with  $\text{ClO}_4^-$  and  $\text{NO}_3^-$  ions were prepared by coprecipitation from aqueous solutions of barium chloride which contained approximately 10% of the dopant ions, at temperatures close to the boiling point of the solutions. The samples were allowed to digest at 340 K overnight, washed free of chloride ions and dried under vacuum for several days prior to their irradiation. If the powders were annealed at temperatures above approximately 450 K some decomposition of the coprecipitated  $\text{ClO}_4^-$  ions occurred. Powdered samples of the doped sulphate were exposed to  $^{60}\text{Co}$   $\gamma$ -rays at both 77 K and room temperature; doses ranging from 2 to 30 Mrads.

Annealing experiments were carried out using a Varian variable-temperature accessory, while spectra at 4.2 K were obtained by employing a Varian V4545B liquid helium accessory and superheterodyne detection.

To facilitate the interpretation of the complex X-band e.s.r. spectra of the irradiated doped powders, further spectra were measured at both Q- and S-band frequencies.

### Results.

Exposure of barium sulphate doped with perchlorate ions to  $\gamma$ -rays at 77 K resulted in the formation of three radicals: the host "sulphate" radical, together with two species A and B which exhibited hyperfine interactions characteristic of radicals containing a single chlorine atom (Figure 6.1). In both A and B features corresponding to the two abundant isotopes  $^{35}\text{Cl}$  and  $^{37}\text{Cl}$

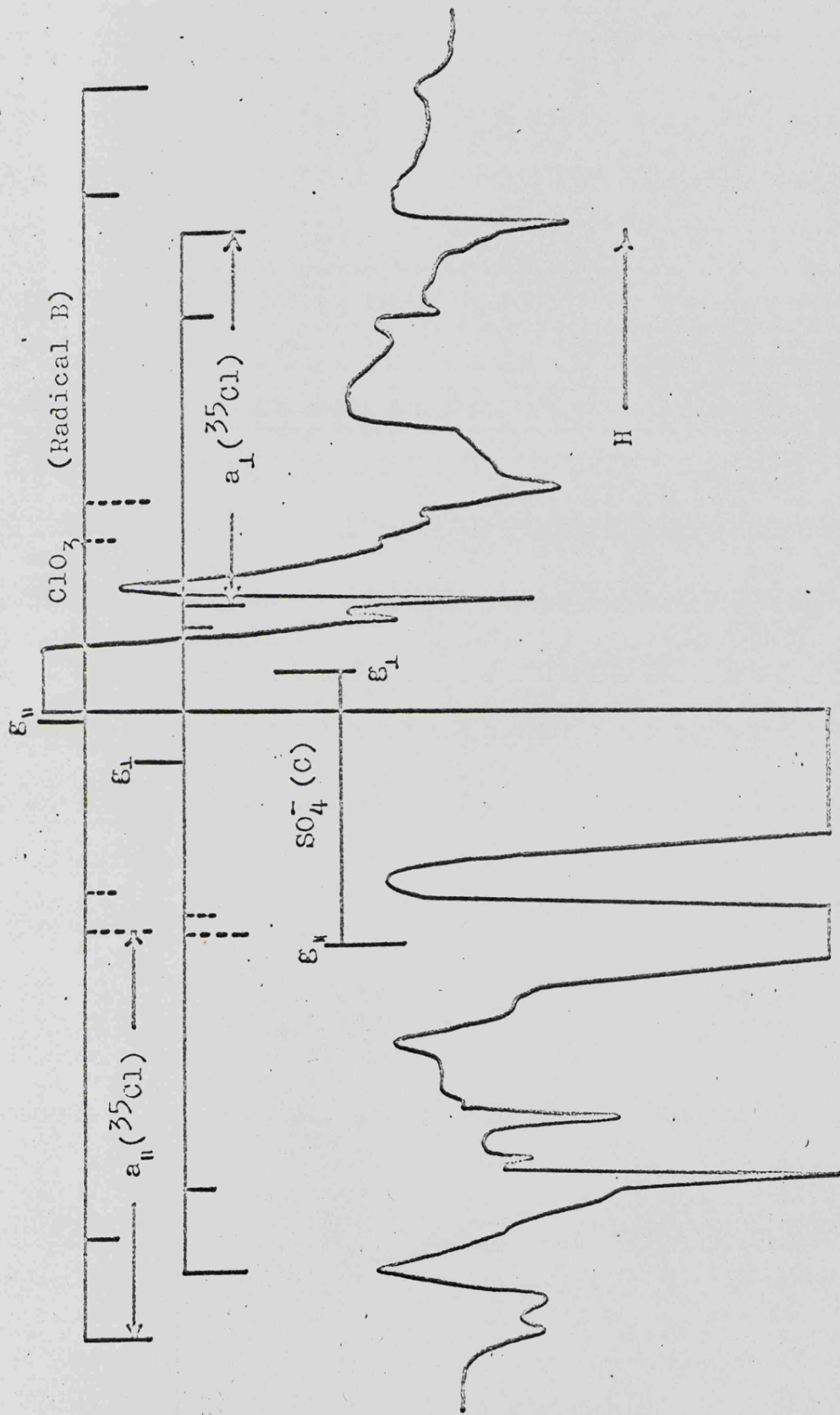


Figure 6.1. An ESR spectrum of irradiated, perchlorate-doped  $\text{BaSO}_4$  measured at 77 K and 10 mV.

were detected, whose relative intensities were in accord with the natural abundance ratio of 3.07 and whose separation was consistent with their magnetic moment ratio of 1.202.

When the sulphate was annealed to 300 K the spectrum changed markedly (Figure 6.2). Whilst the chlorine radical A was stable at this temperature, both radical B and the host sulphate radical C decayed irreversibly; the decomposition of the latter giving rise to a new paramagnetic species D. Irradiation of the doped sulphate at room temperature produced A and D directly. Only radical D was formed when pure barium sulphate was irradiated at 300 K.

Irradiation at 77 K of a sample of barium sulphate containing coprecipitated perchlorate and nitrate anions resulted in the formation of radicals B and C together with the well-characterised  $\text{NO}_3^{2-}$  radical;<sup>4,5,7,13</sup> radical A not being formed in the presence of nitrate ions. (Figure 6.3). When the sample was annealed to 300 K radicals B and C again decayed whilst the nitrate centre was stable at this temperature. Irradiation of the sample at room temperature led to the formation of radical D and  $\text{NO}_3^{2-}$  only; again radical A not being formed due to the presence of nitrate ions.

The only effect of warming the sample from 77 K to room temperature on the spectrum of radical A was that the hyperfine coupling decreased slightly. There was no change in the spectrum when the sample was cooled from 77 K to 4.2 K.

## Discussion.

### Identification of Radical A.

The e.s.r. spectrum of this centre was interpreted in terms of a species with three  $g$ - and  $A$ -values.

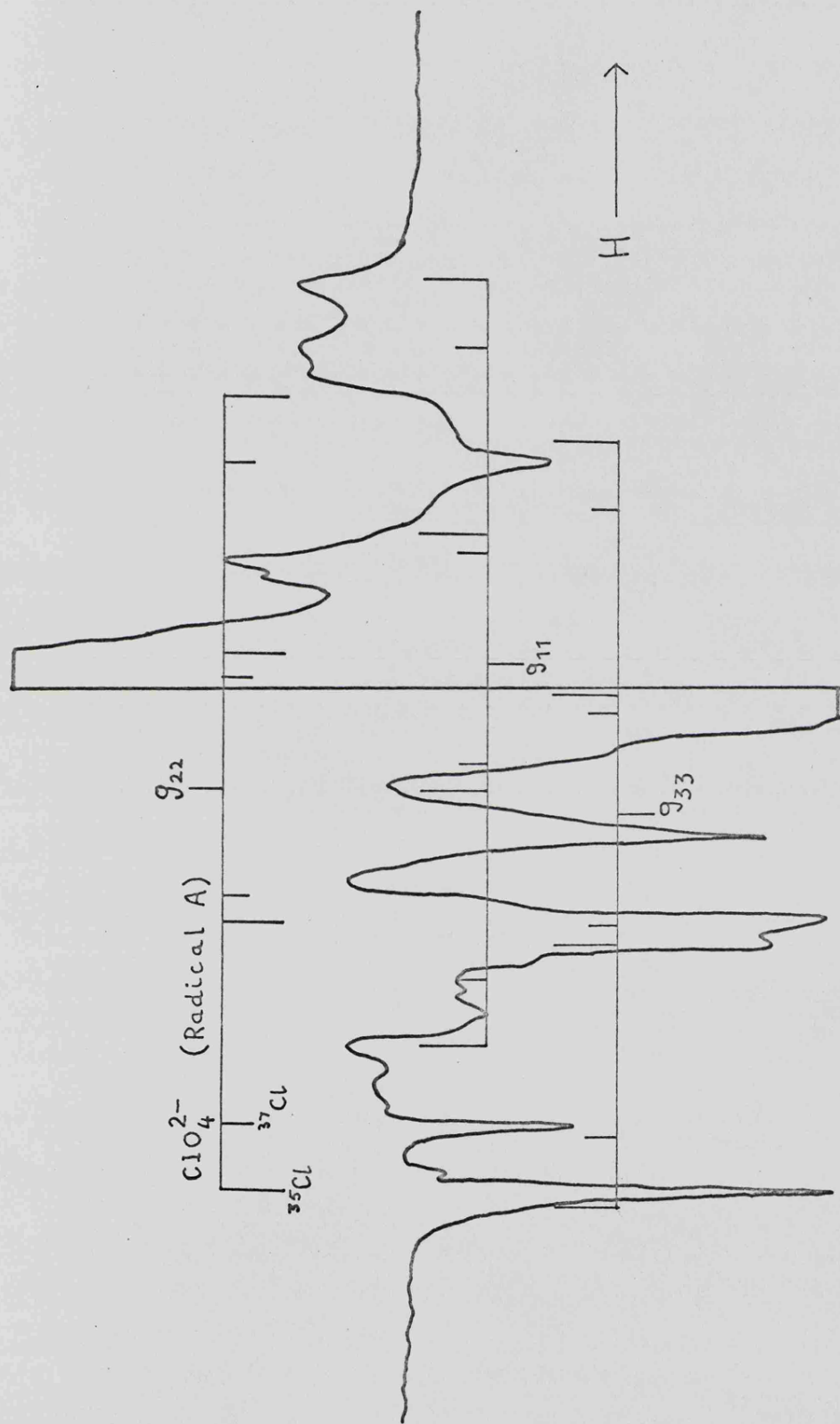
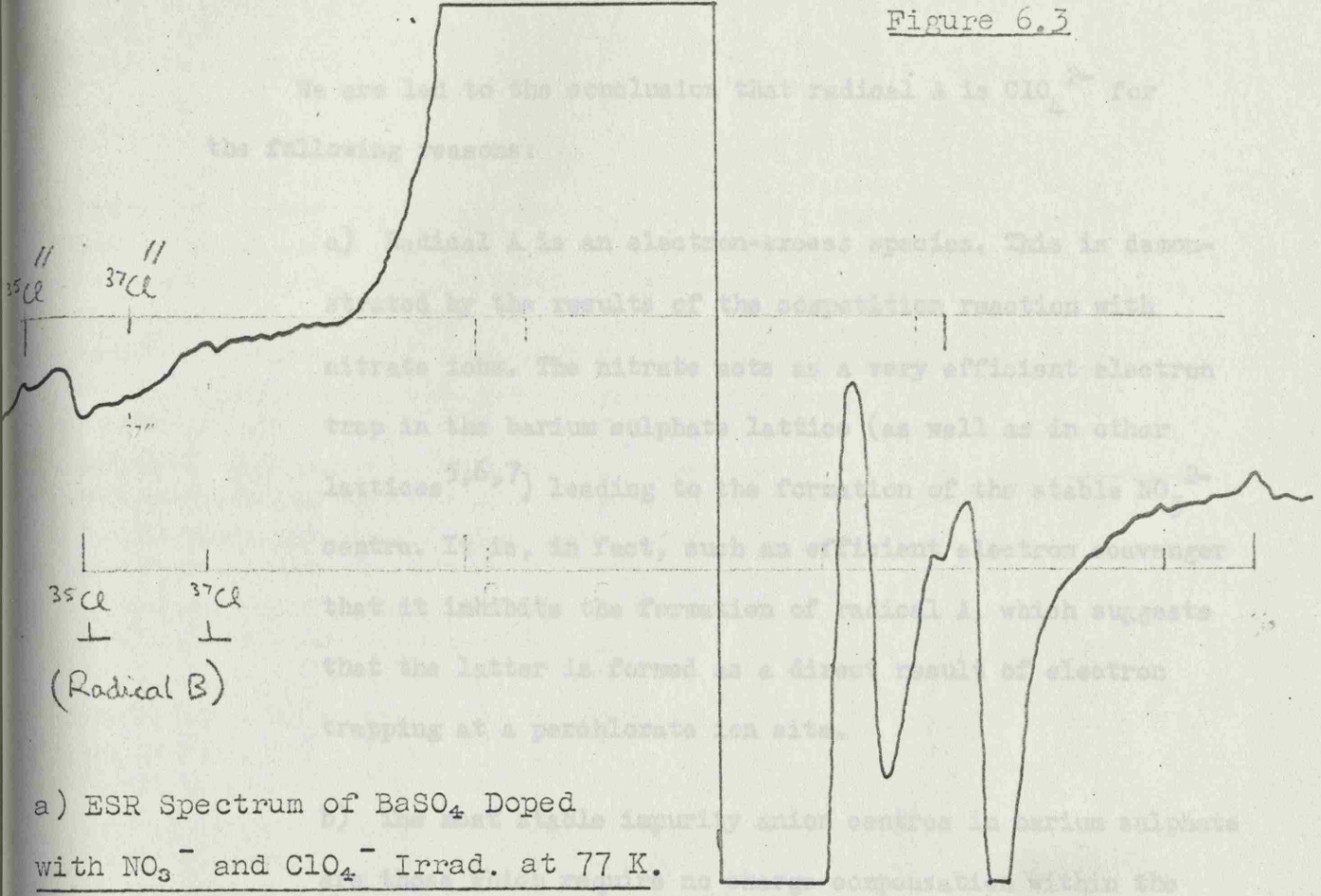
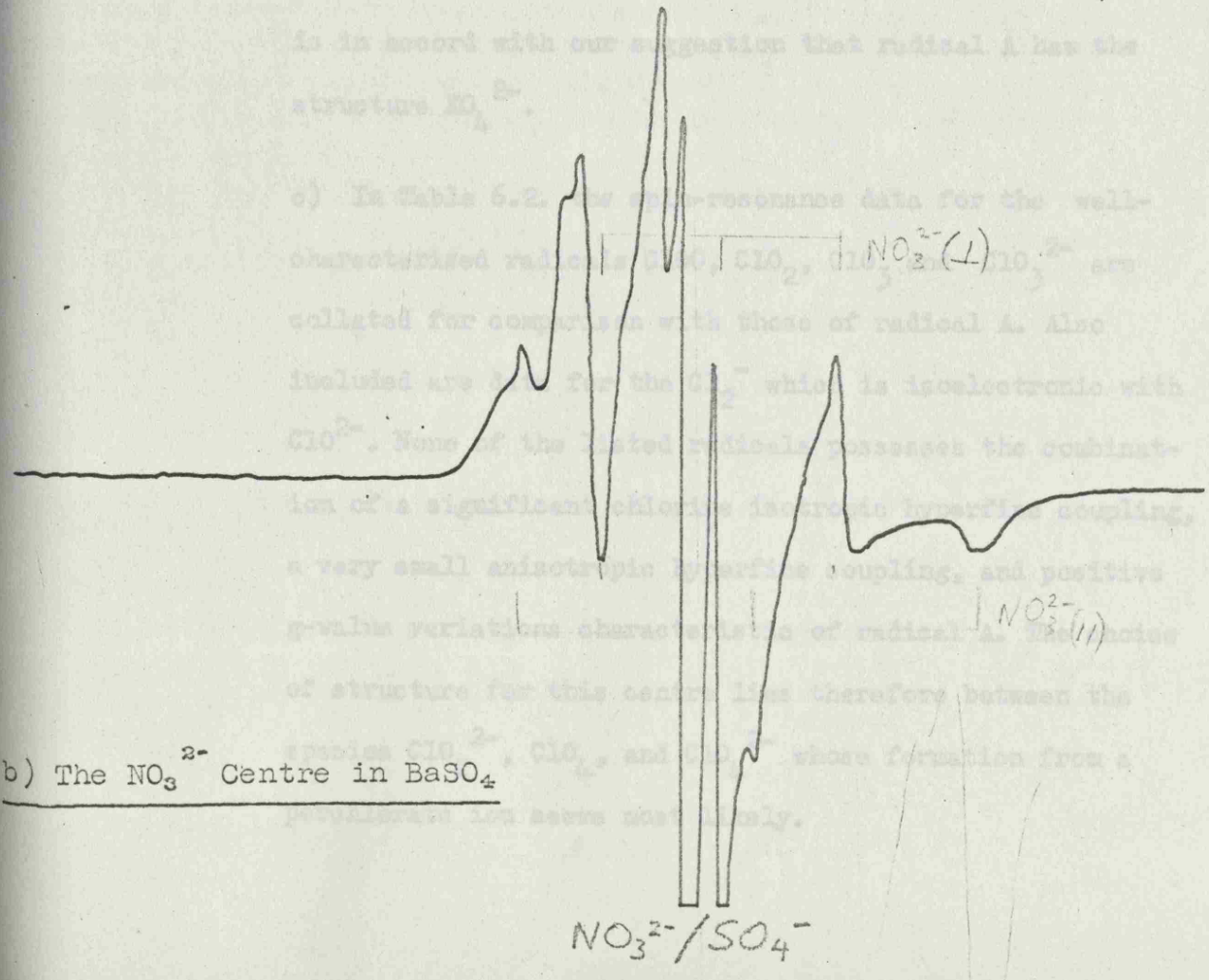


Figure 6.2 ESR Spectrum of Irradiated, Perchlorate-doped  $\text{BaSO}_4$  Measured at 300 K.

Figure 6.3



a) ESR Spectrum of BaSO<sub>4</sub> Doped with NO<sub>3</sub><sup>-</sup> and ClO<sub>4</sub><sup>-</sup> Irrad. at 77 K.



b) The NO<sub>3</sub><sup>2-</sup> Centre in BaSO<sub>4</sub>

We are led to the conclusion that radical A is  $\text{ClO}_4^{2-}$  for the following reasons:

a) Radical A is an electron-excess species. This is demonstrated by the results of the competition reaction with nitrate ions. The nitrate acts as a very efficient electron trap in the barium sulphate lattice (as well as in other lattices<sup>5,6,7</sup>) leading to the formation of the stable  $\text{NO}_3^{2-}$  centre. It is, in fact, such an efficient electron scavenger that it inhibits the formation of radical A, which suggests that the latter is formed as a direct result of electron trapping at a perchlorate ion site.

b) The most stable impurity anion centres in barium sulphate are those which require no charge compensation within the lattice. The observed high thermal stability of this centre is in accord with our suggestion that radical A has the structure  $\text{XO}_4^{2-}$ .

c) In Table 6.2. the spin-resonance data for the well-characterised radicals  $\text{ClO}$ ,  $\text{ClO}_2$ ,  $\text{ClO}_3$  and  $\text{ClO}_3^{2-}$  are collated for comparison with those of radical A. Also included are data for the  $\text{Cl}_2^-$  which is isoelectronic with  $\text{ClO}^{2-}$ . None of the listed radicals possesses the combination of a significant chlorine isotropic hyperfine coupling, a very small anisotropic hyperfine coupling, and positive g-value variations characteristic of radical A. The choice of structure for this centre lies therefore between the species  $\text{ClO}_2^{2-}$ ,  $\text{ClO}_4$ , and  $\text{ClO}_4^{2-}$  whose formation from a perchlorate ion seems most likely.

TABLE 6.2. Electron Spin Resonance and Molecular Parameters for a  
 Number of Well-Characterised Chlorine Radicals

Radical	11	22	33	Direction	$a_s^2(Cl)$	$a_p^2(Cl)$	$a_s^2 + a_p^2$	Ref.
(A) $ClO_4^{2-}$	g	2.0020	2.0255	2.0325				
	$a(^{35}Cl)^*$	74.6	77.5	71.7	0.045	0.03-0.06	0.1	a
$ClO$	g	2.0100	1.9965	2.0035				
	$a(^{35}Cl)^*$	18.7	-4.6	-2.0	0.002	0.14	0.14	25
$ClO_2$	g	2.0025	2.017	2.011				
	$a(^{35}Cl)^*$	72.7	-9.6	-10.0	0.56	0.01	0.57	26
$ClO_3$	g	2.0030	2.0083	2.0083				
	$a(^{35}Cl)^*$	176	122	122	0.083	0.36	0.443	7
$ClO_3^{2-}$	g	2.0121	2.0105	2.0105				
	$a(^{35}Cl)^*$	127	106	106	0.067	0.14	0.207	7
$Cl_2^-$	g	2.0012	2.0426	2.0426				
	$a(^{35}Cl)^*$	91.1	9.3	9.3	0.024	0.582	0.606	27

\* All hyperfine couplings are quoted in Gauss.

a) This work.

The radical  $\text{ClO}_2^{2-}$  would be a 21 valence-electron species and, from Walsh's orbital correlation diagram for  $\text{AB}_2$  radicals,<sup>14</sup> (Figure 6.4) we would predict it to be nearly linear and to approach a  $^2 \Sigma_g$  ground state. The  $g_{\perp}$ -factor for such a linear radical is likely to be close to the free-spin value since the configuration ....

$\pi_g^3 \pi_u^4 \sigma_g^2$ ;  $^2 \pi_g$  would be a highly excited state.

The significant positive  $g$ -shifts observed for radical A would seem to rule out this possibility. Furthermore, the  $\gamma$ -irradiation of samples of barium sulphate doped with chlorite ions produced a high concentration of  $\text{ClO}_2$ , but no other chlorine-containing radical was detected. This suggests that  $\text{ClO}_2^{2-}$  is unstable in barium sulphate.

The observed isotropic hyperfine coupling of 74.6 G is considerably larger than the value we would predict for  $\text{ClO}_4$  by analogy with isoelectronic species such as  $\text{PO}_4^{2-}$  and  $\text{SO}_4^{2-}$ <sup>3,4</sup> (Table 6.1). Further, the arguments expressed in a) and b) above, both militate against  $\text{ClO}_4$ , since we have shown reasonably that the radical must be an electron-excess centre.

We consider therefore, that the foregoing arguments virtually eliminate all possibilities except  $\text{ClO}_4^{2-}$  for the structure of radical A.

#### Identification of Radical B.

The fact that the formation of this radical is not inhibited by the presence of the electron-trapping nitrate ion in barium sulphate indicates that it is not an electron-excess species but

Correlation diagram for AB<sub>2</sub> molecules

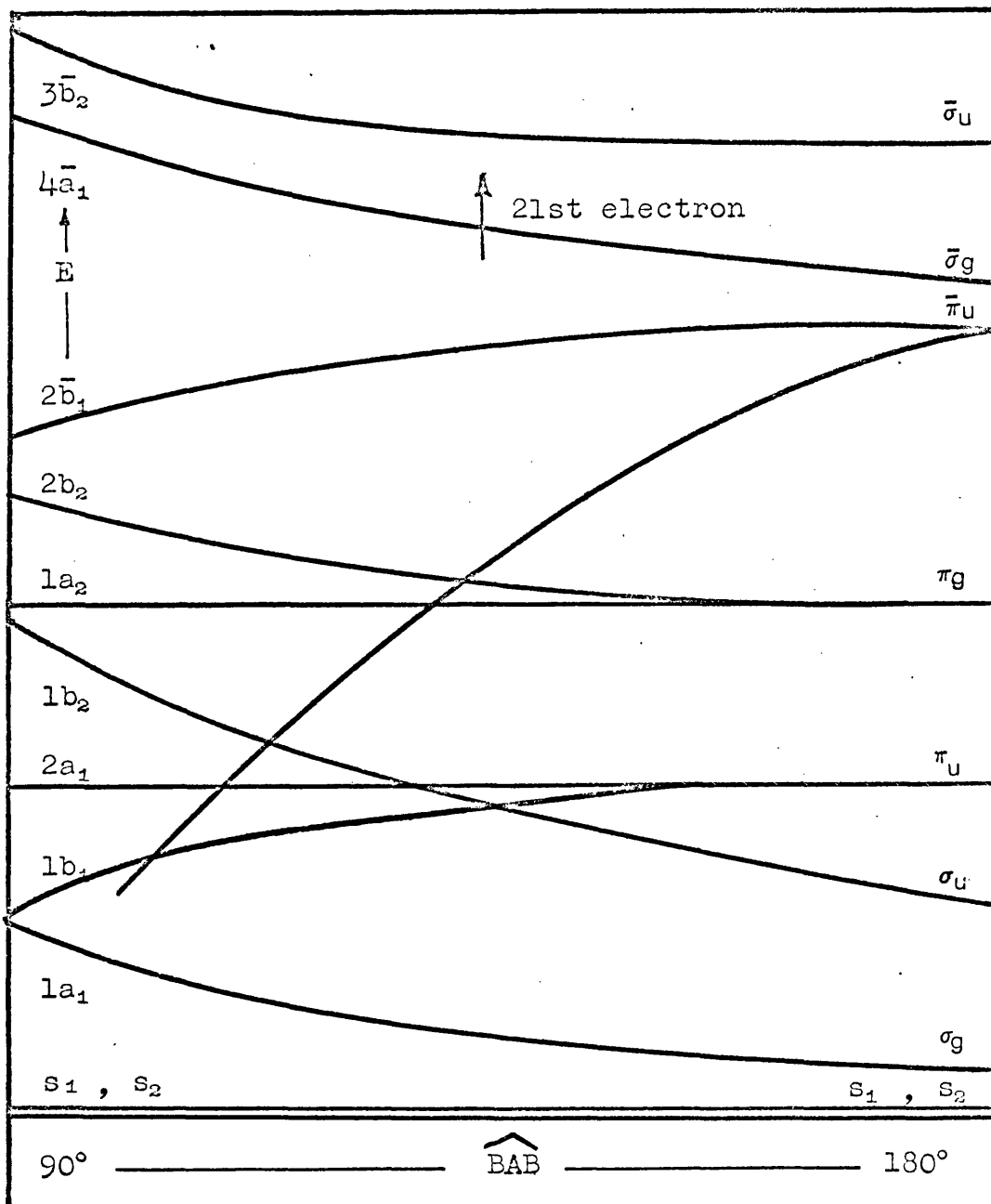


Figure 6.4

likely to be a hole-centre. A comparison of the spin-resonance parameters of radical B with those reported for the  $\text{ClO}_3$  radical trapped in a variety of matrices (Table 6.1) leaves little doubt that this species is chlorine trioxide. The mechanism of formation of this radical will be discussed later.

#### Identification of Radicals C and D.

The identification of these radicals is again based on a comparison of their spectral properties with those of already well-characterised paramagnetic, sulphur-containing oxides and oxyanions (Table 6.3). On this basis it is concluded that radicals C and D are most probably  $\text{SO}_4^-$  and  $\text{SO}_2^-$  respectively. However, we were unable to detect hyperfine interactions involving  $^{33}\text{S}$  for these centres ( $^{33}\text{S}$ ;  $I = 3/2$ , 0.74% isotopic abundance) and therefore, could not confirm these assignments.

#### The Structure of $\text{ClO}_4^{2-}$ .

The energy level scheme for tetrahedral  $\text{XO}_4$  molecules is illustrated in Figure 6.5. The anion  $\text{ClO}_4^{2-}$  is a 33 valence-electron species and, since there is some uncertainty concerning the ground state of such a species, even if the molecule were perfectly tetrahedral, the unpaired electron could be in either the  $2\bar{a}_1$  or the  $3\bar{t}_2$  molecular orbital.<sup>9,15</sup> The energies of the molecular orbitals (and hence the ground state) are very much dependent on the electronegativity ( $\chi_x$ ) of the central X atom. Figure 6.6 illustrates the variation in orbital energies for tetrahedral  $\text{XO}_4$  molecules as the electronegativity of the central atom changes; and for  $\text{ClO}_4$ , where

TABLE 6.3. Electron Spin Resonance Data for Various Sulphur Oxyanions

Radical	Matrix	$g_{11}$	$g_{22}$	$g_{33}$	$g_{av}$	Ref.
$SO_4^-$ (C)	BaSO <sub>4</sub> 77°K	2.0307	2.0076	2.0076	2.0153	a
$SO_4^-$	K <sub>2</sub> SO <sub>4</sub>	2.0486	2.0082	2.0037	2.0202	3
$SO_4^-$	K <sub>2</sub> S <sub>2</sub> O <sub>8</sub>	2.0310	2.0082	2.0064	2.0152	b
$SO_2^-$ (D)	BaSO <sub>4</sub> 300°K	2.0010	2.0168	2.0045	2.0074	a
$SO_2^-$	K <sub>2</sub> S <sub>2</sub> O <sub>5</sub>	2.0018	2.0103	2.0055	2.0058	28
$SO_3^-$	K <sub>2</sub> CH <sub>2</sub> (SO <sub>3</sub> ) <sub>2</sub>	2.0036	2.0036	2.0036	2.0036	29
$SO_3^-$	K <sub>2</sub> SO <sub>4</sub>	2.0033	2.0033	2.0023	2.0030	3

a. This work.

b. P.W. Atkins, J.A. Brivati, A. Horsfield, M.C.R. Symons and P.A. Trevalion, Proc. Int. Symp. on Free Radicals, Cambridge, (1963).

The molecular orbital diagram for  
tetrahedral  $XO_4$  molecules

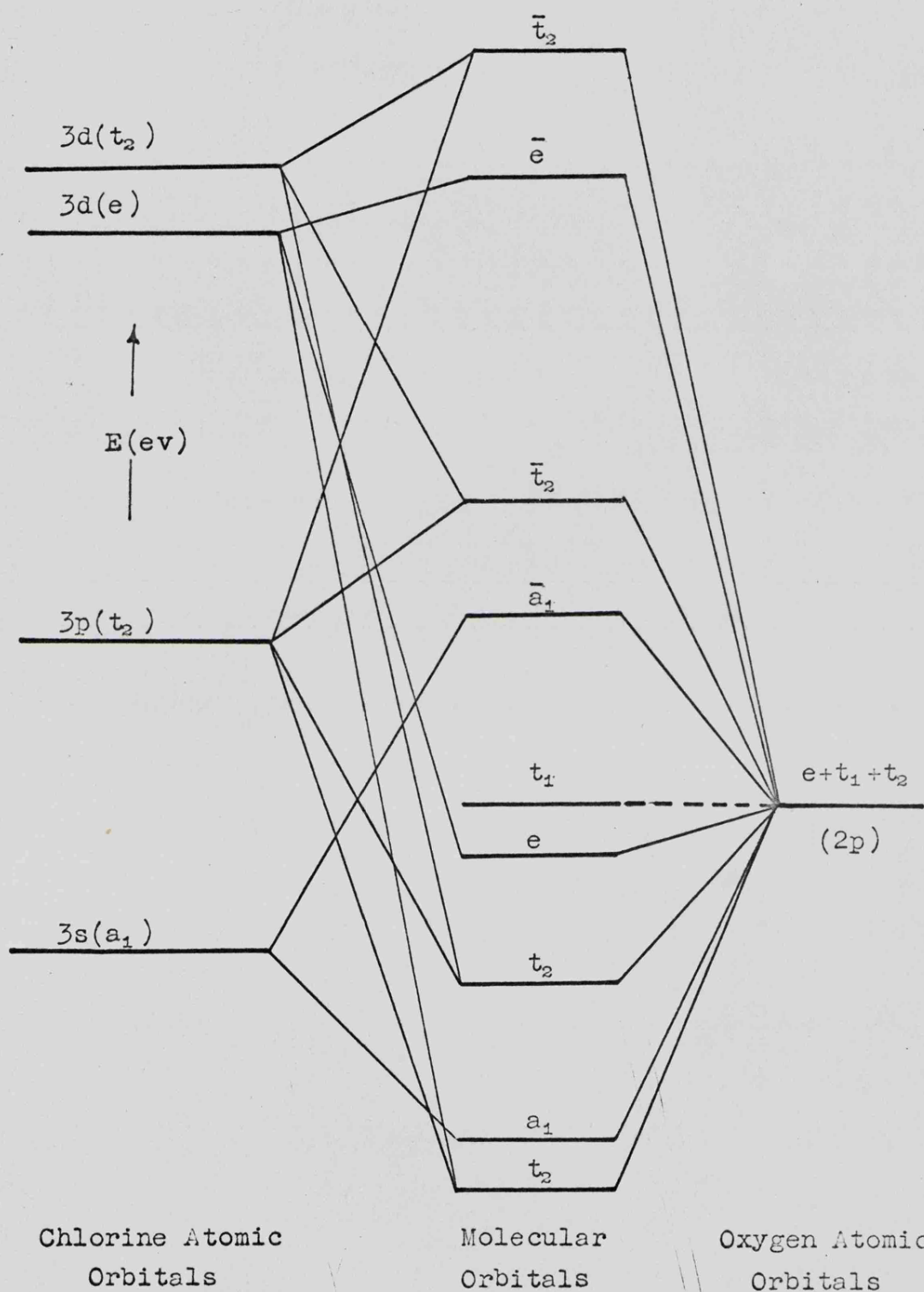
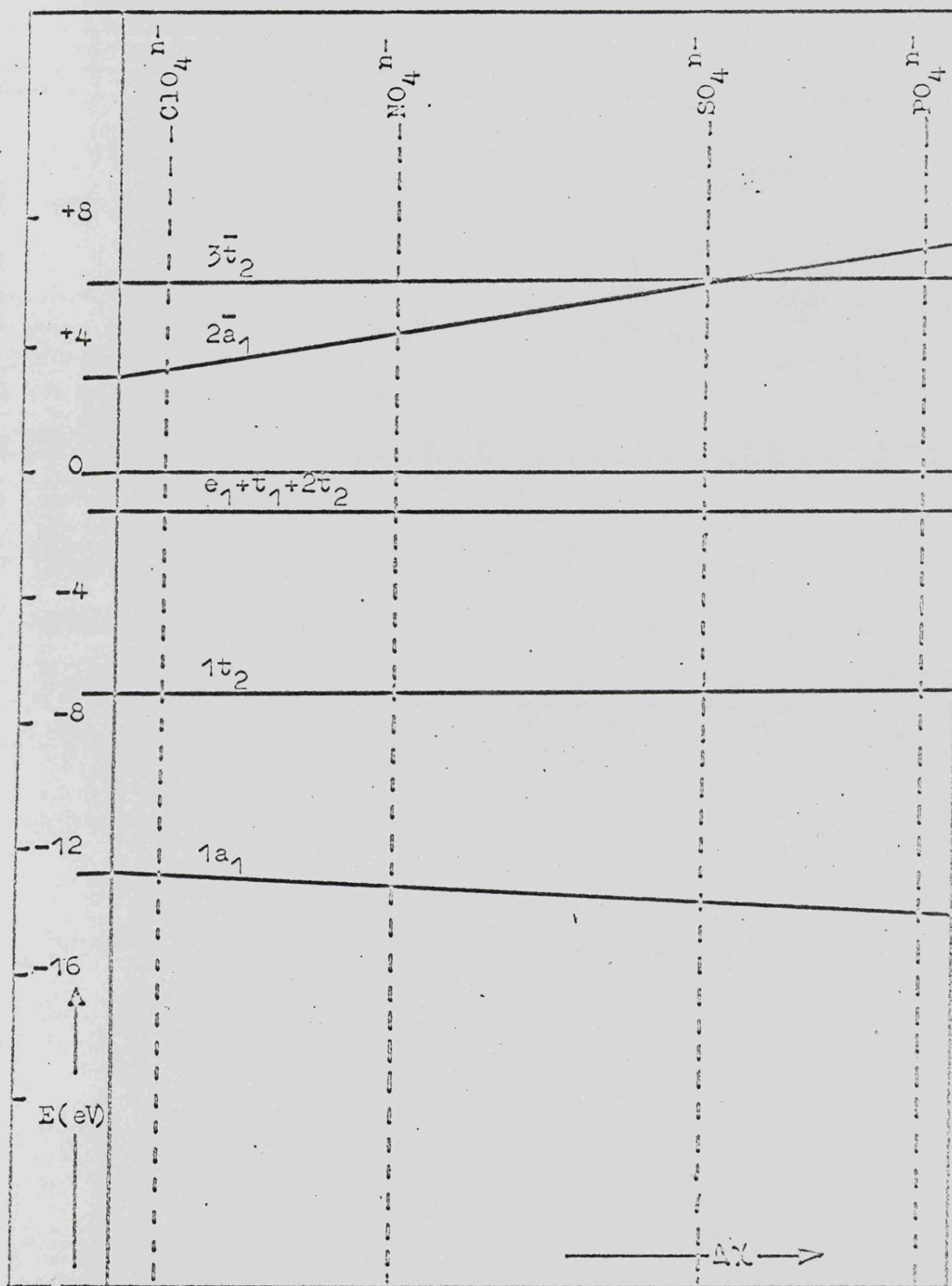


Figure 6.5



The variation of the orbital energies for tetrahedral  $XO_4$  molecules with  $\Delta X$

Figure 6.6

$\chi_0 \approx \chi_{Cl}$ , the  $2\bar{a}_1$ -level has been calculated to be approximately 2.5eV lower than the  $3\bar{t}_2$ -level.<sup>16</sup> We would hesitate to base an assignment on this calculation since the energy difference involved is so small. However, a spin-population analysis of the hyperfine tensor of this radical (Table 6.1) indicates that the contribution of the central atom to the M.O. of the unpaired electron is at least 50% 3s in character. In the absence of any distortion from tetrahedral symmetry, we would infer therefore that the  $2\bar{a}_1$ -level was lower in energy than the  $3\bar{t}_2$ -level.

The observed anisotropic hyperfine coupling, albeit small, is a measure of the distortion of this anion from a purely tetrahedral structure and reflects the presence of p- (or d-) character in the molecular orbital. An intrinsic Jahn-Teller distortion is not expected for a radical having a  ${}^2A_1$ -ground state and therefore the destruction of tetrahedral symmetry may be environmentally induced, perhaps through a non-spherical distribution of adjacent barium cations. If this were so, it would explain why there is a difference between the anisotropic parameters obtained for  $ClO_4^{2-}$  in barium sulphate and those reported by Morton for his radical (II) in  $KClO_4$ ,<sup>1</sup> if, as we suspect, the latter species is also  $ClO_4^{2-}$ . Also, a slight temperature dependence of the isotropic coupling constant for  $ClO_4^{2-}$  (Table 6.1) is probably brought about by changes in the environment. The spin-populations for the 3s- and 3p- orbitals of the chlorine atom are calculated to be approximately 0.05 and 0.06 respectively at 77 K. There still remains the possibility that the anisotropic hyperfine coupling could result from 3d- rather than 3p-orbital character in the molecular orbital which contains the unpaired electron; in this case the spin-population would still remain small. However, since the energy of the

3d-orbital is a good deal higher than that of the 3p-orbital this possibility is remote. The most significant fact to emerge from the spin-population analysis is that the major portion of the unpaired electron density resides on the ligand atoms.

The observed  $g$ -value variations for  $\text{ClO}_4^{2-}$  can be readily explained if we assume that the environmentally or otherwise induced distortion of this anion reduces its symmetry to  $C_{2v}$ . Then, with reference to Figure 6.7, the deviations of the anisotropic  $g$ -factors from the free-spin value would arise through the following excitations:

$$\epsilon_{11}: \dots(a_2)^1(b_1)^2(b_2)^2(a_1)^2; {}^2A_2 \leftarrow \dots(a_2)^2(b_1)^2(b_2)^2(a_1)^1; {}^2A_1$$

$$\epsilon_{22}: \dots(a_2)^2(b_1)^1(b_2)^2(a_1)^2; {}^2B_1 \leftarrow \dots(a_2)^2(b_1)^2(b_2)^2(a_1)^1; {}^2A_1$$

$$\epsilon_{33}: \dots(a_2)^2(b_1)^2(b_2)^1(a_1)^2; {}^2B_2 \leftarrow \dots(a_2)^2(b_1)^2(b_2)^2(a_1)^1; {}^2A_1$$

The effect of distorting the molecule so that its symmetry is reduced to  $C_{2v}$  is to split the non-bonding  $t_1$ -level into orbitals which transform as  $a_2$ ,  $b_1$  and  $b_2$ , and since  $\epsilon_{11} \ll \epsilon_{22} < \epsilon_{33}$  we conclude that the  $a_2$ -level is the lowest in energy as indicated in Figure 6.7.

Although the positive  $g$ -shifts observed can be accommodated using an energy level scheme involving  $C_{2v}$  symmetry, we would not consider this as unequivocal evidence for such an assignment; the exact configuration adopted by a penta-atomic molecule not being easily predicted from M.O. theory.

Effect of Molecular Distortion on the g-tensor  
of an AB<sub>4</sub> Thirty-three Electron Species.

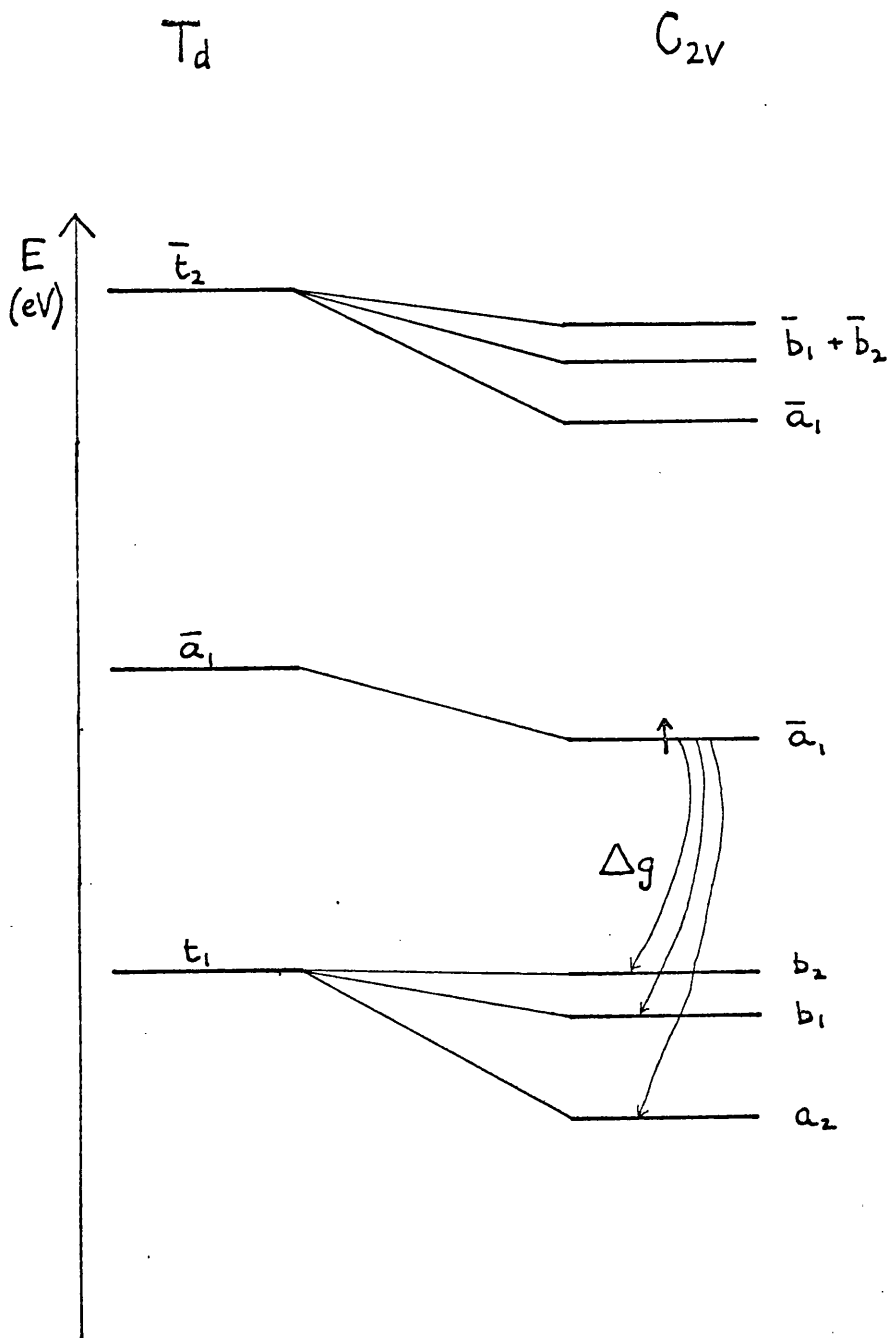


Figure 6.7

### Comparison with Isoelectronic Species.

At room temperature the isoelectronic molecule  $\text{PF}_4$ , prepared by  $\gamma$ -irradiation of ammonium or potassium hexafluorophosphate, gives a completely isotropic e.s.r. spectrum in which all four fluorine atoms appear to be magnetically equivalent.<sup>9,10</sup> When the irradiated samples are cooled, the e.s.r. spectrum broadens markedly before giving a very complex and not fully interpreted envelope spectrum at 200 K.<sup>9</sup> This broadening is considered to arise through a slowing down of a rapid inversion process of the type discussed by Chantry and Ewing<sup>17</sup> for sulphur tetrafluoride, involving two inequivalent pairs of fluorine atoms. This proposal is supported by the observation that  $\text{PF}_4$  in a sulphur hexafluoride matrix at low temperatures gives an isotropic spectrum characterised by two pairs of inequivalent fluorine atoms.<sup>12</sup> (Table 6.4). The analogous chlorine species  $\text{PCl}_4$ , prepared by u.v.-photolysis of phosphorus trichloride, is also reported to possess two pairs of non-equivalent ligand atoms.<sup>11</sup> A trigonal bipyramid structure, where the unpaired electron resides in one of the equatorial  $\text{sp}^2$  orbitals, has been proposed for these molecules.<sup>11,12</sup> In contrast, the isoelectronic radical  $\text{SF}_4^+$  in solid  $\text{SF}_6$  has four magnetically equivalent fluorine atoms even at 98 K.<sup>12</sup> It is not certain whether the radical undergoes rapid inversional motion at 98 K, or whether it possesses four truly equivalent ligands.

We have indicated that the structure of penta-atomic radicals is difficult to predict using M.O. theory. However, a theory which is able to predict the structure of such radicals is the Sidgwick-Powell theory of molecular structure,<sup>18</sup> later developed into the Valence Shell Electron-Pair Repulsion theory.<sup>19-23</sup> This theory assumes

Table 6.4 Electron Spin Resonance and Magnetic Data for some 33 Valence-

electron Radicals.

Radical	Medium	$g_{av}$	Nucleus	Hyperfine Tensor (G)					Ref.	
				$B_{11}$	$B_{22}$	$B_{33}$	$A_{iso}$	$As^2$		$Ap^2$
$PF_4$	$NH_4PF_6$	1.9985	$^{19}F$	-40	-40	80	196			
			$^{31}P$				1346	0.37		10
$PF_4$	$SF_6 + 1\%PF_3$	2.0033	$^{19}F$ (2 equiv nuclei)				59			
			$^{19}F$ (2 equiv nuclei)				282			
			$^{31}P$				1330	0.37		12
$PCl_4$	$PCl_3$	2.013	$^{35}Cl$				62.7			
			$^{31}P$				1206	0.33		11
$SF_4^+$	$SF_6$	2.0041	$^{19}F$				143			
			$^{33}S$				310	0.32		12
$AsO_4^{4-}$ [As(OH) $_4$ ]	$KH_2AsO_4$	2.0016	$^{75}As$	-38.2	-38.2	76.4	1084.7	0.32	.42	8

that it is the repulsive forces between the electron pairs that control their orientation and thus the shape of the resulting molecule. We shall show that the structures of the above 33 valence-electron radicals are consistent with this theory and that the most probable configuration of the  $\text{ClO}_4^{2-}$  anion can be predicted using arguments based on the Sidgwick-Powell theory.

The most energetically favoured configuration for an  $\text{AB}_4$  molecule having five electron pairs is the slightly distorted trigonal bipyramid structure shown in Figure 6.8. For example, the 34 valence-electron  $\text{SF}_4$  molecule is known to have this structure at low temperature,<sup>12</sup> where the axial S-F bonds are larger and weaker than the equatorial S-F bonds and the sulphur non-bonding (or strictly anti-bonding) electrons are accommodated in an equatorial  $\text{sp}^2$ -lone pair orbital. In contrast, the 32 valence-electron perchlorate anion  $\text{ClO}_4^-$ , which does not possess any lone pairs or unpaired electrons, has the fully symmetrical tetrahedral structure. The radicals  $\text{PF}_4$ ,  $\text{PCl}_4$ ,  $\text{SF}_4^+$  and  $\text{ClO}_4^{2-}$  all have 35 valence-electrons, so that we would expect them to adopt configurations between these two extremes. It should be noted that, with reference to Figure 6.8, the tetrahedral structure can be achieved by moving the axial (B') ligands in the direction shown by the arrows. The converse is also true, so that a tetrahedral structure may distort due to lone pair-bonding pair repulsion to give the trigonal bipyramid structure. The amount of distortion will depend on the actual electron density on the central atom's lone pair orbital. The total antibonding electron density ( $a_s^2 + a_p^2$ ) on the central atom in a variety of paramagnetic molecules and ions has been shown to decrease as  $\Delta\chi$  falls, where  $\Delta\chi = \chi_{\text{ligand}} - \chi_{\text{central atom}}$  (Figure 6.9.) For the series of

Most Probable Configuration for an  $AB_4$  Molecule

Having Five Electron Pairs.

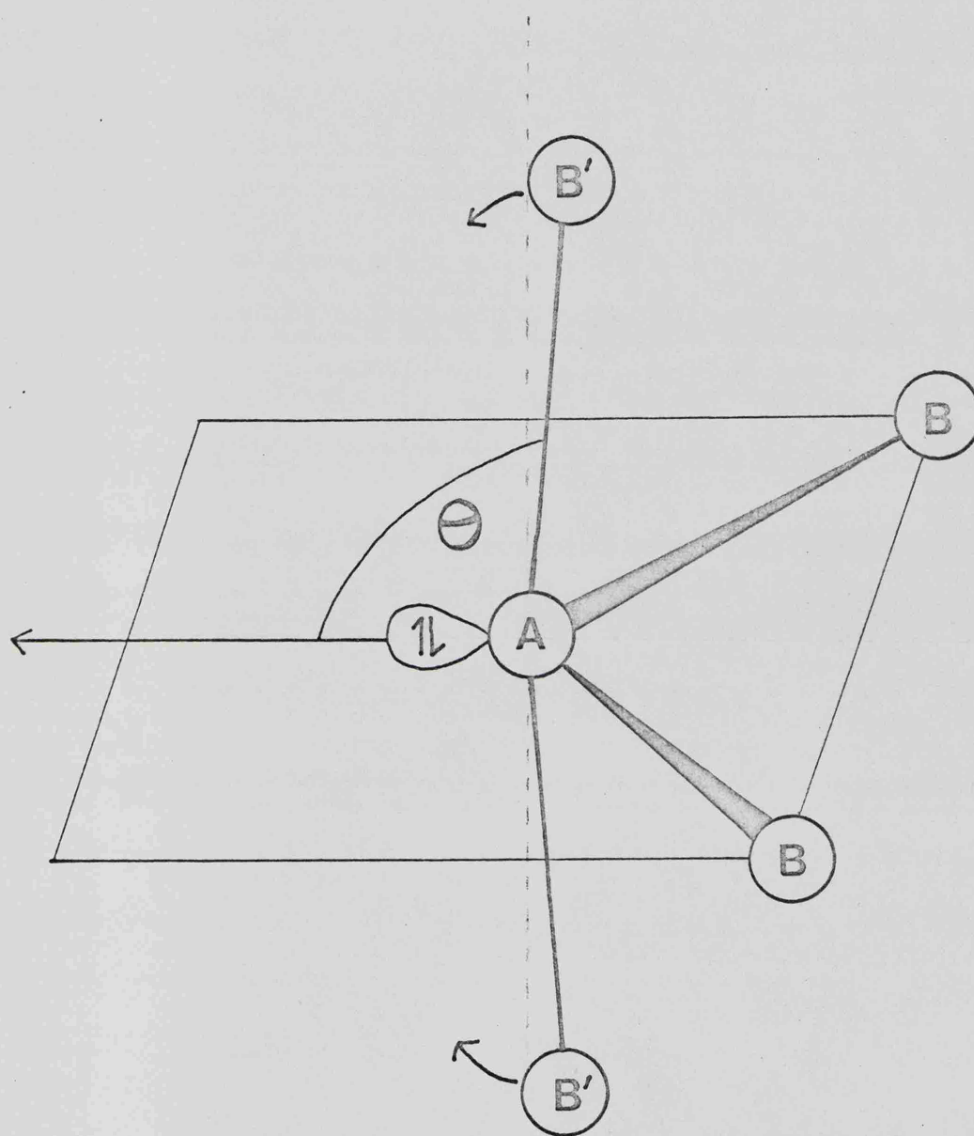


Figure 6.8

Plot of Spin Density on Central Atom against Difference in Electronegativity for some Penta-atomic Radicals.

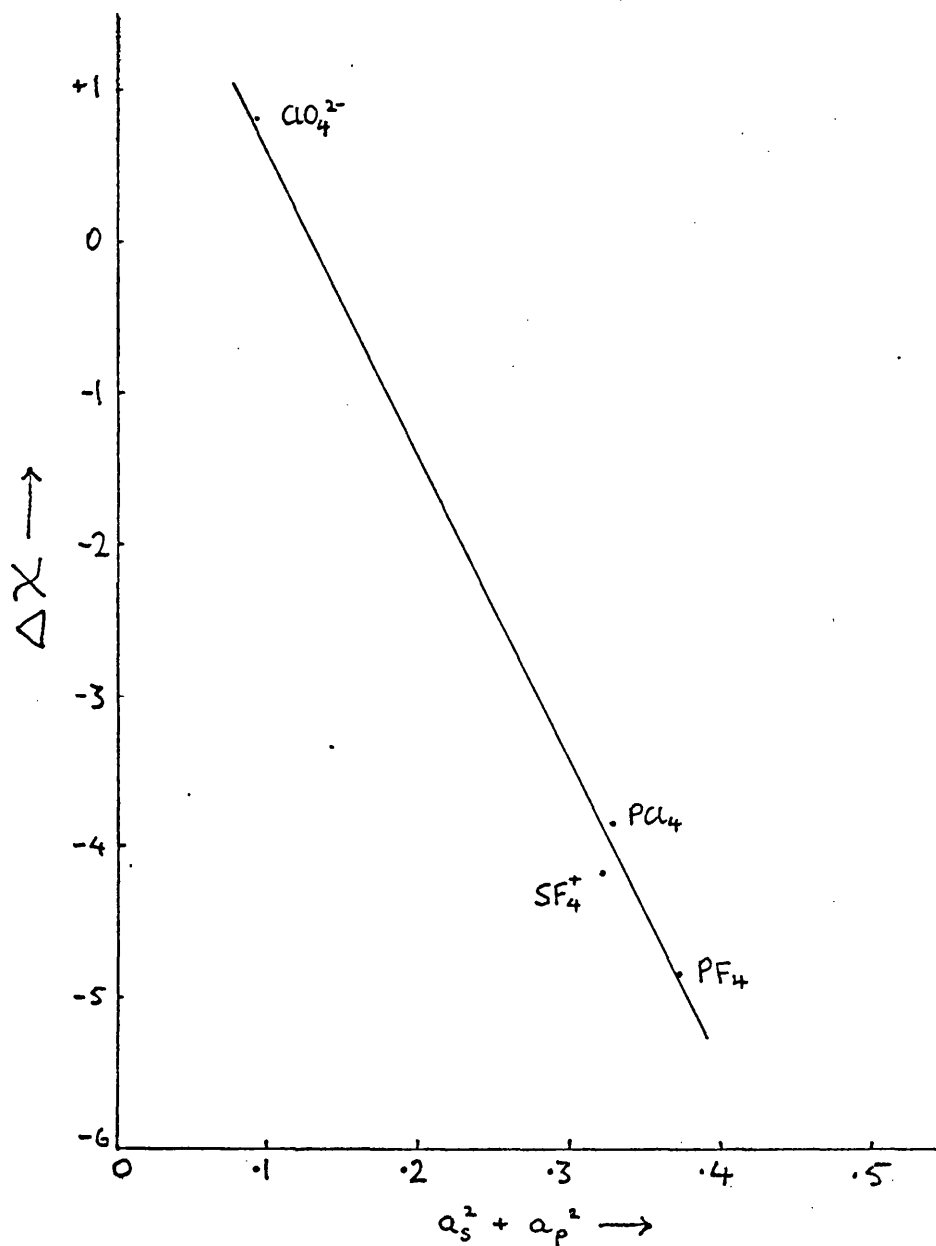


Figure 6.9

radicals  $\text{PF}_4$ ,  $\text{PCl}_4$  and  $\text{SF}_4^+$   $\Delta\chi$  is large, so that the unpaired electrons are expected to be confined largely on the central atoms. In other words, since the highly electronegative ligand atoms take the greater share of the bonding and non-bonding electrons, the central atom will take a correspondingly greater share of the antibonding electrons. Consequently the most favoured configuration for these radicals will be the trigonal bipyramidal structure where the angle  $\theta$  in Figure 6.8 has closed slightly, since there is only one electron in the antibonding orbital to repel the bonding electrons in the A-B' bonds. The anisotropic spin-resonance parameters have not been obtained for these species, but if as we suggest, they do have their unpaired electron in an essentially  $sp^2$ -lone pair orbital on phosphorus or sulphur, then the observed isotropic s-character of the unpaired electron ( $a_s^2$ ) of about 0.3 must correspond to unit occupancy of the central-atom orbitals.

In the case of the isoelectronic tetroxide anion  $\text{AsO}_4^{4-}$ , prepared by the action of  $\gamma$ -rays on  $\text{KH}_2\text{AsO}_4$  at 77 K,  $\Delta\chi$  is again large and  $a_s^2$  on the central atom is close to 0.3.<sup>8</sup> However, the detection of hyperfine coupling to four equivalent protons for certain orientations of this radical would suggest that it is best considered as  $\text{As}(\text{OH})_4$ , where the  $\text{AsO}_4^{4-}$  unit is rigidly held close to the tetrahedral configuration through hydrogen bonding to the protons of adjacent units in the  $\text{KH}_2\text{AsO}_4$  crystal. Hence the unpaired electron of  $\text{AsO}_4^{4-}$  in  $\text{KH}_2\text{AsO}_4$  must be located in an orbital which is constructed principally from the arsenic 4s-level.

In contrast, the value of  $\Delta\chi$  for the anion  $\text{ClO}_4^{2-}$  is small and probably negative, so that we would expect the unpaired electron to be mainly confined to the ligand oxygen atoms. The observed spin-

density on the central chlorine atom is indeed small and bears out this postulate. There being negligible 'lone pair' electron density on chlorine, the 'bonding pair' - 'bonding pair' repulsions of the ligand atoms now become important. Thus for minimum energy we would expect this radical to be only slightly distorted from the tetrahedral structure so that the unpaired electron occupies a molecular orbital having significant 3s-character on chlorine. This is in accord with the spin-resonance parameters of  $\text{ClO}_4^-$  included in Table 6.1.

We conclude therefore, that whilst the radicals  $\text{PF}_4^+$ ,  $\text{PCl}_4^+$  and  $\text{SF}_4^+$  may well have trigonal bipyramidal structures, the species  $\text{ClO}_4^{2-}$  in  $\text{BaSO}_4$  and  $\text{AsO}_4^{4-}$  in  $\text{KH}_2\text{AsO}_4$  are distorted only marginally from the tetrahedral configuration.

#### Mechanism of Formation.

Radiation damage of perchlorate-doped barium sulphate at 77 K results in the formation of the radicals  $\text{SO}_4^-$ ,  $\text{ClO}_4^{2-}$  and  $\text{ClO}_3$ .

The host lattice  $\text{SO}_4^-$  centre is produced by the simple process of electron ejection from a sulphate anion. The 'conduction' electron is then probably trapped at an impurity  $\text{ClO}_4^-$  site producing the  $\text{ClO}_4^{2-}$  paramagnetic centre.

Electrons may also be ejected from a perchlorate ion by interaction with the high energy radiation producing the perchlorate hole-centre  $\text{ClO}_4$ . This is likely to be unstable in the barium sulphate lattice and might undergo homolytic bond fission to give chlorine trioxide. However, we cannot rule out the possibility that  $\text{ClO}_3$  is derived from chlorate ion impurities concurrently coprecipitated with perchlorate ions by the barium sulphate.

On annealing, the  $\text{SO}_4^{\cdot-}$  and  $\text{ClO}_3$  centres decay, the former giving rise to the  $\text{SO}_2^{\cdot-}$  radical, and the latter decomposes into products that are not detectable by e.s.r. spectroscopy. This is unusual, since  $\text{ClO}_3$  is known to undergo thermally initiated decomposition into the relatively stable paramagnetic chlorine dioxide in chlorate and perchlorate matrices, where the process has been monitored spectroscopically.<sup>7,24</sup> Both the  $\text{SO}_2^{\cdot-}$  host radical and  $\text{ClO}_4^{2-}$  are extremely stable in  $\text{BaSO}_4$ .

References for Chapter 6.

1. J.R. Morton, J. Chem. Phys., 45, 1800, (1966).
2. S.A. Marshall and R.A. Serway, J. Chem. Phys., 45, 4098, (1966).
3. V.V. Gromov and J.R. Morton, Canad. J. Chem., 44, 527, (1966).
4. M.C.R. Symons, Adv. in Chem., 82, 1, (1968).
5. R.S. Eachus and M.C.R. Symons, J. Chem. Soc.(A), 2438, (1968).
6. R.S. Eachus and M.C.R. Symons, J. Chem. Soc.(A), 790, (1968).
7. R.S. Eachus and M.C.R. Symons, J. Chem. Soc.(A), 2433, (1968).
8. M. Hampton, F.G. Herring, W.C. Lin and C.A. McDowell, Mol. Phys., 10, 565, (1966).
9. P.W. Atkins and M.C.R. Symons, J. Chem. Soc., 4363, (1964).
10. J.R. Morton, Canad. J. Phys., 41, 706, (1963).
11. G.F. Kokoszka and F.E. Brinkman, Chem. Comm., 349, (1968).
12. R.W. Fessenden and R.H. Schuler, J. Chem. Phys., 45, 1845, (1966).
13. C. Jaccard, Phys. Rev., 124, 60, (1961).
14. A.D. Walsh, J. Chem. Soc., 2266, (1953).
15. P.W. Atkins and M.C.R. Symons, The Structure of Inorganic Radicals, Elsevier, Amsterdam, (1967).
16. P.W. Atkins, Ph.D. Thesis, Leicester, (1964).  
H.W. Wardale, Ph.D. Thesis, Leicester, (1967).

17. G.W. Chantry and V.C. Ewing, *Mol. Phys.*, 5, 210, (1962).
18. N.V. Sidgwick and H.M. Powell, *Proc. Roy. Soc.*, 176A, 153, (1940).
19. R.J. Gillespie and R.S. Nyholm, *Q. Rev.*, 11, 339, (1957); *Prog. Stereochem.*, 2, 261, (1958).
20. J.J. Cox and C.D. Whiston, *Educ. Chem.*, 7, 93, (1970).
21. R.J. Gillespie, *J. Chem. Educ.*, 47, 18, (1970).
22. R.J. Gillespie, *Adv. Chem. Ser.*, 62, 221, (1967).
23. J.W. Linnet and C.E. Mellish, *Trans. Faraday Soc.*, 50, 657, (1954).
24. R.S. Eachus, unpublished result.
25. R.S. Eachus, P.R. Edwards, S. Subramanian and M.C.R. Symons, *J. Chem. Soc.*, (A) 1704, (1968).
26. J.R. Byberg, S.J.K. Jenson and L.T. Muvs, *J. Chem. Phys.*, 46, 131, (1967)
27. T.G. Castner and W. Kanzig, *J. Phys. Chem. Solids*, 3, 178, (1957).
28. P.W. Atkins. A. Horsfield and M.C.R. Symons, *J. Chem. Soc.*, 5220, (1964).
29. G.W. Chantry, A. Horsfield, J.R. Morton, J.R. Rowlands and D.H. Whiffen, *Mol. Phys.*, 5, 223, (1962).

APPENDIX I

CALCULATION OF PRINCIPAL g- AND A-VALUES

FROM SINGLE CRYSTAL DATA

The g-factor in a crystal for an arbitrary orientation is given by :

$$g^2 = \sum_{i,j=1}^3 l_i G_{ij} l_j$$

where  $l_i$  and  $l_j$  are direction cosines and  $G_{ij}$  is an element of a 3 X 3 matrix. Now, for orientation  $\theta$  of the magnetic field with respect to the experimental axis of the crystal,

$$g^2 = \alpha + \beta \sin 2\theta + \gamma \cos 2\theta$$

where  $\alpha$ ,  $\beta$  and  $\gamma$  are functions of  $G_{ij}$ .

If  $g_+$  represents the maximum g-value obtained in one rotation at  $\theta_+$  and  $g_-$  the minimum at  $\theta_-$  then we have

$$2\alpha = g_+^2 + g_-^2$$

$$2\beta = (g_+^2 - g_-^2) \cos 2\theta_+$$

$$2\gamma = (g_+^2 - g_-^2) \sin 2\theta_+$$

In the case where the axes of rotation are orthogonal,  $\beta$  and  $\gamma$  are related to a new parameter  $\delta$  by :

$$\delta = (\beta + \gamma)^{1/2} = 1/2(g_+^2 - g_-^2)$$

and the matrix elements are given by

$$G_{11} = (\alpha_2 + \alpha_3 - \alpha_1)$$

$$G_{22} = (\alpha_3 + \alpha_1 - \alpha_2)$$

$$G_{33} = (\alpha_1 + \alpha_2 - \alpha_3)$$

and

$$G_{12} = (\delta_3 + \alpha_1 - \alpha_2) (\delta_3 - \alpha_1 + \alpha_2)^{1/2}$$

$$G_{23} = (\delta_1 + \alpha_2 - \alpha_3) (\delta_1 - \alpha_2 + \alpha_3)^{1/2}$$

$$G_{31} = (\delta_2 + \alpha_3 - \alpha_1) (\delta_2 - \alpha_3 + \alpha_1)^{1/2}$$

Suffixes 1, 2 and 3 refer to planes 23, 13 and 12 respectively. The above method always gives rise to an ambiguity of sign. In the special case of rotation about three mutually orthogonal axes, one may choose, say  $G_{12}$  and  $G_{31}$  positive, then both possible signs for  $G_{23}$  need to be considered. The situation may be visualised by imagining the construction of a three-dimensional model of the g-value variation from polar diagrams of the variations in each of the planes of measurement. Two of these can be fitted together along their line of intersection; there are then two ways of fitting the third polar diagram into the model.

In order to decide which of the two sets of principal g-values and principal axes obtained in the nitroprusside crystal study (Chapter 3) was correct, the following procedure was applied.

The results of g-value measurements in a direction not included in the previous measurements are compared with the results predicted by the two possible sets of principal values. If we denote the principal axes by x,y,z with corresponding g-values  $g_x, g_y, g_z$ , then the g-value in a direction whose direction cosines with respect to x,y,z are  $l, m, n$  respectively, is given by,

$$g^2 = g_x^2 l^2 + g_y^2 m^2 + g_z^2 n^2$$

On the other hand, if the g-value variation is measured in a plane whose normal has direction cosines  $l, m, n$  with respect to the principal axes, the maximum and minimum g-values in this plane will satisfy the relations

$$g_+^2 + g_-^2 = g_x^2(1 - l^2) + g_y^2(1 - m^2) + g_z^2(1 - n^2) \dots\dots(1)$$

and

$$g_+^2 \cdot g_-^2 = g_x^2 g_y^2 n^2 + g_y^2 g_z^2 l^2 + g_x^2 g_z^2 m^2 \dots\dots (2)$$

simultaneously.

The axis chosen (the  $c'$ -axis) made angles of  $90^\circ$ ,  $105^\circ$  and  $15^\circ$  with the crystallographic  $a$ ,  $b$  and  $c$  axes respectively. When the above procedure was applied, only the first set of principal  $g$ -values and directions satisfied both relationships (1) and (2) simultaneously. (see Table 3.3)

An identical procedure was employed to obtain the principal  $^{14}\text{N}$  hyperfine values and directions.

The next step was to relate the principal directions of the  $g$ -tensor to three bonds in the molecule of unirradiated sodium nitroprusside, comprising a set of co-ordinate axes of the molecule. (viz. the  $\text{Fe-N}$ ,  $\text{Fe-C}_2$  and  $\text{Fe-C}_3$  bonds)

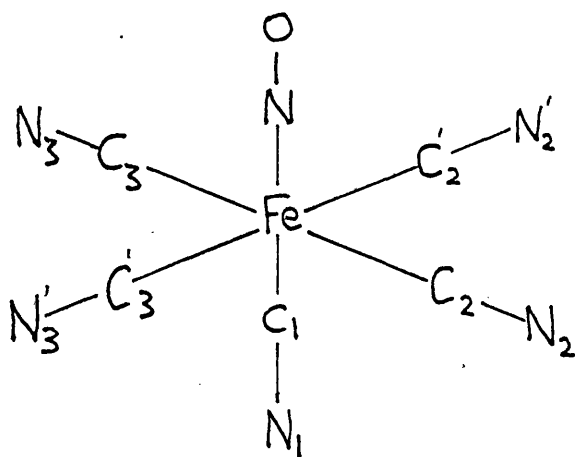


Figure A.1

Since all angles and directions involved in experimental measurement are related to the axes of the unit cell of the crystal (= rotation axes), it is first necessary to calculate the angles the three bonds make with these axes.

The data required for these calculations are to be found in Manoharan and Hamilton's crystal structure paper on sodium nitroprusside (Inorg. Chem. 2, 1043, 1963).

The relevant data are as follows:

cell constants       $a = 6.17$   
                               $b = 11.84$   
                               $c = 15.43$

bond lengths

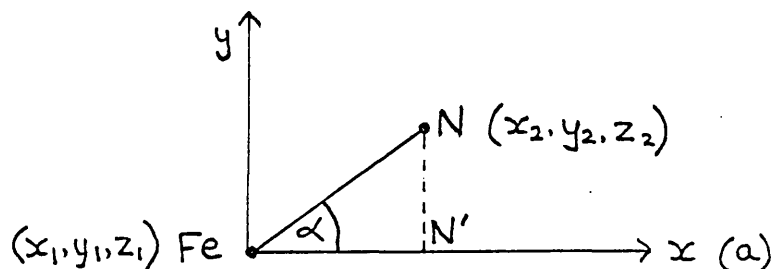
Fe-N      1.63  
 Fe-C<sub>2</sub>    1.91  
 Fe-C<sub>3</sub>    1.93

Atomic parameters

<u>Atom</u>	<u>a-axis (x)</u>	<u>b-axis (y)</u>	<u>c-axis (z)</u>
Fe	.5003	.2797	1/2
N	.7197	.3566	1/2
C <sub>2</sub>	.6038	.1799	.5884
C <sub>3</sub>	.3407	.3599	.4121

The method in principle is as follows.

To find the angle the Fe-N bond makes with the a-axis, say, let Fe have coordinates  $(x_1, y_1, z_1)$  and N  $(x_2, y_2, z_2)$



The perpendicular distance Fe-N' along the x (or a) axis is  $x_2 - x_1$ . In practice this distance is the difference in the two atomic parameters multiplied by the cell constant for

the a-axis.

$$\text{i.e. } \text{Fe-N}' = (.7197 - .5003) \times 6.17$$

$$\alpha = \cos^{-1} \frac{\text{Fe-N}'}{\text{Fe-N}}$$

and the distance Fe-N is known, therefore the angle  $\alpha$  can be computed.

The results are as follows.

<u>Bond</u>		<u>a-axis</u>	<u>b-axis</u>	<u>c-axis</u>
Fe-N	cosine	.8305	.5586	0.0
	angle	33° 51'	56° 3'	90°
Fe-C <sub>2</sub>	cosine	.3343	-.6186	.7141
	angle	70° 34'	51° 47'	47° 1'
Fe-C <sub>3</sub>	cosine	-.5129	.4946	-.7064
	angle	59° 8'	60° 22'	45° 3'

As a routine check, the angles between the bonds N-Fe-C<sub>2</sub> and C<sub>2</sub>-Fe-C<sub>3</sub> in Figure A.1 (taken from Manoharan and Hamilton's paper) were computed. The N-Fe-C<sub>2</sub> bond angle was found to be 93° 53' which agreed with the result of Manoharan and Hamilton. However, the C<sub>2</sub>-Fe-C<sub>3</sub> bond angle calculated from the above data was found to be close to 180°. It was thus unfortunate that the C<sub>2</sub> and C<sub>3</sub> atoms mentioned in Table II of Manoharan and Hamilton's paper were on opposite sides of the iron atom. In effect, only two of the required bond directions have been found. Also the three bonds required do not form a perfectly orthogonal

coordinate system, since the Fe-C<sub>2</sub> bond is bent down from the equatorial plane by nearly four degrees (vide supra).

In order to calculate the direction of the Fe-C<sub>3</sub>' bond, we must assume an orthogonal set of axes.

Let the Fe-N bond have direction cosines  $l, m, n$  and the Fe-C<sub>2</sub> bond  $l', m', n'$ . We shall assume that these bonds are perpendicular. If the Fe-C<sub>3</sub>' bond has direction cosines  $p, q, r$ , then by the perpendicularity condition

$$lp + mq + nr = 0$$

$$\text{and } l'p + m'q + n'r = 0$$

Solving for  $p : q : r$  we have

$$p : q : r = mn' - m'n : n'l' - n'l : lm' - l'm$$

In this particular case  $n = 0$ ,

$$\text{i.e. } p : q : r = mn' : -n'l' : lm' - l'm$$

Thus we find the Fe-C<sub>3</sub>' bond has direction cosines 0.3989 ; -0.5931 ; -0.7798 with respect to the crystallographic a-, b- and c-axes respectively.

Now, we are primarily interested in finding the direction of the N-O bond with respect to the molecular axes of the nitroprusside ion. According to our nomenclature (Chap. 3), the direction of  $g_z$  gives the direction along the N-O bond, whereas the other two g-values ( $g_x$  and  $g_y$ ) have principal directions at right-angles to the N-O bond direction.

Thus, by the usual method of determining the angle between two lines (i.e.  $\cos \theta = ll' + mm' + nn'$ ) the Fe-N-O bond angle is calculated to be  $153^\circ$ .

The next step is to find the angle made by the projection

projection of the N-O bond onto the equatorial plane, with one of the equatorial Fe-CN bonds. We must again make the assumption that the Fe-N, Fe-C<sub>2</sub> and Fe-C<sub>3</sub>' bonds are truly orthogonal. The method is as follows.

Let the Fe-N axis be called a'  
           Fe-C<sub>2</sub> " " " b'  
 and the Fe-C<sub>3</sub>' " " " c'

- (1) We first find the direction cosines of the N-O bond with respect to the a', b', c' set of axes, and then
- (2) project the N-O bond onto the b'c' plane to find the required angle  $\phi$  (vide infra).

(1) i. N-O with a'-axis

$$\begin{aligned}\cos \alpha &= (.9883 \times .8305) + (.1258 \times .5586) \\ &= .8911 \quad (27^\circ)\end{aligned}$$

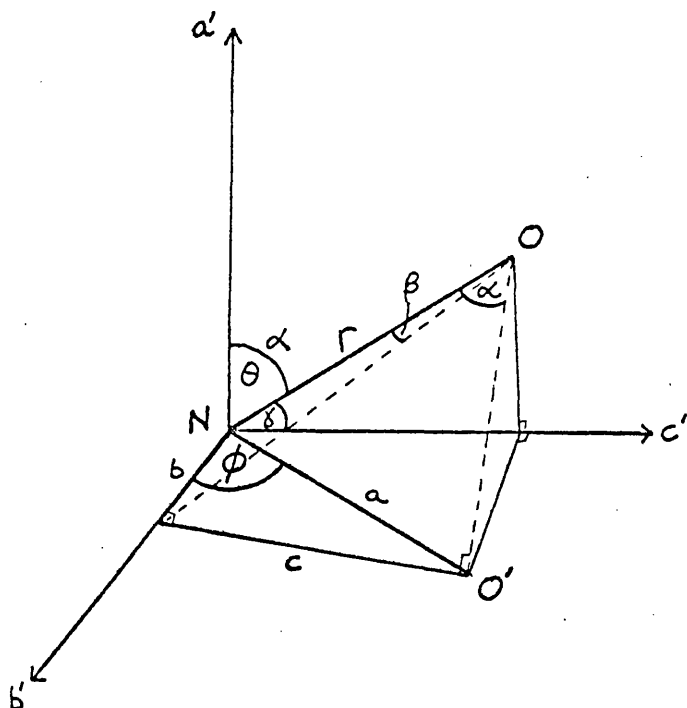
ii. N-O with b'-axis

$$\begin{aligned}\cos \beta &= (.9983 \times .3343) + (.1258 \times -.6186) \\ &\quad + (.0863 \times .7141) \\ &= .3142 \quad (71^\circ 41')\end{aligned}$$

iii. N-O with c'-axis

$$\begin{aligned}\cos \gamma &= (.9883 \times .3989) + (.1258 \times -.5931) \\ &\quad + (.0863 \times -.7798) \\ &= .2523 \quad (75^\circ 23')\end{aligned}$$

So the new direction cosines of the N-O bond are  
 ( .8911, .3142, .2523 ).

Projection of N-O Bond onto b'c' Plane

By simple trigonometry we have the following relationships

$$a = r \cdot \sin \alpha$$

$$b = r \cdot \cos \beta$$

$$c = r \cdot \cos \gamma$$

$$\sin \phi = \frac{c}{a} = \frac{\cos \gamma}{\sin \alpha} = \frac{.2523}{.4540} = .5557 \quad (33^\circ 46')$$

$$\cos \phi = \frac{b}{a} = \frac{\cos \beta}{\sin \alpha} = \frac{.3142}{.4540} = .6921 \quad (46^\circ 12')$$

$$\tan \phi = \frac{c}{b} = \frac{\cos \gamma}{\cos \beta} = \frac{.2523}{.3142} = .8050 \quad (38^\circ 50')$$

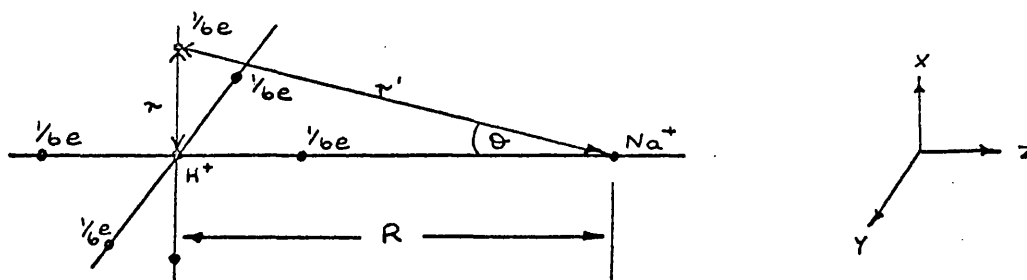
These results for  $\phi$  should be self-consistent, and would be if we had been dealing with a true set of orthogonal axes. Nevertheless, the method does give a rough guide to the required angle. So we conclude that, within the limits of experimental error and computational limitations, the angle made by the N-O' projection with the Fe-C<sub>2</sub> bond is  $40^\circ \pm 10^\circ$ .

APPENDIX II

Calculation of the Dipolar Interaction between an  
Electron Confined to a Hydrogen 1s-orbital and an  
adjacent Na Nucleus.

Calculation of the Dipolar Interaction between an Electron  
Confined to a Hydrogen 1s-orbital and an Adjacent Sodium  
Nucleus.

1. Assume that the electron is distributed octahedrally about the hydrogen nucleus at a distance  $a_0$  (the Bohr radius).



$$r = a_0 = 0.52913 \times 10^{-8} \text{ cm}$$

2. The experimental anisotropic hyperfine term,  $B_{\parallel}$  ( $B_z$ ) is given by.

$$B_{\parallel} = B_z = \frac{2}{3} \left[ g_N \beta_N \left( \frac{3 \cos^2 \theta - 1}{r'^3} \right) \right] + \frac{1}{6} \left[ g_N \beta_N \frac{2}{(R + r)^3} \right] + \frac{1}{6} g_N \beta_N \frac{2}{(R - r)^3}$$

$$\text{where } \cos^2 \theta = \frac{R^2}{r'^2} = \frac{2}{r^2 + R^2}$$

and  $g_N$  = Na nuclear g-factor.

Term A arises from four equivalent charges ( $e/6$ ) at a distance  $r'$  from the Na nucleus. Term B arises from a

charge ( $e/6$ ) at a distance ( $R + r$ ), and term C from a charge ( $e/6$ ) at a distance ( $R - r$ ), where  $\theta = 0$  in both cases.

3. A plot of  $B_{//}$  versus  $R$ , assuming  $r = 0.5293 \text{ \AA}$ , will give the separation of the sodium nucleus and the proton which gives an experimental  $B$  of  $4.2 \text{ G}$  (see Chapter 5).

Thus, when  $R = 1.8 \text{ \AA}$ ,

$$\cos^2 \theta = \frac{R^2}{r^2 + R^2} = 0.9205$$

and we find  $B_{//} = 4.12 \text{ G}$ , which is comparable to the experimental value of  $4.2 \text{ G}$ . So we conclude, on the basis of this calculation, that the internuclear distance  $R$  equals  $1.8 \text{ \AA}$  to a good approximation.

## SUMMARY

Part I deals with the study of various transition metal nitrosyl complexes. The products of radiation-damage in anhydrous sodium nitroprusside are shown to be nitric oxide, trapped at sites with a strong crystal field, and the hitherto unknown pentacyanonitrosylferrate (III) anion. The e.s.r. parameters of the latter are compared with those of the isoelectronic  $d^5$  chromium (I) and manganese (II) pentacyanonitrosyl ions and a general trend is deduced. Irradiation of hydrated nitroprusside at 77 K is shown to produce two new reduced species. These are both interpreted as the ion  $[\text{Fe}(\text{CN})_5\text{NO}]^{3-}$  where the unpaired electron is located in a  $\pi^*$  orbital on the nitrosyl group; the difference being only a subtle one involving the geometry of the molecule. The theory of a librating nitrosyl group is proposed to explain their unusual  $^{14}\text{N}$  hyperfine parameters. Possible mechanisms of radiation-damage in the anhydrous and hydrated systems are discussed.

An infra-red study on the pentacyanonitrosyl chromate (I) and manganate (I) ions, doped into alkali halide lattices, showed a large number of lines in the nitrosyl stretching region of the spectrum, which were interpreted in terms of the N-O group interacting with two cation vacancies in the lattice. Infra-red spectra provide strong evidence to show that both complexes are reduced to the zero oxidation state on irradiation of the doped halides. However, an e.s.r. study on irradiated, manganese-doped halides shows the formation of several new paramagnetic species; the complexity of the spectra being such that the expected manganese (0) complex could not be positively identified.

Part II deals with the stabilisation of inorganic radicals in precipitated powders. Hydrogen atoms produced in irradiated barium sulphate are shown to interact with neighbouring, impurity sodium ions. Hydrogen atoms, formed in other solid matrices, are also shown to be interacting with a second magnetic nucleus. There is also experimental evidence for the formation of the radical-ions  $\text{H}_2^-$  and  $\text{H}_2^+$ .

Finally, we report the formation of the 33 valence-electron  $\text{ClO}_4^{2-}$  radical in barium sulphate and compare its spectral parameters and geometry with those of isoelectronic species.